



# Synthetic Studies Towards Potential Lead(II) Specific Fluorescent Probes

A Thesis Submitted for the  
Degree of Doctor of Philosophy

by

John Vic Valente B.Sc. (Hons.)

The Department of Chemistry  
The University of Adelaide



November 1998

# Contents

<b>Declaration</b> .....	i
<b>Acknowledgements</b> .....	ii
<b>Abbreviations</b> .....	iii
<b>Abstract</b> .....	vi
<b>Chapter 1: Introduction</b> .....	1
1.1 Lead and Heavy Metal Toxicity.....	1
1.1.1 Lead Absorption and Distribution.....	1
1.1.2 The Biological Effects of Lead(II).....	2
1.1.3 Metal Chelation Therapy.....	2
1.2 Current Methods of Lead(II) Measurement.....	4
1.3 Fluorescent Probes.....	6
1.3.1 Zinc(II) and Calcium(II) Fluorescent Probes.....	6
1.3.2 Potential Heavy Metal Probes.....	8
1.3.3 Fluorescent Probes for Other Metal Ions.....	10
<b>Chapter 2: Flavones and Thioflavones</b> .....	11
2.1 Flavones - Background.....	11
2.2 Synthesis.....	13
2.2.1 Synthesis of the 3-Hydroxyflavone Analogues.....	14
2.2.2 Synthesis of the 5-Hydroxyflavone Analogues.....	15
2.2.3 Synthesis of the Flavone Analogues.....	17
2.3 Specificity.....	18
2.3.1 UV-visible Absorption Spectroscopy.....	19
2.3.2 Detecting Complex Formation.....	20
2.3.3 Conditions for Complex Determination.....	21
2.3.4 Determination of Metal Ion-Flavone Complexation.....	24
2.4 Determination of Stability Constants.....	32

2.4.1	Concentration and Activity Constants.....	32
2.4.2	Stability Constant Determination using UV Absorption Spectroscopy.....	33
2.4.3	Conditions of Stability Constant Determination.....	35
2.4.4	Results and Discussion.....	36
2.5	Fluorescence.....	65
2.5.1	Principles of Fluorescence.....	65
2.5.2	Fluorescence of Organic Compounds.....	66
2.5.3	Fluorescent Probe Specifications for the Detection of Lead(II).....	68
2.5.4	Results and Discussion.....	70
2.6	Molecular Modelling and Computational Chemistry.....	84
2.6.1	Molecular Modelling using Gaussian 94.....	84
2.6.2	Results and Discussion.....	85
<b>Chapter 3: Thiazoles and Thiazolines.....</b>		<b>94</b>
3.1	Synthesis.....	94
3.2	Specificity.....	100
3.2.1	Determination of Metal Ion - Thiazole Complexation.....	101
3.3	Fluorescence Measurements on Compounds <b>30 - 33</b> .....	103
3.3.1	The Benzopyran-4-ones <b>30</b> and <b>31</b> .....	105
3.3.2	The Coumarins <b>32</b> and <b>33</b> .....	106
3.3.3	Summary.....	107
<b>Chapter 4: Quinoline and Pyridine Analogues.....</b>		<b>108</b>
4.1	Synthesis.....	108
4.1.1	C <sub>8</sub> Substituted Quinoline Derivatives.....	108
4.1.2	Pyridine and Quinoline 1-Oxides.....	113
4.2	Investigations into the Chelating Properties of the Quinoline and Pyridine Analogues .....	116
<b>Chapter 5: Summary and Conclusions.....</b>		<b>119</b>

<b>Chapter 6: Experimental</b> .....	126
6.1 General Synthesis.....	126
6.2 Flavone and Thioflavone Syntheses.....	127
6.3 Thiazoles Syntheses.....	132
6.4 Quinoline and Pyridine Analogue Syntheses.....	136
6.5 General Physical Methods.....	142
6.6 Standardisation of Metal Ion Solutions.....	143
6.7 UV-visible Absorption Measurements.....	144
6.7.1 Selectivity.....	144
6.7.2 Stability Constant Determination.....	144
6.7.3 Light Decomposition of Ligand <b>7</b> .....	145
6.8 Fluorescence Measurements.....	145
6.8.1 Stability Constant Determinations of the Al <sup>3+</sup> Complexes of Ligands <b>4</b> and <b>5</b> using Fluorescence Spectroscopy.....	146
6.8.2 Fluorescence Determinations of Flavones <b>4 - 7</b> and their Complexes.....	146
6.8.3 Fluorescence and UV-visible Absorption Time Experiments.....	147
6.8.4 Fluorescence Determinations of Thiazoles <b>30 - 33</b> and their Complexes....	147
6.9 Molecular Modelling.....	148
 <b>Appendices</b> .....	 149
Appendix A: UV-visible Absorption Spectra.....	149
A.1 Flavones and Thioflavones.....	150
A.2 Thiazoles <b>30 - 33</b> and their Complexes.....	153
A.3 Quinoline and Pyridine Analogues.....	155
Appendix B: Metal Ion Concentrations for UV-visible Absorption and Fluorescence .....	160
Appendix C: Fluorescence Spectra.....	170
C.1 Flavones and Thioflavones.....	171
C.2 Thiazoles <b>30 - 33</b> .....	175
 <b>Bibliography</b> .....	 177

## Declaration

This thesis contains no material which has been accepted for the award of any other degree or diploma in any university or other tertiary institution and, to the best of my knowledge and belief, contains no material previously published or written by another person, except where due reference has been made in the text.

I give consent to this copy of my thesis, when deposited in the University library, being available for loan and photocopying.

Signed:

Date:

12/11/1998

## Acknowledgements

I would firstly like to express my gratitude towards Dr David Ward and Professor Stephen Lincoln for their guidance and support during my studies. Their reservoir of knowledge (of which I often tapped into) has been greatly appreciated.

I must also especially thank Daniela Caiazza for her friendship, useful advice and her time spent with me having coffee. Her lending ear and undivided attention during seminar practice and times of confusion were very much appreciated. I am forever grateful.

Special thanks go to Kellie Tuck and Kym Hendrickson for their help and advice on the use of the IBM computers and the program 'Specfit' and to Bruce May for proof reading my thesis. Thanks also go to other past and present labmates including Rob, Peter, Francine and Ben who have always been there to lend a helping hand or to just stop and chat.

I would finally like to sincerely thank my parents Anne and Vic for all their support not only during my studies, but throughout the last twenty six years. Their unconditional love and encouragement were truly an inspiration.

## Abbreviations

AAS	atomic absorption spectroscopy
ATPase	adenosine triphosphatase
BAL	2,3-dimercapto-1-propanol: British Anti-Lewisite
BAPTA	1,2-bis(2-aminophenoxy-ethane)- <i>N,N,N',N'</i> -tetraacetic acid
CaEDTA	ethylene diaminetetraacetic acid calcium salt
CHEF	chelation-enhanced fluorescence
CIP	2-(3-Coumarinyl)imidazo[1,2-a]pyridine
dithizone	diphenylthiocarbazone
DMF	<i>N,N</i> -dimethylformamide
DMPS	2,3-dimercapto-1-propanesulfonate
DMSO	dimethylsulfoxide
EDTA	ethylene diamine tetraacetic acid
EGTA	ethylene glycol-bis( $\beta$ -aminoethyl ether)- <i>N,N,N',N'</i> -tetraacetic acid
ether	diethyl ether
Fluo-3	2-[4-(2,7-dichloro-6-oxido-3-oxo-3 <i>H</i> -9-xanthenyl)-2-(2-{5-[di(2-oxido-2-oxoethyl)amino]-2-methylphenoxy}ethoxy)(2-oxido-2-oxyethyl)anilino]acetate
HEDTA	<i>N</i> -(2-hydroxyethyl)ethylenediaminetriacetic acid
$\lambda$	wavelength
Lawesson's Reagent	2,4-bis(4-methoxyphenyl)-1,3-dithia-2,4-diphosphetane-2,4-disulfide
M <sup>+</sup>	molecular ion
morin	3,5,7,2',4'-pentahydroxyflavone
ms	mass spectrometry
<i>m/z</i>	mass to charge ratio
NaPIPES	sodium piperazine- <i>N,N'</i> -bis-(2-ethanesulfonic acid)
NMR	nuclear magnetic resonance
phen green	dipotassium 2-(6-oxido-3-oxo-3 <i>H</i> -9-xanthenyl)-5-[[([1,10]phenanthrolin-5-ylamino)carbothioyl]amino]benzoate
THF	tetrahydrofuran
TLC	thin layer chromatography
Ts	tosyl, <i>p</i> -toluenesulfonyl
Zinquin Acid	2-methyl-8- <i>p</i> -toluenesulfonamido-6-quinolyloxy acetic acid
Zinquin Ester	ethyl(2-methyl-8- <i>p</i> -toluenesulfonamido-6-quinolyloxy)acetate

## Abstract

The adverse health effects of  $Pb^{2+}$  in children has prompted the demand for a fast, sensitive and inexpensive screening method for blood  $Pb^{2+}$  levels. In this regard, an investigation of potential  $Pb^{2+}$  specific fluorescent ligands as probes is reported in this thesis.

A series of flavones were synthesised and their chelation to  $Pb^{2+}$ ,  $Zn^{2+}$ ,  $Al^{3+}$ ,  $Cd^{2+}$ ,  $Ca^{2+}$ ,  $Mg^{2+}$ ,  $Co^{2+}$ ,  $Cu^{2+}$  and  $Ni^{2+}$  was investigated using UV-visible absorption spectroscopy. These qualitative preliminary studies showed that of the flavones studied; 3-hydroxy-2'-methoxyflavone (**4**), 3-hydroxy-4'-methoxyflavone (**5**), 3-hydroxy-2'-methoxythioflavone (**6**) and 3-hydroxy-4'-methoxyflavone (**7**) were the only ligands which coordinated  $Pb^{2+}$ . Other flavones lacking the 3-hydroxy group did not coordinate  $Pb^{2+}$  and were not further studied. Stability constants (using UV-visible absorption spectroscopy) and fluorescence spectra of the  $Pb^{2+}$ ,  $Zn^{2+}$ ,  $Cd^{2+}$  and  $Al^{3+}$  complexes of **4** - **7** were measured under high and low acid concentration conditions. In the presence of a high acid concentration ( $[H^+] = 10^{-2}$  M), ligands **4** and **5** only formed complexes with  $Al^{3+}$  and  $Pb^{2+}$ . Fluorescent studies showed that the  $Al^{3+}$  complexes of **4** and **5** were highly fluorescent while the  $Pb^{2+}$  complexes of **4** and **5** were weakly fluorescent (of equal fluorescence to the free ligands) making **4** and **5** suitable as  $Al^{3+}$  fluorescent probes under these conditions. Under a low acid concentration of  $[H^+] = 10^{-5}$  M, ligands **4** and **5** coordinated all of the metal ions studied producing a relative stability order of  $Pb^{2+} > Al^{3+} > Zn^{2+} > Cd^{2+}$ . The complexes of **4** and **5** produced moderate to weak fluorescence levels with no selective fluorescence being observed for any particular metal ion.

Stability and fluorescence studies were conducted under the same high and low acid concentration conditions on the  $Pb^{2+}$ ,  $Zn^{2+}$  and  $Cd^{2+}$  complexes of the thioflavones **6** and **7**. Neither ligand coordinated  $Al^{3+}$ . In the presence of a high acid concentration ligand **6** produced a stable, detectable complex only with  $Pb^{2+}$ , whereas under the low acid concentration conditions a relative stability order of  $Pb^{2+} > Zn^{2+} > Cd^{2+}$  was determined. Under both conditions the complexes of **6** were either non-fluorescent or very weakly fluorescent. The stability constants of ligand **7** were not determined due to decomposition of the ligand in the presence of light, however, qualitative fluorescence studies were possible. Ligand **7** selectively produced a moderately fluorescent complex with  $Pb^{2+}$  under high acid



concentrations but moderate to weak fluorescent complexes with  $\text{Pb}^{2+}$ ,  $\text{Zn}^{2+}$  and  $\text{Cd}^{2+}$  under low acid concentrations. Thus, Ligand **7** provides a basis for further development of  $\text{Pb}^{2+}$  fluorescent probes.

A further series of ligands were synthesised consisting of benzopyran-4-one thiazoles (**30** and **31**) and coumarin thiazoles (**32** and **33**). These ligands were assessed for their fluorescence in the presence of  $\text{Pb}^{2+}$ ,  $\text{Al}^{3+}$ ,  $\text{Zn}^{2+}$ ,  $\text{Cd}^{2+}$  and  $\text{Mg}^{2+}$ . The unbound benzopyran-4-one thiazole ligands **30** and **31** produced very weak fluorescence, however, upon complexation with each of the metal ions, a slight enhancement of fluorescence was observed. As this fluorescence enhancement was not significant, these compounds were unsuitable as  $\text{Pb}^{2+}$  fluorescent probes. The coumarin thiazoles (**32** and **33**) exhibited intense fluorescence in the unbound state. The ester ethyl-2-(3-2-oxo-2H-1-benzopyran)-2-thiazole-4-carboxylate (**32**) did not produce any change in fluorescence in the presence of any of the metal ions studied, whereas the fluorescence emission of 2-(3-2-oxo-2H-1-benzopyran)-2-thiazole-4-carboxylic acid (**33**) was partially quenched in the presence of  $\text{Pb}^{2+}$  and the emission spectrum was altered in the presence of  $\text{Al}^{3+}$ . Ligand **33** provides the basis for further development of a  $\text{Pb}^{2+}$  selective fluorescent quenching probe.

$\text{C}_8$ -Substituted quinolines, quinoline-1-oxides and pyridine-1-oxides were also investigated. UV-visible absorption studies indicated that of these compounds only 8-mercaptoquinoline and 1-hydroxypyridine-2-thione coordinated the metal ions ( $\text{Pb}^{2+}$ ,  $\text{Zn}^{2+}$  and  $\text{Cd}^{2+}$ ). As the complexes were found to be highly unstable in solution due to oxidation of the ligand, 8-mercaptoquinoline and 1-hydroxypyridine-2-thione were not further studied.

*"I have not failed 10,000 times,  
I have successfully found 10,000 ways that will not work".*

Thomas A. Edison

# Chapter 1: Introduction

## 1.1 Lead and Heavy Metal Toxicity

Lead is the most abundant of the natural heavy metals. Its physical and chemical characteristics are such that lead is uniquely adapted to many industrial uses.<sup>1</sup> Physically, lead is a durable, easily worked metal that has been used since the second century BC.<sup>1,2</sup> Chemically, it will combine with other elements to form compounds with unique and highly useful properties. In spite of its many beneficial uses, lead and its compounds, which have no known physiological function, are a definite hazard to human health when relatively small quantities are taken into and retained within the body.<sup>1</sup> Although the adverse health effects of lead have been recognised for many centuries, its importance as a potentially hazardous environmental contaminant and pollutant has increased with the industrial production and utilisation of lead.<sup>1</sup> Even with stringent safety precautions being established, plants, animals and humans are exposed to, and are being contaminated with lead.<sup>3</sup>

### 1.1.1 Lead Absorption and Distribution

Lead uptake by humans occurs through three main paths. These include 1) absorption of  $Pb^{2+}$  from the gastrointestinal tract, by way of  $Pb^{2+}$  contaminated food and drink, 2) absorption of airborne particles through the lungs, and 3) absorption of organic  $Pb^{2+}$  through the skin.<sup>3-5</sup> Only small amounts of  $Pb^{2+}$  are absorbed from the gastrointestinal tract due to most  $Pb^{2+}$  compounds being insoluble *in vivo*. Since it is only slowly eliminated from the body,  $Pb^{2+}$  accumulates in a variety of organs and bone.<sup>3</sup> The inhalation of  $Pb^{2+}$  as  $PbCO_3$  and  $PbSO_4$  dust results in accumulation of these compounds in the lungs, which is followed by a gradual deposition of  $Pb^{2+}$  to the blood and bones.<sup>3</sup> Lipid soluble  $Pb^{2+}$  compounds, such as tetraalkyllead, are easily absorbed from the respiratory and gastrointestinal tracts and through the skin with a majority of these compounds accumulating in the brain.<sup>3</sup>

Once absorbed,  $Pb^{2+}$  is distributed amongst blood (3%), soft tissue (up to 5%) and mineralised tissue - bone or teeth (90 - 95%).<sup>6</sup> Of  $Pb^{2+}$  in the blood, most (99%) is associated with red blood cells, with the remaining 1% in plasma available for transport to the tissues.<sup>6</sup> Whilst the half life for  $Pb^{2+}$  in blood is around 28 - 35 days, the half life in soft tissues and in the non-

labile compartment of bone may be more than 25 years.<sup>6</sup> Thus, blood  $Pb^{2+}$  levels are a reflection of a dynamic equilibrium between ongoing exposure, tissue (especially bone) storage and release, and loss through excretion.<sup>6</sup> Lead(II) is excreted from the body mainly by urinary and faecal routes, with somewhat less excretion occurring through sweat and integumentary losses, including skin, hair and nails.<sup>7</sup>

### 1.1.2 The Biological Effects of Lead(II)

Exposure of humans to  $Pb^{2+}$  produces a variety of adverse health effects due to its impact on different organs and systems.<sup>8</sup> It has been well documented that the toxicity of  $Pb^{2+}$  affects the functioning of the blood, kidneys, liver, testes, brain, nervous system and other organs of the body.<sup>3,4,8</sup> The toxicity of  $Pb^{2+}$  is due, in general, to its binding affinity to thiol and phosphate groups of numerous enzymes, proteins, and cell membranes, thus inhibiting or interfering with the functions of these entities.<sup>5</sup> The enzymes affected include acetylcholine esterase, acid phosphatase, ATPase, and carbonic anhydrase.<sup>3</sup> Lead(II) also inhibits the biosynthesis of haem, disturbs globin synthesis, increases premature red cell destruction and is toxic to the central nervous system, especially in children.<sup>3,4</sup> The coordination of  $Pb^{2+}$  to functional groups within cell membranes of testes, kidneys, liver and brain cells leads either to complete breakdown or to reduced functioning of their tissues.<sup>3,4</sup> For instance,  $Pb^{2+}$  inhibits the conversion of glucose to amino acids in brain cells.<sup>5</sup> It affects brain mitochondrial respiration and inhibits adenyl cyclase, the enzyme responsible for producing cyclic AMP which mediates the effects of certain neurotransmitters.<sup>5,9</sup>

Lead(II) has long been recognised to be acutely toxic at high dose exposure. Recent findings indicate that  $Pb^{2+}$  is capable of producing toxic effects in adults and children at exposures far lower than those producing gross clinical symptoms.<sup>7,10</sup> Lead(II) exposures that were considered 'safe' only a decade ago are now recognised to produce subtle toxicity. Such effects are not identifiable through routine clinical observations and as a result these effects demand more sophisticated clinical screening methods and more efficient  $Pb^{2+}$  poisoning treatments.

### 1.1.3 Metal Chelation Therapy

Current methods used in the treatment of  $Pb^{2+}$  poisoning involve the use of various  $Pb^{2+}$  chelating therapy agents to promote urinary clearance.<sup>7</sup> The agents used include the following:

EDTA or CaEDTA,<sup>11</sup> *N*-(2-hydroxyethyl)ethylenediaminetriacetic acid (HEDTA),<sup>12,13</sup> a combination of EDTA and the thiol containing ligand 2,3-dimercapto-1-propanol (BAL), sodium 2,3-dimercapto-1-propanesulfonate (DMPS),<sup>14-16</sup> penicillamine, *N*-(2-mercaptopropionyl)glycine, and 2,3-dimercaptoglycine (Figure 1.1).<sup>17</sup> Often these chelators enhance symptomatology, presumably by redistributing  $\text{Pb}^{2+}$  to soft tissues, and they have been found to be non specific, toxic, or both.<sup>2,3</sup> For example, EDTA strongly complexes essential trace-metal ions in the body, resulting in the removal of these metal ions as well as  $\text{Pb}^{2+}$ .<sup>3</sup>

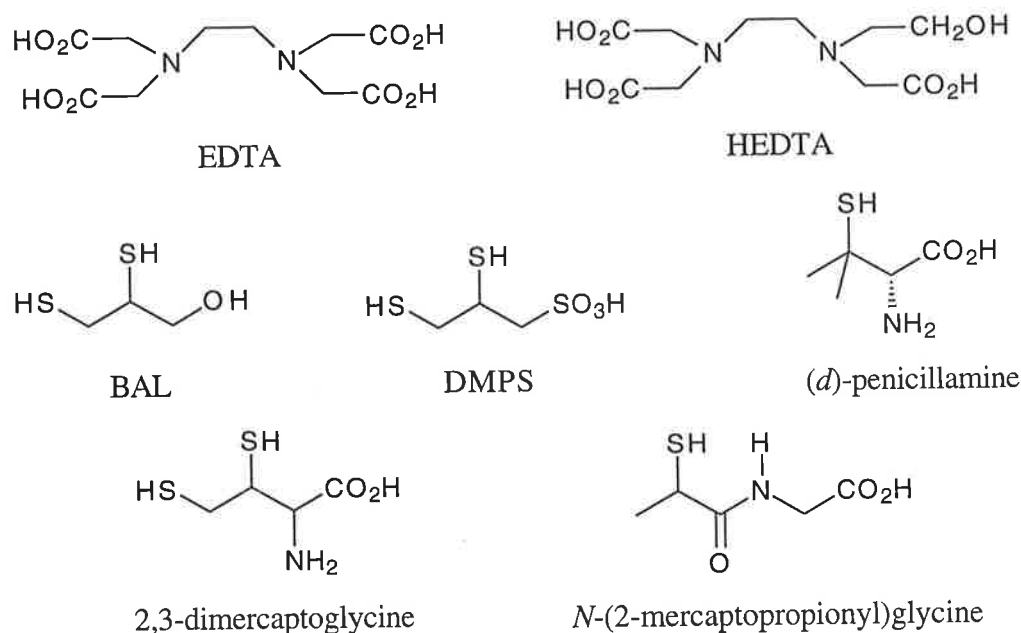
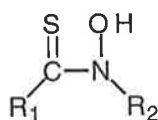


**Figure 1.1**

More recently Raymond *et al* have reported the use of thiohydroxamic acids (Figure 1.2) as  $\text{Pb}^{2+}$  sequestering agents.<sup>3,18</sup> The thiohydroxamic acids form quite stable complexes with  $\text{Pb}^{2+}$ , as indicated by the stability constants of  $\text{Pb}^{2+}$  thiohydroxamate complexes ( $\log \beta_2 = 20.7$  for *N*-phenylthiobenzohydroxamic acid in 70% aqueous dioxane) as compared with that of the  $\text{Pb}^{2+}$  EDTA complex ( $\log \beta_1 = 16.5$ ), and have served as a model for the design of  $\text{Pb}^{2+}$ -chelating agents.<sup>3,18</sup> Although research for highly selective  $\text{Pb}^{2+}$  chelating agents still continues, a non-toxic, highly stable and metal ion specific  $\text{Pb}^{2+}$ -chelating agent has yet to be developed.



Thiohydroxamic acids

**Figure 1.2**

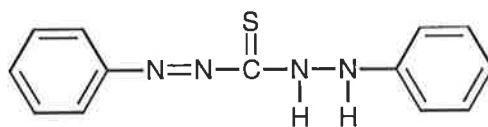
## 1.2 Current Methods of Lead(II) Measurement

For many years the measurement of  $Pb^{2+}$  in whole blood has been the principal biological index of dose, primarily because it has been considered to provide the most practical and accessible estimate of the biologically active part of the body burden of  $Pb^{2+}$ .<sup>7</sup> Hence, blood  $Pb^{2+}$  concentration is the common parameter in the experimental and epidemiological investigation of the toxicological effects of  $Pb^{2+}$ . Furthermore, the collection of blood is relatively simple, harmless and can be performed on large samples of the population. Thus, the blood  $Pb^{2+}$  level is the major criterion on which biological guidelines for population exposure and acceptable limits for occupational exposure are based.<sup>7</sup>

In the analysis of blood  $Pb^{2+}$  levels in humans variations of  $\pm 15\%$  in repeated analyses of the same blood sample is not unusual.<sup>5</sup> Similarly, in inter-laboratory comparisons of the same blood sample the spread of results can be as great. Gross contamination and errors can be introduced at any stage in blood sampling and analysis unless standard precautions are taken. The subjects must be tested in areas reasonably free from  $Pb^{2+}$  contamination which is difficult to find in a lead smelter or an adventitiously contaminated environment. The skin of the subject must be cleansed, the syringe needles must be free from  $Pb^{2+}$  and  $Pb^{2+}$  free collection tubes must be used. Once the sample reaches the laboratory, risk of contamination is low if the analysis is performed by an experienced analyst using a reliable method.<sup>5</sup> Methods commonly used for routine analysis of blood  $Pb^{2+}$  levels include spectrophotometry, flame atomic absorption spectrometry (Flame AAS), furnace AAS and electrochemical methods such as anodic stripping voltammetry (ASV).<sup>5,8</sup>

Spectrophotometric methods for the determination of small amounts of  $Pb^{2+}$  are dominated by a single reagent and a few basic approaches to using it. The dithizone (diphenylthiocarbazone) (Figure 1.3) method has been used for many years.<sup>1</sup> This method has the advantage of a long, well-known history, and it remains the one against which others are judged. Unfortunately, it also suffers from some significant limitations. Dithizone is an intensely coloured compound that non-specifically complexes approximately seventeen metal ions to form chelates that can be extracted into chloroform or carbon tetrachloride.<sup>1</sup> In spite of the large numbers of metal ions that can coordinate, considerable specificity can be gained by careful control of pH and the use

of masking agents. This allows the dithizone method to be used in soil and water samples but unsuccessfully in complex biological systems such as blood.<sup>1</sup> Other disadvantages with the dithizone method are associated with the fact that many steps are required, and numerous reagents must be added. Each step is a potential source of error, and each reagent can be a source of contamination. In biological materials, large samples are required (for example 10 cm<sup>3</sup> of blood) and harmful reagents, such as cyanide, must be used as masking agents.<sup>1</sup>



Dithizone

**Figure 1.3**

Atomic absorption spectroscopy is one of the more generally useful methods for the measurement of Pb<sup>2+</sup> because of its low cost and ease and rapidity of use.<sup>19</sup> Atomic absorption instruments are readily available, relatively inexpensive and simple to operate. Direct flame aspiration gives very rapid analyses that are precise and accurate if appropriate precautions are observed. The method is highly specific and suffers from few interferences. Disadvantages are that the samples must be in solution, and it is usually necessary to destroy organic matter prior to determination making blood analysis difficult.<sup>1</sup>

Prior to the advent of atomic absorption, electrochemical methods, such as ASV, were prime competitors with the dithizone method for determining Pb<sup>2+</sup> at low concentrations.<sup>19</sup> Of these two methods ASV is probably the most sensitive technique for determining Pb<sup>2+</sup> concentrations, and in very low level work the avoidance of contamination is likely to be more of a major problem than the approach of the analytical detection limit.<sup>19</sup> Sensitivity has been enhanced by the use of glassy carbon electrodes.<sup>19</sup> Lead(II) is perhaps an ideal element for many electrochemical determinations as its aqueous complexes are moderately stable.<sup>1</sup> Unfortunately, the organic constituents in many biological and environmental samples act as surface active suppressors which cause large errors using this method.<sup>1</sup>

Despite being well established over many years, the three above mentioned methods used in the determination of blood Pb<sup>2+</sup> levels are not completely satisfactory with each possessing unfavourable aspects. Although blood Pb<sup>2+</sup> is the single most useful index of Pb<sup>2+</sup> exposure

and absorption<sup>5</sup>, a reliable, efficient, inexpensive and accurate method for determining blood  $\text{Pb}^{2+}$  levels at low concentrations has yet to be developed. Therefore, the aim of the research described in this thesis was to develop a sensitive, accurate and inexpensive method for detecting and measuring  $\text{Pb}^{2+}$  concentrations in human blood. The particular method targeted was the use of metal ion, specific fluorescent probes.

### 1.3 Fluorescent Probes

During the last decade, the development of fluorescent indicators (or probes) that selectively respond to biologically important ions has been very successful.<sup>20</sup> These probes have facilitated the measurement of slow and rapid fluxes of ions in single living cells. Fluorescent probes have been described for most of the biologically important ions including  $\text{H}^+$ ,  $\text{Ca}^{2+}$ ,  $\text{Mg}^{2+}$ ,  $\text{Na}^+$ ,  $\text{Cl}^-$  and  $\text{Zn}^{2+}$ .<sup>20-24</sup> The development of a fluorescent probe which is specific for  $\text{Pb}^{2+}$  would be beneficial for monitoring  $\text{Pb}^{2+}$  within cells and therefore could be used as a measure for blood  $\text{Pb}^{2+}$  levels.

For a ligand to be successful as a fluorescent probe for  $\text{Pb}^{2+}$ , certain chemical, physical and structural requirements are necessary. It is obviously essential that the probe must be able to penetrate the cell membrane efficiently but, once inside the cell, be unable to diffuse out. The probe must also be able to function at physiological pH and ionic strength as well as dissolve in aqueous media. More importantly the probe must be specific for  $\text{Pb}^{2+}$  ie. coordinate  $\text{Pb}^{2+}$  in preference to other metal ions. It is also preferable that the probe is non-fluorescent in its uncomplexed state but highly fluorescent on complexation with  $\text{Pb}^{2+}$ . This is to avoid interference from any unbound probe remaining in the sample during measurements.

#### 1.3.1 Zinc(II) and Calcium(II) Fluorescent Probes

One example of a fluorescent probe used to measure  $\text{Zn}^{2+}$  flux within living cells is ethyl (2-methyl-8-*p*-toluenesulfonamido-6-quinolyloxy) acetate, referred to as Zinquin Ester (Figure 1.4).<sup>24,25</sup> On loading Zinquin Ester into cells, cellular esterases hydrolyse the ethyl ester moiety to (the corresponding acid, known as) Zinquin Acid.<sup>26,27</sup> Zinquin Acid then chelates the readily exchangeable  $\text{Zn}^{2+}$  within the cell and, on excitation, an intense fluorescence pattern is observed indicating the presence of exchangeable  $\text{Zn}^{2+}$ .<sup>26,27</sup> Zinquin has been utilised in

many eucaryotic cell systems to determine the role of  $Zn^{2+}$  in life processes such as reproduction and automated cell death (apoptosis).<sup>26,28-31</sup>

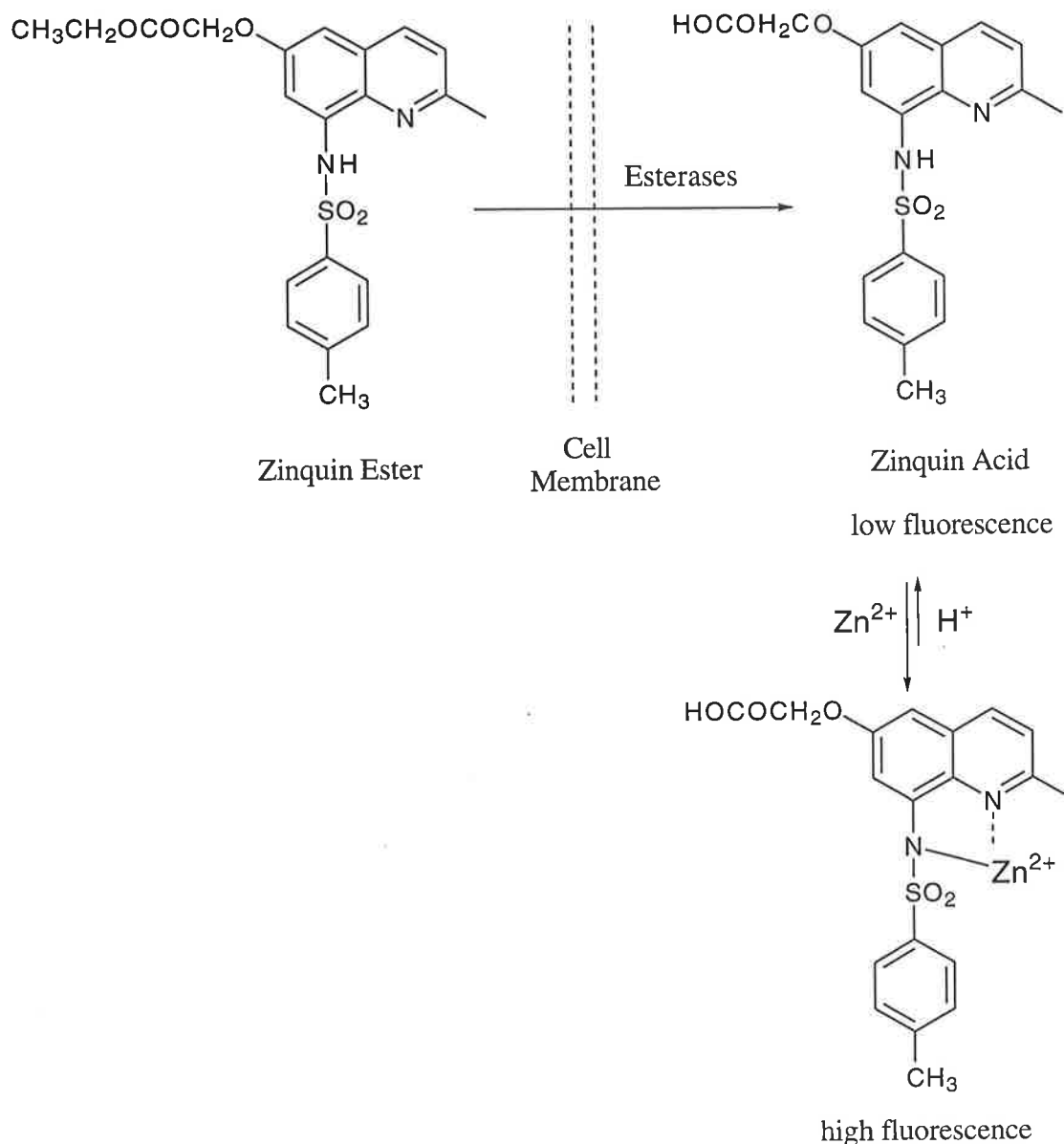
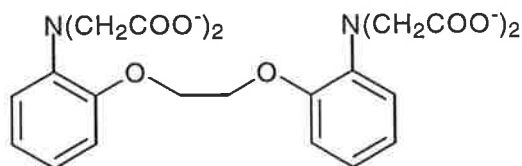


**Figure 1.4**

By far the largest group of fluorescent probes has been that for intracellular  $Ca^{2+}$ .<sup>22,23</sup> Almost all of these probes have been fluorescent derivatives of the chelator BAPTA (1,2-bis(2-aminophenoxy-ethane)- $N,N,N',N'$ -tetraacetic acid) (Figure 1.5) which is an aromatic analogue of the  $Ca^{2+}$  selective chelator ethylene glycol-bis( $\beta$ -aminoethyl ether)- $N,N,N',N'$ -tetraacetic acid (EGTA).<sup>22,23</sup> Advances in techniques for measuring free  $Ca^{2+}$  concentrations, have been essential to the understanding of  $Ca^{2+}$  as an intracellular messenger.<sup>22,23</sup>

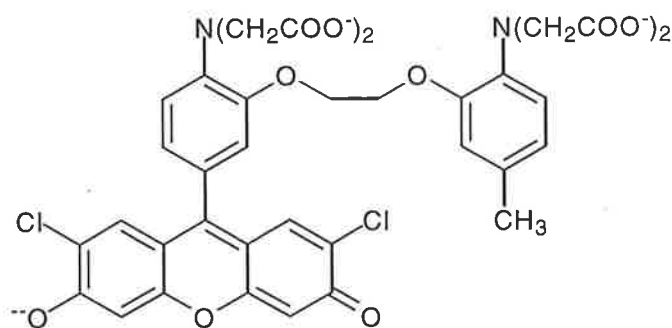




BAPTA

**Figure 1.5**

The most fluorescent of the  $\text{Ca}^{2+}$  fluorescent probes is Fluo-3 (Figure 1.6) which is a BAPTA and fluorescein analogue that has been used in lymphocytes and fibroblasts for biological tests.<sup>22</sup> The  $\text{Ca}^{2+}$  complex of Fluo-3 is 40-fold more fluorescent than the free dye. Although it may produce a high level of fluorescence, the  $\text{Ca}^{2+}$  affinity for Fluo-3 is two to ten fold weaker than those of the other developed  $\text{Ca}^{2+}$  fluorescent probes.<sup>22</sup> Also Fluo-3 has been shown to produce more stable complexes with  $\text{Mn}^{2+}$  and  $\text{Zn}^{2+}$  than for  $\text{Ca}^{2+}$ , the two transition metals known to be able to interact with tetracarboxylate chelators inside cells.<sup>22</sup> Manganese(II) binds to Fluo-3 about 70-fold as strongly as  $\text{Ca}^{2+}$  but interestingly the  $\text{Mn}^{2+}$  complex shows only one-fifth the fluorescence of the  $\text{Ca}^{2+}$  complex.<sup>22</sup> Similarly,  $\text{Zn}^{2+}$  binds to Fluo-3 approximately 300-fold more strongly than  $\text{Ca}^{2+}$ , but the  $\text{Zn}^{2+}$  complex shows only 61% of the fluorescence of the  $\text{Ca}^{2+}$  complex.<sup>22</sup> The significantly greater concentrations of free  $\text{Ca}^{2+}$  as compared with the concentrations of  $\text{Zn}^{2+}$  and  $\text{Mn}^{2+}$  within a cell allow Fluo-3 to be used successfully as a  $\text{Ca}^{2+}$  fluorescent probe.



Fluo-3

**Figure 1.6**

### 1.3.2 Potential Heavy Metal Fluorescent Probes

The high sensitivity and selectivity inherent in fluorescence detection is also of considerable interest for the determination of heavy metal ions in different matrices especially in biological and environmental samples. As only a very few metal ions exhibit a natural luminescence, complexation with suitable ligands is therefore required in most cases.<sup>32</sup> A large number of

fluorescent complexes of 'closed shell' metal ions such as  $Mg^{2+}$ ,  $Ca^{2+}$ ,  $Al^{3+}$ ,  $Ga^{2+}$  and  $In^{2+}$ , are reported in the literature.<sup>21,32</sup> However, most of the transition metal ions have 'open shells' or partially filled  $d$  orbitals. In their complexes, interactions such as intramolecular charge-transfer, paramagnetic influences and heavy atom effects usually lead to fluorescence quenching, even when the free ligands themselves exhibit considerable fluorescence quantum yields.<sup>32</sup>

Although heavy atom quenching may take effect in some systems, examples of CHEF (chelation-enhanced fluorescence) chemosensors for  $Pb^{2+}$  detection have been reported in the literature.<sup>33</sup> Czarnik found that full complexation of  $Pb^{2+}$  to the anthracene thiohydroxamate (1) affords a 13-fold enhancement of fluorescence with the initial fluorescence intensity of (1) being very low (Figure 1.7).<sup>33</sup> It was envisioned that coordination of the less strongly quenching  $Pb^{2+}$  to the strongly quenching thiohydroxamate group might produce a net chelation-enhanced fluorescence (CHEF).<sup>33</sup>

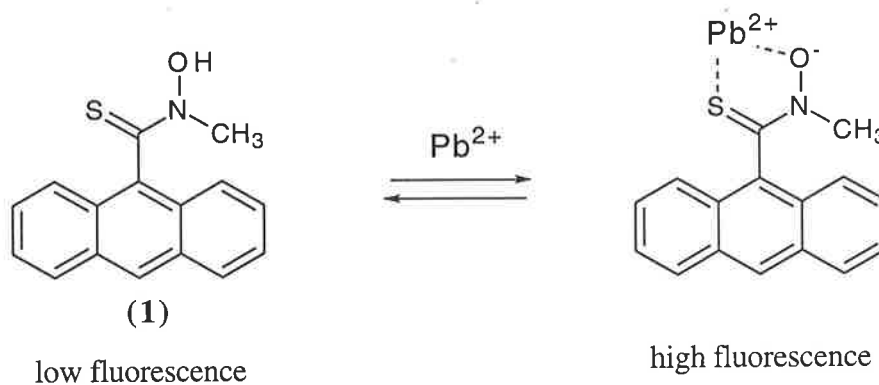
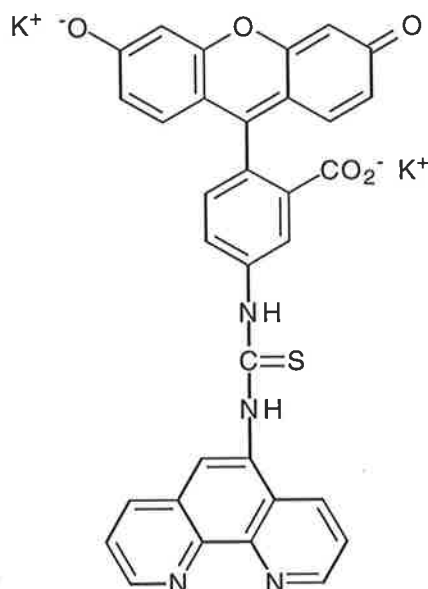


**Figure 1.7**

Other fluorescent heavy metal ion indicators described in the literature take advantage of the quenching heavy metal effect. Phenanthroline-based indicators, such as Phén Green (Figure 1.8), have been used to monitor  $Pb^{2+}$  in micro molar concentrations by measuring the amount of fluorescence quenching.<sup>21</sup> The disadvantage with this technique is that Phén Green is an excellent general-purpose heavy metal sensor capable of detecting a broad range of metal ions, and therefore is non-specific for the metal ion of interest,  $Pb^{2+}$ .<sup>21</sup>

The predominant aim of the research described in this thesis was to develop different fluorescent probes specific for  $Pb^{2+}$ , which could be utilised in detecting and measuring  $Pb^{2+}$  concentrations in biological and water samples. In so doing, it was hoped to produce a series

of probes, whose  $\text{Pb}^{2+}$  complexes had different excitation and emission maxima and a varying range of suitable stability constants. It was thought that from this series, a probe could be selected which had the optimum properties for the measurement of  $\text{Pb}^{2+}$  concentrations in a selected medium.



Phen Green

**Figure 1.8**

### 1.3.3 Fluorescent Probes for Other Metal Ions

Although the main part of this research is concerned with the attempted development of a fluorescent probe specific for  $\text{Pb}^{2+}$ , development of probes specific for other metal ions has also been considered. The use of fluorescent probes for detecting and determining concentrations of a range of metal ions in biological systems is possible, so long as each particular metal ion has a fluorescent probe which binds specifically to that metal ion. Each fluorescent probe developed also needs to meet the conditions outlined previously (Section 1.3, page 6).

There is great interest in developing fast and efficient methods for detecting metal ions which are known to be, or suspected as being, harmful to humans, such as  $\text{Cd}^{2+}$  and  $\text{Al}^{3+}$ . As a secondary aim of this research, investigation into the specificity of any probes developed for metal ions such as these has been undertaken. It was hoped that the data obtained would lead to the development of fluorescent biological probes for metal ions such as  $\text{Cd}^{2+}$  and  $\text{Al}^{3+}$ .

## Chapter 2: Flavones and Thioflavones

### 2.1 Flavones - Background

The study of flavones or flavonoids, which are compounds of plant origin, has given insight into such subjects as the fermentation of tea, the tanning of leather, and the manufacture of cocoa and flavours of foodstuffs.<sup>34,35</sup> Flavonoids are also used as anti-oxidants, with flavonols exhibiting these properties better than other flavones.<sup>35</sup> The  $\alpha,\beta$ -unsaturated ketonic structure of the pyrone ring, the hydroxyl group in the C<sub>3</sub> position and the presence of *o*-dihydroxy groups on ring B are all believed to be responsible for the anti-oxidant activity.<sup>34,35</sup>

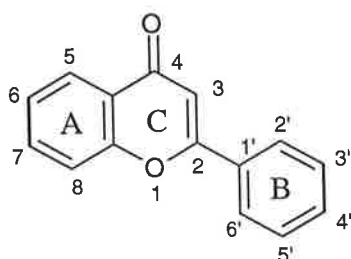
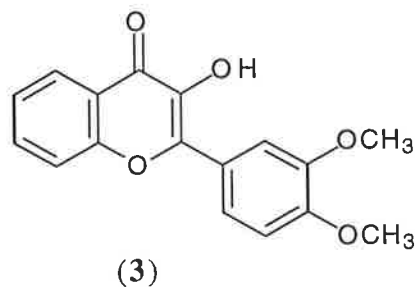
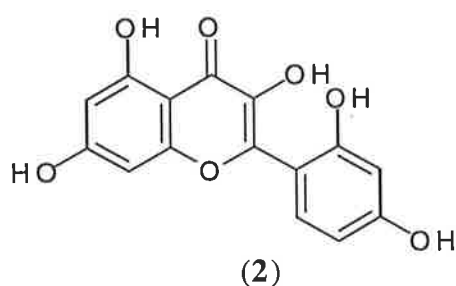


**Figure 2.1:** *The numbering and labelling of flavones.*

The flavonoid nucleus is composed of three rings A, B and C as shown in Figure 2.1. The rings A and B react similarly to those of any aromatic compound, but the reactions of the pyrone ring C are typical of the flavones.<sup>34</sup> Although ring C contains the carbonyl group, flavones do not react with carbonyl reagents such as hydroxylamine, semicarbazide or phenylhydrazine.<sup>34,35</sup> The treatment of flavones with alkaline solutions opens the pyrone ring to yield a 1,3 diketone which may be further degraded.<sup>34,35</sup>

Flavonoids contain a highly conjugated aromatic system and consequently exhibit intense and characteristic absorption spectra.<sup>34,35</sup> Dissociation of the flavonoid or chelation with various reagents causes shifts in the spectra which can give additional information regarding the structure of the flavonoid.<sup>35</sup> Flavonols, such as the 3-hydroxyl and 5-hydroxyl types, can form analytically useful metal ion chelates through the carbonyl group and the 3-hydroxyl or 5-hydroxyl groups.<sup>36</sup> These metal chelates are usually coloured and are suitable for the spectrophotometric determination of the metal ions. Some of them produce characteristic fluorescence and thus the metal ions can be determined fluorimetrically.<sup>36</sup>

Most flavones can be extracted from appropriate plants or synthesised with the majority of the analytically important compounds being commercially available. Amongst them morin (2) is probably the most extensively studied and used for analytical work.<sup>36</sup> Morin is a naturally occurring, poly-oxygenated, flavonol which produces a yellow-green fluorescence in solution on complexation with  $\text{Pb}^{2+}$ .<sup>37</sup> Morin also produces fluorescent species with other metal ions such as  $\text{Sb}^{3+}$ ,  $\text{Mo}^{2+}$ ,  $\text{Mg}^{2+}$ ,  $\text{Zn}^{2+}$ ,  $\text{Ga}^{2+}$ ,  $\text{Cd}^{2+}$ ,  $\text{Be}^{2+}$  and  $\text{Al}^{3+}$ .<sup>37</sup> Therefore, morin is regarded as a non-specific metal binding fluorescent ligand.



Flavones such as 3-hydroxy-3',4'-dimethoxyflavone (3) have also been used to produce new methods for the fluorometric determination of metal ions.<sup>38</sup> One such method measures  $\text{Mg}^{2+}$  concentrations in urine and blood serum using a reagent which contains flavone 3, DMF and a buffer, forming a fluorescent  $\text{Mg}^{2+}$ -flavone 3 complex.<sup>38</sup> The disadvantage with this method is that certain biologically prevalent ions, such as phosphate, interfere with the fluorescence intensity of the metal - ligand complex, and therefore the urine and serum samples must be purified by ion exchange chromatography prior to analysis. Although  $\text{Mg}^{2+}$  is not one of the metal ions targeted in this project, such a precedence illustrates the potential of flavones as metal ion fluorescent probes.

The chelation of  $\text{Pb}^{2+}$  to flavones, such as morin, and the ability of these complexes to form fluorescent species are important factors when designing a fluorescent probe. For these reasons, the flavone chromophore was chosen as a model on which the design of new ligands for use as fluorescent probes was based. By making additions and modifications to the flavone structure, for example by replacement of the heteroatoms in the pyrone ring with other heteroatoms or by adding electron donating substituents to the B ring (to promote fluorescence), a number of compounds were identified which were to be assessed for their ability to perform as  $\text{Pb}^{2+}$  fluorescent probes. Results obtained from such studies would then

give direction into the development of a  $\text{Pb}^{2+}$  specific fluorescent probe for use in aqueous and biological systems.

## 2.2 Synthesis

The potential ligands for  $\text{Pb}^{2+}$  chelation were based upon the structures of 3-hydroxyflavones, 5-hydroxyflavones and flavone type compounds, and are shown in Figure 2.2. Each of the chosen compounds contains an electron donating methoxy substituent on the B ring to promote fluorescence (see Section 2.5.2).

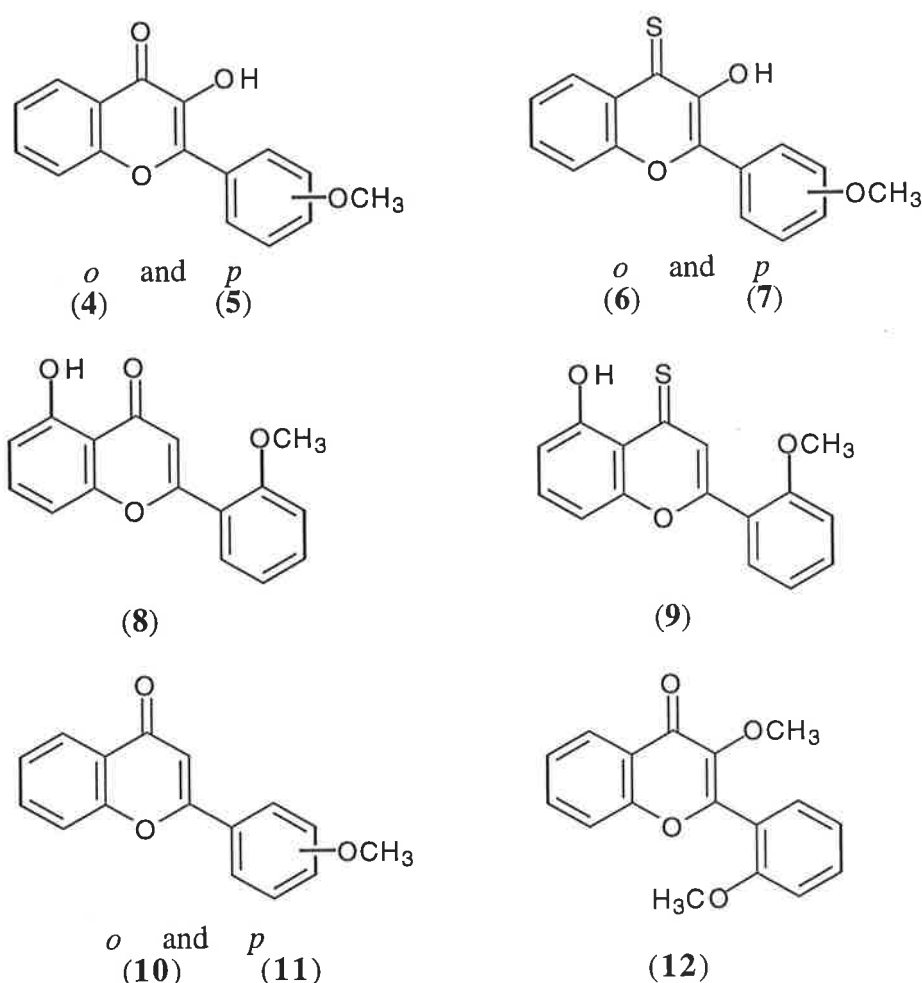


**Figure 2.2**

The flavonols **4** and **5** were chosen as part of the ligand series to determine the effects of the methoxy substituent on the fluorescence intensity and stability of the  $\text{Pb}^{2+}$ -ligand complex. The thioflavone analogues, **6** and **7**, were chosen to enable comparisons to be made between oxygen and sulfur as electron donor atoms, and to increase the 'bite' size of the ligand to further increase the stability and selectivity for  $\text{Pb}^{2+}$  (assuming that coordination occurs between the  $\text{C}_4$  carbonyl and  $\text{C}_3$  hydroxyl group). According to the theory of hard and soft

acids and bases  $Pb^{2+}$  is a soft acid metal ion and should have a greater binding affinity for the soft base sulfur donor atom than for the hard base oxygen donor atom.<sup>39</sup> Typically thiocarbonyl carbon to sulfur bond lengths are longer than the carbonyl carbon to oxygen bond lengths.<sup>40,41</sup> Therefore introducing sulfur atoms and increasing the 'bite' size of the ligand should allow better accommodation of the large  $Pb^{2+}$  cation.

Other suitable targets were those of the 5-hydroxyflavone type such as **8** and **9** as it has been documented that 5-hydroxyflavones as well as 3-hydroxyflavones form complexes with metal ions. 5-Hydroxy-2'-methoxyflavone (**8**) and its thio analogue **9** were chosen to compare the specificity, stability and fluorescence intensity of their complexes with those of the 3-hydroxyflavone ligands (**4** - **7**).

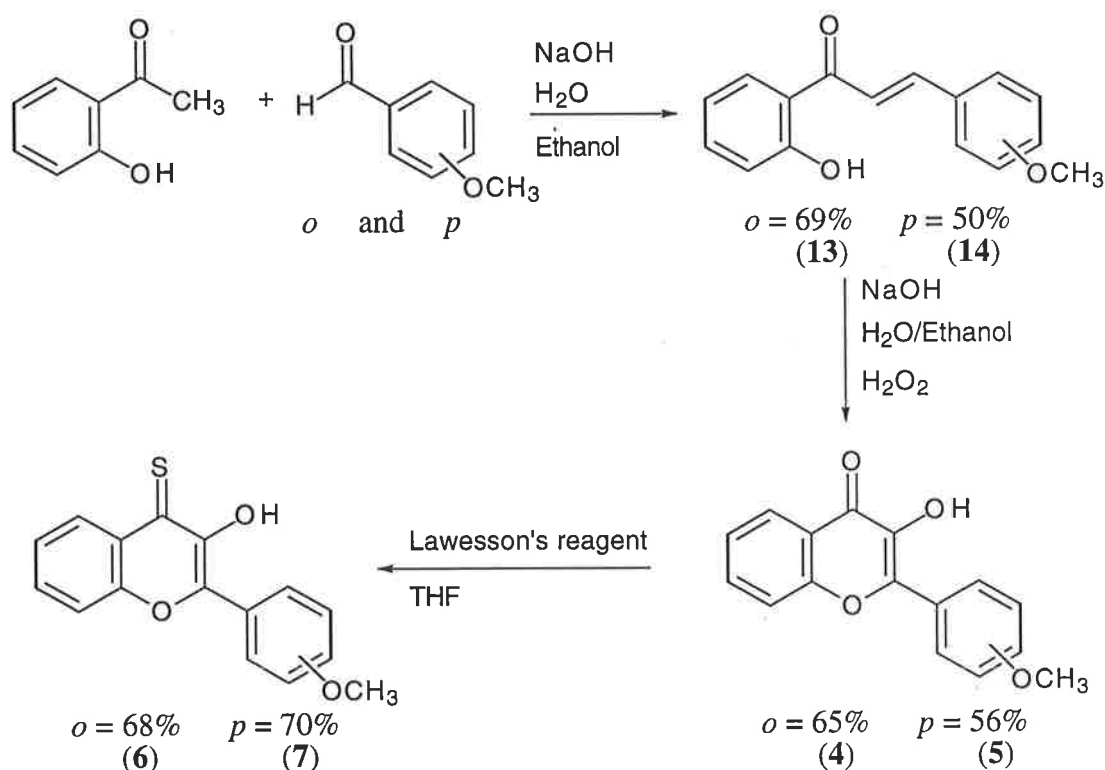
In the interest of determining whether the  $C_3$  hydroxyl group was essential for metal ion coordination, and whether the methoxy substituents on the B ring are metal ion coordinating sites for ligands **4** and **5**, the flavones **10** and **11** were produced. Lack of metal ion coordination to **10** and **11** would suggest that the  $C_4$  carbonyl and the  $C_3$  hydroxyl functional groups are the coordination sites for **4** and **5**.

To further determine whether the hydroxyl group present in 3-hydroxyflavones are necessary for metal ion complexation, the 3-methoxy flavone **12** was produced. This compound contains a methyl group in place of the phenolic hydrogen in compound **4**. No metal ion coordination to **12** would indicate the requirement of a  $C_3$  hydroxy group for complex formation. The relatively small size of the methoxy substituent should not introduce great steric factors into complex stability.

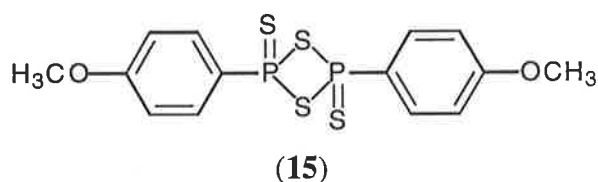
### 2.2.1 Synthesis of the 3-Hydroxyflavone Analogues

To obtain flavones **4** and **5**, the precursor chalcones **13** and **14** were first required. 2-Hydroxyacetophenone and *o*-methoxybenzaldehyde were stirred at room temperature under basic conditions for twenty four hours.<sup>42</sup> After an acidic workup the corresponding chalcone **13** was produced in 69% yield. 2'-Hydroxy-4-methoxychalcone (**14**) was also made (50%) *via* an aldol condensation, using a modified procedure of the above (Scheme 2.1).<sup>43</sup> The chalcones **13** and **14** were cyclised and oxidised to the flavones **4** and **5** using a 32% aqueous

solution of hydrogen peroxide under alkaline conditions followed by an acidic workup (Scheme 2.1).<sup>44</sup>



Thioflavones have been produced in the literature by treatment of flavones with phosphorous pentasulfide in various solvents but never with Lawesson's reagent (**15**).<sup>45-47</sup> Lawesson's reagent (**15**), which converts carbonyls to thiocarbonyls and has previously been used on aldehydes, ketones, amides, carboxylic acids and other types of carbonyls, is produced by a procedure which involves refluxing phosphorous pentasulfide in anisole for six hours.<sup>48</sup> The reagent **15** is very moisture sensitive and must be stored in a dry environment. Treatment of flavones **4** and **5** with Lawesson's reagent (**15**) in dry THF at room temperature produced the required thioflavones **6** and **7** as orange solids in 68% and 70% respectively (Scheme 2.1).

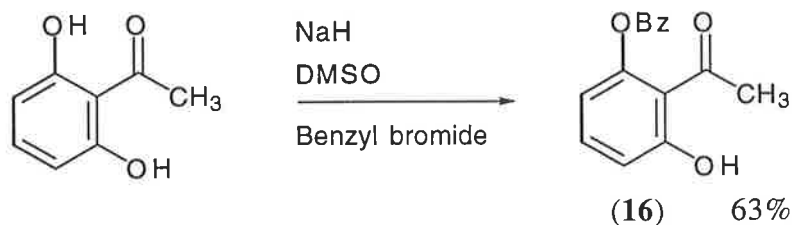


### 2.2.2 Synthesis of the 5-Hydroxyflavone Analogues

In the first attempt to produce 2',6'-dihydroxy-2-methoxychalcone (**17**), 2',6'-dihydroxyacetophenone was stirred with *o*-methoxybenzaldehyde under basic conditions for several days, however a multiple product mixture was obtained. Literature reports on the

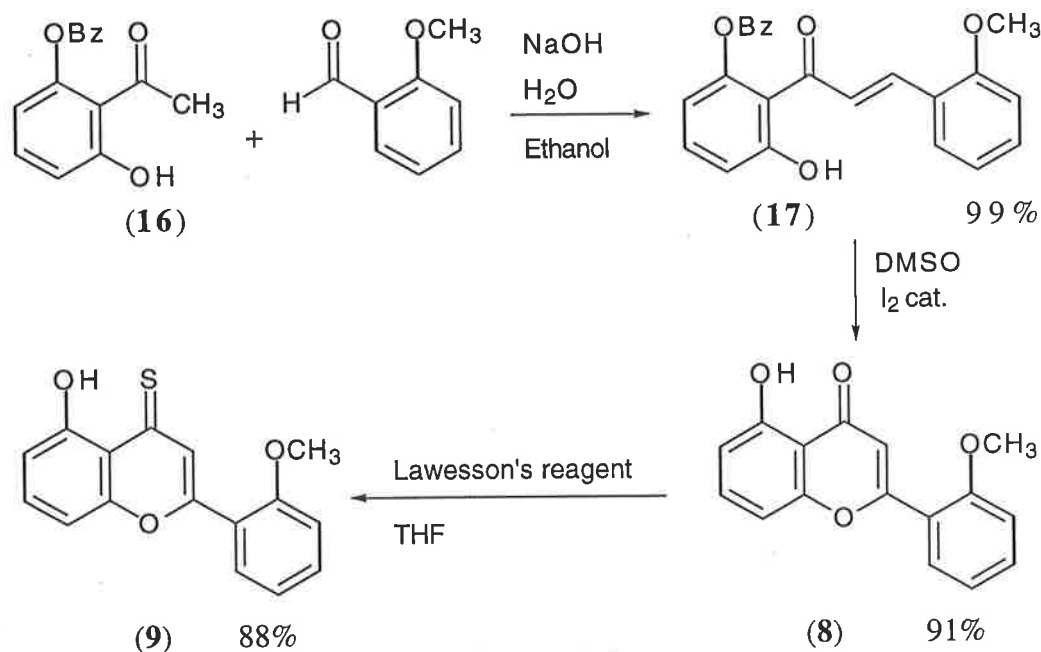


synthesis of 2',6'-dihydroxychalcones are characterised by low yields and the formation of by-products which is often associated with the difficulty of preventing the cyclisation of these reactive compounds to give 5-hydroxyflavanones.<sup>49</sup> To overcome this problem the mono benzyl protected 2',6'-dihydroxyacetophenone derivative **16** was prepared by treating 2',6'-dihydroxyacetophenone with one molar equivalent of sodium hydride in DMSO followed by the addition of one molar equivalent of benzyl bromide.<sup>50</sup> The mono-protected product, **16**, was isolated in 63% yield after flash chromatography (Scheme 2.2).



Compound **16** was stirred with *o*-methoxybenzaldehyde in ethanol with an aqueous potassium hydroxide solution at room temperature for six hours (Scheme 2.3). After work up with dilute hydrochloric acid followed by extraction, the chalcone **17** was obtained as orange crystals in 99% yield. The product, **17**, was identified by its mass spectrum which showed a molecular ion at  $m/z$  360 and another peak at  $m/z$  269 due to the characteristic loss of the benzyl protecting group from the molecular ion. Structure **17** was further supported by the  $^1\text{H}$  NMR spectrum which contained two doublets, one at  $\delta$  7.85 ppm and the other at  $\delta$  8.18 ppm, which correspond to the  $\text{C}_2$  -  $\text{C}_3$  vinylic protons. The 15.7 Hz coupling constant between these protons suggests that **17** was formed as its *trans* isomer.

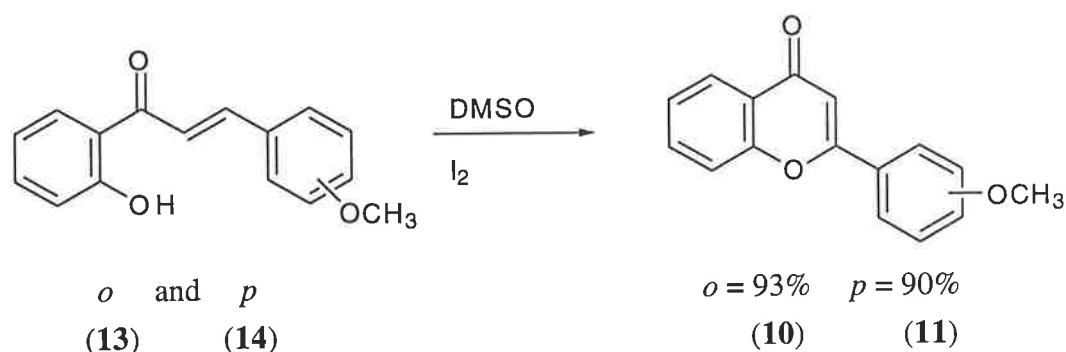
Chalcone **17** was treated with a catalytic amount of iodine in DMSO at reflux, according to a literature procedure to produce the required 5-hydroxyflavone **8** (Scheme 2.3).<sup>51</sup> The outcome was two fold in that the chalcone had cyclised to the flavone as required but also the benzyl protecting group was fortuitously removed. The 5-debenzylation is most likely due to the action of hydrogen iodide, formed in catalytic amounts during the cyclisation steps, reacting with the benzyloxy group to form benzyl iodide, which after being oxidised by DMSO to benzaldehyde, generates more hydrogen iodide molecules to continue the debenzylation process.<sup>51</sup> The result of this reaction was the required 5-hydroxyflavone, **8**.



The 5-hydroxythioflavone **9** was made from **8** using Lawesson's reagent (**15**) as previously described for the thioflavones **6** and **7** (Scheme 2.3). After purification using flash chromatography, compound **9** was isolated in 88% yield. The product **9** was identified by its mass spectrum with a molecular ion at  $m/z$  284 and another peak at  $m/z$  253 as a result of the loss of the methoxy group from the molecular ion. The structure was further supported by microanalytical and NMR data.

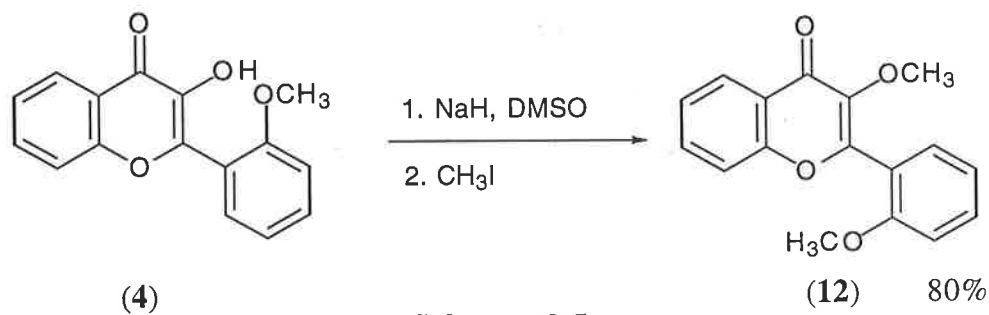
### 2.2.3 Synthesis of the Flavone Analogues

Flavones **10** and **11** were prepared in yields of 90 and 93% respectively by heating the chalcones **13** and **14** for three hours in refluxing DMSO with a catalytic amount of iodine (Scheme 2.4).<sup>52</sup>



Methylation of flavone **4** by treatment with sodium hydride and DMSO followed by the addition of iodomethane produced flavone **12** within one hour in 88% yield (Scheme 2.5).

The  $^1\text{H}$  NMR of the product showed singlets at  $\delta$  3.82 ppm and  $\delta$  3.85 ppm for the two methyl ether protons.



**Scheme 2.5**

### 2.3 Specificity

One of the essential requirements for a ligand to be a suitable  $\text{Pb}^{2+}$  fluorescent probe in either aqueous or biological samples is that the ligand should be specific for  $\text{Pb}^{2+}$ , that is, the ligand should discriminate between  $\text{Pb}^{2+}$  and other metal ions in a particular system. The means by which a potential ligand can discriminate between metal ions, within the confines of the project's objectives, is either through metal-ligand coordination or fluorescence. A specific ligand should have a higher complexation affinity for  $\text{Pb}^{2+}$  than for other metal ions, or ideally coordinate  $\text{Pb}^{2+}$  only. Although selective coordination of a ligand with  $\text{Pb}^{2+}$  is the preferred scenario, methods such as selective metal chelation-enhanced fluorescence (CHEF) or selective fluorescence quenching can also allow discrimination between metal ions. If a ligand's fluorescence emission is strongly modified by metal-ligand interaction with  $\text{Pb}^{2+}$  alone then  $\text{Pb}^{2+}$  discrimination has been accomplished. Therefore, whether a ligand will be selective for  $\text{Pb}^{2+}$  depends on the electronic and physical interactions between the studied ligand and the other competitor metal ions present in the particular system studied.

Since a ligand needs to be specific for  $\text{Pb}^{2+}$  to act as a suitable  $\text{Pb}^{2+}$  probe, the complexing ability and electronic effects on coordination with a series of metal ions needs to be assessed as a measure of selectivity. To investigate these properties with the potential flavone ligands (4 - 12), a series of possible competitor metal ions were studied. The series consisted of the following nine metal cations,  $\text{Pb}^{2+}$ ,  $\text{Cd}^{2+}$ ,  $\text{Zn}^{2+}$ ,  $\text{Al}^{3+}$ ,  $\text{Co}^{2+}$ ,  $\text{Ni}^{2+}$ ,  $\text{Cu}^{2+}$ ,  $\text{Ca}^{2+}$  and  $\text{Mg}^{2+}$ .

The metal ions  $\text{Zn}^{2+}$  and  $\text{Ca}^{2+}$  were chosen because of their prevalence in biological systems. Zinc(II) is an essential trace element in biological systems and is required in all phases of the

metabolic life cycle of a cell.<sup>53</sup> One of the reasons why  $Zn^{2+}$  is widely found in biological systems is because it is a borderline hard Lewis acid, which can act to polarise a bond making it more susceptible to reaction.<sup>54</sup> Zinc(II) can consequently form tightly coordinated complexes with donor atoms nitrogen, sulfur and oxygen on various proteins and metalloenzymes in the cell. The majority of the total concentration of  $Zn^{2+}$  within a cell is mainly in the cytoplasm of cells, ranging in concentration from  $10^{-9}$  M to  $10^{-3}$  M.<sup>25</sup> Calcium(II) as well as  $Zn^{2+}$  can be found in relatively high concentrations in the cytoplasm of cells, and can therefore interfere in  $Pb^{2+}$  determination in biological samples. Furthermore the chemical similarity between  $Pb^{2+}$  and  $Ca^{2+}$  in relation to their ionic radii (for a coordination number of 6,  $Ca^{2+} = 1.00 \text{ \AA}$  and  $Pb^{2+} = 1.19 \text{ \AA}$ )<sup>55</sup> and stable 2+ oxidation states may explain the alteration in the functioning of calcium-dependent systems due to  $Pb^{2+}$  contamination.<sup>7</sup>

Both  $Cd^{2+}$  and  $Al^{3+}$ , in relatively high doses, have detrimental effects on human health.<sup>7</sup> Cadmium(II) is considered to be non essential to humans while  $Al^{3+}$  is not classified as an essential trace element, but has been difficult to prove as non essential because of the high  $Al^{3+}$  concentration in the earth's crust.<sup>7</sup> Despite recent interest in the possible link between Alzheimer's disease and  $Al^{3+}$ , and the biotoxicity of  $Cd^{2+}$ , there is still considerable difficulty in measuring  $Al^{3+}$  and  $Cd^{2+}$  ion concentrations in biological and aqueous samples. Therefore, there is also an interest in developing fluorescent probes for these metal ions as well as  $Pb^{2+}$ .

The remaining ions,  $Co^{2+}$ ,  $Ni^{2+}$ ,  $Mg^{2+}$  and  $Cu^{2+}$ , were chosen because they are classified as trace elements in biological systems.<sup>7,53</sup>

### 2.3.1 UV-visible Absorption Spectroscopy

The method chosen to investigate whether complex formation of the series of metal ions occurred with the ligands **4 - 12** was UV-visible absorption spectroscopy. UV-visible absorption spectroscopy is a sensitive technique that produces absorption spectra for most organic compounds and many inorganic ions and complexes.<sup>56</sup> This technique involves the absorption of UV or visible light by a molecule when it encounters a photon of a discrete energy,  $E$ , and results in an increase in the energy of the electrons or atoms in the molecule.<sup>56</sup> This photon's energy,  $E$ , is related to the frequency,  $\nu$ , and wavelength,  $\lambda$ , of the radiation by;

$$E = h\nu = hc/\lambda \quad (\text{eqn 2.1})$$

This photonic energy absorption results in the promotion of one of the bonding electrons from a ground state energy level into one of higher energy. A plot of this absorption against wavelength is called an absorption spectrum which has a specific shape that is characteristic of a particular compound.<sup>56</sup>

The relationship of the absorption spectra of organic compounds to their structure has been extensively studied and is well understood. Current explanations of absorption spectra are based on the assignment of the spectral bands to the excitations of different electronic environments. The three main types of environments experienced by electrons in organic compounds are,  $\sigma$ -covalent bonds,  $\pi$ -bonds in double and triple bonds, and non-bonding orbitals associated with hetero atoms such as nitrogen and oxygen.<sup>56</sup>

Two main factors that effect the separation of the electronic energy levels of a compound are the presence of substituents on the molecule and the polarity of the solvent in which the molecule is dissolved. Since these factors effect the electronic energy levels of a molecule, they also produce a marked effect on the UV-visible spectrum of the molecule. Those which reduce the number or delocalisation of  $\pi$  or  $n$  electrons tend to increase the energy differences between the ground and excited electronic states of the molecule. Hence the molecule will absorb photons of higher energy and the absorption maxima of the compound will shift to shorter wavelengths. Such a displacement is referred to as a hypsochromic or blue shift. On the other hand, if the number or delocalisation of  $\pi$  and  $n$  electrons is increased, the energy differences between a molecules's ground and excited electronic states are reduced. In this case the molecule will absorb photons of lower energy and the absorption maxima of the molecule will be shifted to longer wavelengths. This is known as a bathochromic or red shift. Thus, the absorption spectrum of a class of molecules is very dependent on the nature of the substituents and their effects on the conjugation.

### 2.3.2 Detecting Complex Formation

When a metal ion coordinates to a ligand, a redistribution of the electron density of the ligand will occur between the ligand and the metal ion, and consequently the ligand may undergo a conformational change or adopt a new geometrical arrangement. Such coordination affects the energy differences between the ground and excited electronic states of the ligand, and provided

the metal coordination affects the separation of the ligand's chromophoric electronic energy levels, a change or shift in the ligand's absorption spectrum should be observed. Therefore, it is possible to determine whether a complex is formed between a ligand and a metal ion by comparing UV-visible absorption spectra of the ligand in the absence and presence of the metal ion.

Previous UV-visible spectrophotometric studies have shown that some flavones coordinate metal ions.<sup>34,36,57</sup> The extensive conjugation and UV-visible light absorption properties of the flavones **4 - 12** allow this method to be used in the complexation studies of the selected metal ions. The absorption spectrum of each of the synthesised flavones (**4 - 12**) was measured in the presence of each metal ion of the chosen series. An intensity change (hyperchromic or hypochromic effect) or a shift (bathochromic or hypsochromic) in the absorption spectrum of the uncomplexed flavone by comparison with that observed in the presence of the metal ion indicated complexation.

### 2.3.3 Conditions for Complex Determination

Whether the flavones **4 - 12** will complex the listed series of metal ions in solution depends on a variety of factors including the pH, solvent polarity and the ionic strength of the solution. These factors must remain constant with each free ligand and metal-ligand solution measured to allow consistent comparisons to be made between each metal ion studied. Since the predominant aim of this research was to develop a fluorescent probe to detect the concentration of  $Pb^{2+}$  in human cells, it was preferable to simulate the conditions of a biological cell as closely as possible. Ideally, the conditions require a pH of approximately 7 and an ionic strength of 0.1 in a 100% aqueous medium.

To select a set of standard conditions in which to measure metal-ligand complexation, firstly the solvent or medium in which the UV-visible absorption spectra were to be determined was established. Although using a 100% aqueous solvent system was the ideal, the flavone ligands **4 - 12** were not soluble in water. To overcome this problem a solvent system containing water and DMF was chosen. DMF is a very polar, water miscible organic solvent in which the studied ligands (**4 - 12**) are soluble. A solution made up of 75% DMF and 25% water was the solvent system found to contain the highest percentage of water in which the

flavone ligands were soluble. This solvent system was used to prepare all sample solutions used in the UV-visible absorption spectroscopy measurements. The next stage required the establishment of a set ionic strength and pH conditions standardised for the complete study.

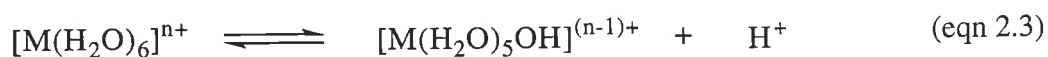
Besides replicating physiological conditions, the ionic strength of the solution  $I$ , [which is defined as half the sum of the molarity,  $m$ , of each ionic species in solution, multiplied by the square of their ionic charge,  $z$  (eqn 2.2)], must remain constant so that no significant activity coefficient variations occur upon the addition of metal ion solutions to ligand solutions.<sup>58</sup> This is achieved when an inert electrolyte is present in a solution at a much higher concentration than all other ionic species in solution. Therefore the ionic strength of the solution is predominantly based on the contribution of the more highly concentrated species, with little effect being made by all other dilute species present. Thus, it can be stated that the ionic strength of the solution is controlled by the inert electrolyte.<sup>59</sup>

$$I = 1/2 \sum m z^2 \quad (\text{eqn 2.2})$$

The most suitable inert electrolyte to be used in the detection of complex formation between the flavones and the series of metal ions is one that dissolves readily in the medium that is being measured, does not coordinate with any of the flavones or interact with the metal ions studied, and does not absorb UV-visible light in the region of the flavone absorptions. Accordingly, sodium perchlorate was chosen. Previous UV-visible absorption and fluorescence experiments performed on flavone complexes (similar to the complexes of ligands **4** - **12**) used sodium ions in their solutions in the form of sodium acetate buffers with no interference being observed.<sup>57,60</sup> The perchlorate salt was used because the perchlorate ion,  $\text{ClO}_4^-$ , does not form strong associations with metal ions in solution.<sup>59</sup> Therefore, the metal ions considered in this study interacted with the flavone ligands without competition from the perchlorate ions present. The perchlorate salts are also readily soluble in a number of organic solvents as well as aqueous media. Because of these favourable qualities, the studied metal ions were used as metal perchlorates and sodium perchlorate was chosen as the electrolyte to control the ionic strength of ligand and metal ion-ligand solutions.

To maintain a constant pH of approximately 7 (to mimic cellular conditions) a buffer NaPIPES [sodium piperazine-*N,N'*-bis-(ethanesulfonic acid)] was added to each of the studied

solutions. To ensure the buffer did not interfere in the absorption measurements of the metal-ligand complexes, NaPIPES was used at a concentration of  $1.0 \times 10^{-3}$  M in both the reference and sample UV-visible cells. However, the buffer caused precipitation of metal hydroxides in the solutions containing the metal ions  $\text{Al}^{3+}$ ,  $\text{Cu}^{2+}$  and  $\text{Pb}^{2+}$  (eqn 2.3).<sup>61</sup> These metal ions produce highly acidic hydrated species in aqueous media, and as the buffer counteracts the production of acid more of the insoluble metal hydroxide is formed (eqn 2.3). To avoid the interference of these precipitates in the UV-visible absorption measurements the solutions containing these metal ions were filtered prior to analysis. Although the total concentrations of these metal ion solutions were consequently not accurately known, the metal ion concentrations were still in great excess of the ligand concentration and hence conditions within these solutions were favourable to complexation. Thus, it was still possible to observe coordination of the ions  $\text{Al}^{3+}$ ,  $\text{Cu}^{2+}$  or  $\text{Pb}^{2+}$  with the ligands **4 - 12** and to make qualitative comparisons from the spectra obtained.



To determine accurately the absorption maxima and intensity from a UV-visible spectrum of an organic or inorganic compound, the concentration of the measured species should be such that the absorption maxima occurs between the absorption range 0.3 and 1.5.<sup>56</sup> For the absorption maxima of the ligands **4 - 12** to lie within this range a concentration of  $4.0 \times 10^{-5}$  M was required. To ensure substantial complex formation, the studied metal ions were present in the sample solutions at a 200 fold concentration excess to that of the flavone ligands **4 - 12** (ligand:metal ion ratio of 1:200). This ligand to metal ion ratio was used for each of the sample solutions containing the flavone ligands **4 - 12**. The concentration of the metal ions in the sample solutions was  $8.0 \times 10^{-3}$  M as made up, but the precipitation mentioned above decreased this to a small extent for  $\text{Pb}^{2+}$ ,  $\text{Al}^{3+}$  and  $\text{Cu}^{2+}$ .

The UV-visible absorption spectra of the flavones **4 - 12** were recorded at a thermostatted temperature of 298.2 K under the previously described conditions which have been summarised in Table 2.1. A comparison of the spectra measured of each ligand in the absence and presence of the metal ions was then made to determine which metal ions coordinated to the ligands **4 - 12**. A shift in the absorption maxima wavelengths of the tested ligands of greater



than 5 nm was taken as indicating that significant coordination had occurred between the ligand and metal ion.

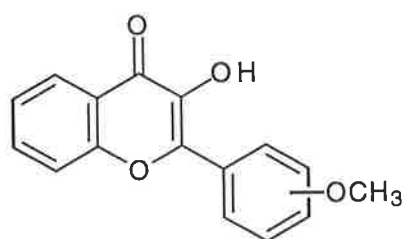
**Table 2.1:** A summary of the conditions used to measure the UV-visible spectra of ligands 4 - 12 in the presence of the listed metal ions.

Ligands	4 - 12
Metal ions	Pb <sup>2+</sup> , Zn <sup>2+</sup> , Ca <sup>2+</sup> , Al <sup>3+</sup> , Cd <sup>2+</sup> , Ni <sup>2+</sup> , Cu <sup>2+</sup> , Co <sup>2+</sup> , Mg <sup>2+</sup>
Solvent	25% H <sub>2</sub> O/75% DMF
Ionic strength	0.1
pH	Approximately 7 *
[Ligand]	4.0 x 10 <sup>-5</sup> M
[Metal ion]	8.0 x 10 <sup>-3</sup> M *

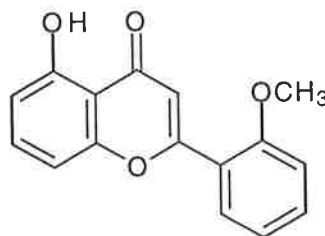
\* Variable value in the solutions containing Pb<sup>2+</sup>, Al<sup>3+</sup> or Cu<sup>2+</sup>.

### 2.3.4 Determination of Metal ion-Flavone Complexation

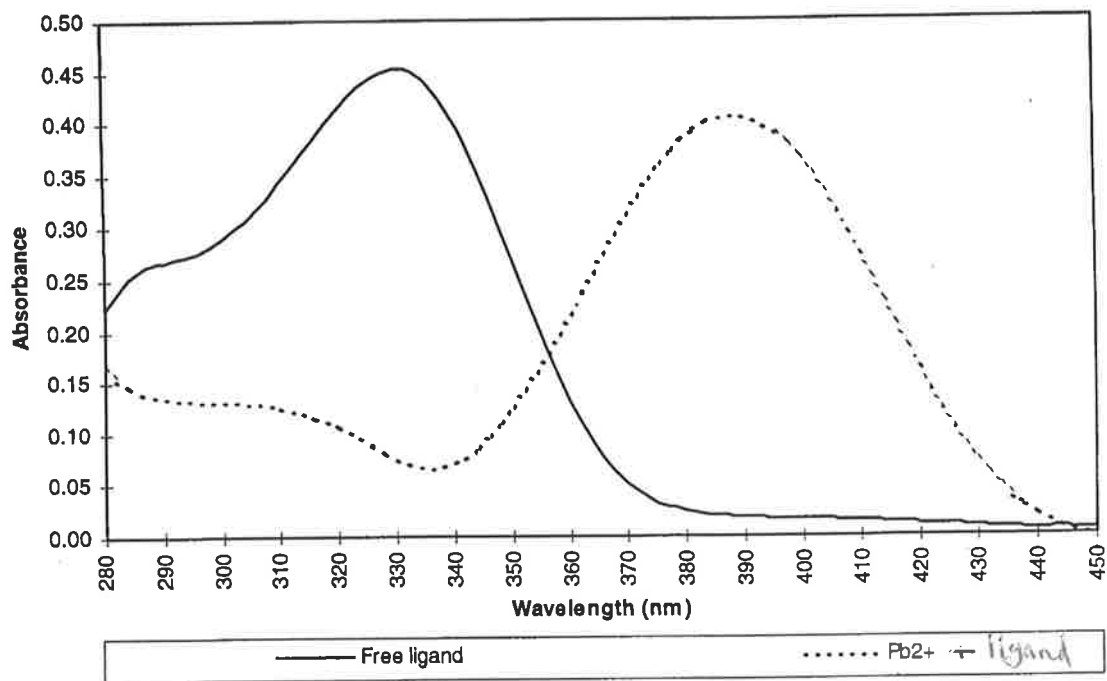
The first three ligands chosen for investigation into their coordinating properties with Pb<sup>2+</sup> were the geometric isomers 3-hydroxy-2'-methoxyflavone (**4**), 3-hydroxy-4'-methoxyflavone (**5**) and 5-hydroxy-2'-methoxyflavone (**8**). The UV-visible spectra of these ligands were determined in the absence and presence of Pb<sup>2+</sup> using the method described in section 6.7 and are presented in the Figures 2.3 - 2.5. The spectra were measured between the wavelength range 280 - 450 nm for the ligands **4** and **8** and 280 - 500 nm for ligand **5**.



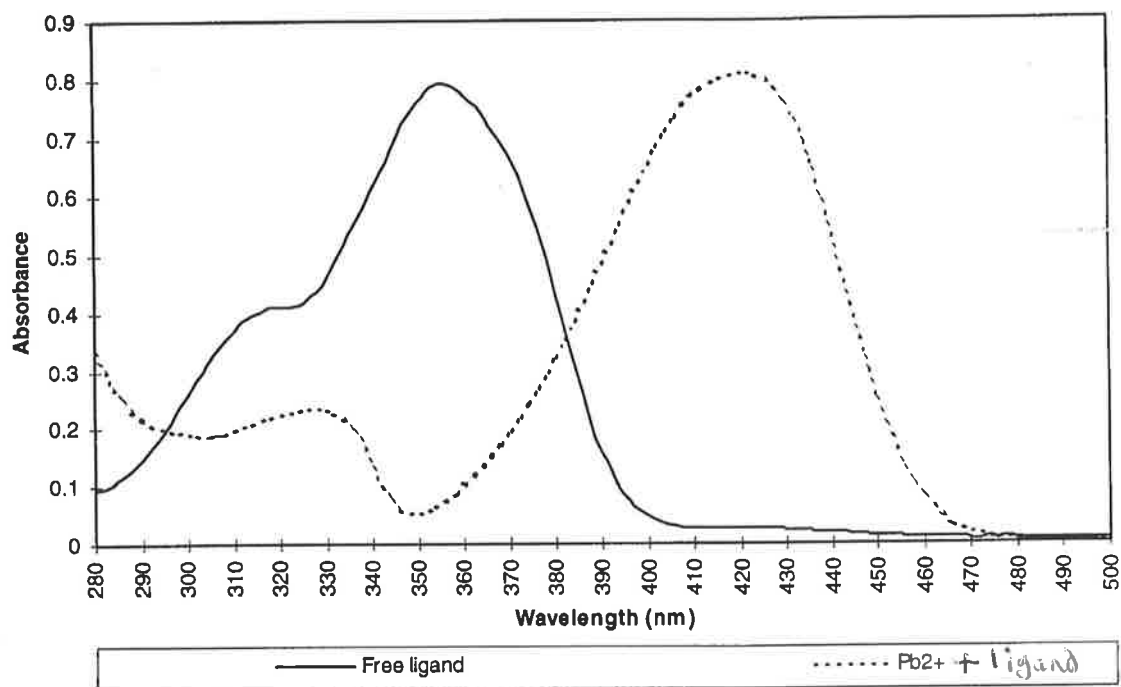
*o* and *p*  
(4) (5)



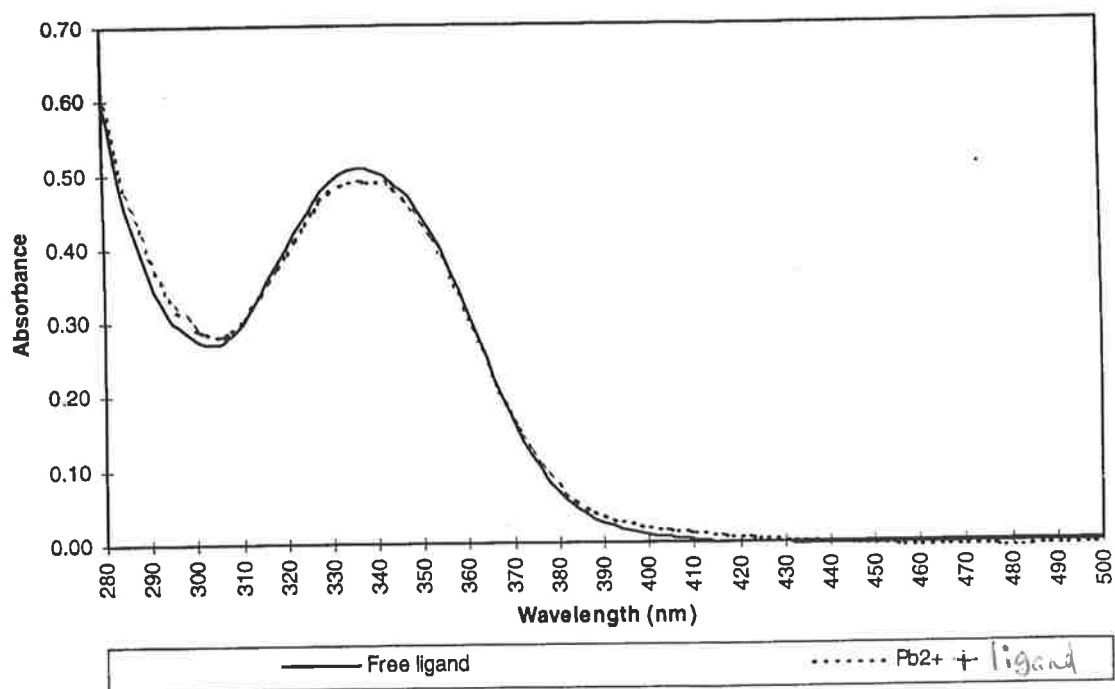
(8)



**Figure 2.3:** A comparison of the UV-visible absorption spectrum of 3-hydroxy-2'-methoxyflavone (4) in the absence and presence of  $Pb^{2+}$ . The solid line represents the spectrum of 4 alone, and the broken line represents the spectrum of 4 in the presence of  $Pb^{2+}$ .



**Figure 2.4:** A comparison of the UV-visible absorption spectrum of 3-hydroxy-4'-methoxyflavone (5) in the absence and presence of  $Pb^{2+}$ . The solid line represents the spectrum of 5 alone, and the broken line represents the spectrum of 4 in the presence of  $Pb^{2+}$ .

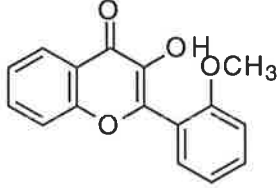
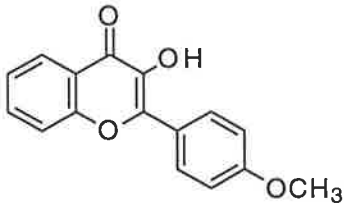
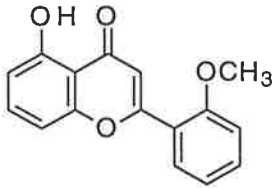


**Figure 2.5:** A comparison of the UV-visible absorption spectrum of 5-hydroxy-2'-methoxyflavone (**8**) in the absence and presence of  $\text{Pb}^{2+}$ . The solid line represents the spectrum of **5** alone, and the broken line represents the spectrum of **4** in the presence of  $\text{Pb}^{2+}$ .

The absorption spectra of the ligands alone as compared to the ligands in the presence of excess  $\text{Pb}^{2+}$  resulted in bathochromic shifts of 59 nm and 65 nm for the ligands **4** and **5** respectively and no change for ligand **8**. It was apparent that ligands **4** and **5** were coordinating to  $\text{Pb}^{2+}$  and ligand **8** was not. To investigate further the metal ion selectivity of these ligands, the change in absorption spectra of the other eight metal ions in the series with the ligands **4**, **5** and **8** were recorded and are presented in Appendix A (Figures A.1.1, A.1.2 and A.1.3). The UV-visible absorption maxima of the ligands and their metal complexes are listed in Table 2.2.

As can be seen from Table 2.2, the wavelength values at which the absorption maximum of ligand **4** occurred, were shifted to longer wavelengths when any one of  $\text{Pb}^{2+}$ ,  $\text{Co}^{2+}$ ,  $\text{Ni}^{2+}$ ,  $\text{Cu}^{2+}$ ,  $\text{Al}^{3+}$ ,  $\text{Cd}^{2+}$ ,  $\text{Zn}^{2+}$  were added to a solution of **4**, signifying coordination of these metal ions. No shift in the ultraviolet absorption maximum of **4** was observed when  $\text{Ca}^{2+}$  was added, and a slight absorbance increase around 390 nm was observed when  $\text{Mg}^{2+}$  was added to a solution of **4**. These observations indicate no coordination between  $\text{Ca}^{2+}$  and the ligand, but a weak coordination between  $\text{Mg}^{2+}$  and **4**.

**Table 2.2:** UV-visible absorption maxima of the flavones (4, 5, 8) and their metal complexes.

Ligand	Metal Ion	Absorption Maxima <sup>a</sup> (nm)
 <p>3-Hydroxy-2'-methoxyflavone (4)<sup>b</sup></p>	Pb <sup>2+</sup> Co <sup>2+</sup> Ni <sup>2+</sup> Cu <sup>2+</sup> Al <sup>3+</sup> Ca <sup>2+</sup> Mg <sup>2+</sup> Cd <sup>2+</sup> Zn <sup>2+</sup>	330  389 400 405 398 386 330 330 396 390
 <p>3-Hydroxy-4'-methoxyflavone (5)<sup>c</sup></p>	Pb <sup>2+</sup> Co <sup>2+</sup> Ni <sup>2+</sup> Cu <sup>2+</sup> Al <sup>3+</sup> Ca <sup>2+</sup> Mg <sup>2+</sup> Cd <sup>2+</sup> Zn <sup>2+</sup>	356  421 429 437 432 421 356 356;429 428 422
 <p>5-Hydroxy-2'-methoxyflavone (8)<sup>b</sup></p>	Pb <sup>2+</sup> Co <sup>2+</sup> Ni <sup>2+</sup> Cu <sup>2+</sup> Al <sup>3+</sup> Ca <sup>2+</sup> Mg <sup>2+</sup> Cd <sup>2+</sup> Zn <sup>2+</sup>	336  336 322 315;403 332;405 338 337 334 337 333

<sup>a</sup> Errors in the absorption maxima values are  $\pm 1$  nm

<sup>b</sup> Measured between wavelengths 280 - 450 nm

<sup>c</sup> Measured between wavelengths 280 - 500 nm

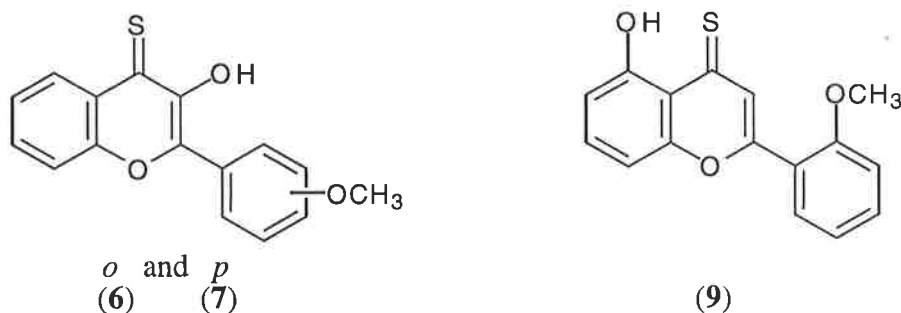
Ligand 5, which varies in structure from ligand 4 only by the position of the methoxy substituent on the B ring of the flavone, complexed the same metal ions as 4 as expected. It

was assumed that the substituents on the B ring of the flavones **4** and **5** did not contribute to the coordination of metal ions. The most significant differences between the absorption spectra of **4** and **5** and their metal complexes are the wavelengths at which the absorption maxima occur.

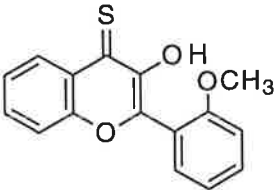


The 5-hydroxyflavone **8**, which did not coordinate  $\text{Pb}^{2+}$ , coordinated  $\text{Co}^{2+}$ ,  $\text{Ni}^{2+}$ ,  $\text{Cu}^{2+}$ ,  $\text{Al}^{3+}$ ,  $\text{Mg}^{2+}$  and  $\text{Zn}^{2+}$ . This was shown either by a bathochromic or hypsochromic shift in the ultraviolet absorption maxima of **8**, when **8** was recorded in the presence of these metal ions. The absorption maxima of these complexes are listed in Table 2.2. No change in the absorption spectrum of **8** was observed when  $\text{Pb}^{2+}$ ,  $\text{Cd}^{2+}$  and  $\text{Ca}^{2+}$  were added to solutions of **8**, indicating no coordination to these metal ions.

In summary, of the three ligands tested, **4**, **5** and **8**, the 5-hydroxyflavone, **8**, was the only ligand which did not coordinate  $\text{Pb}^{2+}$  or  $\text{Cd}^{2+}$ . None of the ligands formed complexes with  $\text{Ca}^{2+}$ , which was highly desirable, however, total selectivity for  $\text{Pb}^{2+}$  was not achieved.

The compounds **6**, **7** and **9**, the thiocarbonyl analogues of the flavones **4**, **5** and **8**, were the next ligands tested for metal ion coordination with the same series of nine metal ions. As explained in Section 2.2, it was expected that ligands containing a thiocarbonyl would be more selective for larger, softer acid metal ions such as  $\text{Pb}^{2+}$ , than ligands containing carbonyl functional groups. It was anticipated that smaller, harder metal ions would bind less readily to these thioflavone ligands. The UV-visible absorption spectra of the ligands **6**, **7** and **9** and their metal ion complexes were recorded in the same manner as those of ligands **4**, **5** and **8** and their absorption maxima are listed in Table 2.3. All UV-visible absorption spectra of the flavones **6**, **7** and **9** in the presence of several metals are presented in Appendix A (Figures A.1.4, A.1.5 and A.1.6).



**Table 2.3:** UV-visible absorption maxima of the thioflavones (6, 7, 9) in the presence of several metal ions.

Ligand	Metal Ion	Absorption Maxima <sup>a</sup> (nm)
 <p>3-Hydroxy-2'-methoxythioflavone (6)<sup>b</sup></p>	Pb <sup>2+</sup> Co <sup>2+</sup> Ni <sup>2+</sup> Cu <sup>2+</sup> Al <sup>3+</sup> Ca <sup>2+</sup> Mg <sup>2+</sup> Cd <sup>2+</sup> Zn <sup>2+</sup>	411;333 465;358 463;356 488; 466;361 411;333 411;332 411;332 477;362 465;356
 <p>3-Hydroxy-4'-methoxythioflavone (7)<sup>b</sup></p>	Pb <sup>2+</sup> Co <sup>2+</sup> Ni <sup>2+</sup> Cu <sup>2+</sup> Al <sup>3+</sup> Ca <sup>2+</sup> Mg <sup>2+</sup> Cd <sup>2+</sup> Zn <sup>2+</sup>	449;368 500;383 494;377 522; 500;385 449;369 449;369 449;368 514;384 501;382
 <p>5-Hydroxy-2'-methoxythioflavone (9)<sup>b</sup></p>	Pb <sup>2+</sup> Co <sup>2+</sup> Ni <sup>2+</sup> Cu <sup>2+</sup> Al <sup>3+</sup> Ca <sup>2+</sup> Mg <sup>2+</sup> Cd <sup>2+</sup> Zn <sup>2+</sup>	409;351 409;351 510;405;350 491;384;313 408;351 409;351 409;351 408;351 409;351

<sup>a</sup> Errors in the absorption maxima values are  $\pm 1$ .

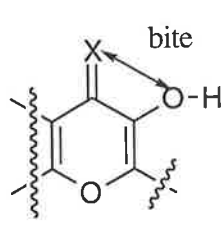
<sup>b</sup> Measured between wavelengths 280 - 600 nm.

The observed absorption maxima, as presented in Table 2.3, for the ligands 6 and 7 and their metal complexes suggest that these ligands coordinate the same metal ions. Like their

oxygenated counterparts (**4** and **5**), ligands **6** and **7** vary in structure only by the position of the methoxy substituent on the B ring, which is believed to have little effect on the binding of metal ions to the coordination site. The metal ions to which these ligands coordinate are  $\text{Pb}^{2+}$ ,  $\text{Co}^{2+}$ ,  $\text{Ni}^{2+}$ ,  $\text{Cu}^{2+}$ ,  $\text{Cd}^{2+}$  and  $\text{Zn}^{2+}$ . No coordination was observed with  $\text{Ca}^{2+}$ ,  $\text{Mg}^{2+}$  and  $\text{Al}^{3+}$ .

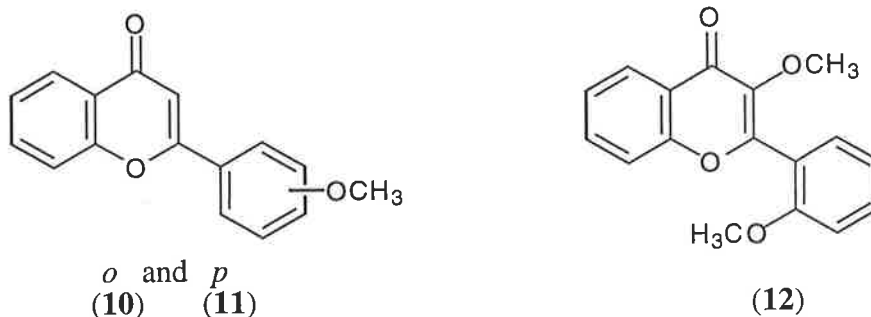
A comparison of the number of metal ion types that coordinate to the oxygenated flavones **4** and **5** and the metal ions that coordinate the thioflavones **6** and **7** demonstrates the greater metal ion specificity for the latter. Of the nine metal ions in the series, the oxygenated flavones complexed eight of these, whereas the thioflavones complexed only six. As suggested previously, it was expected that the thioflavones would have a preference for larger, softer acid metal ions due to the relatively large distance between the two coordination sites on these ligands and also due to the presence of the soft donor atom sulfur. Therefore it is most likely that the ligands **6** and **7** would exclude smaller cations such as  $\text{Mg}^{2+}$  and  $\text{Al}^{3+}$ . Computer aided molecular modelling studies have supported these ideas by showing that the 'bite' distance of the thioflavones (the distance between the thiocarbonyl S and the hydroxyl O) is significantly greater than the bite distance of the oxygenated flavones (the distance between the carbonyl O and the hydroxyl O) (Table 2.4).

**Table 2.4:** The calculated 'bite' distances of the flavones **4** and **5**, and the thioflavones **6** and **7** determined by *ab initio* calculations using Gaussian 94.<sup>62</sup>

Ligand	Ligand 'Bite' Distance (Å)	
<b>4</b>	2.69474	
<b>5</b>	2.67063	
<b>6</b>	3.00401	
<b>7</b>	2.97919	

Ligand **9**, the thiocarbonyl analogue of compound **8**, only coordinated the metal ions  $\text{Ni}^{2+}$  and  $\text{Cu}^{2+}$  according to the data tabulated in Table 2.4. The UV-visible absorption spectrum of **9** did not alter on the addition of the metal ions  $\text{Pb}^{2+}$ ,  $\text{Mg}^{2+}$ ,  $\text{Ca}^{2+}$ ,  $\text{Co}^{2+}$ ,  $\text{Zn}^{3+}$ ,  $\text{Cd}^{2+}$  and  $\text{Al}^{3+}$  indicating no interaction of these metal ions with ligand **9**.

Previous work performed on 3-hydroxyflavones (eg **4** and **5**) has inferred that metal ions coordinate to the C<sub>4</sub> carbonyl and C<sub>3</sub> hydroxyl functional groups on these ligands.<sup>34,35</sup> To confirm these findings and to illustrate that the metal ions studied do not coordinate to the methoxy substituents on the B ring of the flavones **4** - **12**, the UV-visible absorption spectra of the three flavones **10**, **11** and **12** were recorded in the absence and presence of the nine metal ions. The spectra were determined using the method described in Section 6.7.1 between the wavelengths 280 - 400 nm.



The UV-visible absorption spectra of the ligands **10**, **11** and **12**, as expected, did not produce any changes in the ligands wavelength maxima in the presence of any of the tested metal ions. The absorption maxima values of the flavones **10** - **12** measured in the presence of the metal ions were identical to those of the flavones themselves, indicating no metal ion coordination. Consequently, the presence of a C<sub>3</sub> or C<sub>5</sub> hydroxyl group is considered to play a predominant part in the chelation of flavones to metal ions. In the case of flavone **12**, the presence of the methyl group obviously reduces the availability of the electrons of the C<sub>3</sub> ether O through inductive or steric means.

In summary, none of the ligands tested (**4** to **12**) coordinated the biologically prevalent metal ions Na<sup>+</sup> or Ca<sup>2+</sup> which is a first requirement for these compounds to be useful as probes in biological systems. However, the ligands **10**, **11** and **12** did not coordinate any of the tested metal ions rendering them unfavourable as metal ion specific probes. The only ligands which coordinated Pb<sup>2+</sup>, the metal ion of major interest, were **4** - **7**. Of these ligands **4** and **5** also coordinated the metal ions Mg<sup>2+</sup>, Co<sup>2+</sup>, Cu<sup>2+</sup>, Ni<sup>2+</sup>, Zn<sup>2+</sup>, Cd<sup>2+</sup> and Al<sup>3+</sup> whereas **6** and **7** also coordinated the metal ions Co<sup>2+</sup>, Cu<sup>2+</sup>, Ni<sup>2+</sup>, Zn<sup>2+</sup> and Cd<sup>2+</sup>. Therefore, none of the tested ligands **4** to **12** bind specifically with Pb<sup>2+</sup>. However, ligands **4** to **7** may still prove useful as probes for Pb<sup>2+</sup>, if they produce fluorescent chelates, only with Pb<sup>2+</sup>, in the presence of the other metal ions.



To further study the potential ability of the ligands 4 - 7 to act as  $Pb^{2+}$  specific fluorescent probes, quantitative selectivity and fluorescence of these ligands needed to be investigated. Therefore, stability constant determinations and fluorescence spectroscopy measurements of the metal-ligand complexes were required. Information obtained from these studies would aid in assessing the suitability of these compounds as fluorescent probes for  $Pb^{2+}$ .

## 2.4 The Determination of Stability Constants

For a ligand to be a suitable probe for measuring  $Pb^{2+}$  ion concentrations within a biological cell or in aqueous samples, certain requirements are placed on the ability of the ligand to form complexes with  $Pb^{2+}$ . The ligand must form complexes of a relatively high stability with  $Pb^{2+}$  as compared to other metal ions, so that  $Pb^{2+}$  is rapidly coordinated in preference to these metal ions. The stability of these  $Pb^{2+}$  complexes should be such that little, if any, competitive displacement reactions, by other biologically prevalent cations, such as  $Mg^{2+}$ ,  $Ca^{2+}$  and  $Zn^{2+}$ , occur. Essentially, the stability of the  $Pb^{2+}$ -ligand complexes should be high enough so that the probe ligand can compete for the  $Pb^{2+}$  ions which are tightly bound to enzymes and other chelating sites within human cells. Hence, the stability of the  $Pb^{2+}$  complexes formed by the ligands 4 to 7, needed to be examined.

### 2.4.1 Concentration and Activity Constants

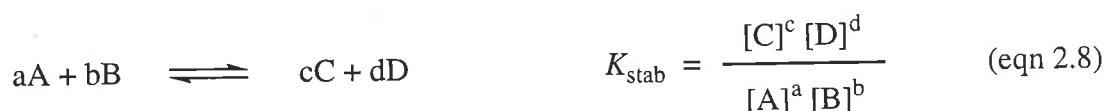
Stability constants, for metal complex formation, have long been employed as an effective measure of the affinity of a ligand for a metal ion in solution, and have served as a quantitative indication of the success or failure of ligand design.<sup>63</sup> These stability constants, which characterise the stability of the complexes, can be used to describe the stepwise formation of complexes from a metal ion,  $M^{n+}$ , and a ligand  $L^-$ .<sup>59</sup> In eqns 2.4 to 2.6, stepwise stability constants are expressed in terms of concentration and are often referred to as apparent or concentration stability constants, and in these cases have units of  $M^{-1}$ ,  $M^{-2}$  and  $M^{-n}$ , respectively.



Thermodynamic stability constants are defined as the ratio of products of the activities of the reaction products, raised to the appropriate power, to the product of the activities of the reactants, raised by the appropriate power, illustrated by eqn 2.7, and are dimensionless.<sup>63</sup>



The problem with determining thermodynamic stability constants is that the activities of all species in solution are required to be known. The determination of the activities of complex ionic species at both infinite dilution and in real solutions is a complicated and time consuming task. Thus, the more readily determined apparent stability constants are often preferred. Since the concentrations vary in direct proportion to the activities of ionic solutes when the ionic strength is controlled by a non-reacting electrolyte present at a concentration far in excess (approximately 100 times) that of the reacting ionic species under investigation, it has become general practice to measure apparent stability constants involving coordination compounds at constant ionic strength maintained by a supporting electrolyte.<sup>63</sup> The inert electrolyte must not interfere with any of the ionic species under investigation, nor with the physical or chemical properties being measured. It must have a significantly high solubility in the solvent used and readily dissociate into ionic form. All equilibrium constants then quoted are those of concentration,  $K_{\text{stab}}$ , (eqn 2.8) and not the thermodynamic  ${}^T K_{\text{stab}}$ . This practice has been adopted throughout this study and from this point 'apparent' is dropped from the term apparent stability constants.

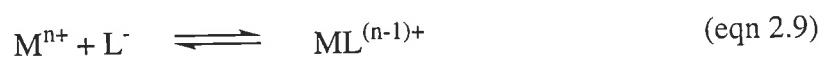


#### 2.4.2 Stability Constant Determination using UV-Visible Absorption Spectroscopy.

Stability constants can be determined by measurement of any parameter which alters due to complex formation, provided the composition of the equilibrium state can be calculated from such a measurement. Many methods have been employed for the determination of stability constants of various complexes; some of these include potentiometry, spectrophotometry, NMR spectroscopy and polarography.<sup>63</sup> Of these, UV-visible absorption spectroscopy is

ideally suited to the present study since the measurement need not disturb the system and it is often possible to determine, from one spectrum, the concentrations of two or more compounds participating in equilibrium.<sup>64</sup>

Using UV-visible absorption spectroscopy, the changes in shift and/or intensity of the absorption bands of a metal ion or of a ligand resulting from complex formation can be used to determine stability constants.<sup>65</sup> For example when a metal ion interacts with a ligand that significantly absorbs UV-visible light to form a complex where this UV-visible absorption changes (eqn 2.9), then the absorbance  $A$ , defined by Beer's law, is given by eqn 2.10, where  $l$  denotes the length of the light paths and  $\epsilon$  represents the molar extinction coefficients of the two absorbing species.



$$A = l\epsilon_L[L^-] + l\epsilon_{ML}[ML^{(n-1)+}] \quad (\text{eqn 2.10})$$

It is seen that, if  $\epsilon_L$  and  $\epsilon_{ML}$  can be determined, then absorbance measurements at two wavelengths (for solutions in which the formation of the complex is incomplete) allow the calculation of the concentration of all species in the equilibrium expression. If the absorption maximum of the complex is shifted considerably from that of the uncomplexed ligand, a wavelength may be found where the absorption of the latter is negligible compared to that of the complex. In this case measurements at one wavelength allow the calculation of all species in equilibrium.<sup>65</sup> Hence complex stability constants can be determined.

The various UV-visible absorption methods used to determine complex stability constants in two-component systems are based on the systematic variation of the total concentrations of either the ligand ( $T_L$ ) or the metal ion ( $T_M$ ) studied, or both of these.<sup>59</sup> The individual methods differ from one another in the manner in which the total concentrations are varied. Some of the methods include:

- 1) The Job method, or the method of continuous variation, in which  $T_L + T_M$  is kept constant, and the ratio  $T_L/T_M$  is varied<sup>59</sup>;
- 2) The mole ratio ligand method, in which  $T_M$  is kept constant and  $T_L$  is varied;
- 3) The mole ratio metal ion method, in which  $T_L$  is kept constant and  $T_M$  is varied; and

4) The stoichiometric dilution method in which  $T_L/T_M$  is kept constant, and  $T_L$  and  $T_M$  are varied.

The systems studied here exhibit isosbestic points consistent with the ligands chromophore occupying two dominant environments. An isosbestic point is defined as the wavelength at which the absorbing species in solution have equal absorptivity.<sup>66</sup> The existence of such an isosbestic point is not proof of the presence of only two chemical entities, since the third might very well have zero absorptivity at this particular frequency. However, the absence of an isosbestic point is usually strong evidence of the presence of a third constituent.<sup>64</sup>

The method chosen to determine the stability constants of the complexes formed by the flavone ligands **4** to **7** was the mole ratio metal ion method. This method involves the measurement of the absorbance of the complex in the presence of various concentrations of the metal ion studied. The metal ion concentrations usually vary in increments up to a concentration which is in great excess of the measured ligand, whose concentration is held constant, so that formation of the complex approaches completion. The stability constants were calculated using the MATLAB computer program Specfit.<sup>67</sup> This program calculates a  $\log K_{stab}$  value from the best possible least squares fit between the calculated and experimentally determined data based on eqns 2.9 and 2.10. The program fits for 1:1 (metal ion:ligand), 1:2, 1:3, 2:1, 1:2 one step, 1:4 one step stoichiometric models. Complete simultaneous fitting of equations for different complex stoichiometry to the resulting experimental spectral variations were tested. The stoichiometry which provided the best fit was invariably of much better fit than those arising from other stoichiometries.

### 2.4.3 Conditions of Stability Constant Determination.

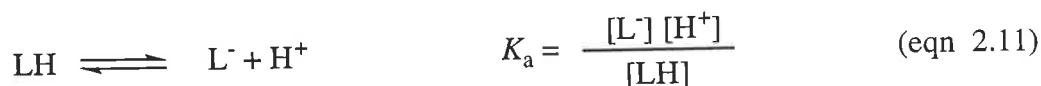
To determine the stability constants of the complexes formed by the ligands **4** to **7**, a set of standard conditions such as solvent composition, pH and ionic strength is required. The set of conditions used are as follows. A solvent system comprising of 95% ethanol and 5% water was chosen to prepare the solutions. Ethanol was used as flavones and flavonoids usually exhibit intense absorption spectra in this solvent.<sup>34</sup> Water was used in 5% so a totally dry environment, which is difficult to maintain, was not required in the preparation and measurement of solutions. Sodium perchlorate (0.10 M) and perchloric acid ( $1.0 \times 10^{-2}$  M)

were also present in the solutions prepared for UV-visible absorbance determination. The sodium perchlorate was the inert electrolyte used to maintain ionic strength (as explained in Sections 2.3.3 and 2.4.1), and the perchloric acid was used to maintain a constant, low pH of the measured solutions. As explained in Section 2.3.3, metal ions such as  $\text{Al}^{3+}$  and  $\text{Pb}^{2+}$  form hydroxo species in solution at high pH levels, so the pH of the solutions was kept low to maintain the metal ions as monomeric hydrated species.

The metal ions studied with the ligands **4** to **7** were  $\text{Pb}^{2+}$ ,  $\text{Al}^{3+}$ ,  $\text{Zn}^{2+}$ ,  $\text{Cd}^{2+}$   $\text{Mg}^{2+}$  as perchlorate salts. The perchlorate salts were used since the perchlorate ion,  $\text{ClO}_4^-$ , does not significantly complex to metal ions in solution.

#### 2.4.4 Results and Discussion.

The stability constants for complex formation, as represented in eqns 2.4 to 2.6, are determined when a fully deprotonated ligand,  $\text{L}^-$ , forms a complex with a metal ion,  $\text{M}^{n+}$ . Therefore if the stability constants are to be determined for a complex, the acid dissociation constant,  $K_a$ , of the free ligand,  $\text{LH}$ , also needs to be known. The acid dissociation constant is a quantitative measure of how readily the free ligand will ionise, releasing a proton, and is commonly referred to in terms of its  $\text{p}K_a$  (eqns 2.11 and 2.12).



$$\text{p}K_a = -\log K_a \quad (\text{eqn 2.12})$$

To determine the  $\text{p}K_a$  of the flavone ligands **4** to **7**, acid-base titrations of the ligands and the determination of the  $\text{p}K_w$  of the 95% ethanol/5% water solvent mix are required. However, since the flavone ligands tend to decompose under highly basic conditions at which appreciable dissociation of the hydroxyl proton occurs, determination of this  $\text{p}K_a$  was impractical. Even so, relative stability constants could still be determined for each metal complex under identical conditions to give relative orders of stability.

#### Ligand 4-Lead(II) Complex (in solutions with $[\text{H}^+] = 10^{-2}$ M)

The first metal-ligand combination studied was  $\text{Pb}^{2+}$  with ligand **4**. A series of twenty five solutions containing ligand **4** at a concentration of  $5.00 \times 10^{-5}$  M and  $\text{Pb}(\text{ClO}_4)_2$  at

concentrations ranging from 10 times to 400 times the ligand concentration were prepared. The  $\text{Pb}^{2+}$  concentration of 400 times the ligand concentration was found to give almost complete complexation of the ligand. The UV-visible absorption spectra of the twenty five solution series were measured in succession over a wavelength range of 260 to 450 nm as explained in Section 6.7.2. The results are illustrated by Figure 2.6, and were used to calculate the stability constant for the complex formed between  $\text{Pb}^{2+}$  and ligand 4.

The absorbance data from Figure 2.6 in the ranges 310 - 338 nm and 370 - 410 nm were collated and then submitted to Specfit for processing and a  $\log K_{\text{stab}}$  of 2.20 was obtained for a 1:1 (metal ion:ligand) model for ligand 4 with  $\text{Pb}^{2+}$ . To reduce statistical error, which is likely to be greatest in the wavelength regions of the smallest absorption difference between each absorption spectrum (ie the absorbance values near the isosbestic point), only the data between the specified wavelength ranges was used in the calculations. A graphical representation of the best possible least squares fit between the experimentally determined data (shown as circles) and the calculated data (represented as a solid line) at  $\lambda = 380$  nm is shown in Figure 2.7.

#### **Ligand 4-Aluminium(III) Complex (in solutions with $[\text{H}^+] = 10^{-2}$ M)**

The next metal ion to be studied with ligand 4 was  $\text{Al}^{3+}$ . A series of twenty four solutions containing ligand 4 at a concentration of  $5.00 \times 10^{-5}$  M and  $\text{Al}(\text{ClO}_4)_3$  at a range of concentrations ( $6.25 \times 10^{-6}$  -  $2.50 \times 10^{-4}$  M) were prepared, as for the  $\text{Pb}^{2+}$  stability constant determination. The concentration of  $\text{Al}^{3+}$  ranged from 0.125 times to 5.0 times the ligand concentration (cf. the  $\text{Pb}^{2+}$  concentration range of 10 to 400 times the ligand concentration). The UV-visible absorption spectra of the twenty four solution series were measured and a stability constant of  $\log K_{\text{stab}} = 4.51$  was determined from the absorbance data for a 1:1 fit. Figures 2.8 and 2.9 show the absorbance spectra and a graphical representation of the fit.

A comparison of the values obtained for the  $K_{\text{stab}}$  determination of ligand 4 with  $\text{Pb}^{2+}$  and  $\text{Al}^{3+}$ , under the stated conditions (see Section 2.4.3), shows that the  $\text{Al}^{3+}$  complex is at least one hundred times more stable than the  $\text{Pb}^{2+}$  complex. To allow further selectivity comparisons to be made with ligand 4 and a range of metals,  $\text{Zn}^{2+}$  and  $\text{Cd}^{2+}$  were chosen for further stability constant determinations.

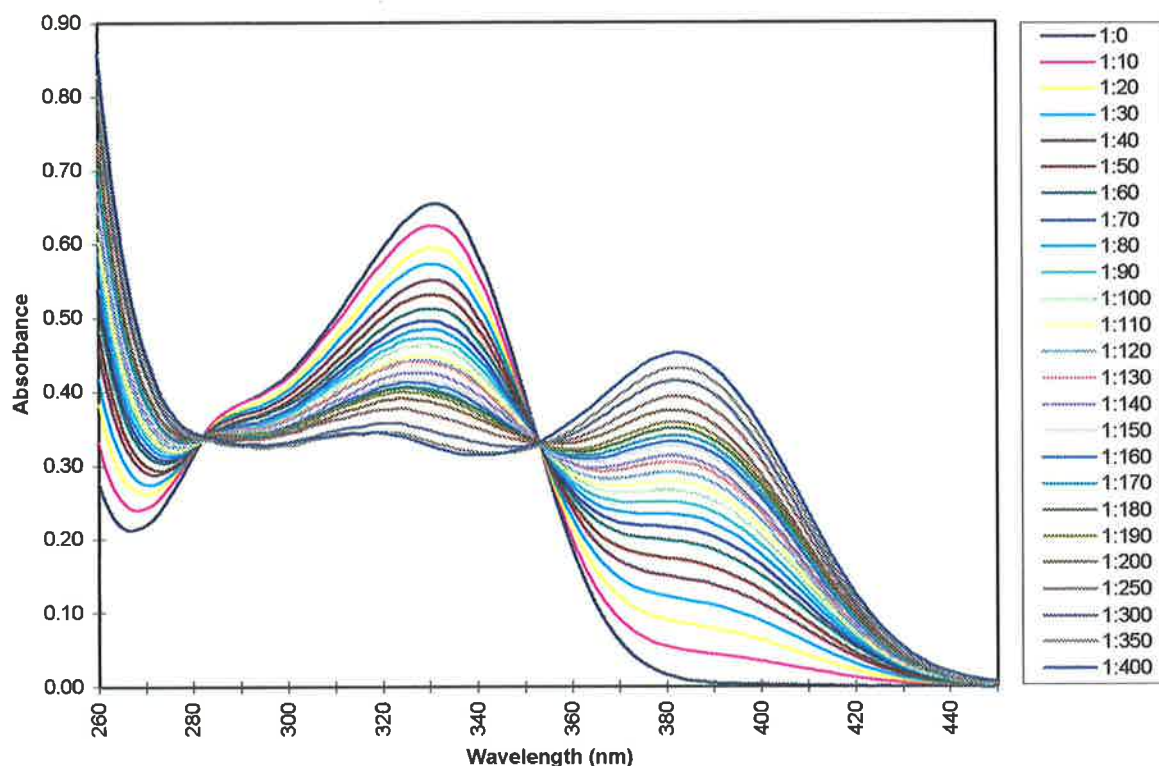


**Figure 2.6:** UV-visible absorption spectra of 3-hydroxy-2'-methoxyflavone (**4**) at  $5.0 \times 10^{-5} M$  in  $[H^+] = 1.0 \times 10^{-2} M$  with varying concentrations of  $Pb(ClO_4)_2$  as shown in Appendix B, Table B.1. The vertical, right legend represents the ratio of  $[4]$  to  $[Pb^{2+}]$ . For **4**  $\lambda_{max} = 332$  nm and for  $[Pb4]$   $\lambda_{max} = 385$  nm. The isosbestic points occur at 282 and 353 nm.

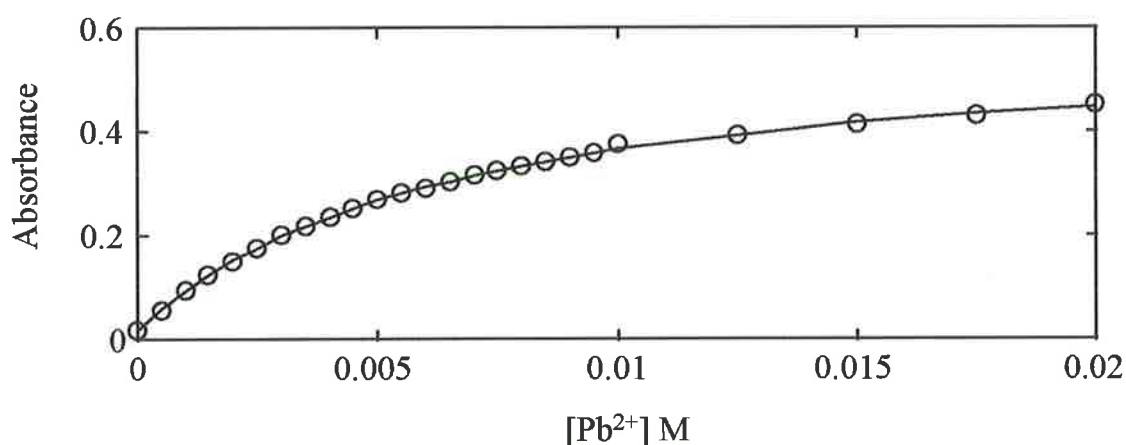


**Figure 2.7:** A graphical representation of the data fitting of Figure 2.6 at  $\lambda = 380$  nm. The circles represent the experimentally obtained data and the solid line represents the best fit.

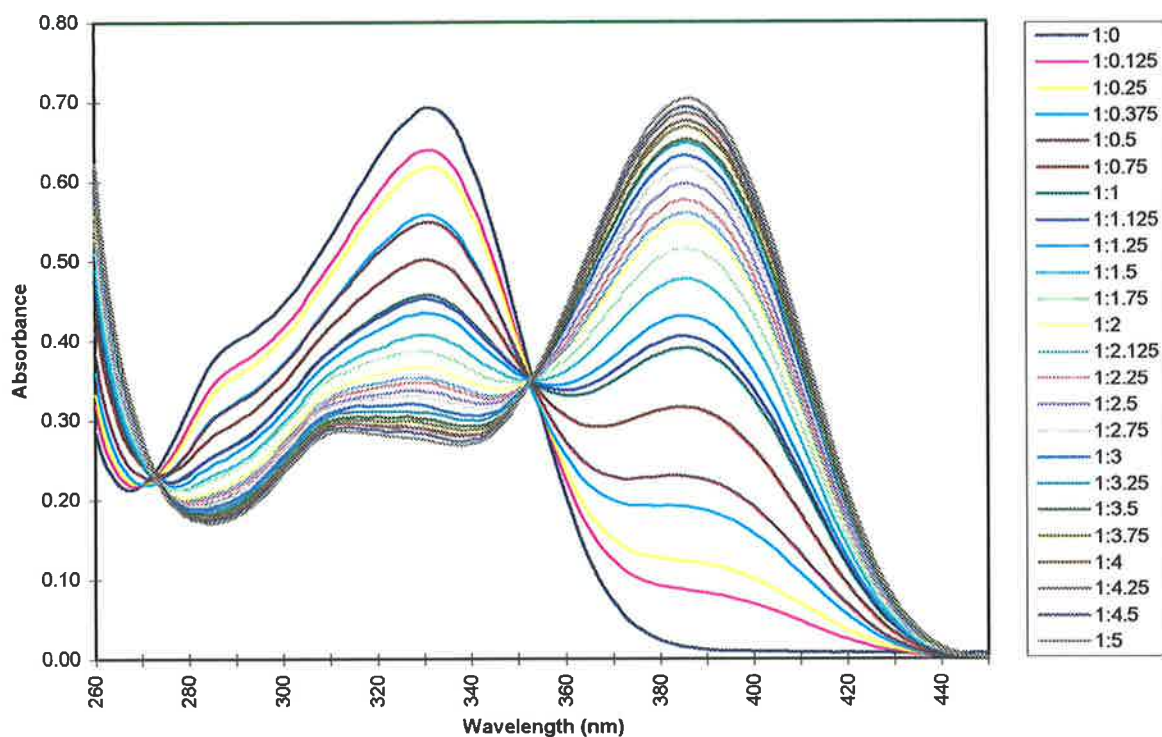


**Figure 2.8:** UV-visible absorption spectra of 3-hydroxy-2'-methoxyflavone (**4**) at  $5.0 \times 10^{-5} M$  in  $[H^+] = 1.0 \times 10^{-2} M$  with varying concentrations of  $Al(ClO_4)_3$  as shown in Appendix B, Table B.3. The vertical, right legend represents the ratio of  $[4]$  to  $[Al^{3+}]$ . For **4**  $\lambda_{max} = 332$  nm and for  $[Al4]$   $\lambda_{max} = 385$  nm. The isosbestic points occur at 273 and 353 nm.

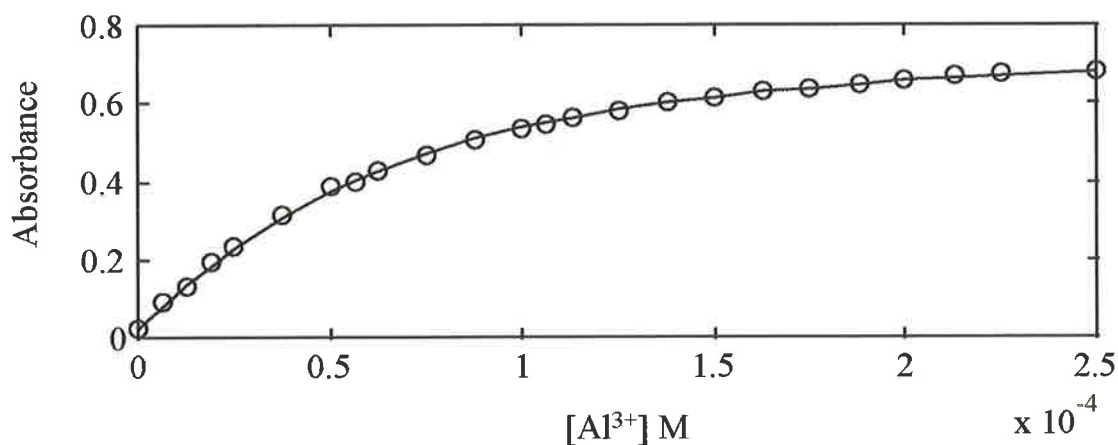
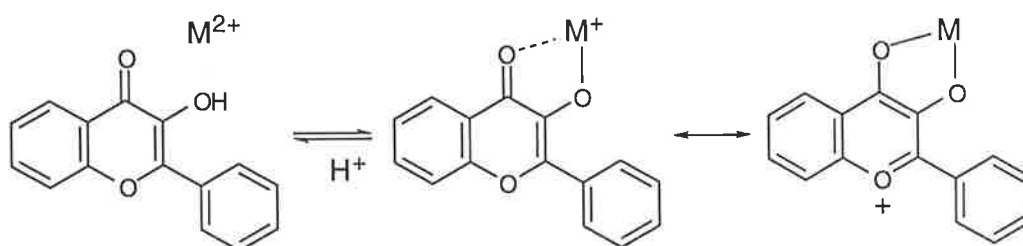


**Figure 2.9:** A graphical representation of the data fitting of Figure 2.8 at  $\lambda = 380$  nm. The circles represent the experimentally obtained data and the solid line represents the best fit.



In determining the concentrations of  $Zn^{2+}$  and  $Cd^{2+}$  required to produce complete complexation of the ligand in solution, it was evident that complexes of these metal ions had not formed to a significant extent. The UV-visible spectra of the  $Zn^{2+}$  and  $Cd^{2+}$  metal ion-ligand complexes as compared with the absorption spectra of the free ligand had not produced a significant bathochromic shift even with each metal ion concentration as high as 200 times the ligand concentration. Although both  $Zn^{2+}$  and  $Cd^{2+}$  produced significant changes in the UV-visible absorption spectrum of ligand **4** under the conditions used for qualitative selectivity (75% DMF/25%  $H_2O$  with NaPIPES buffer) suggesting coordination, such changes were not observed in solutions containing 95% Ethanol/5%  $H_2O$  with  $1.0 \times 10^{-2}$  M perchloric acid. Besides a different solvent system and different ligand concentration the main difference between the conditions for qualitative complex determination and quantitative stability constant determination was the pH of the solutions. The qualitative absorption spectra were determined in NaPIPES buffer whereas the quantitative stability constant determinations were performed under acidic conditions of  $[H^+] = 10^{-2}$  M. Since metal ion chelation with 3-hydroxyflavones results in the loss of a proton from the hydroxyl group, as suggested by Jurd and Geissman (Scheme 2.6),  $H^+$  competes strongly with  $Zn^{2+}$  and  $Cd^{2+}$ , and therefore no complex is formed with  $Zn^{2+}$  or  $Cd^{2+}$ .<sup>57</sup> At low pH the complex stability decreases because protons tend to displace the metal ion. Therefore unlike  $Pb^{2+}$  and  $Al^{3+}$ ,  $Zn^{2+}$  and  $Cd^{2+}$  must form relatively weak complexes with ligand **4**. To enable stability constants to be determined for  $Zn^{2+}$  and  $Cd^{2+}$ , the stabilities of the complexes formed between ligand **4** and the listed metal ions need to be determined under less acidic conditions of  $[H^+] = 10^{-5}$  M.

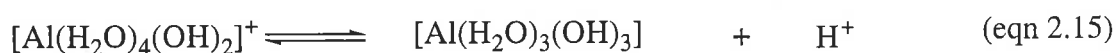
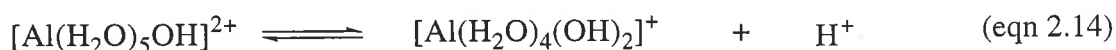
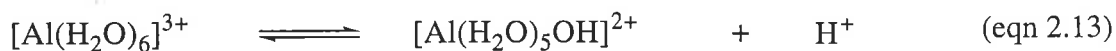


Scheme 2.6

#### Ligand **4**-Lead(II) and Aluminium(III) Complexes (in solutions with $[H^+] = 10^{-5}$ M)

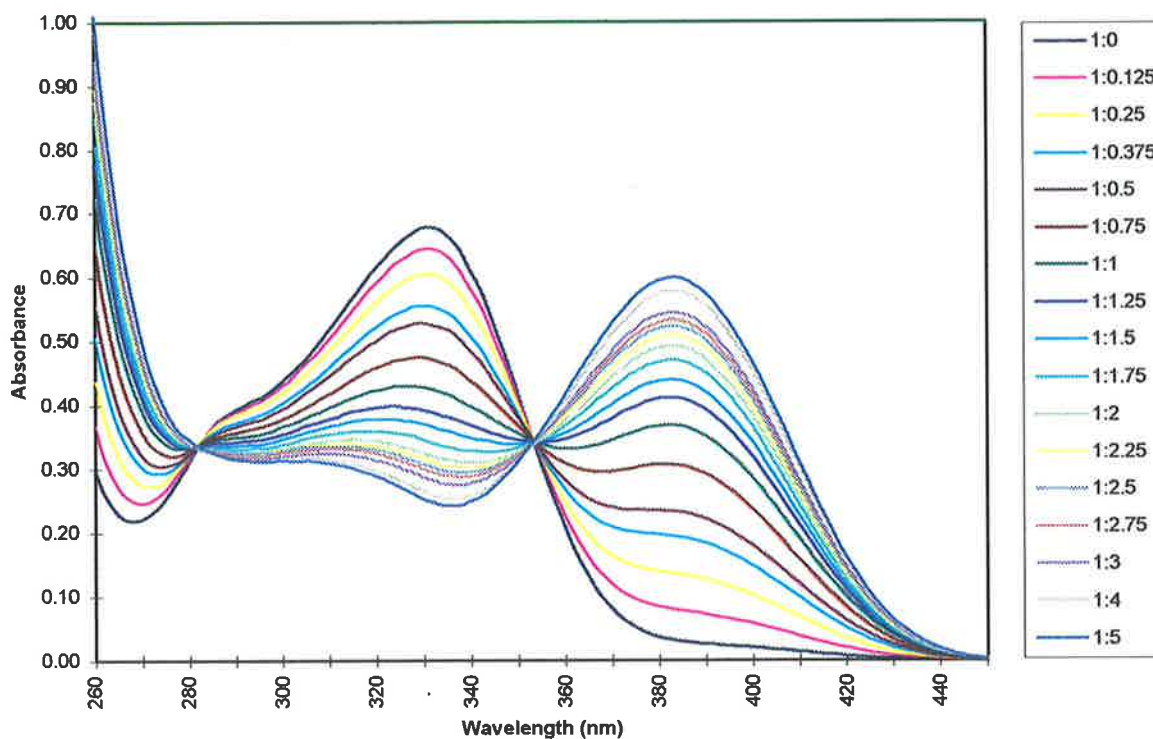
The stability constants were also determined for  $Pb^{2+}$  and  $Al^{3+}$  with ligand **4** under the lower acid concentration conditions and the  $\log K_{stab}$  values obtained are 4.70 and 4.21 respectively.

Their spectra and fits are illustrated in Figures 2.10 to 2.13. As predicted the  $\text{Pb}^{2+}$  complex formed under the less acidic conditions was more stable than the complex formed under the more acidic conditions ( $\log K_{\text{stab}}$  of 4.70 as compared with 2.20), supporting the theory that the pH of the solution alters the position of equilibrium and therefore the stability of the complex. However, the  $\text{Al}^{3+}$  complex formed with ligand **4** had only a slightly lower stability constant in  $10^{-5}$  M perchloric acid compared with its complex in  $10^{-2}$  M perchloric acid ( $\log K_{\text{stab}}$  of 4.21 as compared with 4.51). This result is not unexpected since  $\text{Al}^{3+}$  produces different hydroxo species in aqueous solutions depending on the pH of the solution (which influences the position of equilibrium in eqns 2.13 to 2.15) and so the number and type of  $\text{Al}^{3+}$  hydroxo species in solutions with differing pH are not known with certainty.<sup>69</sup> Therefore the stability constant values obtained for the  $\text{Al}^{3+}$  complexes under the different acid concentrations conditions reflect changes in the protonation of ligand **4** and the formation of hydroxo species of  $\text{Al}^{3+}$ . In their search for an immobilised fluorescent sensor for  $\text{Al}^{3+}$ , Saarl and Seltz also reported similar differences in their determined stability constants for  $\text{Al}^{3+}$  and morin (**2**) (a poly-oxygenated flavone, see Section 2.1) complexes at varying pH.<sup>70</sup> The  $\text{Al}^{3+}$  and morin complexes produced  $\log K_{\text{stab}}$  values of 4.52 and 4.25 at the respective pHs of 5.1 and 6.5.

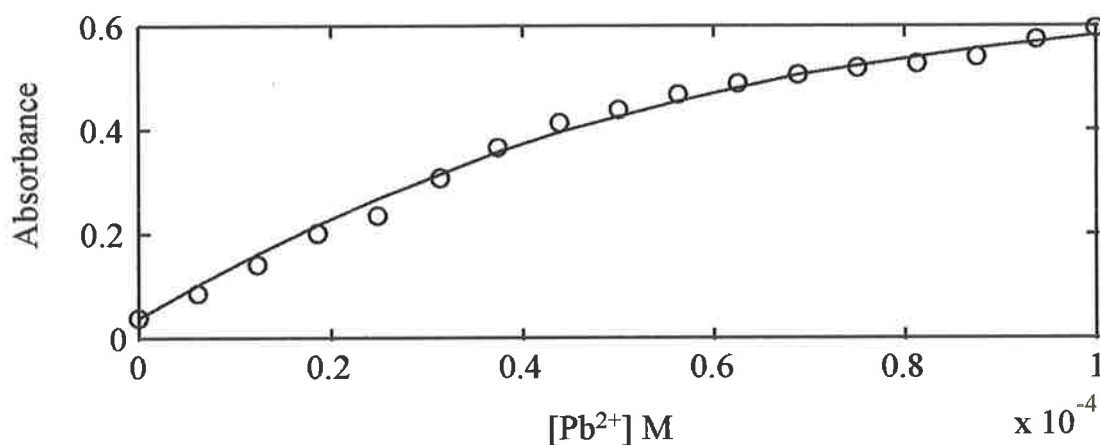


#### **Ligand 4-Zinc(II) and Cadmium(III) Complexes (in solutions with $[\text{H}^+] = 10^{-5}$ M)**

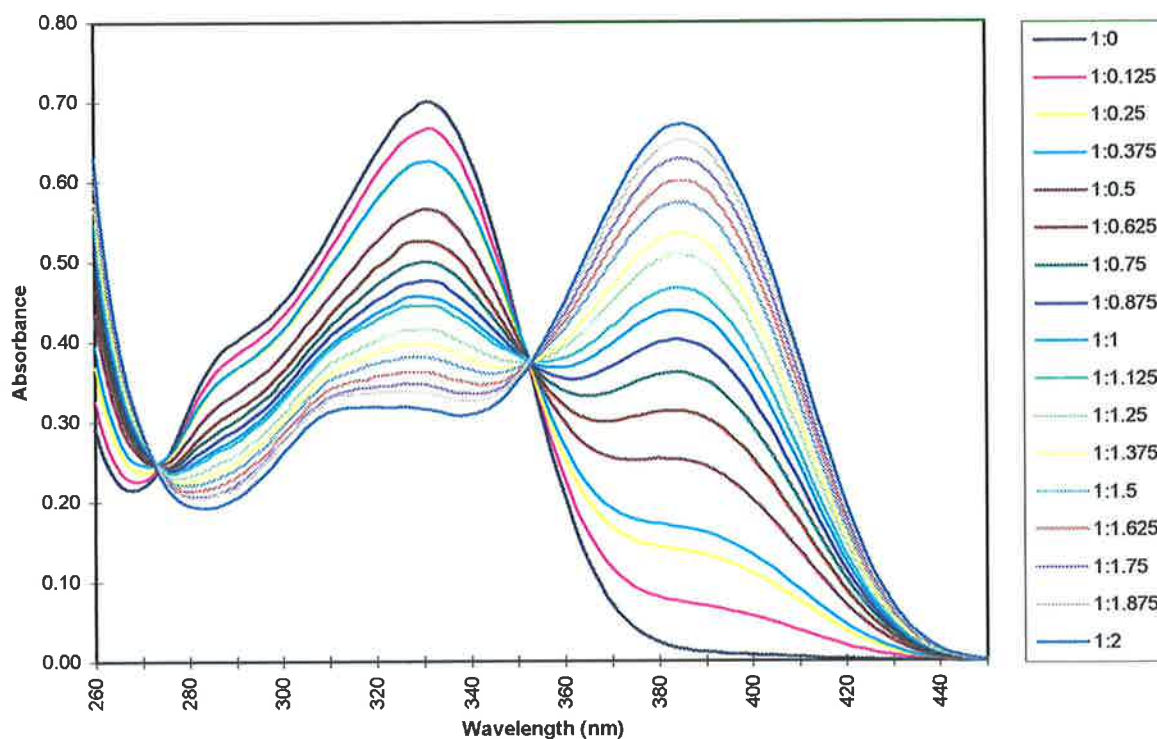
Under the less acid conditions, the stability of the  $\text{Zn}^{2+}$  and  $\text{Cd}^{2+}$  complexes with ligand **4** were investigated. In the preparation of the solutions used to measure the UV-visible absorption spectra of the metal-ligand complexes,  $\text{Zn}(\text{ClO}_4)_2$  did not dissolve in the 95% ethanol/25% water solvent mix. Solubility trials on various  $\text{Zn}^{2+}$  salts led to the use of  $\text{Zn}(\text{NO}_3)_2$ , as it was completely soluble in the solvent. The amount of  $\text{Zn}^{2+}$  required to produce a maximum bathochromic shift in the UV-visible absorption spectrum of ligand **4** was 100 times the ligand concentration. The spectra of  $\text{Zn}^{2+}$  and ligand **4** were recorded (see



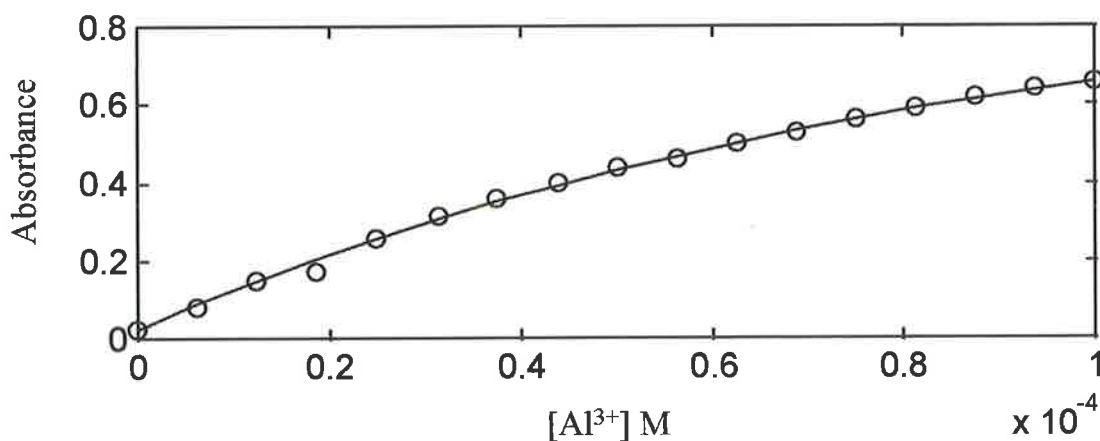
**Figure 2.10:** Ultraviolet absorption spectra of 3-hydroxy-2'-methoxyflavone (**4**) at  $5.0 \times 10^{-5} M$  in  $[H^+] = 1.0 \times 10^{-5} M$  with varying concentrations of  $Pb(ClO_4)_2$  as shown in Appendix B, Table B.2. The vertical, right legend represents the ratio of  $[4]$  to  $[Pb^{2+}]$ . For **4**  $\lambda_{max} = 332 nm$  and for  $[Pb4]$   $\lambda_{max} = 385 nm$ . The isosbestic points occur at 282 and 353 nm.



**Figure 2.11:** A graphical representation of the data fitting of Figure 2.10 at  $\lambda = 380 nm$ . The circles represent the experimentally obtained data and the solid line represents the best fit.



**Figure 2.12:** UV-visible absorption spectra of 3-hydroxy-2'-methoxyflavone (**4**) at  $5.0 \times 10^{-5} M$  in  $[H^+] = 1.0 \times 10^{-5} M$  with varying concentrations of  $Al(ClO_4)_3$  as shown in Appendix B, Table B.4. The vertical, right legend represents the ratio of **4** to  $[Al^{3+}]$ . For **4**  $\lambda_{max} = 332 nm$  and for **[Al4]**  $\lambda_{max} = 385 nm$ . The isosbestic points occur at 273 and 353 nm.



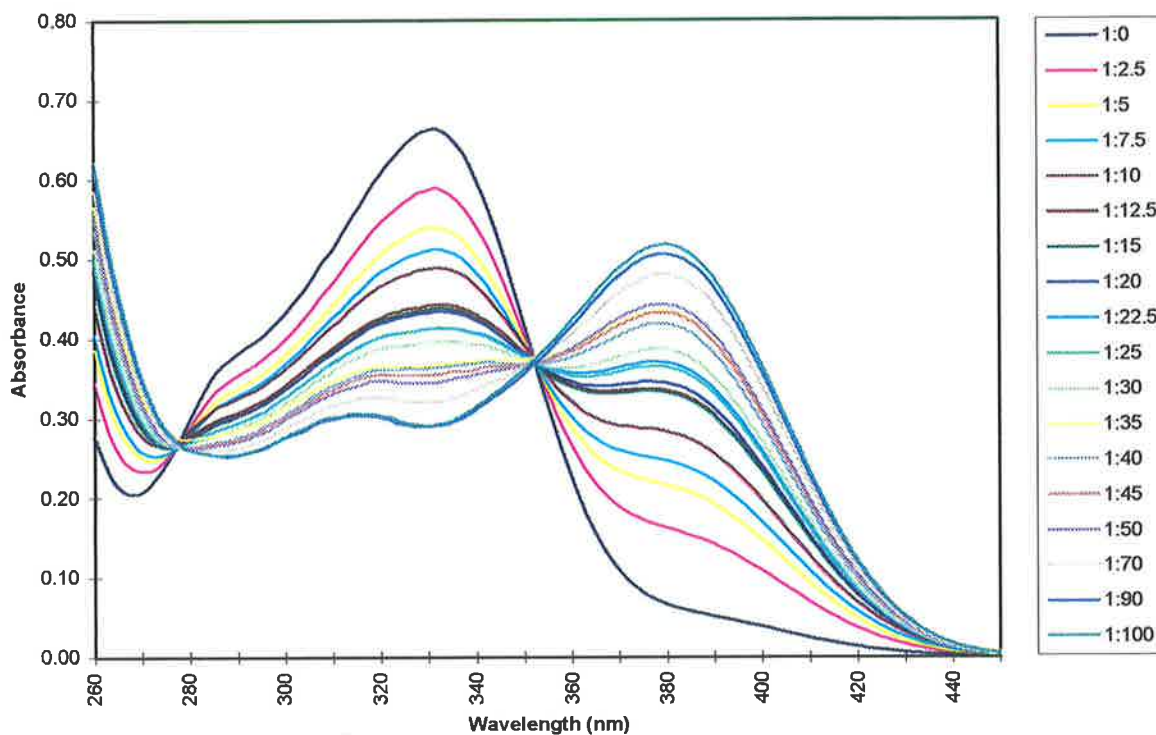
**Figure 2.13:** A graphical representation of the data fitting of Figure 2.12 at  $\lambda = 380 nm$ . The circles represent the experimentally obtained data and the solid line represents the best fit.

Figure 2.14) and  $\log K_{\text{stab}} = 3.22$  was obtained from the spectra. The fit for the data extracted from Figure 2.14 is graphically represented in Figure 2.15.

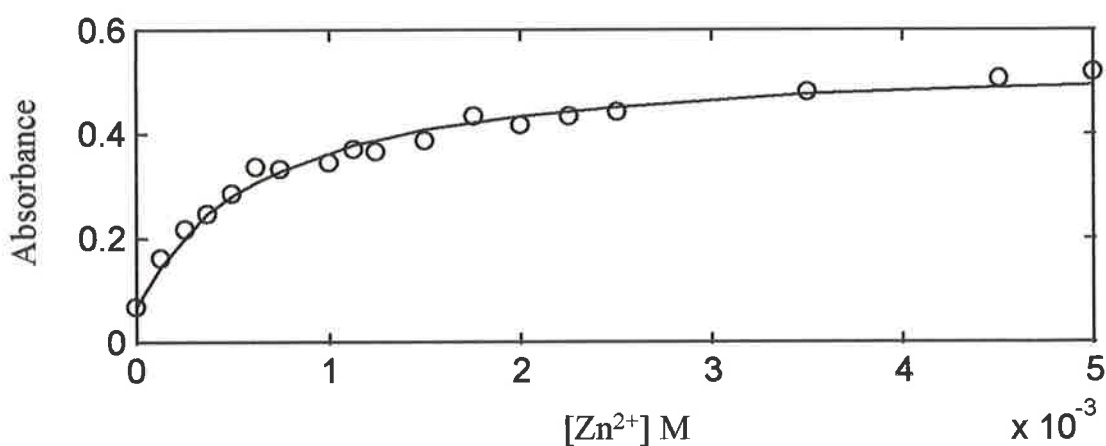
The stability constant for the  $\text{Cd}^{2+}$  and ligand **4** complex was determined in a similar manner to that described above, except the maximum amount of  $\text{Cd}(\text{ClO}_4)_2$  used was 400 times the concentration of the ligand (Figure 2.16). Similarly to the other metal ion complexes with ligand **4**, the absorption spectra were submitted to the computer program Specfit and a  $\log K_{\text{stab}}$  value (2.39) was obtained for a 1:1 (metal ion:ligand) model (Figure 2.17a). Since some of the experimentally determined points do not coincide with the theoretical line, the data was fitted to a 1:2 (metal ion:ligand) model (fitted to equations 2.16 and 2.17) giving stepwise stability constants of  $\log K_{\text{stab1}} = 2.29$  and  $\log K_{\text{stab2}} = 5.45$ . (It should be noted that the isosbestic points observed in Figure 2.16 do not preclude the formation of  $\text{ML}_2^{(n-2)+}$  as they are indicative of free and coordinated environments for  $\text{L}^-$  and evidently do not distinguish between the  $\text{ML}^{(n-1)+}$  and  $\text{ML}_2^{(n-2)+}$  environments). A graphical representation of the fit is shown in Figure 2.17b. Although a comparison of the 1:1 and 1:2 fits shows a greater coincidence of experimentally determined points with the theoretical line for the 1:2 model, arguments for one model are inconclusive on the basis of the calculated errors. The errors for both fits are of similar magnitude indicating reliability in both calculations (see Table 2.5 and Table 2.6). However, as the  $\text{Cd}^{2+}$  concentration is in great excess of the ligand concentration (up to 400 times as concentrated), the presence of a 1:1 complex is more likely.



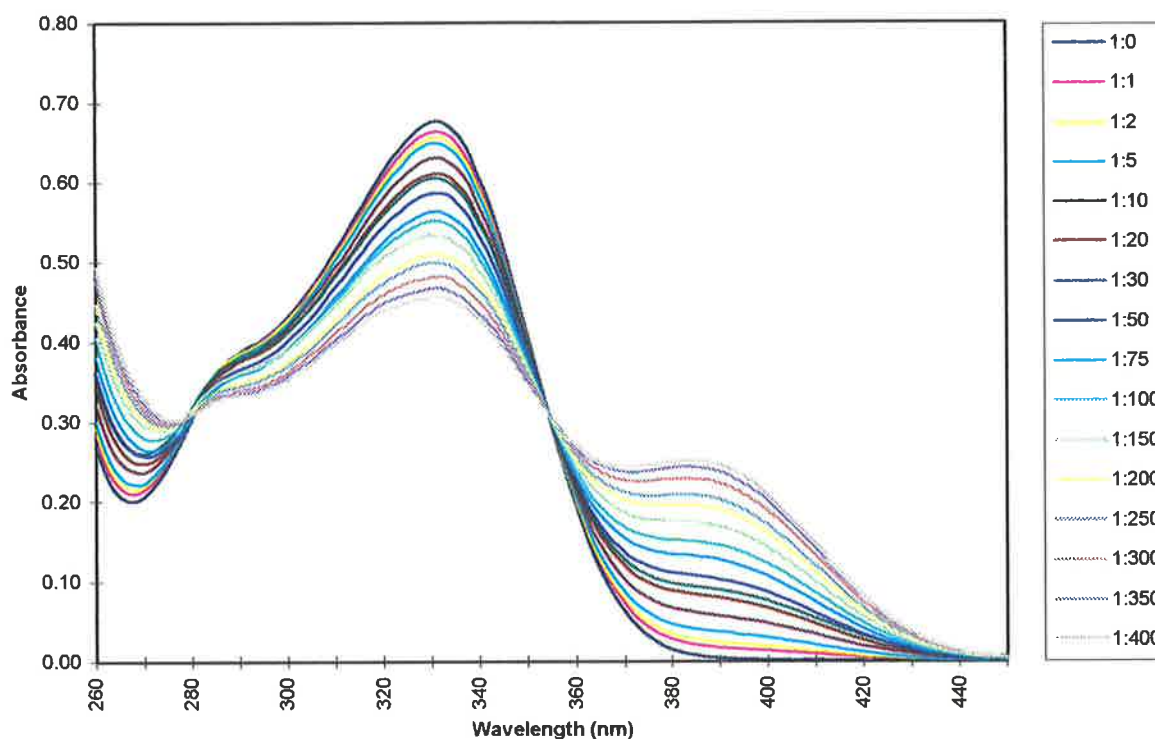
From the stepwise stability constants determined for the 1:2 ( $\text{Cd}^{2+}$ :ligand **4**) model, it can be seen that  $\log K_{\text{stab2}}$  is larger than  $\log K_{\text{stab1}}$ . It is mostly found that in the formation of a complex there is a decrease in successive stepwise stability constants, this effect arises at least in part from the statistics of substitution.<sup>71,72</sup> However, there are examples in which the initial complexes are less stable than their more highly substituted relatives. Deviations from a regular decreasing trend of stepwise stability constants is usually due to a change in the



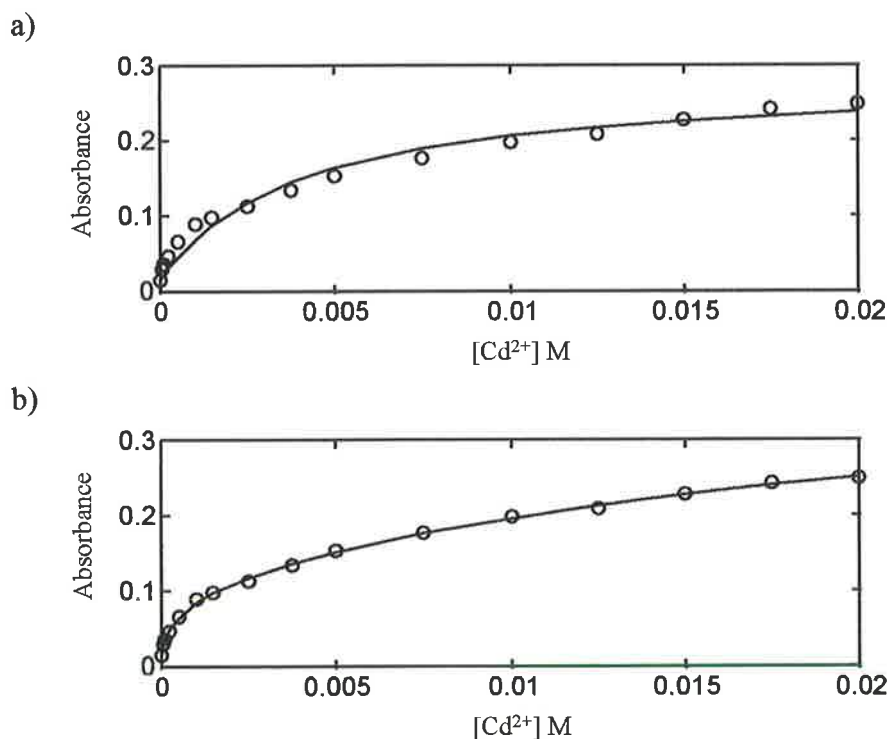
**Figure 2.14:** UV-visible absorption spectra of 3-hydroxy-2'-methoxyflavone (**4**) at  $5.0 \times 10^{-5}$  M in  $[H^+] = 1.0 \times 10^{-5}$  M with varying concentrations of  $Zn(NO_3)_2$  as shown in Appendix B, Table B.5. The vertical, right legend represents the ratio of ligand concentration to  $Zn^{2+}$  concentration. For **4**  $\lambda_{max} = 332$  nm and for  $[Zn4]$   $\lambda_{max} = 380$  nm. The isosbestic points occur at 278 and 352 nm.



**Figure 2.15:** A graphical representation of the data fitting of Figure 2.14 at  $\lambda = 380$  nm. The circles represent the experimentally obtained data and the solid line represents the best fit.



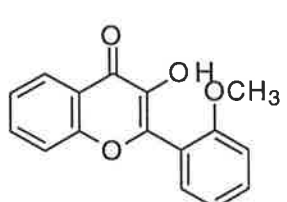
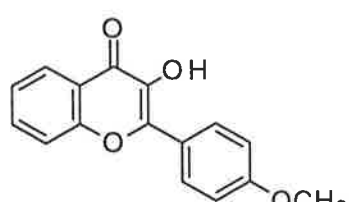
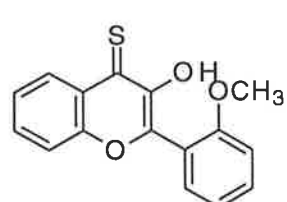
**Figure 2.16:** UV-visible absorption spectra of 3-hydroxy-2'-methoxyflavone (**4**) at  $5.0 \times 10^{-5}$  M in  $[H^+] = 1.0 \times 10^{-5}$  M with varying concentrations of  $Cd(ClO_4)_2$  as shown in Appendix B, Table B.6. The vertical, right legend represents the ratio of **4** to  $[Cd^{2+}]$ . For **4**  $\lambda_{max} = 332$  nm and for  $[Cd4]$   $\lambda_{max} = 332$  nm. The isosbestic points occur at 280 and 354 nm.



**Figure 2.17:** A graphical representation of the data fitting of Figure 2.16 at  $\lambda = 380$  nm. Graph a) is the fit for a 1:1 metal ion:ligand model and b) for a 1:2 metal ion:ligand model. The circles represent the experimentally obtained data and the solid line represents the best fit.

coordination number of the metal ion and/or the chelate effect (the chelate effect is where chelating ligands form more stable complexes than their monodentate analogues and is explained in terms of the favourable entropy for the chelation process).<sup>71</sup>

**Table 2.5:** Calculated stability constants fit for the 1:1 complexes formed by ligands **4**, **5** and **6** with various metal ions determined in  $[H^+] = 10^{-2}$  and  $10^{-5}$  M.

Ligand	Metal Ion	$\log K_{stab}$ [H <sup>+</sup> ] = 10 <sup>-2</sup> M	$\log K_{stab}$ [H <sup>+</sup> ] = 10 <sup>-5</sup> M
 <p>(4)</p>	Pb <sup>2+</sup>	2.20 ± 0.01	4.70 ± 0.01
	Al <sup>3+</sup>	4.51 ± 0.01	4.21 ± 0.01
	Zn <sup>2+</sup>	– <sup>a</sup>	3.22 ± 0.01
	Cd <sup>2+</sup>	–	2.39 ± 0.02
 <p>(5)</p>	Pb <sup>2+</sup>	2.57 ± 0.01	5.38 ± 0.01
	Al <sup>3+</sup>	4.73 ± 0.01	4.61 ± 0.01
	Zn <sup>2+</sup>	–	3.74 ± 0.01
	Cd <sup>2+</sup>	–	2.40 ± 0.02
 <p>(6)</p>	Pb <sup>2+</sup>	3.22 ± 0.01	5.74 ± 0.04
	Al <sup>3+</sup>	–	–
	Zn <sup>2+</sup>	–	4.46 ± 0.01
	Cd <sup>2+</sup>	–	3.72 ± 0.01

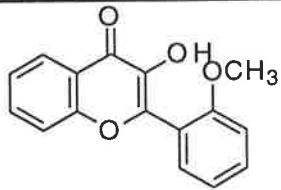
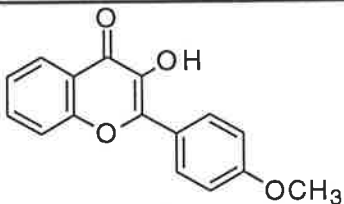
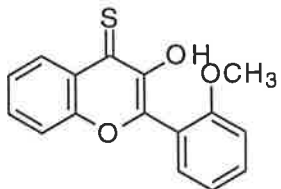
<sup>a</sup> A dash (–) indicates that either no complex has formed or the complex is too unstable to be measured.

In summary, the stability constants of ligand **4** with Pb<sup>2+</sup>, Al<sup>3+</sup>, Zn<sup>2+</sup> and Cd<sup>2+</sup> have been determined. Only the constants of the complexes with Pb<sup>2+</sup> and Al<sup>3+</sup> could be determined under the higher acid concentration conditions ( $[H^+] = 10^{-2}$  M) producing 1:1  $\log K_{stab}$  values of 2.20 and 4.51 respectively, indicating a higher stability of ligand **4** with Al<sup>3+</sup>. Under the low acid concentration conditions of  $[H^+] = 10^{-5}$  M a relative stability order for ligand **4** with



the list of metal ions was determined giving  $Pb^{2+} > Al^{3+} > Zn^{2+} > Cd^{2+}$  for 1:1 complexes (Table 2.5). Cadmium(II) was the only metal ion whose data could also fit to a 1:2 complex with ligand 4 (Table 2.6).

**Table 2.6:** Calculated stability constants fit for the 1:2 complexes formed by ligands 4, 5 and 6 with various metal ions determined in  $[H^+] = 10^{-2}$  and  $10^{-5}$  M.

Ligand	Metal Ion	$\log K_{stab1}$ and $\log K_{stab2}$ $[H^+] = 10^{-2}$ M	$\log K_{stab1}$ and $\log K_{stab2}$ $[H^+] = 10^{-5}$ M
 (4)	$Cd^{2+}$	– <sup>a</sup>	$\log K_1 = 2.29 \pm 0.01$ $\log K_2 = 5.45 \pm 0.01$
 (5)	$Pb^{2+}$ $Cd^{2+}$	X <sup>b</sup> –	$\log K_1 = 5.79 \pm 0.03$ $\log K_2 = 5.27 \pm 0.04$ $\log K_1 = 2.41 \pm 0.01$ $\log K_2 = 5.28 \pm 0.05$
 (6)	$Pb^{2+}$ $Zn^{2+}$ $Cd^{2+}$	$\log K_1 = 3.03 \pm 0.05$ $\log K_2 = 4.00 \pm 0.07$ – –	$\log K_1 = 6.48 \pm 0.08$ $\log K_2 = 5.32 \pm 0.12$ $\log K_1 = 4.65 \pm 0.15$ $\log K_2 = 5.26 \pm 0.10$ $\log K_1 = 3.22 \pm 0.10$ $\log K_2 = 4.56 \pm 0.10$

<sup>a</sup> A dash (–) indicates that either no complex has formed or the complex is too unstable to be measured.

<sup>b</sup> A cross (X) indicates that a stability constant could not be fit to a 1:2 (metal ion:ligand) stoichiometric model.

### Ligand 5 Complexes

Ligand 5, whose structure differs from 4 in the position of the methoxy group on ring B of the flavone, was the next ligand to be studied with the metal ions  $Pb^{2+}$ ,  $Al^{3+}$ ,  $Zn^{2+}$  and  $Cd^{2+}$ . Similarly to ligand 4, under the conditions of  $[H^+] = 10^{-2}$  M, ligand 5 only significantly complexed  $Pb^{2+}$  and  $Al^{3+}$  giving the same relative stability order with the two metal ions and comparatively slightly higher stability constants (Table 2.5). Under the conditions of  $[H^+] =$

$10^{-5}$  M, ligand **5** produced the same relative stability order and relatively slightly higher stability constants as those of ligand **4**. The UV-visible absorption data used to obtain the above mentioned stability constants, and the graphically represented fits at  $\lambda = 420$  nm for each set of spectra are shown in Figures 2.18 to 2.29. Ligand **5** produced 1:1 fits as well as 1:2 fits with the  $\text{Cd}^{2+}$  complexes, showing a greater coincidence of experimentally determined points with the theoretical line for the 1:2 model, as with ligand **4**. However, ligand **5** also produced equally valid 1:1 as well as 1:2 fits for the  $\text{Pb}^{2+}$  complexes at  $[\text{H}^+] = 10^{-5}$  M. Again, since the  $\text{Cd}^{2+}$  concentration is in great excess of the ligand concentration (up to 400 times as concentrated), the presence of a 1:1 complex is more likely.

A comparison of the  $\log K_{\text{stab}}$  values for the complexes formed by ligand **4** and ligand **5** (Tables 2.5 and 2.6) shows that for each complex, slightly higher stability constants were obtained for ligand **5**. This suggests that the position of the methoxy group on the B ring has a significant effect on the stabilities of the flavones metal-ligand complexes. Computer aided molecular modelling studies show that the globally minimised structure of ligand **4** has the B ring twisted out of plane with the A and C rings, due to steric hindrance and repulsion between the hydroxyl O and the methoxy O, whereas ligand **5** has all three rings coplanar (Figures 2.30 and 2.31). This coplanarity extends the conjugation of the lone pair of electrons on the electron donating methoxy group, increasing the electron density on the carbonyl O and therefore increasing the strength of the bond between the carbonyl O and the metal ion. Since the B ring is out of plane in ligand **4**, the extent of conjugation is decreased (due to restricted  $\pi$  orbital overlap between the B and C rings). This theory is further supported by the UV-visible absorption spectra of ligand **4** and ligand **5**. The  $\lambda_{\text{max}}$  of ligand **5** is 380nm whereas the  $\lambda_{\text{max}}$  of ligand **4** is 350nm suggesting ligand **5** is more extensively conjugated. If chromophores or multiple bonds are linearly conjugated within an organic molecule, both the  $\pi$ - $\pi^*$  and the  $n$ - $\pi^*$  bands in the UV-visible absorption spectrum are shifted to longer wavelengths.<sup>73</sup> Therefore, due to less conjugation within ligand **4** as compared with ligand **5**, the electron donating effect of the methoxy group on the carbonyl is reduced. Hence the stability constants produced for ligand **4** are relatively lower than those of ligand **5**.

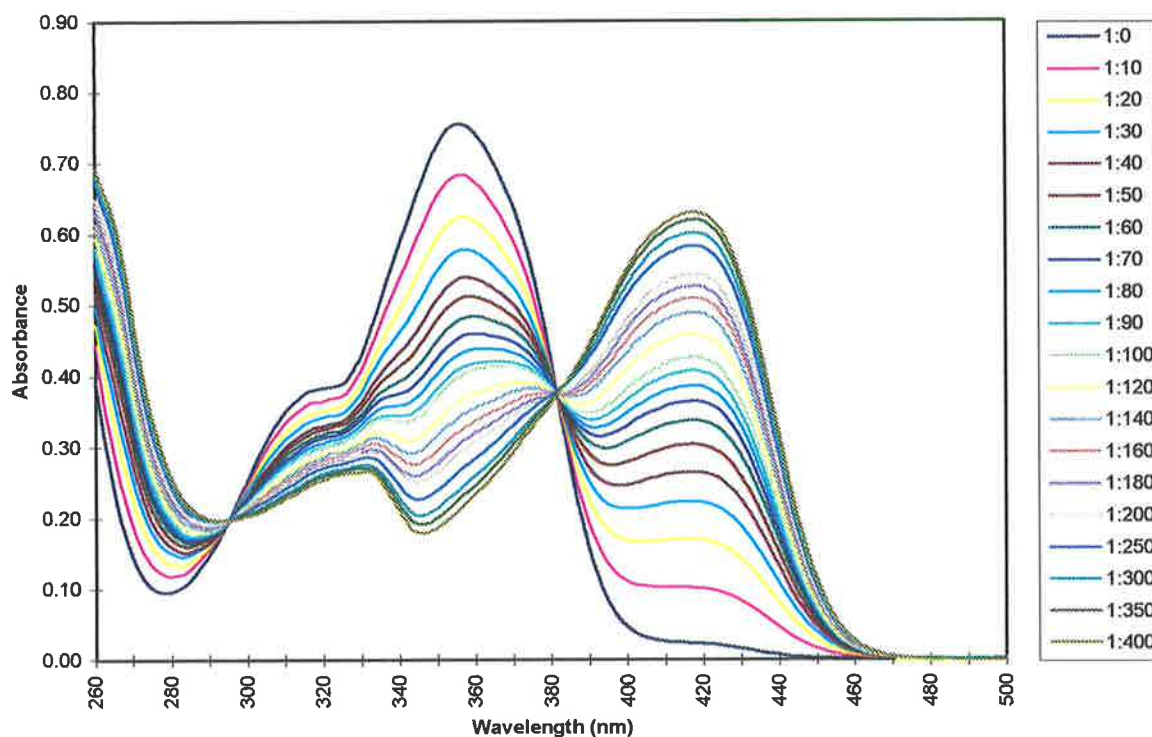


**Figure 2.18:** UV-visible absorption spectra of 3-hydroxy-4'-methoxyflavone (**5**) at  $3.33 \times 10^{-5}$  M in  $[H^+] = 1.0 \times 10^{-2}$  M with varying concentrations of  $Pb(ClO_4)_2$  as shown in Appendix B, Table B.7. The vertical, right legend represents the ratio of  $[5]$  to  $[Pb^{2+}]$ . For **5**  $\lambda_{max} = 356$  nm and for  $[Pb5]$   $\lambda_{max} = 418$  nm. The isosbestic points occur at 295 and 382 nm.

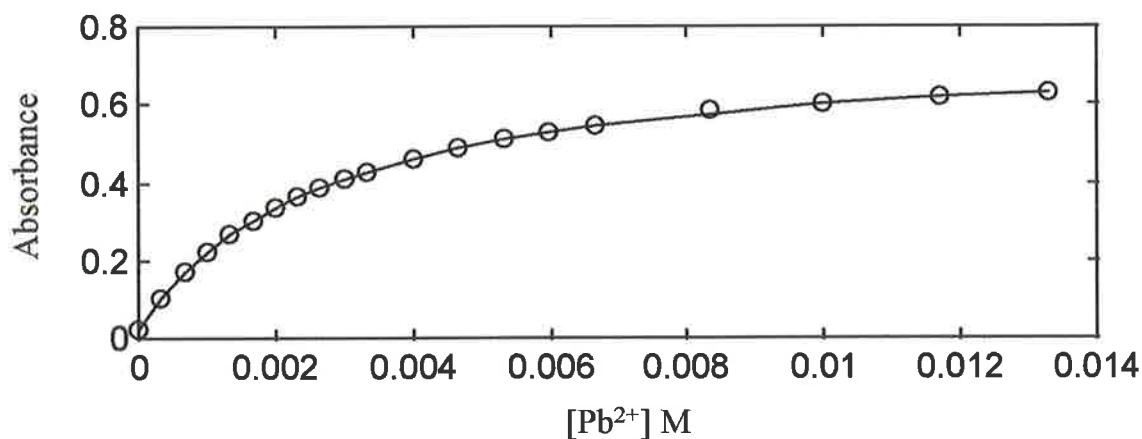


**Figure 2.19:** A graphical representation of the data fitting of Figure 2.18 at  $\lambda = 420$  nm. The circles represent the experimentally obtained data and the solid line represents the best fit.

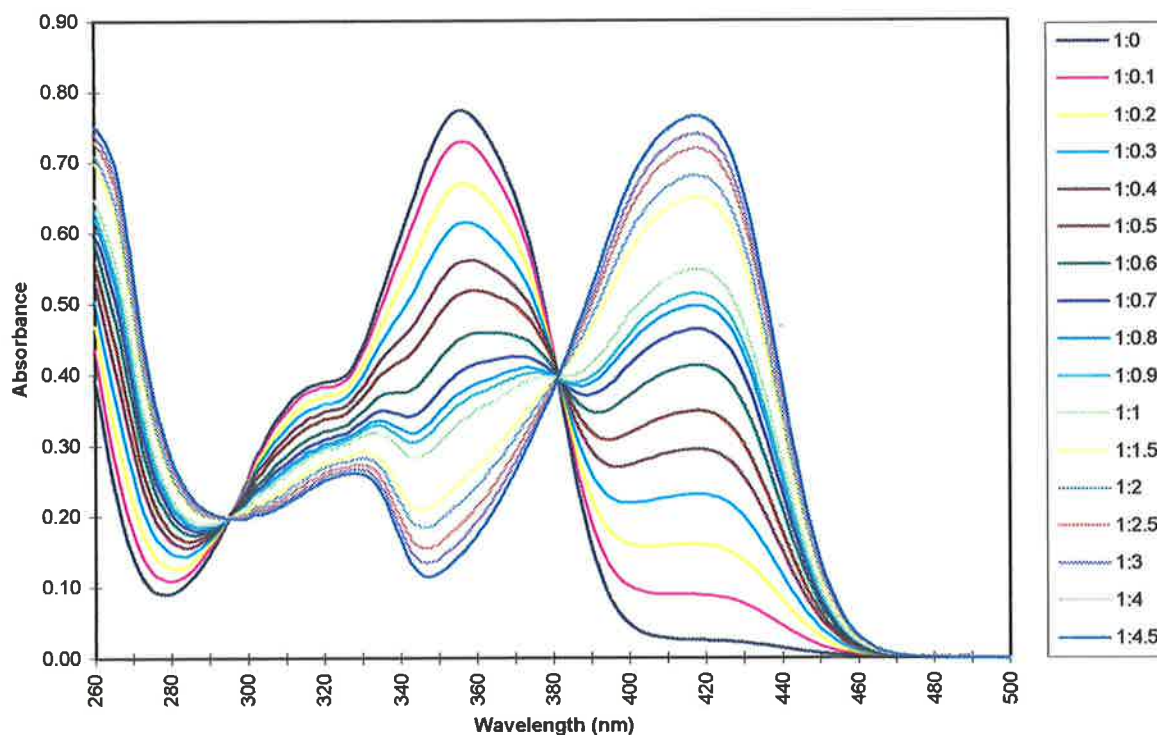


**Figure 2.20:** UV-visible absorption spectra of 3-hydroxy-4'-methoxyflavone (**5**) at  $3.33 \times 10^{-5} M$  in  $[H^+] = 1.0 \times 10^{-5} M$  with varying concentrations of  $Pb(ClO_4)_2$  as shown in Appendix B, Table B.8. The vertical, right legend represents the ratio of [**5**] to  $[Pb^{2+}]$ . For **5**  $\lambda_{max} = 356 nm$  and for  $[Pb5]$   $\lambda_{max} = 418 nm$ . The isosbestic points occur at 295 and 382 nm.

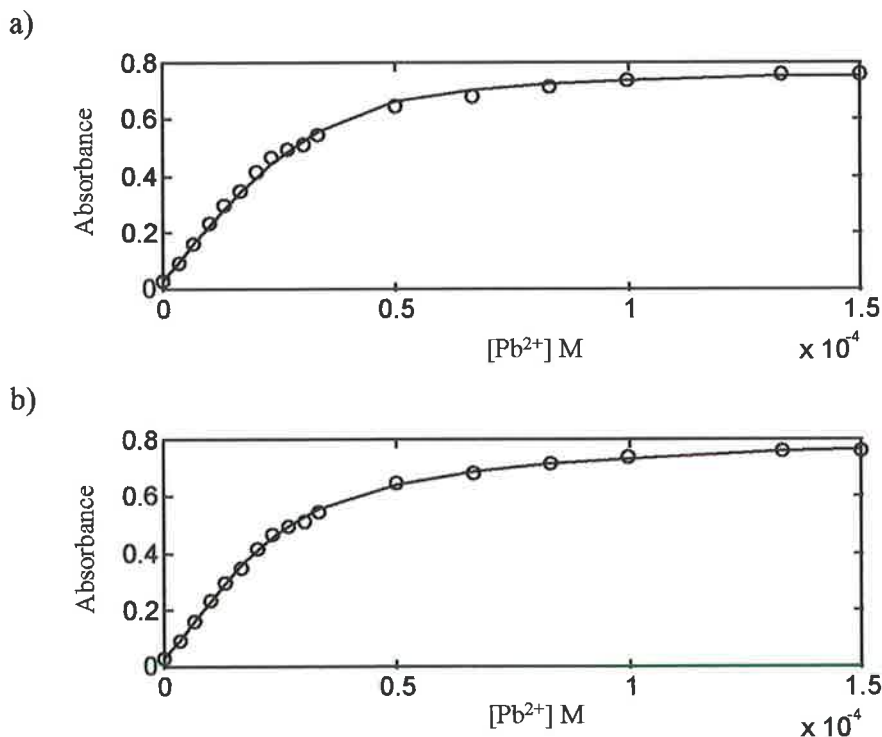


**Figure 2.21:** A graphical representation of the data fitting of Figure 2.20 at  $\lambda = 420 nm$ . Graph a) is the fit for a 1:1 metal ion:ligand model and b) for a 1:2 metal ion:ligand model. The circles represent the experimentally obtained data and the solid line represents the best fit.

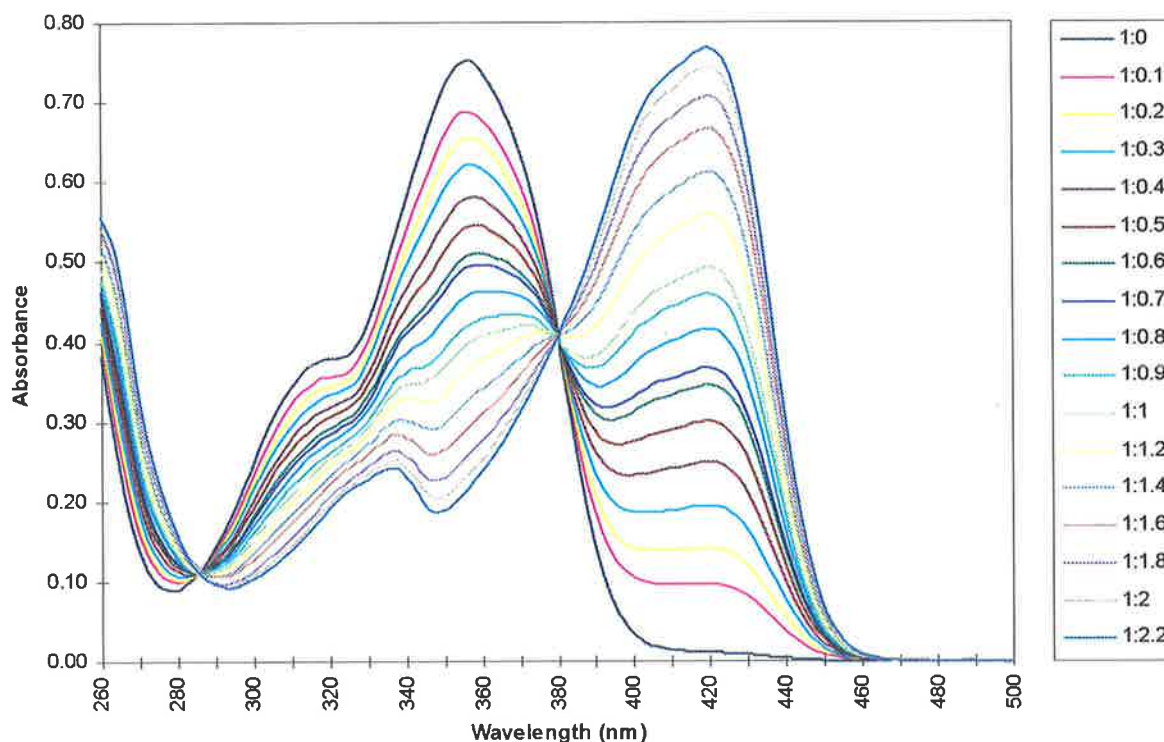


**Figure 2.22:** UV-visible absorption spectra of 3-hydroxy-4'-methoxyflavone (**5**) at  $3.33 \times 10^{-5}$  M in  $[H^+] = 1.0 \times 10^{-2}$  M with varying concentrations of  $Al(ClO_4)_3$  as shown in Appendix B, Table B.9. The vertical, right legend represents the ratio of **[5]** to  $[Al^{3+}]$ . For **5**  $\lambda_{max} = 356$  nm and for **[Al5]**  $\lambda_{max} = 420$  nm. The isosbestic points occur at 286 and 380 nm.

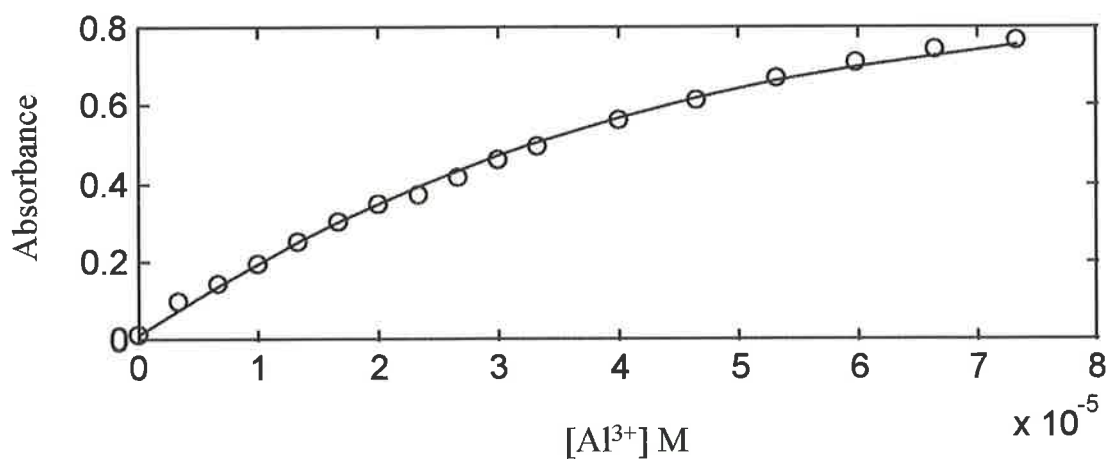


**Figure 2.23:** A graphical representation of the data fitting of Figure 2.22 at  $\lambda = 420$  nm. The circles represent the experimentally obtained data and the solid line represents the best fit.

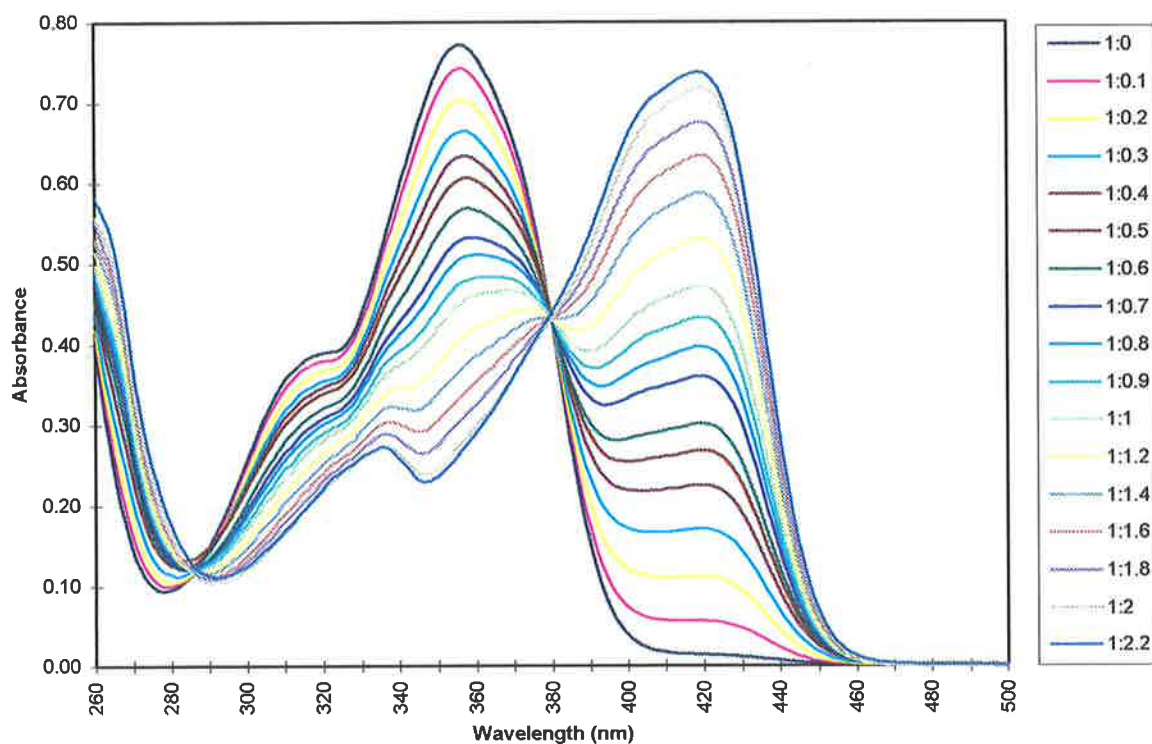


**Figure 2.24:** UV-visible absorption spectra of 3-hydroxy-4'-methoxyflavone (**5**) at  $3.33 \times 10^{-5}$  M in  $[H^+] = 1.0 \times 10^{-5}$  M with varying concentrations of  $Al(ClO_4)_3$  as shown in Appendix B, Table B.10. The vertical, right legend represents the ratio of **[5]** to  $[Al^{3+}]$ . For **5**  $\lambda_{max} = 356$  nm and for **[Al5]**  $\lambda_{max} = 420$  nm. The isosbestic points occur at 286 and 380 nm.

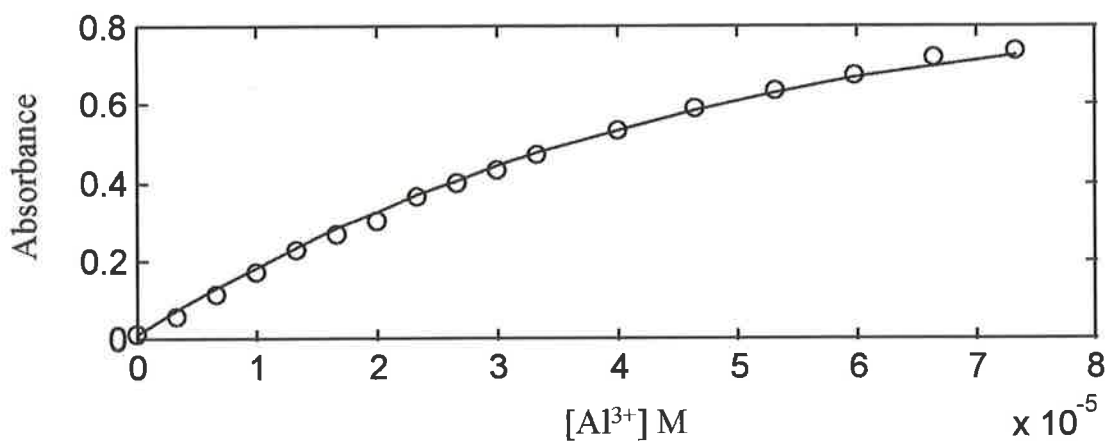


**Figure 2.25:** A graphical representation of the data fitting of Figure 2.24 at  $\lambda = 420$  nm. The circles represent the experimentally obtained data and the solid line represents the best fit.

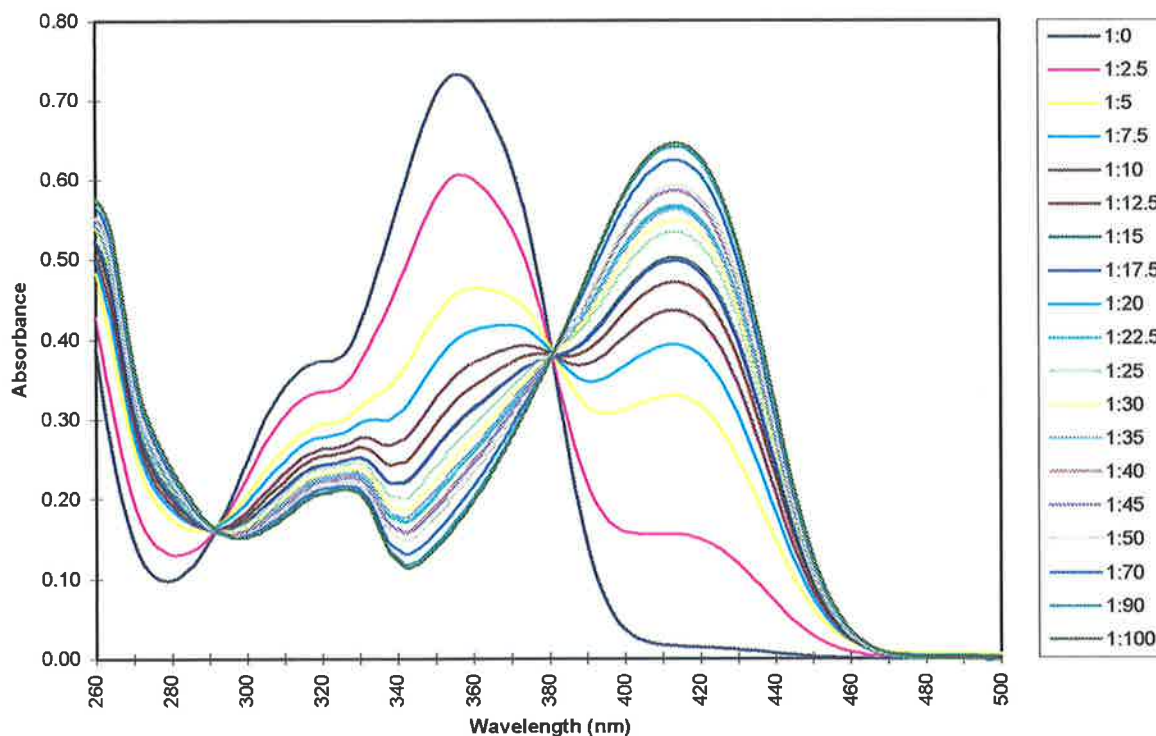


**Figure 2.26:** UV-visible absorption spectra of 3-hydroxy-4'-methoxyflavone (**5**) at  $3.33 \times 10^{-5} M$  in  $[H^+] = 1.0 \times 10^{-5} M$  with varying concentrations of  $Zn(NO_3)_2$  as shown in Appendix B, Table B.11. The vertical, right legend represents the ratio of [**5**] to  $[Zn^{2+}]$ . For **5**  $\lambda_{max} = 356 nm$  and for  $[Zn5]$   $\lambda_{max} = 414 nm$ . The isosbestic points occur at 292 and 380 nm.

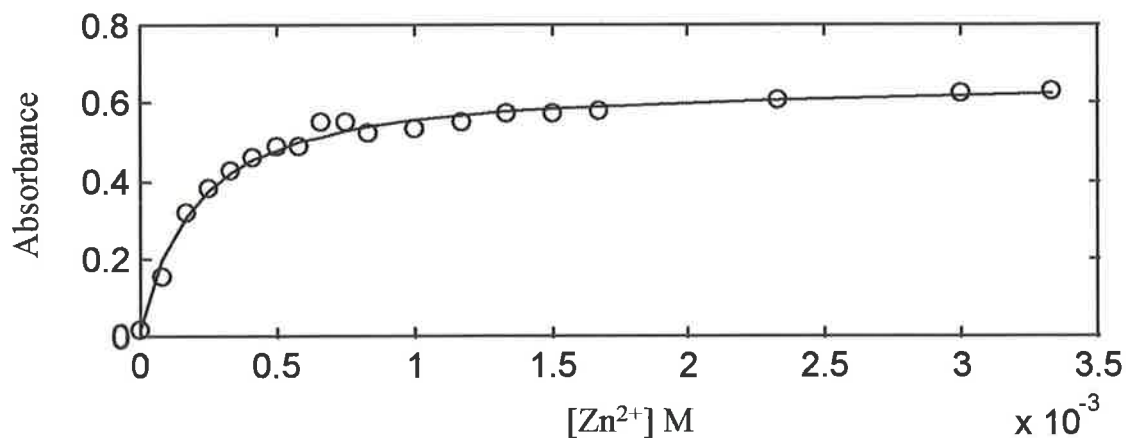


**Figure 2.27:** A graphical representation of the data fitting of Figure 2.26 at  $\lambda = 420 nm$ . The circles represent the experimentally obtained data and the solid line represents the best fit.

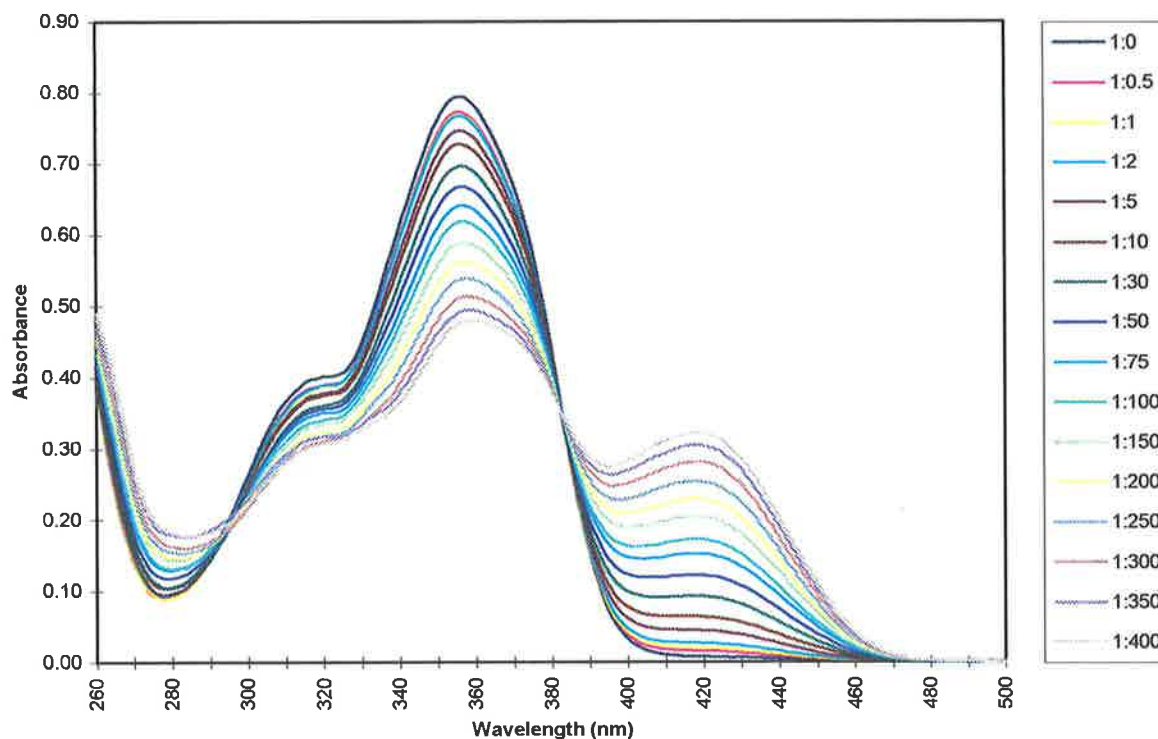


**Figure 2.28:** UV-visible absorption spectra of 3-hydroxy-4'-methoxyflavone (**5**) at  $3.33 \times 10^{-5} M$  in  $[H^+] = 1.0 \times 10^{-5} M$  with varying concentrations of  $Cd(ClO_4)_2$  as shown in Appendix B, Table B.12. The vertical, right legend represents the ratio of **5** to  $[Cd^{2+}]$ . For **5**  $\lambda_{max} = 356$  nm and for  $[Cd5]$   $\lambda_{max} = 356$  nm. The isosbestic points occur at 294 and 383 nm.

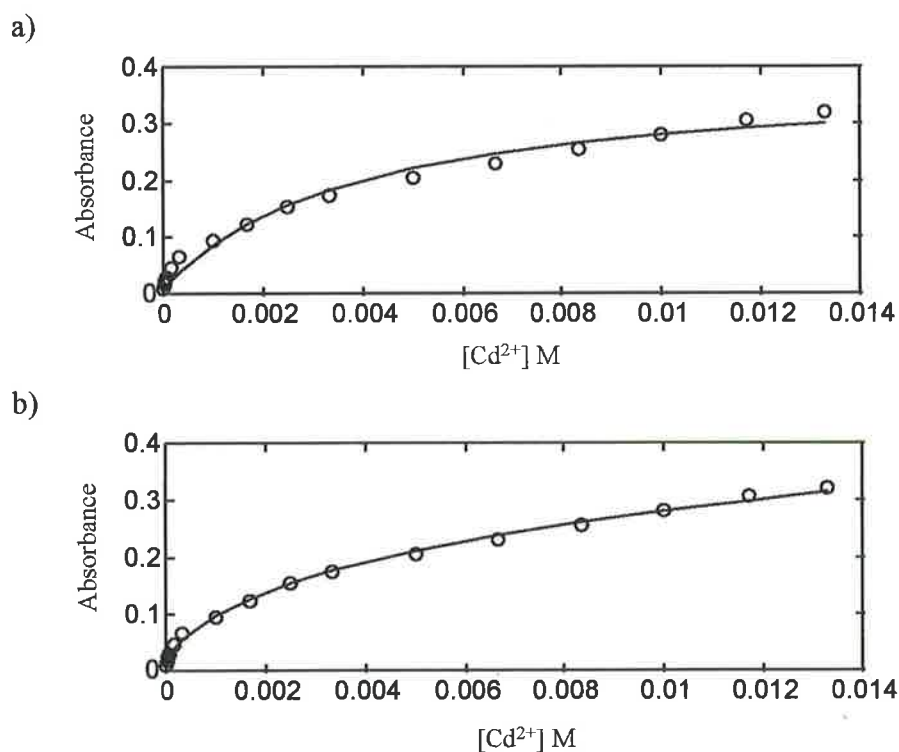


**Figure 2.29:** A graphical representation of the data fitting of Figure 2.28 at  $\lambda = 460$  nm. Graph a) is the fit for a 1:1 metal ion:ligand model and b) for a 1:2 metal ion:ligand model. The circles represent the experimentally obtained data and the solid line represents the best fit.



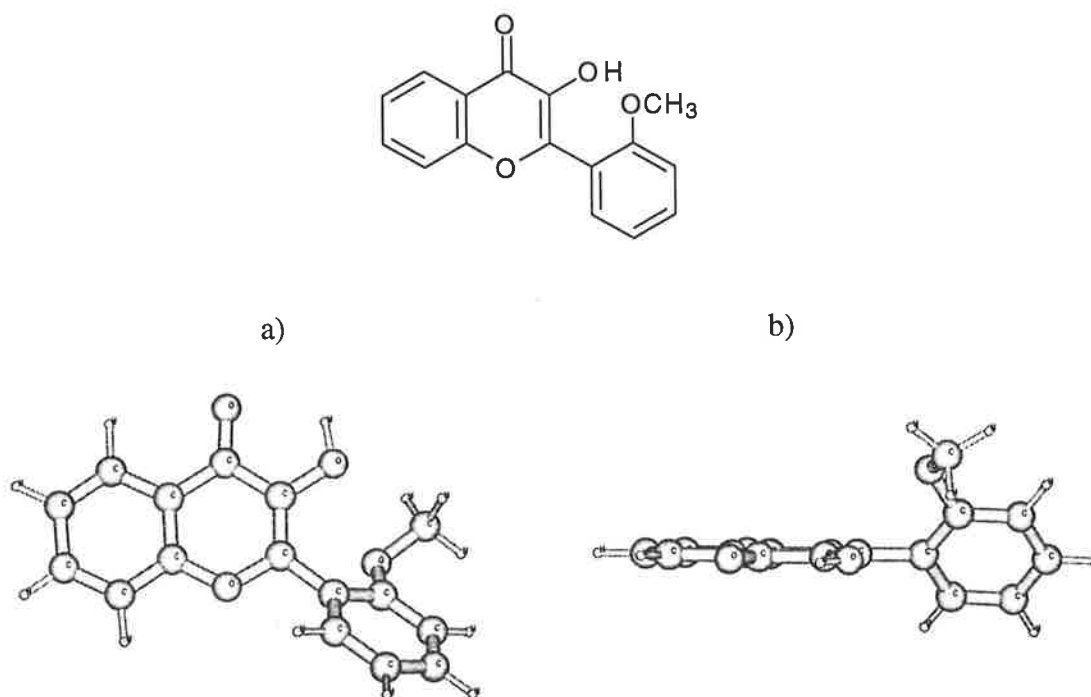


**Figure 2.30:** The globally minimised structure of ligand 4 as calculated using *ab initio* calculations by the use of Gaussian 94. Figure a) represents the view perpendicular to the AC ring plane. Figure b) represents the view parallel to the AC ring plane.

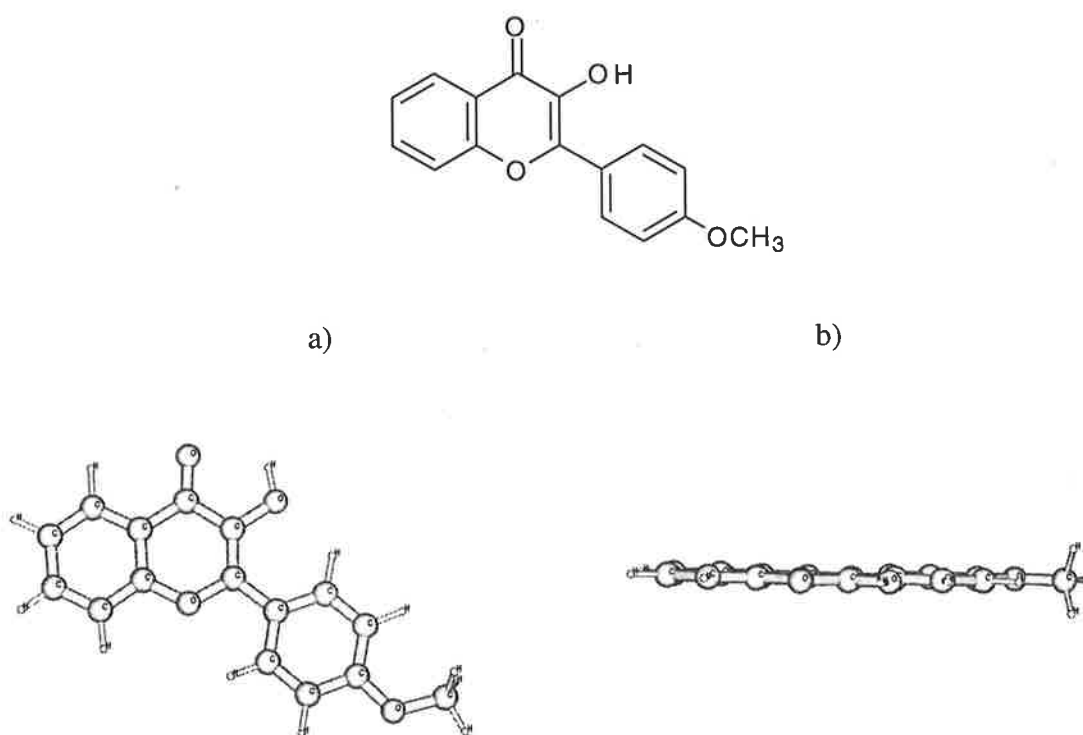


**Figure 2.31:** The globally minimised structure of ligand 5 as calculated using *ab initio* calculations by the use of Gaussian 94. Figure a) represents the view perpendicular to the AC ring plane. Figure b) represents the view parallel to the AC ring plane.

### Ligand 6 Complexes

Ligand **6**, the thioflavone analogue of ligand **4**, was the next ligand to be investigated. The stability constants were determined with the same metal ions used for ligands **4** and **5**, except for  $\text{Al}^{3+}$  which did not produce any shift in the UV-visible absorption spectrum of the free ligand in either of the two acid concentration conditions. This is consistent with  $\text{Al}^{3+}$  not coordinating **6**. At  $[\text{H}^+] = 10^{-2}$  M only  $\text{Pb}^{2+}$  showed evidence for complex formation. The data could be fitted to both 1:1 and 1:2 complex formation. The UV-visible absorption spectra and the graphically represented fits at  $\lambda = 460$  nm for  $\text{Pb}^{2+}$  as a 1:1 and 1:2 complex formed with ligand **6** are shown in the Figures 2.32 and 2.33. The correlation between the experimentally determined data and the calculated data was equally as good for the 1:1 model as the 1:2 model, however, the error in the 1:1  $\log K_{\text{stab}}$  calculation is smaller than the error in the 1:2  $\log K_{\text{stab}1}$  and  $\log K_{\text{stab}2}$  calculations (see Tables 2.5 and 2.6). This suggests that the 1:1 stoichiometry of the  $\text{Pb}^{2+}$ -ligand **6** complex is more likely than the 1:2 stoichiometry. Since the  $\text{Pb}^{2+}$  concentrations used were in great excess of the ligand **6** concentration (up to 250 times as great) it is more likely that the complex exists in a 1:1 stoichiometry.

Stability constants were determined for the  $\text{Pb}^{2+}$ ,  $\text{Zn}^{2+}$  and  $\text{Cd}^{2+}$  complexes of ligand **6** at the lower acid concentration of  $[\text{H}^+] = 10^{-5}$  M. Again  $\text{Al}^{3+}$  did not modify the UV-visible absorption spectrum of **6**. The UV-visible absorption spectra and the graphically represented fits at  $\lambda = 460$  nm for each determined stability constant are shown in Figures 2.34 to 2.39. The data for each complex could be fitted to a 1:1 (metal ion:ligand) model as well as a 1:2 model. The relative stability order produced from the metal ion complexes of ligand **6**,  $\text{Pb}^{2+} > \text{Zn}^{2+} > \text{Cd}^{2+}$ , is the same order as that of the ligands **4** and **5**. The magnitude of the constants obtained with ligand **6** were greater than those for ligand **4** and ligand **5**.

When the  $\log K_{\text{stab}}$  of the complex formed between  $\text{Pb}^{2+}$  and ligand **7** (the thioflavone analogue of ligand **5**) was determined by recording the UV-visible absorption spectra of the free ligand and of a series of  $\text{Pb}^{2+}$ -ligand **7** solutions with varying  $\text{Pb}^{2+}$  concentration, no isosbestic points were observed. It was also noted that there was no consistent increase in the absorbance values as the concentration of  $\text{Pb}^{2+}$  was increased, and that with time (in the presence of light) the deep yellow colour of the solution faded, which is consistent with the

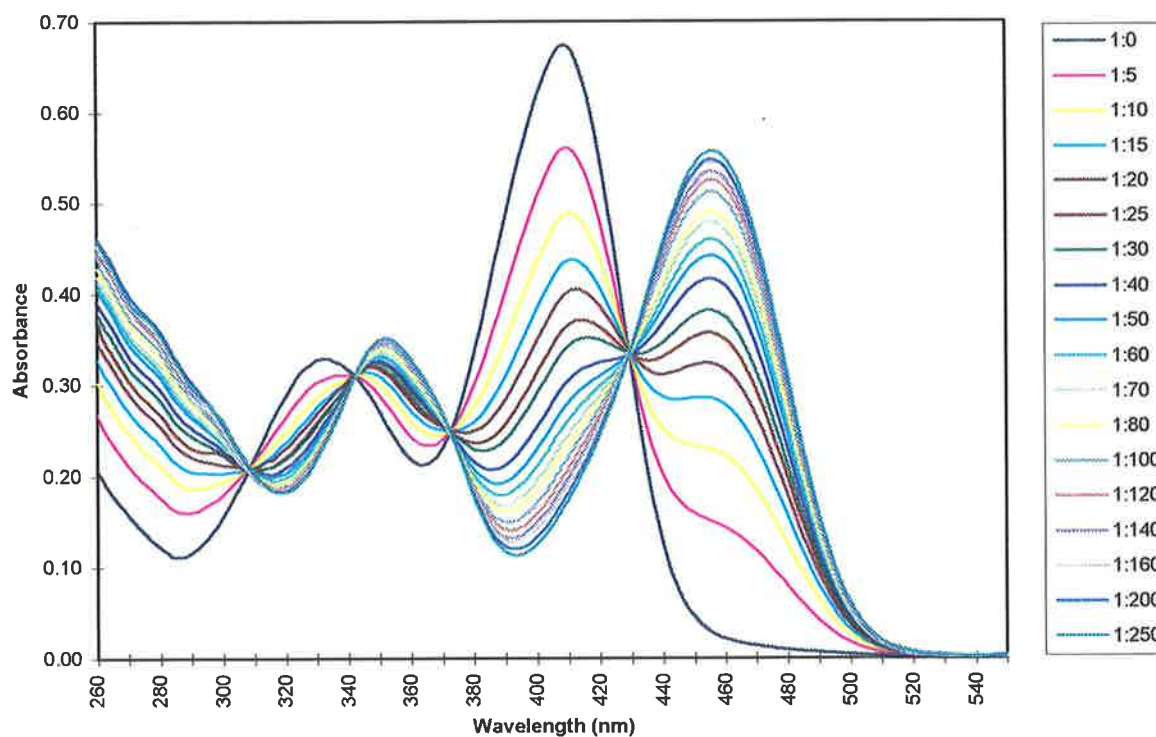


**Figure 2.32:** UV-visible absorption spectra of 3-hydroxy-2'-thiomethoxyflavone (**6**) at  $3.33 \times 10^{-5} \text{ M}$  in  $[\text{H}^+] = 1.0 \times 10^{-2} \text{ M}$  with varying concentrations of  $\text{Pb}(\text{ClO}_4)_2$  as shown in Appendix, Table B.13. The vertical, right legend represents the ratio of [**6**] to  $[\text{Pb}^{2+}]$ . For **6**  $\lambda_{\text{max}} = 409 \text{ nm}$  and for  $[\text{Pb6}]$   $\lambda_{\text{max}} = 457 \text{ nm}$ . The isosbestic points occur at 308, 342, 372 and 430 nm.

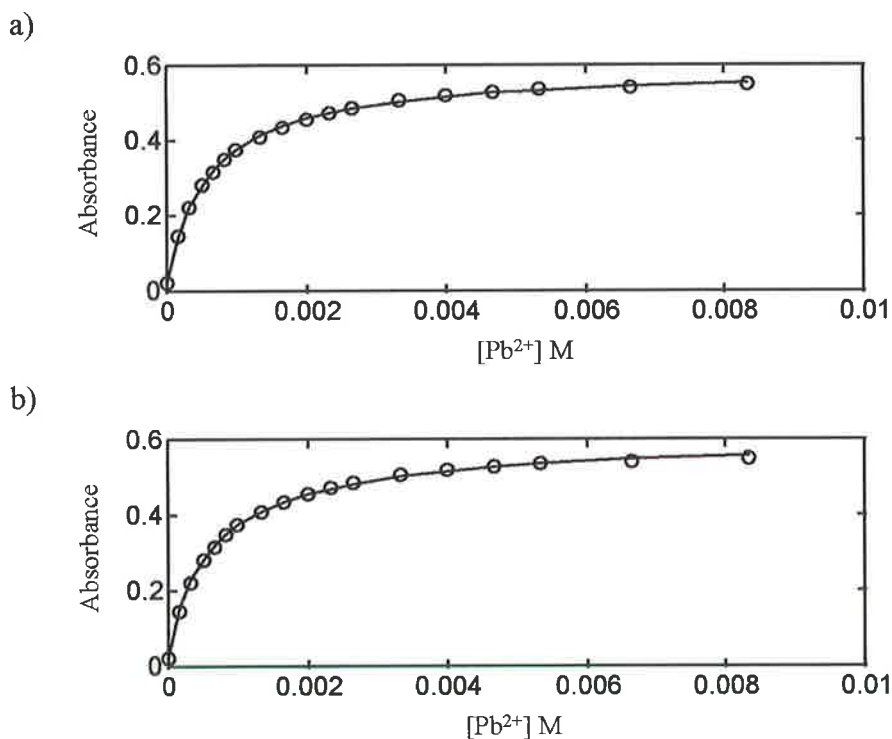


**Figure 2.33:** A graphical representation of the data fitting of Figure 2.32 at  $\lambda = 460 \text{ nm}$ . Graph a) is the fit for a 1:1 metal ion:ligand model and b) for a 1:2 metal ion:ligand model. The circles represent the experimentally obtained data and the solid line represents the best fit.

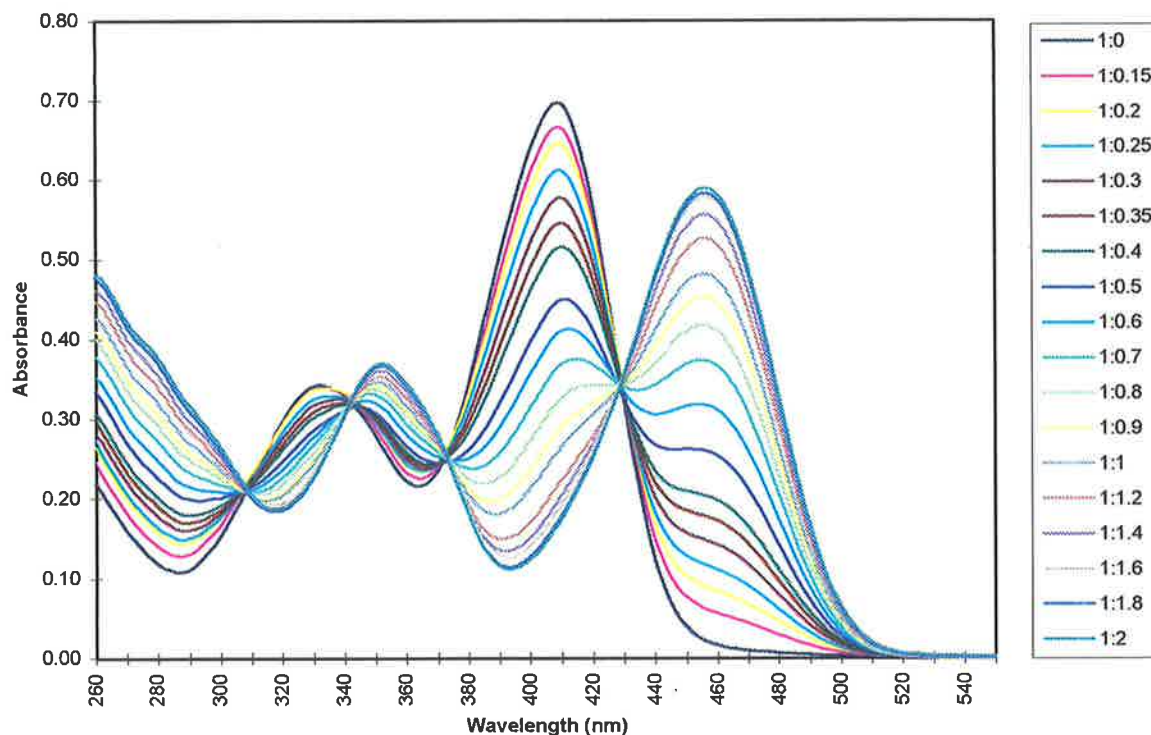
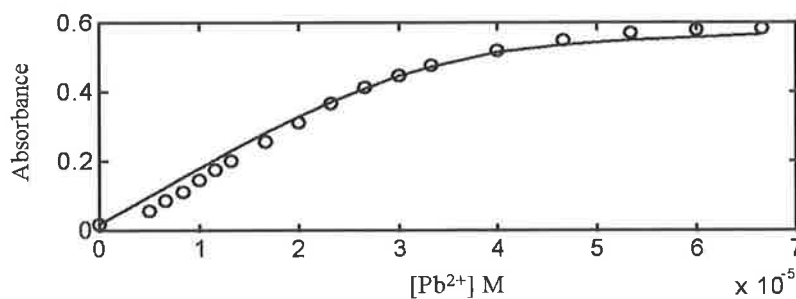


**Figure 2.34:** UV-visible absorption spectra of 3-hydroxy-2'-thiomethoxyflavone (**6**) at  $3.33 \times 10^{-5} \text{ M}$  in  $[\text{H}^+] = 1.0 \times 10^{-5} \text{ M}$  with varying concentrations of  $\text{Pb}(\text{ClO}_4)_2$  as shown in Appendix B, Table B.14. The vertical, right legend represents the ratio of [**6**] to  $[\text{Pb}^{2+}]$ . For **6**  $\lambda_{\text{max}} = 409 \text{ nm}$  and for  $[\text{Pb6}]$   $\lambda_{\text{max}} = 457 \text{ nm}$ . The isosbestic points occur at 308, 342, 372 and 430 nm.

a)



b)

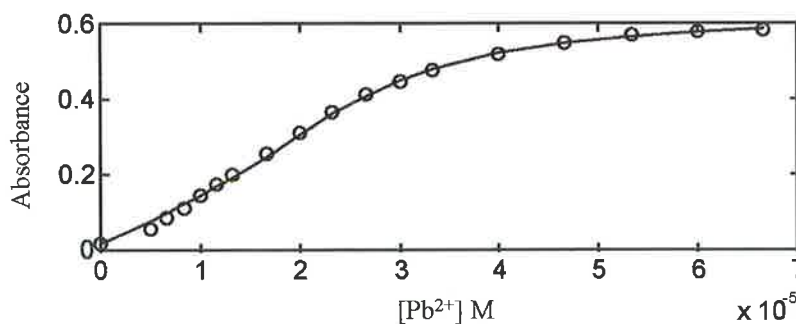


**Figure 2.35:** A graphical representation of the data fitting of Figure 2.34 at  $\lambda = 460 \text{ nm}$ . Graph a) is the fit for a 1:1 metal ion:ligand model and b) for a 1:2 metal ion:ligand model. The circles represent the experimentally obtained data and the solid line represents the best fit.

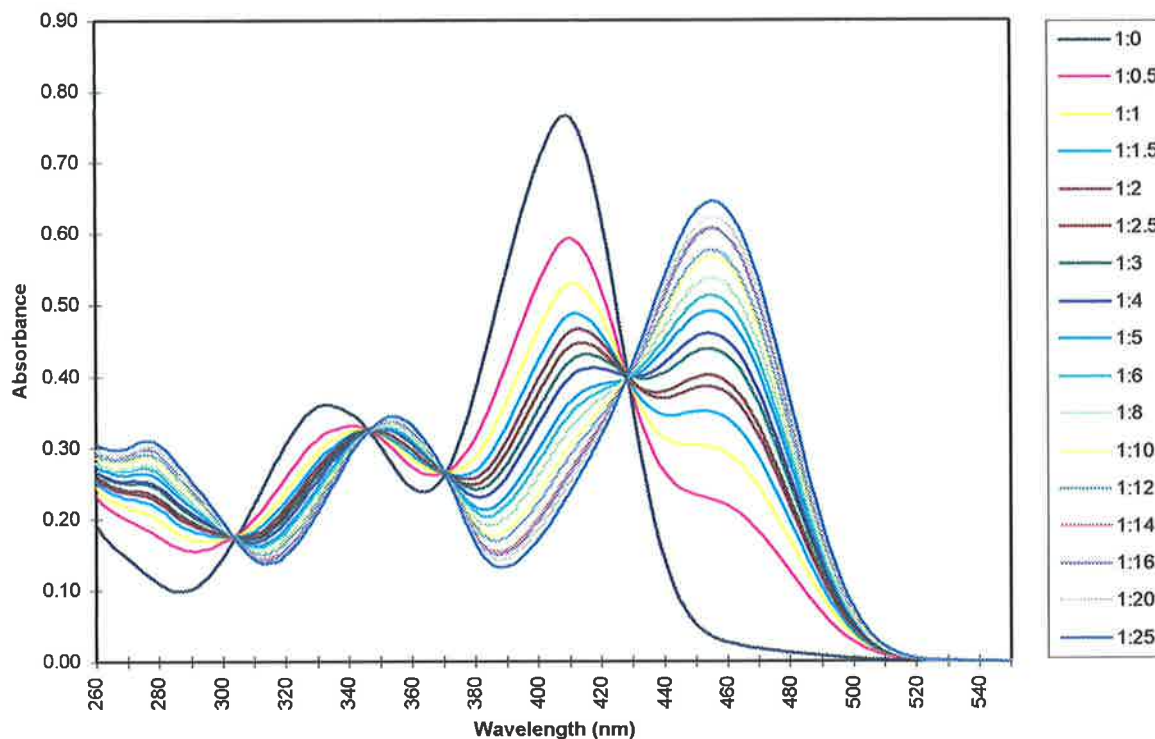


**Figure 2.36:** UV-visible absorption spectra of 3-hydroxy-2'-thiomethoxyflavone (**6**) at  $3.33 \times 10^{-5} \text{ M}$  in  $[\text{H}^+] = 1.0 \times 10^{-5} \text{ M}$  with varying concentrations of  $\text{Zn}(\text{NO}_3)_2$  as shown in Appendix B, Table B.15. The vertical, right legend represents the ratio of [**6**] to  $[\text{Zn}^{2+}]$ . For **6**  $\lambda_{\text{max}} = 408 \text{ nm}$  and for  $[\text{Zn6}]$   $\lambda_{\text{max}} = 457 \text{ nm}$ . The isosbestic points occur at 304, 346, 370 and 429 nm.

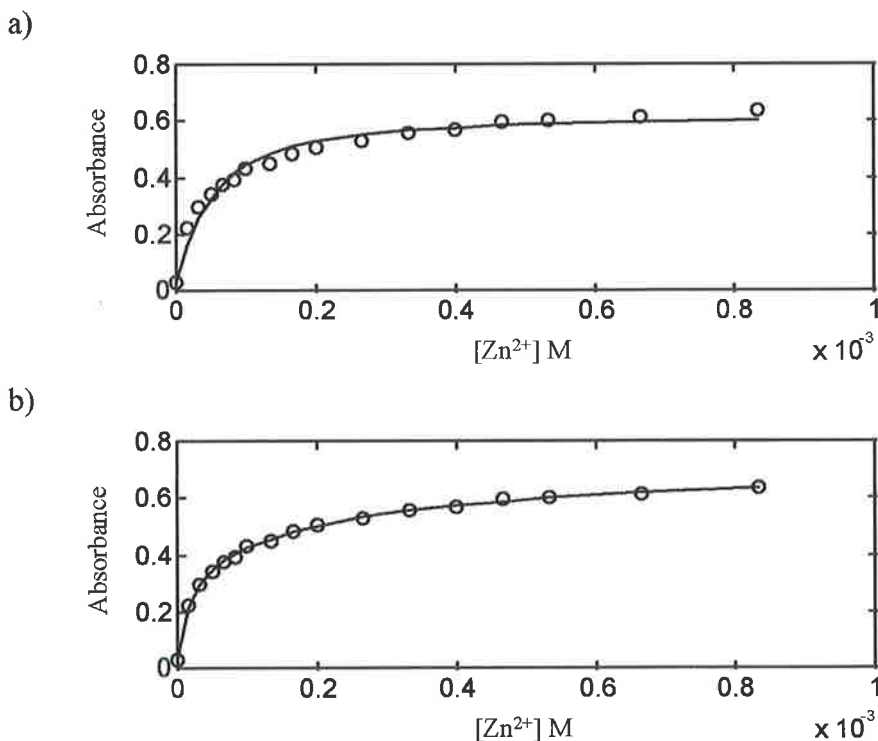


**Figure 2.37:** A graphical representation of the data fitting of Figure 2.36 at  $\lambda = 460 \text{ nm}$ . Graph a) is the fit for a 1:1 metal ion:ligand model and b) for a 1:2 metal ion:ligand model. The circles represent the experimentally obtained data and the solid line represents the best fit.

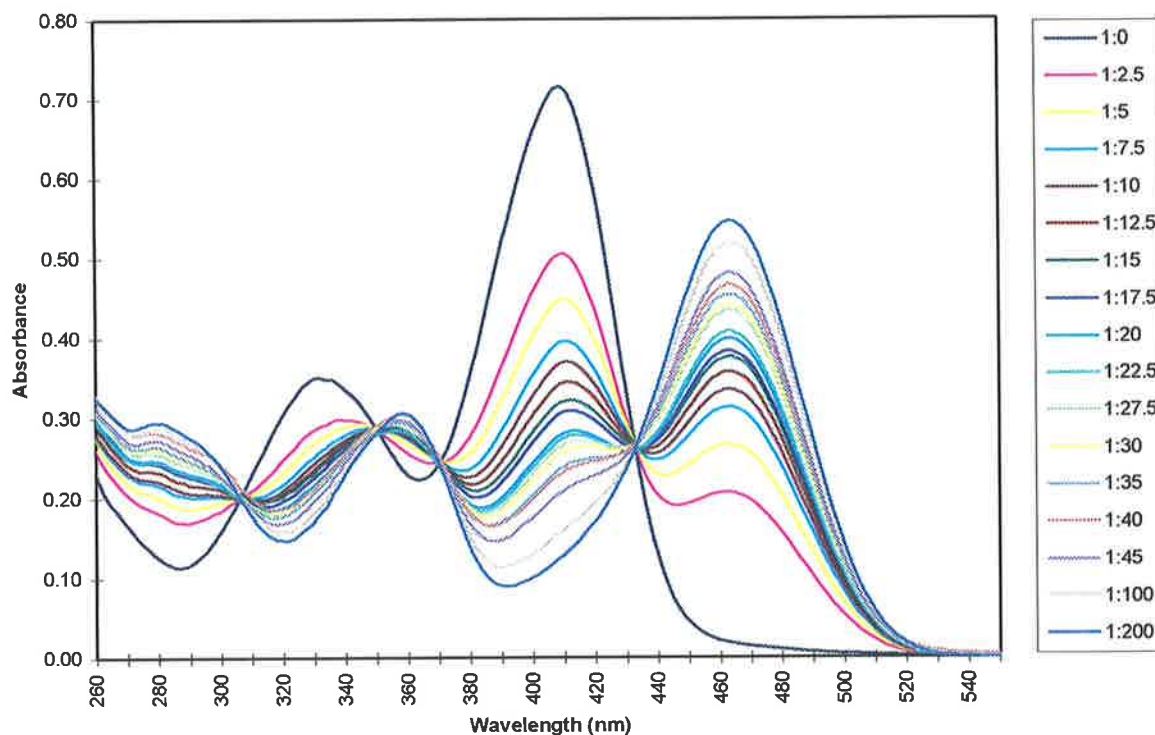


**Figure 2.38:** UV-visible absorption spectra of 3-hydroxy-2'-thiomethoxyflavone (**6**) at  $3.33 \times 10^{-5} \text{ M}$  in  $[\text{H}^+] = 1.0 \times 10^{-5} \text{ M}$  with varying concentrations of  $\text{Cd}(\text{ClO}_4)_2$  as shown in Appendix B, Table B.16. The vertical, right legend represents the ratio of [**6**] to  $[\text{Cd}^{2+}]$ . For **6**  $\lambda_{\text{max}} = 410 \text{ nm}$  and for  $[\text{Cd6}]$   $\lambda_{\text{max}} = 464 \text{ nm}$ . The isosbestic points occur at 306, 350, 370 and 433 nm.

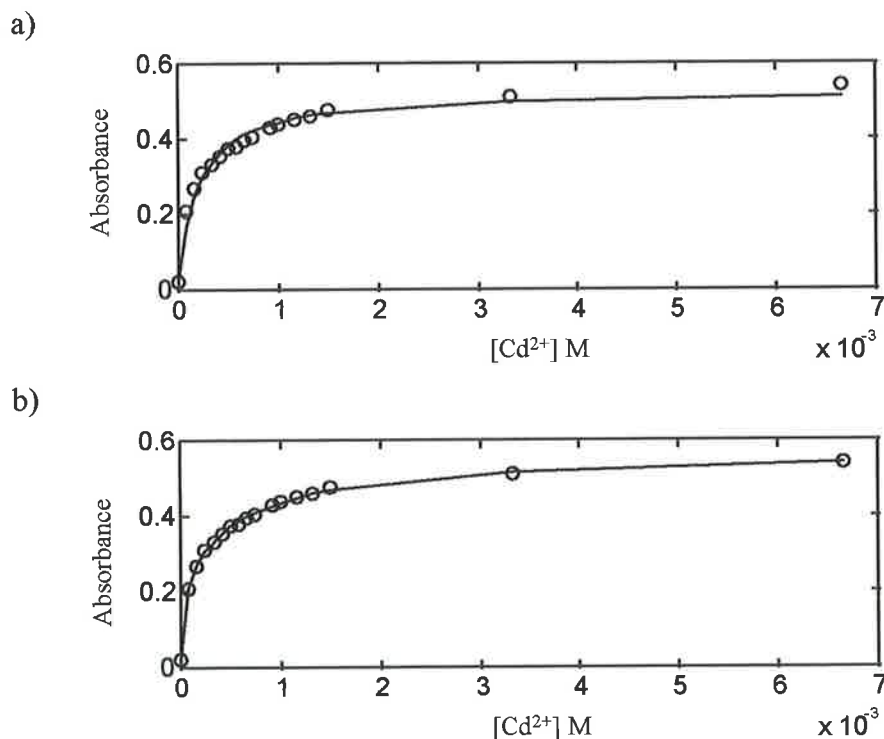


**Figure 2.39:** A graphical representation of the data fitting of Figure 2.38 at  $\lambda = 460 \text{ nm}$ . Graph a) is the fit for a 1:1 metal ion:ligand model and b) for a 1:2 metal ion:ligand model. The circles represent the experimentally obtained data and the solid line represents the best fit.

ligand decomposing in the presence of ultraviolet or visible light. To test this hypothesis a series of experiments were performed in which the UV-visible absorption spectra of a solution of the free ligand **7** exposed to sunlight and a solution of the free ligand **7** stored in the dark were recorded. The absorption spectrum of each solution was recorded at 20 minute intervals for a total of 60 minutes as described in section 6.7.3. After the 60 minute period the sunlight exposed solution containing ligand **7** was totally devoid of colour and the flavanoid chromophore was no longer present as indicated by the UV-visible absorption spectra shown in Figure 2.40. The solution containing ligand **7**, which was stored in the dark, showed little change in the spectrum recorded at 20 minute intervals over 60 minutes indicating that ultraviolet or visible light was the cause of ligand decomposition (Figure 2.41). To investigate whether the  $\text{Pb}^{2+}$ -ligand **7** complex was also unstable in solution in the presence of light, the above experiments were repeated on a solution of ligand **7** with  $\text{Pb}^{2+}$  at a concentration of 2 times the ligand concentration. The spectra are shown in Figure 2.42 and 2.43. As with the free ligand, the absorbance of the complex exposed to light was significantly reduced after 60 minutes while the spectrum of the complex stored in the dark was unchanged. Due to the instability of ligand **7** in solution as the free ligand or in the metal-ligand complex, no further work was carried out with this ligand.

In summary, stability constants have been determined for ligands **4**, **5** and **6** with the metal ions  $\text{Pb}^{2+}$ ,  $\text{Al}^{3+}$ ,  $\text{Zn}^{2+}$  and  $\text{Cd}^{2+}$ , under both conditions of  $[\text{H}^+] = 10^{-2} \text{ M}$  and  $[\text{H}^+] = 10^{-5} \text{ M}$ . Greater  $\log K_{\text{stab}}$  values were obtained for the thioflavone ligand **6** complexes as those compared with the oxygenated ligands **4** and **5** metal complexes. The higher  $\log K_{\text{stab}}$  values for these complexes may be due in part to the presence of the soft donor atom sulfur and possibly the theoretically larger bite size of ligand **6** as indicated by molecular modelling (Table 2.4 page 30). The general stability order determined for complexes of the ligands **4** and **5** formed with the listed series of metal ions is  $\text{Pb}^{2+} > \text{Al}^{3+} > \text{Zn}^{2+} > \text{Cd}^{2+}$  at the lower acid concentration conditions and  $\text{Al}^{3+} > \text{Pb}^{2+}$  at the higher acid concentration conditions. For ligand **6** the stability order is  $\text{Pb}^{2+} > \text{Zn}^{2+} > \text{Cd}^{2+}$ . To further investigate the potential ability for these metal-ligand complexes to act as fluorescent probes, fluorescence measurements were required.

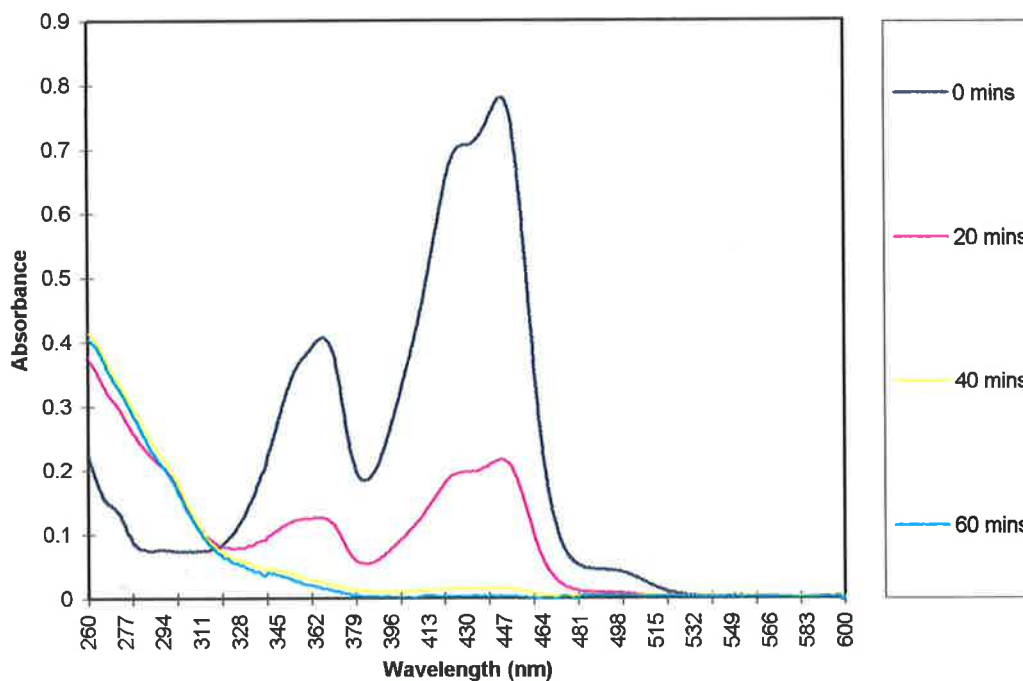


**Figure 2.40:** The absorbance spectra of a solution of ligand 7 exposed to light which were recorded over 60 minutes with 20 minute intervals as indicated in the vertical, right legend.

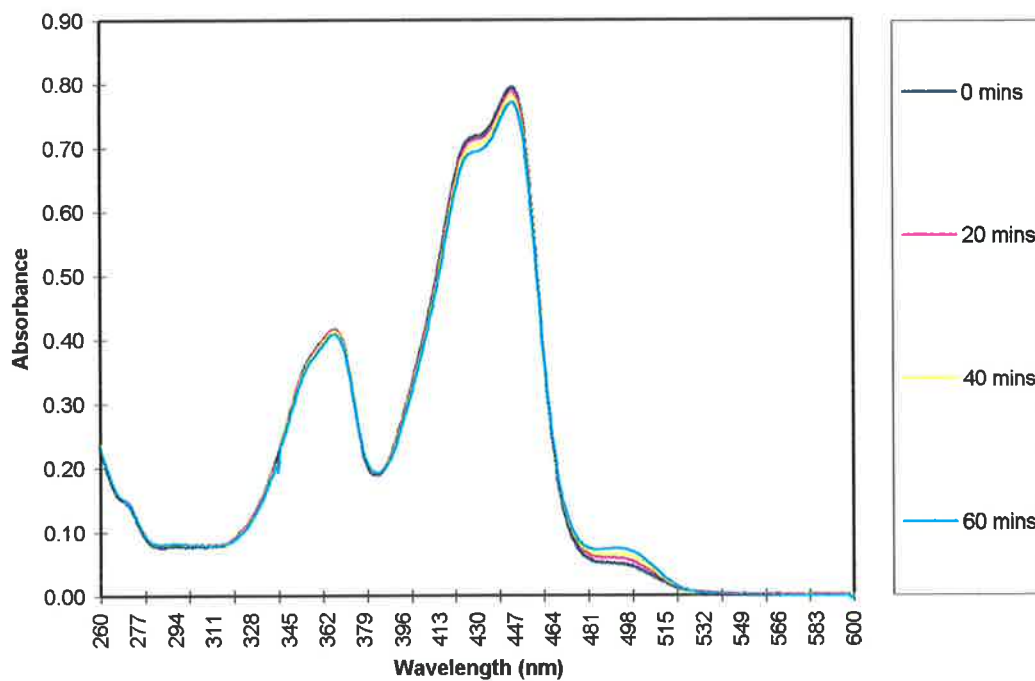


**Figure 2.41:** The absorbance spectra of a solution of ligand 7 stored in the dark which were recorded over 60 minutes with 20 minute intervals as indicated in the vertical, right legend.



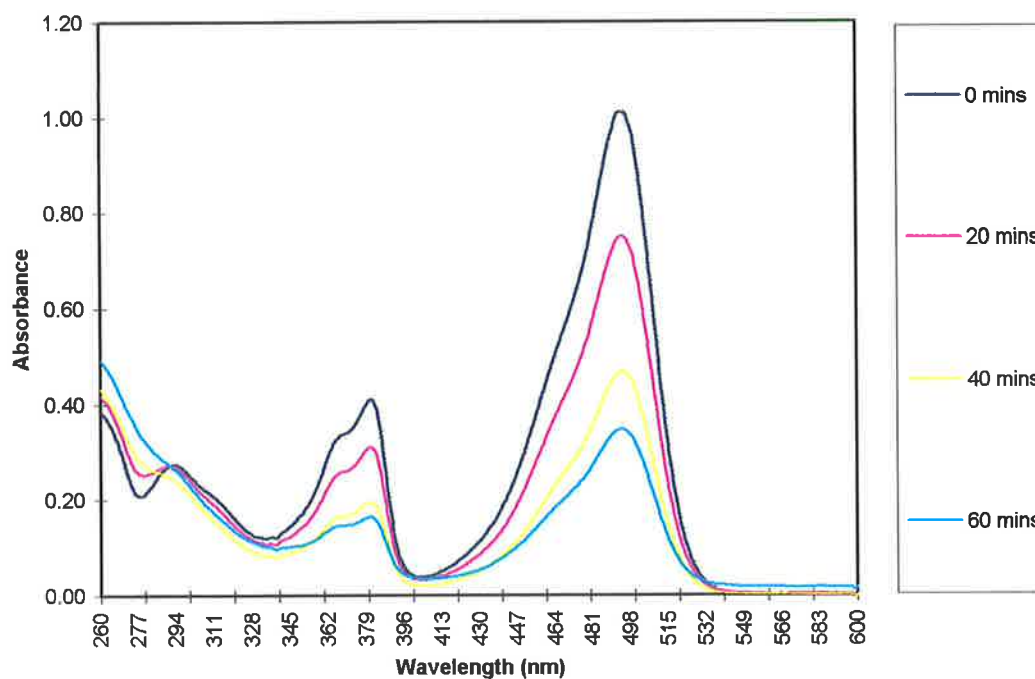


**Figure 2.42:** The absorbance spectra of a solution of the  $Pb^{2+}$ -ligand 7 complex exposed to light which were recorded over 60 minutes with 20 minute intervals as indicated in the vertical, right legend.

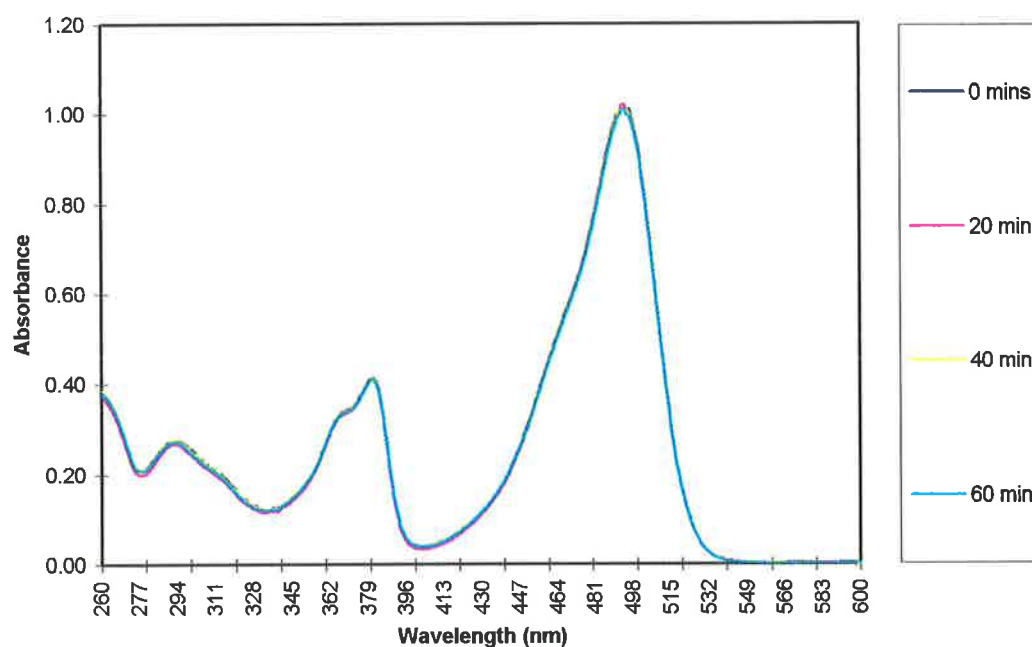


**Figure 2.43:** The absorbance spectra of a solution of the  $Pb^{2+}$ -ligand 7 complex stored in the dark which were recorded over 60 minutes with 20 minute intervals as indicated in the vertical, right legend.

## 2.5 Fluorescence

### 2.5.1 Principles of Fluorescence

When ultraviolet or visible radiation encounters an organic molecule, an interaction between the radiation and the electrons of the molecule may take place. This absorption process is very specific and results in an attenuation of the radiation and an increase in the energy of the electrons of the organic molecule. This may be regarded as the promotion of one of the paired outer or bonding electrons from a singlet ground electronic energy state,  $S_0$ , into one of a higher energy orbit,  $S_{1,2,\dots,n}$ .<sup>56</sup> These levels are separated by discrete energy increments,  $\Delta E$ , which are determined by the nature of the organic molecule, and only a photon of energy  $\Delta E$  can be absorbed.<sup>56</sup> This photon and its energy is related to the frequency and wavelength of radiation by:

$$\Delta E = h\nu = hc/\lambda \quad (\text{eqn 2.18})$$

where  $h$  is Planck's constant ( $6.63 \times 10^{-34}$  Js),  $c$  is the velocity of light ( $2.998 \times 10^8$  ms<sup>-1</sup>) and  $\lambda$  is in m.<sup>56</sup>

When light is absorbed by an organic molecule, and one of the paired electrons within that molecule has been excited from its ground state to one of the various vibrational levels, several processes can occur. Firstly the excited molecule will vibrate more vigorously and possibly collide with other molecules transferring excess energy in the form of vibrational energy or heat until it has relaxed to its first excited singlet state,  $S_1$ . This thermal equilibration is called internal conversion and occurs in about  $10^{-12}$  seconds.<sup>74</sup>

Once in the first excited single state, the organic molecule may further undergo internal conversion to the ground singlet state,  $S_0$ .<sup>74</sup> However, if the energy gap between the first excited singlet state, and the ground singlet state is relatively large, the excess energy will dissipate as a quantum of light by either the process of fluorescence or phosphorescence.<sup>74</sup>

Fluorescence is the radiative decay, or the emission of light, which results from the return of the first excited singlet state electron to the ground state in a molecule. Such transitions are quantum mechanically 'allowed' and occur over a lifetime of approximately  $10^{-8}$  seconds.<sup>74</sup>

Phosphorescence is also a process by which energy is released from a molecule in the form of light. The difference between fluorescence and phosphorescence is that phosphorescence occurs through a quantum mechanically 'forbidden' process known as intersystem crossing. Intersystem crossing involves a spin state change in an electron as the molecule goes from its first excited singlet state to its first triplet state,  $T_1$ .<sup>74</sup> In a singlet excited state, the electron in the higher-energy orbital has the opposite spin orientation to that of the second electron in the lower energy orbital. These two electrons are said to be paired. In a triplet state these electrons are unpaired, that is, their spins have the same orientation. Therefore transitions from a triplet excited state to a singlet ground state are said to be 'spin forbidden' and the emission of energy as phosphorescent light is slow.<sup>74</sup> Typical phosphorescent lifetimes range from milliseconds to seconds.<sup>74</sup>

The terms internal conversion, fluorescence, phosphorescence and intersystem crossing are illustrated in Figure 2.44.<sup>75</sup>

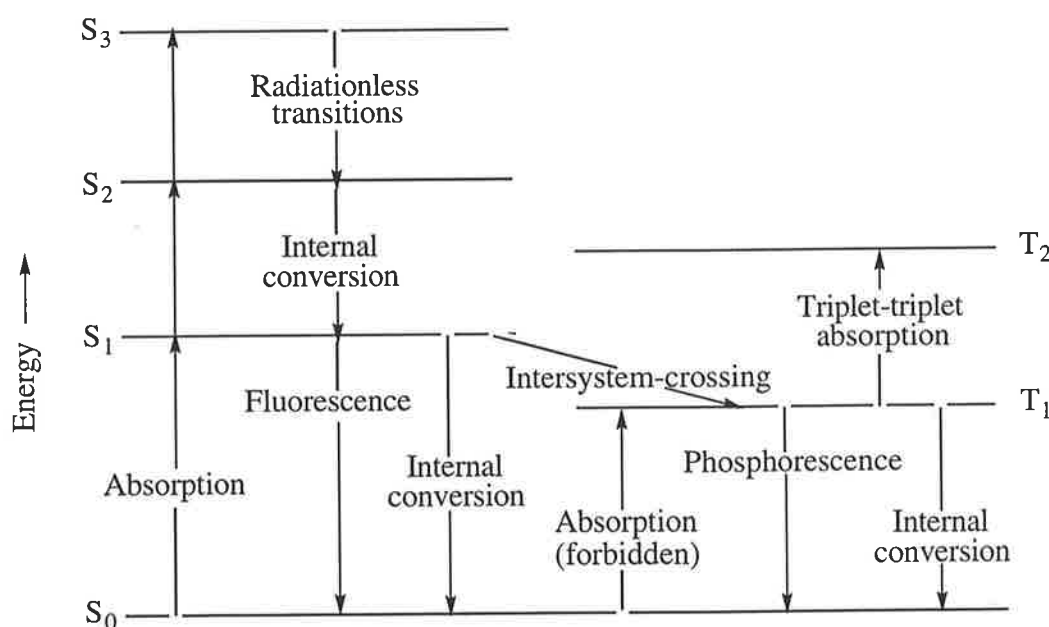


**Figure 2.44:** Schematic state energy level diagram: *S* is singlet and *T* is triplet. The  $S_0$  state is the ground state and the subscript numbers identify individual states.

### 2.5.2 Fluorescence of Organic Molecules

Fluorescence, as explained previously, is the result of the rapid emission of light energy from a molecule which has become excited by light absorption. In order to fluoresce, therefore, a compound must absorb light. However, relatively few light absorbing organic molecules are

strongly fluorescent either in the solid state or in solution.<sup>76</sup> Much of the light energy absorbed by a molecule may be lost by processes other than fluorescence, including internal and external conversions. Energy loss by internal conversions arises either because of intersystem crossing from the excited singlet to the triplet state or through predissociation (the disruption of the chemical bonds of the compound).<sup>76</sup> Energy loss by external conversions (quenching) occurs through collisions with other molecules, and may result in the radiationless transfer of energy to the colliding molecules or the production of heat. Therefore the extent to which an organic molecule will fluoresce depends upon how energy is dissipated from the molecule, which in turn depends upon its electronic and molecular structure and also its environment.

Fluorescent properties of organic molecules are often very sensitive to slight structural modification.<sup>76</sup> The structural requirements for the fluorescence of an organic molecule are dependent on three main factors; the nature of the carbon skeleton, the geometrical arrangement of the molecule, and the type and position of any substituents.<sup>76</sup>

The carbon skeleton - All fluorescent molecules contain a conjugated system of double bonds. When the extent of conjugation is increased in a molecule the absorption is shifted towards the red end of the spectrum and therefore so is the fluorescence wavelength (thus reducing the possibility of predissociation which often occurs in molecules which absorb high energy frequencies) and the delocalisation of the  $\pi$  electrons is enhanced.<sup>76</sup> This increase in the number and delocalisation of the  $\pi$  electrons often results in an increase in fluorescence intensity.<sup>76</sup>

The geometrical arrangement: - In addition to the requirement for a conjugated system of double bonds, certain geometrical considerations are also important. Planarity of the conjugated system appears to be essential for maximum fluorescence. When the planarity of a system is destroyed through steric hindrance, the free delocalisation of the  $\pi$  electrons will be decreased resulting in a loss of fluorescence.<sup>76</sup> Molecular rigidity is also necessary for maximum fluorescence. In a non-rigid molecule the absorbed energy can be readily dissipated as heat through thermal motions. This need for molecular rigidity explains the greater fluorescence of cyclic systems as compared to linear chain systems.<sup>76</sup>

The type and position of substituents: - The extent to which the fluorescence properties of a conjugated system are modified by a particular substituent depends largely on the change produced in  $\pi$  electron delocalisation. Substituents which enhance  $\pi$  electron delocalisation will normally increase fluorescence, while those which decrease it will reduce fluorescence. Thus, electron donating (positively mesomeric) substituents tend to enhance fluorescence while electron withdrawing substituents tend to diminish or abolish it.<sup>76</sup> Wherever atoms which have a large magnetic field associated with them (eg bromine and iodine) occur as substituents, fluorescence will also be reduced. The presence of bromine, iodine or heavy metal substituents in either a mono or poly-substituted aromatic compound invariably leads to a reduction in fluorescence by encouraging intersystem crossing from the excited singlet to the triplet states.<sup>76</sup> This effect is known as the heavy atom effect and is brought about *via* spin-orbit coupling.<sup>77</sup>

In general, it appears that the fluorescent magnitude depends upon the molecular rigidity which decreases the vibrational degrees of freedom. This is why aliphatic compounds, with their non-rigid molecular skeletons and their many degrees of vibrational freedom are mostly non-fluorescent. Rigidity of organic compounds is achieved through the conjugation of double bonds and formation of ring systems. This is why many aromatic molecules are fluorescent. The more extensive the conjugation in a molecule, the greater is the delocalisation of the  $\pi$  electrons within the molecule and the more fluorescent the molecule becomes.

### 2.5.3 Fluorescent Probe Specifications for the Detection of Lead(II)

In addition to the previously mentioned general structural requirements of fluorescent organic molecules, there exists a number of other properties desirable for molecules to be useful as fluorescent probes for the detection and measurement of  $\text{Pb}^{2+}$  in biological and aqueous systems. Along with the required specificity to be a useful probe for  $\text{Pb}^{2+}$  the ligand also needs to produce a highly fluorescent species once chelated to  $\text{Pb}^{2+}$ . Normally a fluorescent organic ligand will lose its tendency to fluoresce when it forms a complex with divalent metal ions from the first transition series. This is because these metal ions (with the exception of  $\text{Zn}^{2+}$ ) have partially filled  $d$  orbitals and can absorb the excess excited energy of the ligand by excitation of a  $d$  electron to a higher energy state.<sup>75</sup> This process is known as a  $d-d$  transition

and quenches the fluorescence of the attached ligand. Although  $\text{Pb}^{2+}$  has filled  $d$  orbitals and therefore tends not to quench *via* this mechanism,  $\text{Pb}^{2+}$  is a large atomic weight ion with a large ionic radius and therefore tends to quench *via* the heavy metal or heavy atom effect (Section 2.5.2). Although  $\text{Pb}^{2+}$  has the tendency to quench the fluorescence of ligands, examples of  $\text{Pb}^{2+}$  fluorescence enhanced probes have been reported in the literature (see Section 1.4). Therefore  $\text{Pb}^{2+}$  has the potential to enhance the fluorescence of a ligand if the formation of a complex tends to lock the ligand in a geometry of greater rigidity, reducing the number of degrees of vibrational freedom of the ligand. This is provided that on forming a complex, the delocalisation of the  $\pi$  electrons is not adversely affected, for example, by the breakdown of planarity of the conjugated system of the ligand.

Another probe specification is that the fluorescent properties of the unbound ligand must be significantly different from that of the  $\text{Pb}^{2+}$  complex to enable differentiation between the two. For a ligand to be useful as a fluorescent probe for  $\text{Pb}^{2+}$ , it is desirable to be able to measure the fluorescence of the  $\text{Pb}^{2+}$ -ligand complex without interference from any uncomplexed ligand which may be present. Thus, it is preferable that the free and coordinated ligand have differing fluorescence emission spectra. Ideally there should be minimal fluorescence of the free ligand at an emission maxima of the complexed ligand. The optimum situation is where the  $\text{Pb}^{2+}$  complexed ligand is highly fluorescent and the unbound ligand is non-fluorescent, or at least weakly fluorescent, with emission maxima different from those of its  $\text{Pb}^{2+}$  complex. However, if the unbound ligand is highly fluorescent and only  $\text{Pb}^{2+}$  coordinates to this ligand quenching its fluorescence,  $\text{Pb}^{2+}$  may be detected through the decreased fluorescence.

If the ligand has a tendency to form complexes with other metal ions present in a sample, then these complexes formed should have differing emission spectra from that of the  $\text{Pb}^{2+}$  complexed ligand. For the ligand to be a useful fluorescent probe for  $\text{Pb}^{2+}$ , no interference from other metal complexes formed by the ligand should occur during fluorescence measurements of the  $\text{Pb}^{2+}$ -ligand complex. Once again, the optimum situation would be where metal complexes of the ligand other than those with  $\text{Pb}^{2+}$  are non-fluorescent or at least weakly fluorescent with emission maxima different from those of its  $\text{Pb}^{2+}$ -ligand complex.

The ligands **4** - **7** are not  $\text{Pb}^{2+}$  specific as they chelate to other metal ions as well as  $\text{Pb}^{2+}$  (Section 2.3). The fluorescence spectra of these ligands were measured along with those of the various metal complexes, which they form. A comparison of these results was expected to give more information on the suitability of these ligands as fluorescent probes for measuring  $\text{Pb}^{2+}$  concentrations, and to provide a basis for the design of more specific probes.

#### 2.5.4 Results and Discussion

Initially, to determine which metal ions produce fluorescent complexes upon coordination with ligands **4** to **7**, qualitative visual fluorescence measurements were performed. The visual tests required the use of the stock solutions of the free ligands **4** - **7** under the conditions of  $[\text{H}^+] = 10^{-5}$  M used in the stability constant determinations (Section 2.4). The source of light was from a 360 nm UV lamp. For each of the ligands tested, nine solutions were prepared consisting of 10  $\text{cm}^3$  of the free ligand solution to which was added 1  $\text{cm}^3$  of one of the nine aqueous metal ion solutions tested. The metal ion series consisted of  $\text{Pb}^{2+}$ ,  $\text{Mg}^{2+}$ ,  $\text{Ca}^{2+}$ ,  $\text{Co}^{2+}$ ,  $\text{Cu}^{2+}$ ,  $\text{Ni}^{2+}$ ,  $\text{Zn}^{2+}$ ,  $\text{Cd}^{2+}$  and  $\text{Al}^{3+}$  as perchlorate salts. Each metal type was chosen as for reasons explained in Section 2.2. Each of the metal ion-ligand solutions were placed under the lamp in a dark room for the observation of fluorescence by the naked eye. No fluorescence for any of the tested ligands with any of the divalent metal ions from the transition series except for  $d_{10} \text{Zn}^{2+}$  was observed. For the ligands **4** and **5**, only the solutions containing  $\text{Pb}^{2+}$ ,  $\text{Al}^{3+}$ ,  $\text{Cd}^{2+}$  and  $\text{Zn}^{2+}$  produced fluorescent chelates as did  $\text{Pb}^{2+}$ ,  $\text{Cd}^{2+}$  and  $\text{Zn}^{2+}$  for the ligands **6** and **7**. The ligands **4** and **5** produced blue fluorescent chelates of which the  $\text{Al}^{3+}$  complexes were the most fluorescent, and the ligands **6** and **7** produced green fluorescent chelates. From these results it was evident that quantitative fluorescence measurements were required for the complexes of ligands **4** - **7** with the metal ions  $\text{Pb}^{2+}$ ,  $\text{Al}^{3+}$ ,  $\text{Cd}^{2+}$  and  $\text{Zn}^{2+}$ . Magnesium(II) was also added to this list of metal ions due to its biological significance and the literature reports of fluorescent flavone complexes of  $\text{Mg}^{2+}$ .<sup>36,38,60,78</sup>

To allow comparisons to be made between the stability constants of the metal ion complexes of the ligands **4** - **7** and the relative fluorescence levels of these complexes, the quantitative fluorescence measurements were performed using the same solvent, ionic strength and pH conditions as those used to determine the stability constants as described in Section 2.3. The

only differences in the conditions between the relative fluorescence and stability constant measurements were the concentrations at which the ligands and the metal-ligand complexes were measured. Since fluorescence spectroscopy is generally a more sensitive technique than ultraviolet absorption spectroscopy, lower concentrations of the studied species were required.

#### **Aluminium(III)-Ligand 4 Complex (in solutions containing $[H^+] = 10^{-2}$ M)**

Ligand 4 was the first ligand to be investigated in solutions containing  $[H^+] = 10^{-2}$  M. Since  $Al^{3+}$  produced the most fluorescent chelate with ligand 4 from the qualitative experiments, the  $Al^{3+}$ -ligand 4 complex was used to determine the required concentration of ligand 4 to produce a significant relative fluorescence level. The sample was excited at 385 nm (which is the maximum absorbance wavelength of the  $Al^{3+}$ -ligand 4 complex as determined in Section 2.3) and produced a maximum emission at  $\lambda = 454$  nm. A relative fluorescence value of 346 was determined for ligand 4 at a concentration of  $1.00 \times 10^{-6}$  M (50 times less than the concentration used for stability constant determinations) with  $Al^{3+}$  at a concentration of  $2.5 \times 10^{-6}$  M.

To determine the stability of ligand 4 with  $Al^{3+}$  in the excited state, a series of fluorescence spectra were recorded of the ligand in the presence of various concentrations of  $Al^{3+}$ . Nineteen solutions were prepared with ligand 4 in a concentration of  $1.00 \times 10^{-6}$  M (as determined from above) in each and  $Al^{3+}$  in concentrations ranging from  $1.25 \times 10^{-7}$  M to  $5.00 \times 10^{-6}$  M as described in Section 6.8.1. The concentrations of  $Al^{3+}$  in each solution are listed in Appendix B. The fluorescence spectra (400 - 600 nm) of the nineteen solutions were measured in succession with an incident wavelength of  $\lambda = 385$  nm and the results are illustrated in Figure 2.45.

To be able to compare the stability of the  $Al^{3+}$ -ligand 4 complex in the ground state (as determined by ultraviolet absorption spectroscopy) and in the excited state, the fluorescence spectra mentioned above were used to calculate a stability constant in conjunction with the MATLAB computer program 'Specfit'. As described in Section 2.4.4, the fluorescence emission values from Figure 2.45 in the range 440 - 500 nm were collated and submitted to 'Specfit' to produce a  $\log K_{stab} = 6.31$ . A graphical representation of the fitting is shown in Figure 2.46. In comparison to the value obtained *via* ultraviolet absorption spectroscopy ( $\log$



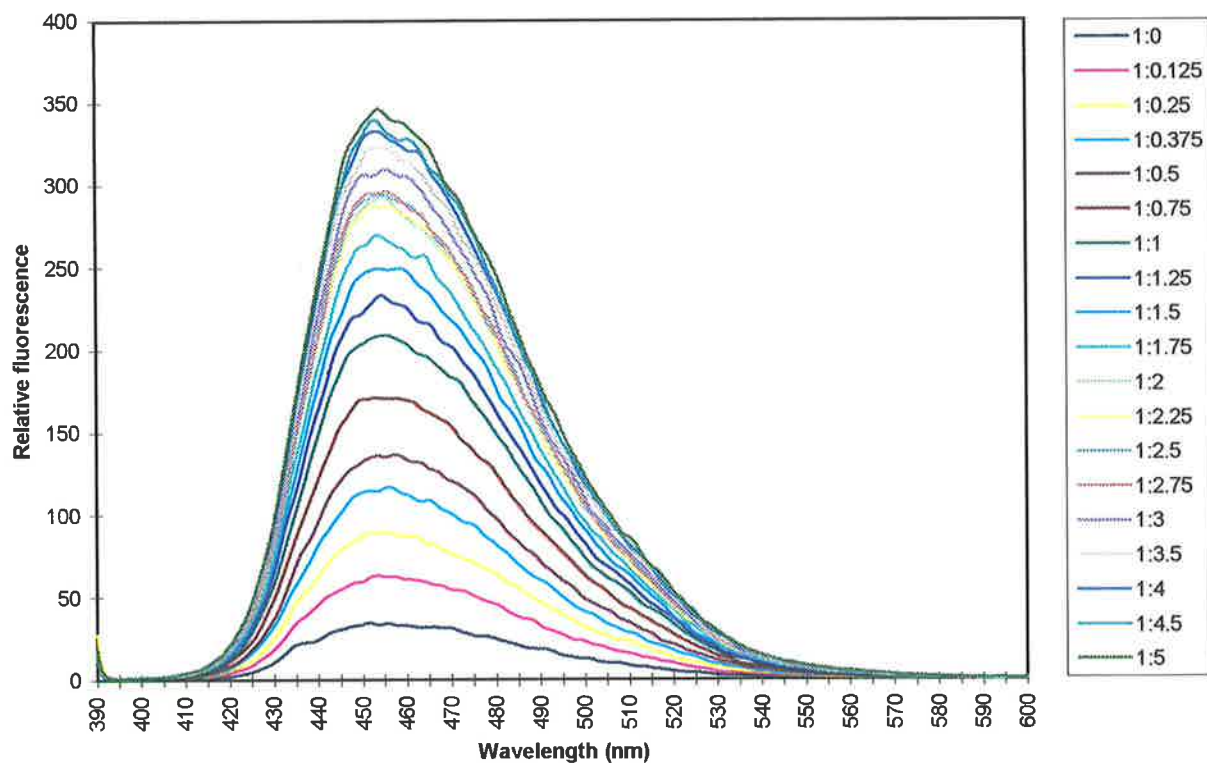


**Figure 2.45:** Fluorescence spectra of ligand **4** at a concentration of  $1.0 \times 10^{-6} \text{ M}$  in  $[\text{H}^+] = 1.0 \times 10^{-2} \text{ M}$  with varying concentrations of  $\text{Al}(\text{ClO}_4)_3$  as shown in Appendix B, Table B.17. The vertical, right legend represents the ratio of  $[\mathbf{4}]$  to  $[\text{Al}^{3+}]$ .

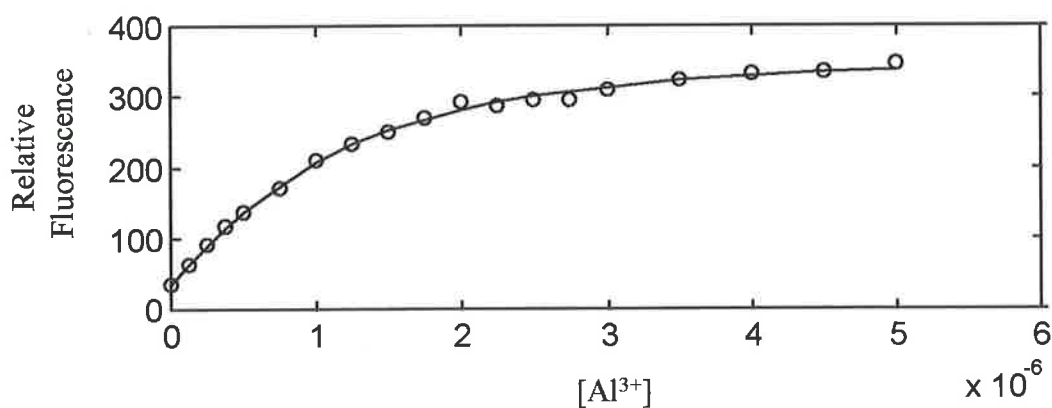


**Figure 2.46:** A graphical representation of the data fitting of Figure 2.45 at  $\lambda = 455 \text{ nm}$ . The circles represent the experimentally obtained data and the solid line represents the best fit.

$K_{\text{stab}} = 4.51$ ), the value from fluorescence spectroscopy ( $\log K_{\text{stab}} = 6.31$ ) is considerably larger indicating that the excited state of the complex is more stable. Such changes in the physical properties of molecules upon electronic excitation is not uncommon as changes in the  $pK_a$  of certain compounds in the excited state compared with the ground state have been reported.<sup>75</sup> According to the Franck-Condon principle, the absorption of light occurs in about  $10^{-15}$  seconds, a time too short for significant displacement of nuclei, but evidently adequate for the redistribution of electrons.<sup>74</sup> For example, 2-naphthylamine shows a change from  $pK_a = 4.1$  in the ground state to  $-2$  in the excited state, and thus becomes a considerably stronger acid.<sup>75</sup>

In order to compare the relative fluorescence of the ligand **4** complexes formed with the selected metal ions, fluorescence spectra of  $\text{Pb}^{2+}$ ,  $\text{Cd}^{2+}$ ,  $\text{Zn}^{2+}$  and  $\text{Mg}^{2+}$  with ligand **4** were required. To ensure that any observed fluorescence was due to complex formation, each of the metal ions tested were used in a 100 fold concentration excess to that of ligand **4** ( $[\text{4}] = 1 \times 10^{-6}$  M, as used with  $\text{Al}^{3+}$ ). Again the incident wavelength used was  $\lambda = 385$  nm, so that the emission intensities of the complexes could be compared to that of  $\text{Al}^{3+}$ , and the emission wavelength range used was 400 - 600 nm. The results are tabulated in Table 2.7 and the spectra are presented in Appendix C. None of the metal ions tested showed any significant fluorescence upon complexation when compared to the fluorescence of the uncomplexed ligand, except for  $\text{Al}^{3+}$ . This suggests that under highly acidic conditions ligand **4** produces high fluorescence levels only when it chelates to  $\text{Al}^{3+}$ . To further investigate the selective fluorescence of ligand **4** with  $\text{Al}^{3+}$ , the fluorescence spectra of ligand **4** with the same list of metal ions under the lower acid concentration conditions of  $[\text{H}^+] = 10^{-5}$  M were determined.

#### **Ligand 4 Complexes in $[\text{H}^+] = 10^{-5}$ M**

The fluorescence spectra of ligand **4** with the series of metal ions were determined, with ligand **4** at a concentration of  $1 \times 10^{-6}$  M in  $[\text{H}^+] = 10^{-5}$  M. Under these conditions,  $\text{Zn}^{2+}$  and  $\text{Pb}^{2+}$  showed significant fluorescence enhancement upon complexation to ligand **4** with respective relative fluorescence levels of 64 and 37 (as compared to 1 for the uncomplexed ligand) (Table 2.6). The metal ions  $\text{Cd}^{2+}$  and  $\text{Mg}^{2+}$  produced no significant change in the fluorescence of ligand **4**.

**Table 2.7:** Comparison of the fluorescence intensities of the ligands 4, 5, 6 and 7 in the absence and presence of the listed metal ions.

Ligand	Metal Ion <sup>a</sup>	Excitation Wavelength (nm)	Fluorescence Maximum (nm) at [H <sup>+</sup> ] =		Maximum Emission Intensity at [H <sup>+</sup> ] =	
			10 <sup>-2</sup> M	10 <sup>-5</sup> M	10 <sup>-2</sup> M	10 <sup>-5</sup> M
(4) <sup>b</sup>		385	452	467	26	1
	Al <sup>3+</sup>	385	454	-	346	-
	Pb <sup>2+</sup>	385	453	467	34	37
	Zn <sup>2+</sup>	385	452	476	34	64
	Cd <sup>2+</sup>	385	453	467	28	4
	Mg <sup>2+</sup>	385	453	467	27	1
(5) <sup>c</sup>		416	465	474	36	4
	Al <sup>3+</sup>	416	463	-	931	-
	Pb <sup>2+</sup>	416	464	475	38	42
	Zn <sup>2+</sup>	416	463	482	33	129
	Cd <sup>2+</sup>	416	465	477	38	23
	Mg <sup>2+</sup>	416	465	474	32	3
(6) <sup>d</sup>		460	519	519	0	0
	Pb <sup>2+</sup>	460	519	519	2	5
	Zn <sup>2+</sup>	460	519	514	0	15
	Cd <sup>2+</sup>	460	519	519	0	5
(7) <sup>e</sup>		492	524	522	1	0
	Pb <sup>2+</sup>	492	524	522	47	115
	Zn <sup>2+</sup>	492	522	522	5	331
	Cd <sup>2+</sup>	492	524	529	1	69

<sup>a</sup> The concentration of all metal ions in solution were 100 times greater than the corresponding ligand concentration except for Al<sup>3+</sup> which was 2.5 times greater for 5 and 5 times greater for 4

<sup>b</sup> The concentration of ligand 4 was 1 x 10<sup>-6</sup> M.

<sup>c</sup> The concentration of ligand 5 was 3.33 x 10<sup>-7</sup> M.

<sup>d</sup> The concentration of ligand 6 was 3.33 x 10<sup>-6</sup> M.

<sup>e</sup> The concentration of ligand 7 was 2.5 x 10<sup>-6</sup> M.

Aluminium(III), which produced the most fluorescent chelate with ligand **4** at  $[H^+] = 10^{-2}$  M, did not provide reproducible fluorescence values after several measurements with ligand **4** at  $[H^+] = 10^{-5}$  M. As a result, a time dependent fluorescence experiment was performed on a solution of ligand **4** containing  $Al^{3+}$  ( $[4] = 1.0 \times 10^{-6}$  M and  $[Al^{3+}] = 5.0 \times 10^{-6}$  M), which showed a substantial decrease in fluorescence within a 2 hour time period indicating a loss or change in the flavone chromophore (Figure 2.47). To investigate further, a series of experiments were performed which measured the UV-visible absorption and relative fluorescence of ligand **4** and its  $Al^{3+}$  complex over time at the UV absorbance wavelength maxima. These experiments were expected to provide insight into the cause of the fluorescence decrease with time in the  $[H^+] = 10^{-5}$  M solutions of the ligand **4** -  $Al^{3+}$  complex. Although no loss or change in the chromophore of ligand **4** was observed during previous UV-visible absorbance measurements (ie. during stability constant determinations, see Section 2.4) the first experiment performed was the measurement of the absorbance of the  $Al^{3+}$ -ligand **4** complex ( $[4] = 5.0 \times 10^{-5}$  M and  $[Al^{3+}] = 1.0 \times 10^{-4}$  M) at 385 nm over 2 hours. The absorption of the complex at 385 nm did not vary over time as illustrated in Figure 2.48.

Since there was clearly a change in the ligand **4** chromophore during the fluorescence measurement but not during the UV-absorbance measurement of the  $Al^{3+}$ -ligand **4** complex it became apparent that a dilution factor was the cause, as the concentrations of the species present were the only factors that varied between the two measurements. Photodecomposition was unlikely since both experiments involved irradiation of the solutions at the same wavelength over the same period of time (385 nm over 2 hours). As fluorescence spectroscopy is generally a more sensitive technique than UV-visible absorbance spectroscopy the fluorescence measurements were performed with the ligand solution diluted by a factor of ten ( $Al^{3+}$  was used at a concentration of two times the ligand concentration in each case). To determine whether the dilution factor had an effect on the measurement, the absorbance of the  $Al^{3+}$ -ligand **4** complex was measured again over 2 hours with an incident  $\lambda = 385$  nm but with the ligand concentration and  $Al^{3+}$  concentration at one tenth of those used previously (ie.  $[4] = 5.0 \times 10^{-6}$  M and  $[Al^{3+}] = 1.0 \times 10^{-4}$  M). This time the absorption of the complex decreased significantly with time as illustrated in Figure 2.49.

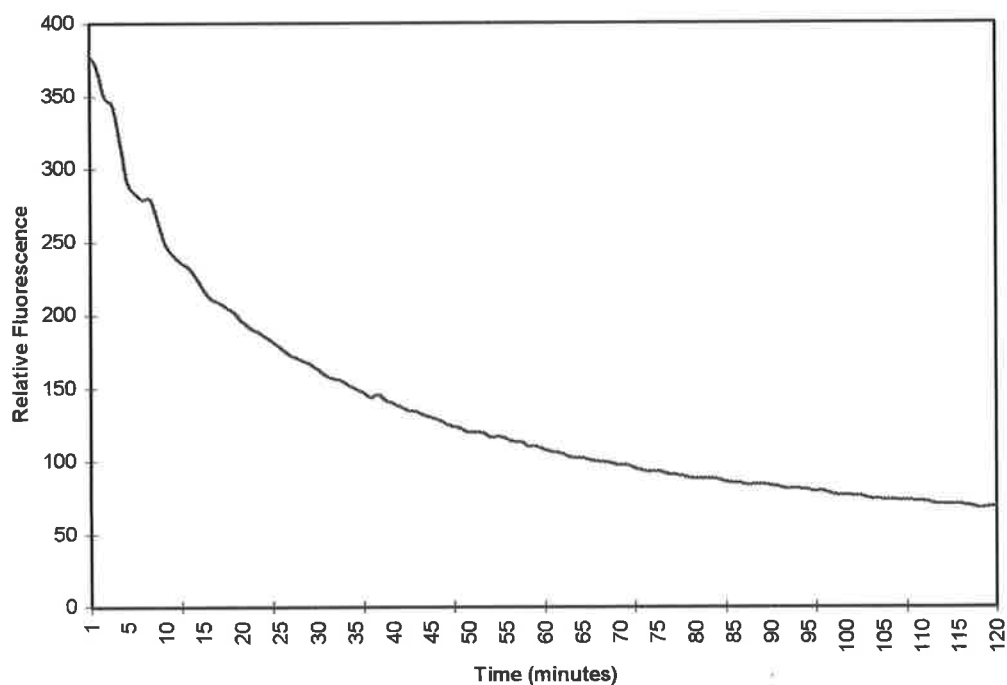


**Figure 2.47:** The relative fluorescence of the  $Al^{3+}$ -ligand 4 complex in a solution of  $[H^+] = 10^{-5} M$  measured over a period of 120 minutes with an incident wavelength of 385 nm. The concentrations of ligand 4 and  $Al^{3+}$  used were  $1.0 \times 10^{-6} M$  and  $5.0 \times 10^{-6}$  respectively.

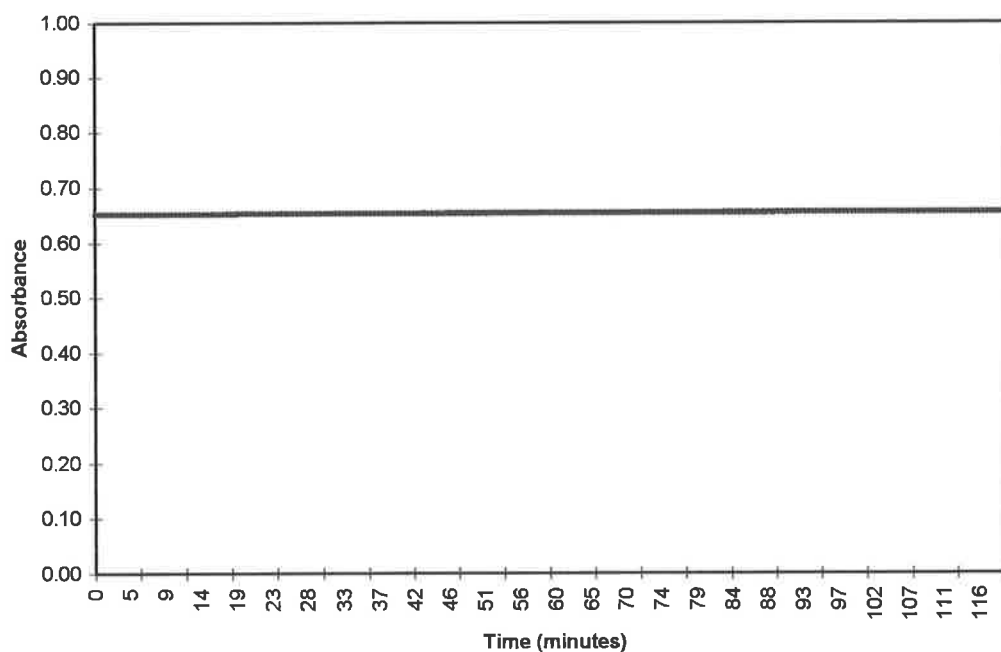
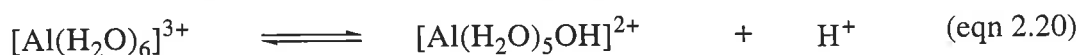
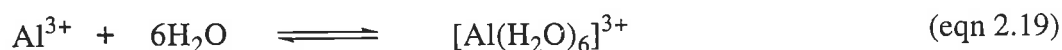
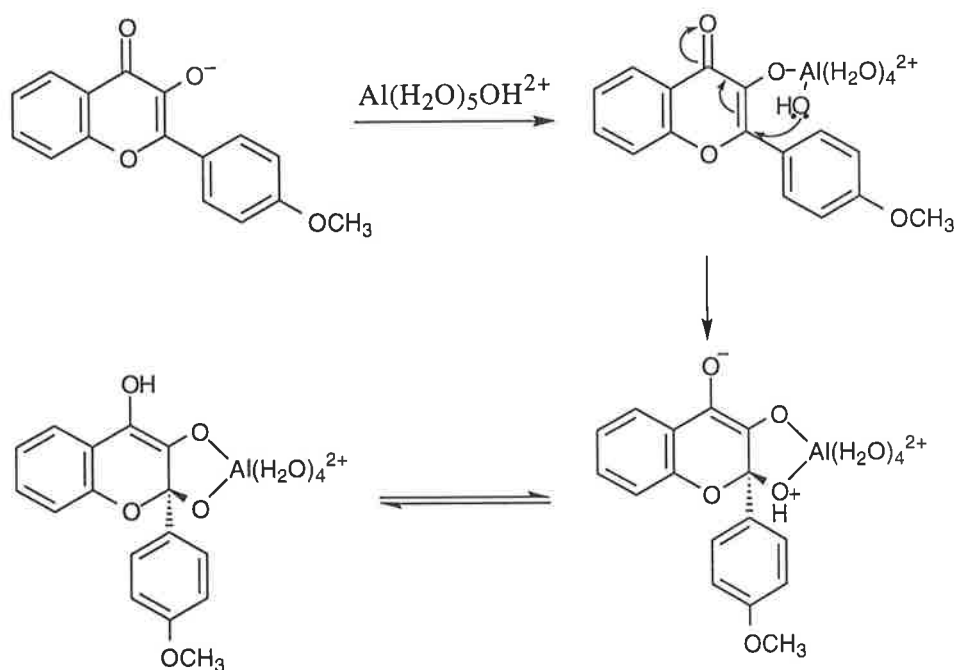


**Figure 2.48:** The absorbance of the  $Al^{3+}$ -ligand 4 complex in a solution of  $[H^+] = 10^{-5} M$  measured over a period of 120 minutes with an incident wavelength of 385 nm. The concentrations of ligand 4 and  $Al^{3+}$  used were  $5.0 \times 10^{-5} M$  and  $1.0 \times 10^{-4} M$  respectively.

It was expected that upon dilution, the pH of the solution would increase due to less contribution of  $H^+$  ions from the ligand and from the hydrated  $Al^{3+}$  ions as their concentrations had been decreased by a factor of ten. The increase in pH (or the decrease in  $[H^+]$ ) would increase the concentration of the hydroxo  $Al^{3+}$  species shifting the equilibrium to the right in eqn 2.20. Therefore it is most likely that the various hydroxo  $Al^{3+}$  species are causing the loss of conjugation and therefore the loss of fluorescence of the flavone ligands. To support this explanation, the pH of the solutions at the UV-visible concentrations ( $[4] = 1.0 \times 10^{-5}$  M and  $[Al^{3+}] = 5.0 \times 10^{-5}$  M) and at the fluorescence concentrations ( $[4] = 1.0 \times 10^{-6}$  M and  $[Al^{3+}] = 5.0 \times 10^{-6}$  M) were measured. The solution containing  $[4] = 1.0 \times 10^{-5}$  M and  $[Al^{3+}] = 5.0 \times 10^{-5}$  M had a pH of 3.73 and the solution containing  $[4] = 1.0 \times 10^{-6}$  M and  $[Al^{3+}] = 5.0 \times 10^{-6}$  M had a pH of 4.56 indicating a significant pH difference.



The hydroxo  $Al^{3+}$  species is a localised source of hydroxide which could attack flavones at the  $C_2$  position (as with a free hydroxyl anion) deconjugating the flavone system and therefore significantly reducing the fluorescence (Scheme 2.7). Similarly, the treatment of flavones with alkaline solutions opens the pyrone ring (C ring) to yield a 1,3 diketone, suggesting an attack by hydroxide at the  $C_2$  position (Scheme 2.8).<sup>34,35</sup>



Scheme 2.7

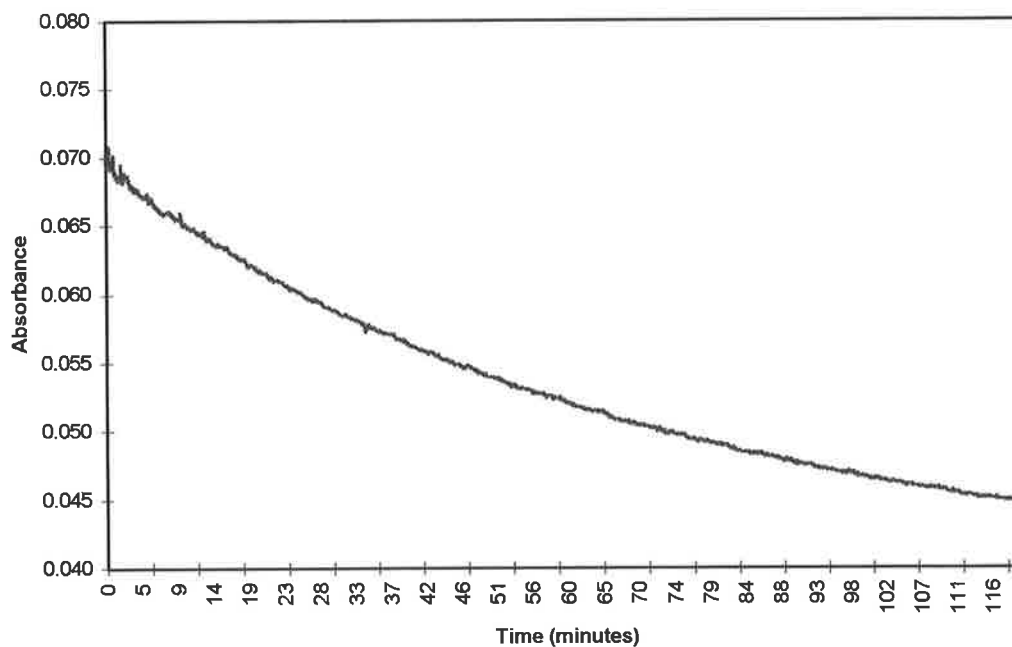


**Figure 2.49:** The absorbance of the  $Al^{3+}$ -ligand 4 complex in a solution of  $[H^+] = 10^{-5} M$  measured over a period of 120 minutes with an incident wavelength of 385 nm. The concentrations of ligand 4 and  $Al^{3+}$  used were  $5.0 \times 10^{-6} M$  and  $1.0 \times 10^{-5} M$  respectively.

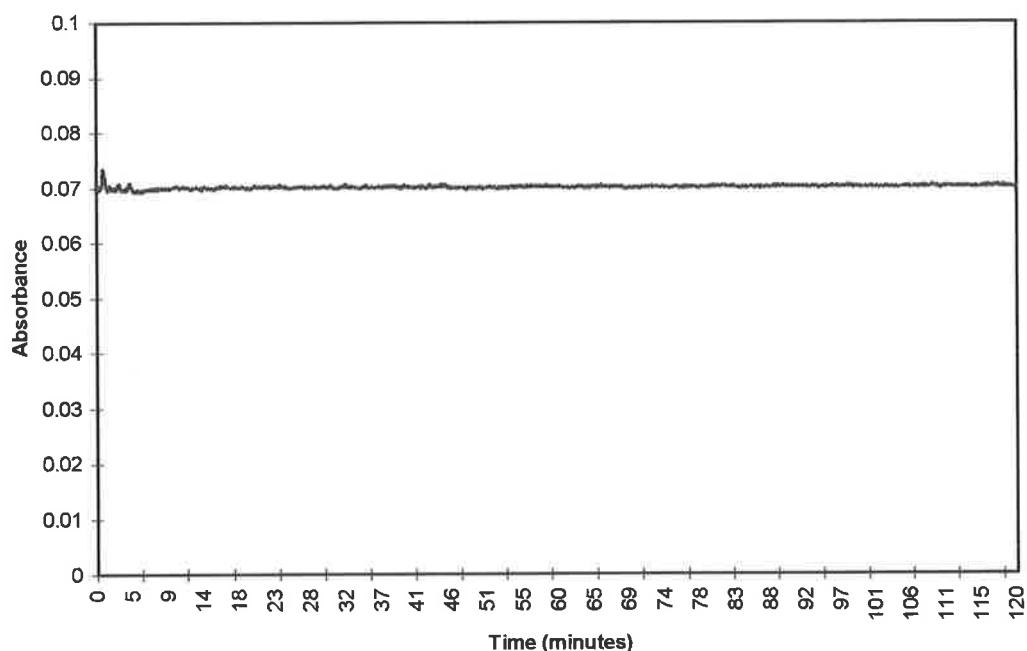
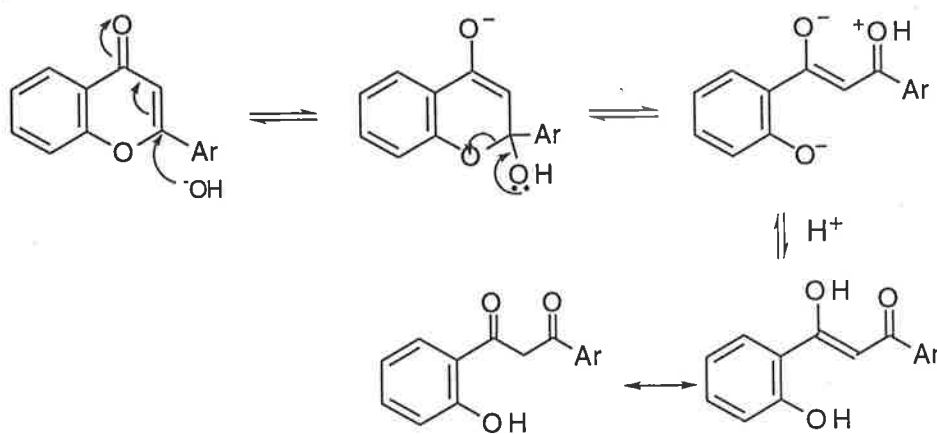


**Figure 2.50:** The absorbance of ligand 4 in a solution of  $[H^+] = 10^{-5} M$  measured over a period of 120 minutes with an incident wavelength of 330 nm. The concentration of ligand 4 was the same as that used above in Figure 2.49 ( $5.0 \times 10^{-6} M$ ).



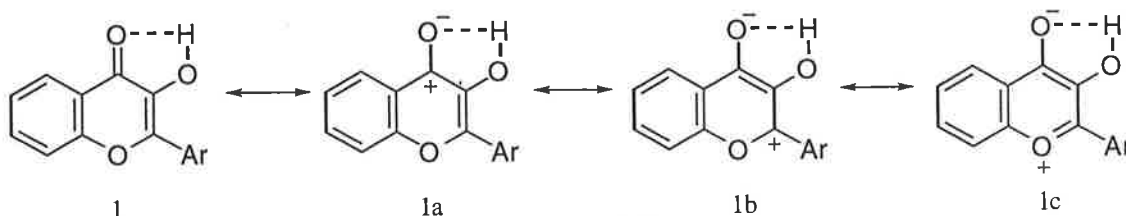
Scheme 2.8

To test this hypothesis a solution of ligand **4** without  $\text{Al}^{3+}$  present (at one tenth the usual concentration) was prepared and its UV-absorbance measured over 2 hours at its maximum absorbance wavelength (330 nm). No absorbance decrease was noted suggesting that  $\text{Al}^{3+}$  plays a key role in the loss of conjugation in ligand **4** (Figure 2.50).

Besides the reduction in fluorescence of the  $\text{Al}^{3+}$  complex, the other significant difference between the fluorescence spectra of ligand **4** measured in the high and low acid concentration was the relative fluorescence of the free ligand. Under the acidic conditions of  $[\text{H}^+] = 10^{-2}$  M, the fluorescence of the free ligand was notably larger (relative fluorescence of 26) than that of the free ligand under the conditions of  $[\text{H}^+] = 10^{-5}$  M (relative fluorescence of 1) suggesting that the presence of the acid has an electronic effect on the fluorophore which enhances fluorescence. This theory is supported by the work of Hayashi *et. al.*<sup>78</sup> In their explanation for 3-hydroxyflavones fluorescing while 3-methoxyflavones do not, Hayashi *et. al.* found that the introduction of a hydroxyl group on  $\text{C}_3$  of flavone causes a frequency shift of the carbonyl IR absorption band to a shorter wavenumber, and that methylation of the 3-hydroxyl group shifts the band back.<sup>78</sup> This phenomenon has been interpreted from a well-known observation in IR spectroscopy that hydrogen bonding to carbonyl groups causes the shifts toward lower carbonyl frequencies. As a result of the hydrogen bonding, participation of the ionic resonance forms 1a, 1b and 1c are more prominent, as shown in Scheme 2.9, promoting the aromaticity of the pyrone ring and hence causing an increase in fluorescence. Therefore the low level of fluorescence under the low acid concentration conditions may be due to less

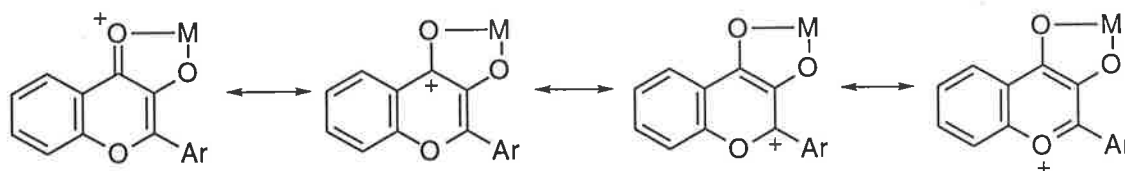


hydrogen bonding as a result of a low concentration of  $H^+$  ions. A similar explanation may apply to **4**.



Scheme 2.9

This observed phenomenon can also provide a feasible explanation as to why metal ion complexes of 3-hydroxyflavones are fluorescent. The strong bond formed between the metal ion and the carbonyl group would most likely make the ionic resonance forms of the complexes (shown in Scheme 2.10) more prominent (more so than when only weakly bonded to  $H^+$ ) promoting the aromaticity of the pyrone ring, hence causing an increase in fluorescence.



Scheme 2.10

### Ligand **5** Complexes (in solutions containing $[H^+] = 10^{-2}$ M)

To compare the fluorescent properties of ligand **4** with ligand **5**, the relative fluorescence of ligand **5** and its metal ion complexes were determined. Again,  $Al^{3+}$  was the first metal ion to be investigated with ligand **5** and  $[H^+] = 10^{-2}$  M. As expected, due to the delocalisation of the  $\pi$  electrons within ligand **5** which is more planar (as explained in Section 2.4), the  $Al^{3+}$  complex of ligand **5** is more fluorescent than that of ligand **4** (see Table 2.7, page 74). Consequently, the concentration of ligand **5** required for the fluorescence measurements was lower than that of ligand **4** so that the resulting fluorescence of the  $Al^{3+}$  complex did not exceed the upper level of detection of the fluorimeter. The concentration of ligand **5** was  $3.33 \times 10^{-7}$  M (100 times less than the concentration of ligand **5** used in the UV-visible absorption measurements in Section 2.3). The excitation wavelength was  $\lambda = 416$  nm which is the maximum absorbance wavelength of the  $Al^{3+}$ -ligand **5** complex. Seventeen solutions containing ligand **5** were prepared with the concentration of  $Al^{3+}$  ranging from  $3.33 \times 10^{-8}$  M

to  $8.33 \times 10^{-7}$  M and their fluorescence spectra were recorded. As with ligand **4**, the series of fluorescence spectra of ligand **5** with  $\text{Al}^{3+}$  were used to determine a stability constant of the complex in the excited state and the spectra are illustrated in Figure 2.51. A graphical fit of the data is shown in Figure 2.52. Again, the complex was more stable in the excited state with a  $\log K_{\text{stab}}$  of 7.49 as shown in Table 2.8.

The maximum relative fluorescence level obtained for ligand **5** with  $\text{Al}^{3+}$  was 931 (see Table 2.7). In comparison to the  $\text{Al}^{3+}$  complex of ligand **4** (relative fluorescence of 346), the ligand **5** complex is almost three times as fluorescent at one third the ligand concentration. This suggests that ligand **5** is a much more sensitive probe than ligand **4**. However, to determine if ligand **5** is as selective for  $\text{Al}^{3+}$  as ligand **4** is at  $[\text{H}^+] = 10^{-2}$  M, the fluorescence spectra of the other metal ions in the series with ligand **5** were determined. The spectra were recorded and the results are tabulated in Table 2.7. These metal complexes produced comparable fluorescence to that of the free ligand indicating no significant metal ion fluorescence enhancement.

**Table 2.8:** Calculated stability constants of the  $\text{Al}^{3+}$  complexes of ligands **4** and **5** as determined by UV-visible absorption spectroscopy (in solutions containing  $[\text{H}^+] = 10^{-2}$  M) compared with those as determined by fluorescence spectroscopy.

Ligand	Metal Ion	UV-visible Absorption Spectroscopy	Fluorescence
		$\log K_{\text{stab}}$ in $[\text{H}^+] = 10^{-2}$ M	$\log K_{\text{stab}}$ in $[\text{H}^+] = 10^{-2}$ M
(4)	$\text{Al}^{3+}$	$4.51 \pm 0.01$	$6.30 \pm 0.01$
(5)	$\text{Al}^{3+}$	$4.73 \pm 0.01$	$7.49 \pm 0.01$

#### Ligand **5** Complexes (in solutions containing $[\text{H}^+] = 10^{-5}$ M)

The fluorescence spectra of ligand **5** with the metal ions  $\text{Pb}^{2+}$ ,  $\text{Al}^{3+}$ ,  $\text{Zn}^{2+}$ ,  $\text{Cd}^{2+}$  and  $\text{Mg}^{2+}$  were determined under the conditions of  $[\text{H}^+] = 10^{-5}$  M. Similarly to ligand **4** under the low acid concentration conditions, the relative fluorescence of the  $\text{Al}^{3+}$  complex with ligand **5** decreased over time which is consistent with the previously suggested reason for fluorescence loss (pp 75-79). The other metal ions produced varying degrees of enhanced fluorescence in the same relative order as that obtained for ligand **4**. Zinc(II) produced the most fluorescent

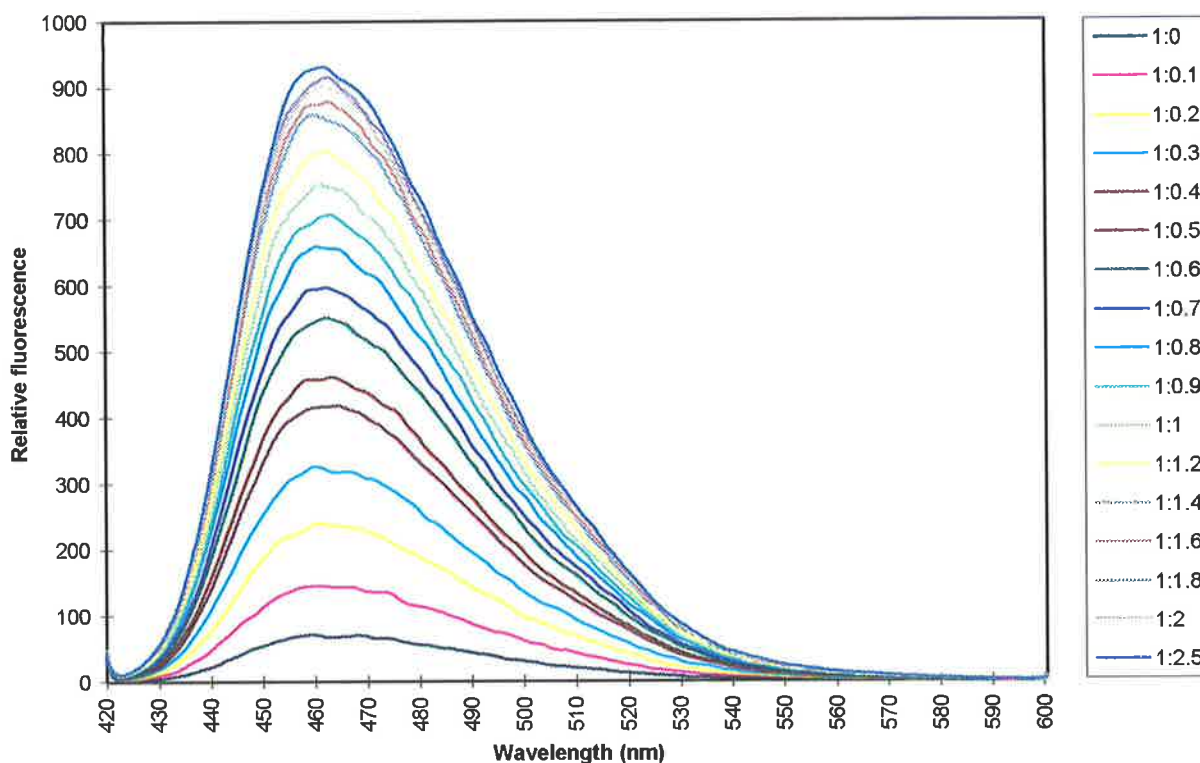


**Figure 2.51:** Fluorescence spectra of ligand 5 at a concentration of  $3.33 \times 10^{-7} \text{ M}$  in  $[\text{H}^+] = 1.0 \times 10^{-2} \text{ M}$  with varying concentrations of  $\text{Al}(\text{ClO}_4)_3$  as shown in Appendix B, Table B.18. The vertical, right legend represents the ratio of [5] to  $[\text{Al}^{3+}]$ .

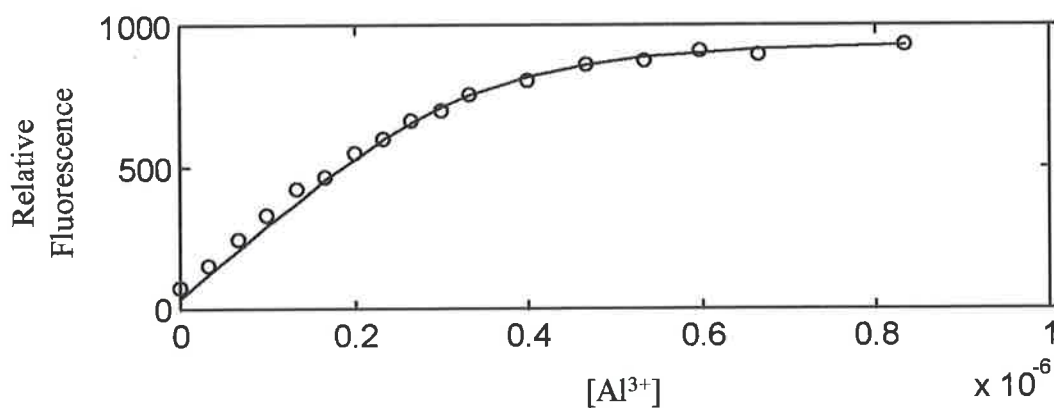


**Figure 2.52:** A graphical representation of the data fitting of Figure 2.51 at  $\lambda = 460 \text{ nm}$ . The circles represent the experimentally obtained data and the solid line represents the best fit.

chelate with a relative fluorescence intensity of 129, followed by  $\text{Pb}^{2+}$  with 42 and  $\text{Cd}^{2+}$  with 23. Again  $\text{Mg}^{2+}$  produced a relative fluorescence level comparable to the fluorescence of the free ligand.

### Ligand 6 and 7 Complexes

Ligands **6** and **7**, the thioflavone analogues of **4** and **5**, were also studied for their fluorescent properties. The metal ions chosen for study were  $\text{Pb}^{2+}$ ,  $\text{Zn}^{2+}$  and  $\text{Cd}^{2+}$ . Aluminium(III) and  $\text{Mg}^{2+}$  were omitted from these studies as they did not coordinate to the ligands **6** and **7** as determined from UV-visible absorbance spectroscopy (Section 2.3). The fluorescence spectra are presented in Appendix C and the fluorescence values are listed in Table 2.7 (page 74). The fluorescence spectra for both ligands **6** and **7** were determined at one tenth the concentration of those used in the UV-visible studies.

Ligand **6**, in solutions containing  $[\text{H}^+] = 10^{-2}$  M, produced no fluorescence for the free ligand,  $\text{Zn}^{2+}$  or  $\text{Cd}^{2+}$  complex, but complexation with  $\text{Pb}^{2+}$  produced a small fluorescence (relative fluorescence of 2). In  $[\text{H}^+] = 10^{-5}$  M, a slight fluorescence enhancement was observed with each of the studied metal ions. Again the free ligand produced no fluorescence.

Although the stability constants for ligand **7** were not determined, due to the instability of **7** in solution in the presence of light, fluorescence measurements were still performed on this ligand. If stored in the absence of light, the solutions of ligand **7** were stable long enough to give reproducible fluorescence data. At  $[\text{H}^+] = 10^{-2}$  M, ligand **7** only produced significant fluorescent enhancement with  $\text{Pb}^{2+}$  giving a value of 47 as compared to 1 for the free ligand. However, at  $[\text{H}^+] = 10^{-5}$  M, fluorescence enhancement was shown for each of the metal ion complexes formed with ligand **7**. Zinc(II) produced the most fluorescent chelate with a relative fluorescence of 331, followed by  $\text{Pb}^{2+}$  with 115 and  $\text{Cd}^{2+}$  69. The free ligand did not produce any fluorescence under these conditions.

In summary, the ligands **4** - **7** were tested for their fluorescence enhancement upon complexation with a series of metal ions under two acid concentration conditions of  $[\text{H}^+] = 10^{-2}$  M and  $10^{-5}$  M. The ligands **4** and **5** produced selective fluorescence enhancement with  $\text{Al}^{3+}$  when  $[\text{H}^+] = 10^{-2}$  M (making it potentially useful as an  $\text{Al}^{3+}$  fluorescent probe) and varying

degrees of fluorescence with all of the metal ions when  $[H^+] = 10^{-5}$  M. The relative order of fluorescence enhancement observed for the metal complexes decreased with metal ion in the order  $Zn^{2+} > Pb^{2+} > Cd^{2+} > Mg^{2+}$ . Ligand **6** produced little if any fluorescence enhancement upon metal ion complexation under both acid conditions whereas ligand **7**, the geometrical isomer of **6**, produced selective fluorescence enhancement with  $Pb^{2+}$  in solutions containing the higher acid concentration and varying degrees of fluorescence with all of the tested metal ions in the solutions containing the lower concentration of acid.

## 2.6 Molecular Modelling and Computational Chemistry

### 2.6.1 Molecular Modelling using Gaussian 94

Computational chemistry is one of the fastest growing areas of chemistry.<sup>79,80</sup> Chemical calculations can predict the structures, energies and other properties of known or unknown molecules and have recently been heralded as important new tools in chemical research.<sup>80</sup> Widespread quantitative applications have only become practically possible in recent times, primarily because of rapid developments in computer hardware and associated achievements in the design of efficient algorithms.<sup>81</sup> It is now possible to study reactive intermediates and transition states by computational means.

The computational calculations performed in this thesis have been carried out using the Gaussian 94 suite of programs which generates globalised energy minimum structures using *ab initio* molecular orbital methods. These *ab initio* methods allow the calculation of an approximate electronic wavefunction by utilising numerical approximation techniques and the fundamental laws of quantum mechanics (The Schrödinger equation). Before the Schrödinger equation can be solved for a particular molecule, a basis set must be chosen. Basis sets assign a group of basis functions to each atom within a molecule to approximate its orbitals.<sup>82</sup> Almost all modern *ab initio* calculations employ Gaussian type orbital (GTO) basis sets.<sup>80</sup> These basis sets, in which each atomic orbital is made up of a number of Gaussian probability functions, have considerable advantages over other types of basis sets as exemplified by those containing Slater type orbitals (STO).<sup>80</sup> The Gaussian series of programs deals, as the name implies, exclusively with Gaussian type orbitals and includes several optional GTO basis sets of varying size.<sup>80</sup> The basis set used for the molecules studied in this thesis is the LanL2DZ

basis set. This basis set, unlike other basis sets, is appropriate for calculations of systems comprised of heavier atoms such as those beyond the first three periods of the periodic table.<sup>83-85</sup> The LanL2DZ basis set varies from other basis sets by the implementation of effective core potential approximations (ECP's) for the inner core structure of heavier atoms. ECP approximations are a means of treating valence electrons in a different manner to those in the core.<sup>86</sup>

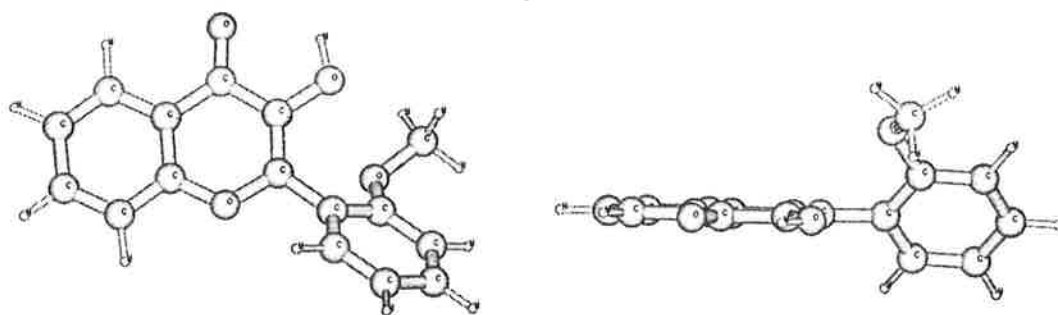
The purpose of employing computational chemistry and molecular modelling techniques in this study was to allow comparisons to be made between the experimentally obtained data and the theoretical, gas phase calculations. It was hoped that the theoretically obtained minimised structures would help explain why one ligand or complex may be more stable or more fluorescent than another, and would also provide a guide to the optimum bite size for Pb<sup>2+</sup>. In particular, the exploration of whether molecular orbital theory can be used as a means of predicting the suitability of a molecule as a Pb<sup>2+</sup> fluorescent probe based upon its structural characteristics is of interest. Good correlation between the computer generated minimised structures and the experimentally obtained results would therefore support the use of molecular modelling (using Gaussian 94) as a tool for future Pb<sup>2+</sup> specific ligand design.

### 2.6.2 Results and Discussion

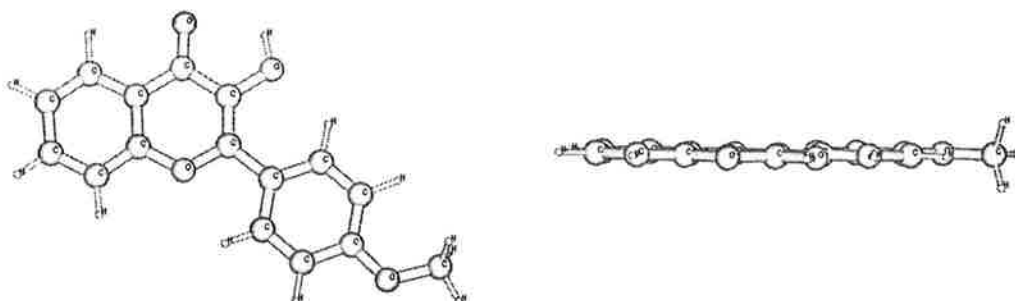
The free ligands **4** - **7** were the first molecules to be examined using Gaussian 94, and their global energy minimised structures are represented with parallel and perpendicular views to the AC ring plane of the flavone structure in Figure 2.53. It was hoped that the calculated bond lengths, interatomic distances and dihedral angles of these free ligands would provide support to the previously mentioned reasons as to why the thioflavones (**6** and **7**) are more metal ion selective than the flavones (**4** and **5**), and why the *p*-methoxyflavone (**5**) produced more stable and more fluorescent complexes than the *o*-methoxyflavone (**4**).

The calculated bite distances of the ligands **4** - **7** are presented in Table 2.4 (Section 2.3.4, page 30). The bite distances for flavone ligands **4** and **5** (2.69 Å and 2.67 Å respectively) were shown to be considerably smaller than those for the thioflavones **6** and **7** (3.00 Å and 2.97 Å respectively) supporting the experimental findings (Section 2.3.4) that the thioflavones are more selective for the larger metal ions than the flavones.

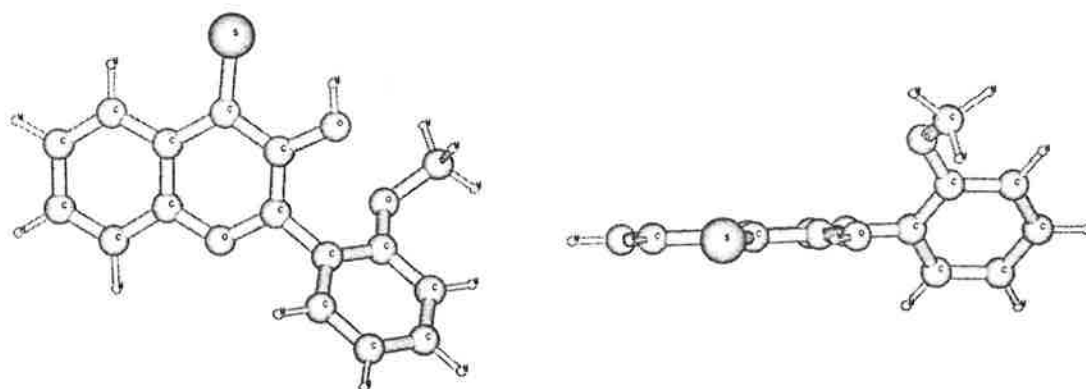
4)



5)



6)



7)

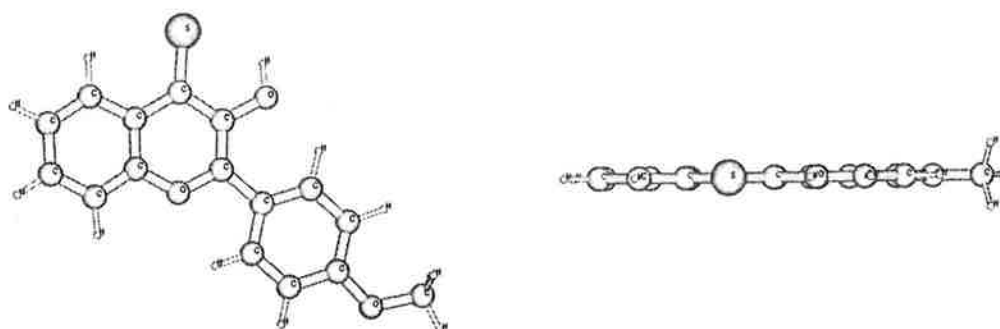


**Figure 2.53:** The minimised structures of ligands 4 - 7 as calculated using *ab initio* molecular orbital calculations by the use of Gaussian 94 with views parallel and perpendicular to the AC ring plane.

The global energy minimised structures shown in Figure 2.53 also assist in the reasoning as to why the complexes of **5** are more stable (Section 2.4) and more fluorescent (Section 2.5) than those complexes of **4**. Figure 2.53 shows that ligand **4** has the B ring twisted out of plane with the A and C rings whereas ligand **5** has all three rings coplanar. This coplanarity would extend the conjugation of the lone pair of electrons on the electron donating *p*-methoxy group, increasing the electron density on the carbonyl O and therefore increasing the strength of the bond between the carbonyl O and the metal ion making the complex more stable. The more extensive electron delocalisation in **5** as compared with **4** would also be expected to increase the fluorescent properties of ligand **5** (and possibly its complexes) for reasons explained in Section 2.5.2. The experimental results (Section 2.5.4) agree with these suggested concepts derived from the computed molecular geometries. It is interesting to note that the more highly fluorescent complexes as determined experimentally (namely those of **5** compared with **4** and **7** compared with **6**) have the free ligand dihedral angles (through the bonds C<sub>3</sub>-C<sub>2</sub>-C<sub>1</sub>'-C<sub>2</sub>' as illustrated in Figure 2.54) of less than 1° whereas the non or weakly fluorescent complexes (those of **4** compared to **5** and **6** compared to **7**) have the free ligand ring B out of alignment with rings A and C by approximately 53° (Table 2.9).

**Table 2.9:** The calculated dihedral angles of the ligands **4** - **7** through the bonds C<sub>3</sub>-C<sub>2</sub>-C<sub>1</sub>'-C<sub>2</sub>' (illustrated in Figure 2.54) as determined by gas phase *ab initio* calculations using Gaussian 94.

Ligand	(4)	(5)	(6)	(7)
Dihedral Angle	-53.209°	0.008°	-54.584°	-0.069°

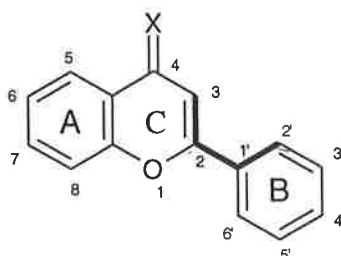


**Figure 2.54:** An illustration of the bonds (in bold) through which the dihedral angles were calculated for Table 2.9.



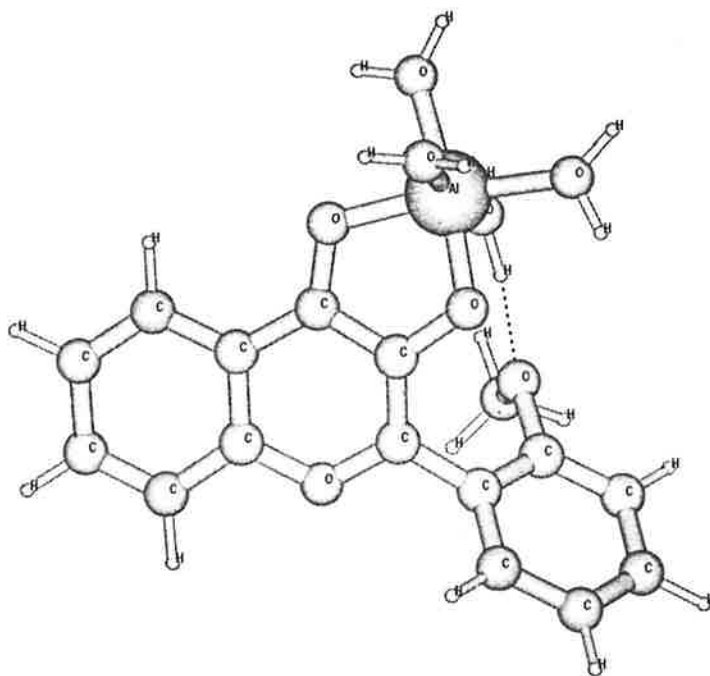
Although much molecular information can be obtained quite accurately by computer <sup>79-81</sup>, differences can be expected between the optimised structures and experimentally obtained data due to the different phases (gaseous versus solution) used for calculation and experiment. While gas phase predictions are appropriate for many purposes, they are inadequate for describing the characteristics of many molecules in solution.<sup>82</sup> Indeed, the properties of molecules can differ considerably between the gas phase and solution.<sup>82</sup> Therefore the next obvious step required molecular orbital calculations of the solvated metal ion complexes.

To ascertain that solvation of the metal ion may have a significant impact on structure optimisation, the  $\text{Pb}^{2+}$ ,  $\text{Zn}^{2+}$ ,  $\text{Cd}^{2+}$  and  $\text{Al}^{3+}$  complexes of ligand **4** were reoptimised with hydrated metal ions. To remain consistent with each complex studied, four water molecules were assigned to each metal complex to reasonably approximate the first coordination sphere (suggesting six coordinate species). The optimised structures are presented in Figure 2.55.

The global energy minimised structure of  $[\text{Al}(\text{H}_2\text{O})_4\mathbf{4}]^{2+}$  (as shown in Figure 2.55) illustrates a bidentate complex with  $\text{Al}^{3+}$  coordinating to the deprotonated  $\text{C}_3$  hydroxyl group, the  $\text{C}_4$  carbonyl group and the four water molecules. Upon examination of the other hydrated metal ion complexes (Figures 2.56 to 2.58), it is evident that these complexes prefer to exist as five coordinate species as the detachment of a water molecule was observed starting from the six coordinate species. Since the coordination number had not been established experimentally, conclusions cannot be drawn on the validity of the calculated five coordinate species. However, the experimentally obtained Gibbs free energies of hydration of the metal ions studied <sup>61</sup> show that the hydration of  $\text{Al}^{3+}$  is much more favourable than the hydration of the other studied metal ions (Table 2.10). This may help explain why the  $\text{Al}^{3+}$  complex prefers to remain coordinated to four waters while the other complexes prefer three. It is probable that in water the  $\text{Pb}^{2+}$ ,  $\text{Zn}^{2+}$  and  $\text{Cd}^{2+}$  complexes would be six coordinate with four water molecules in the first coordination sphere. Further study on a system with more water molecules present may be required to make relevant comments regarding coordination number.

The results of this comparative study suggest that molecular modelling and computational chemistry can assist in the explanation of some observed experimental results such as greater metal ion selectivity and higher fluorescence for metal ion-ligand complexes. To obtain more

a)



b)

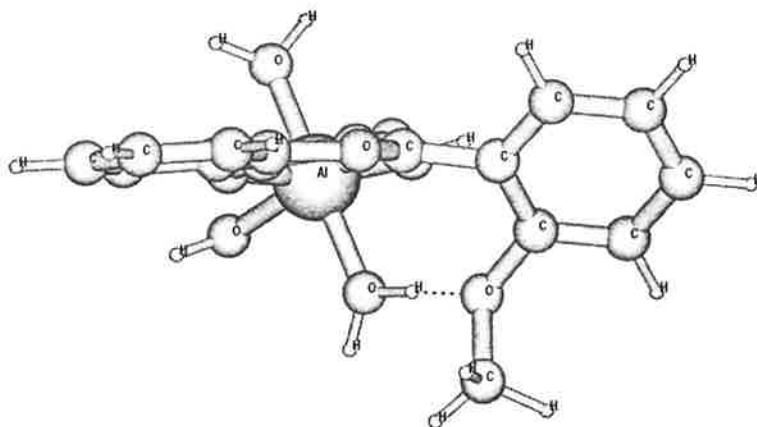
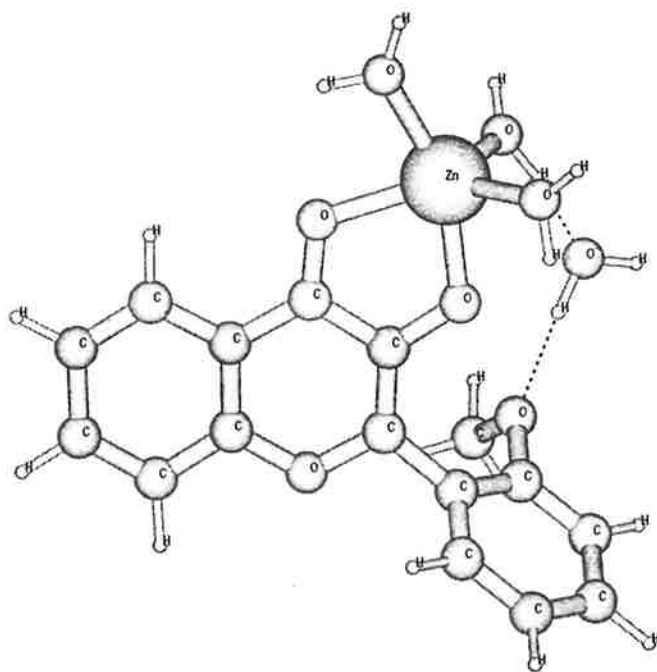


**Figure 2.55:** The global energy minimised structure of the  $[Al(H_2O)_4]^{2+}$  complex as calculated by the use of Gaussian 94. Figure a) represents the view perpendicular to the AC ring plane and Figure b) represents the view parallel to the AC ring plane.

a)



b)

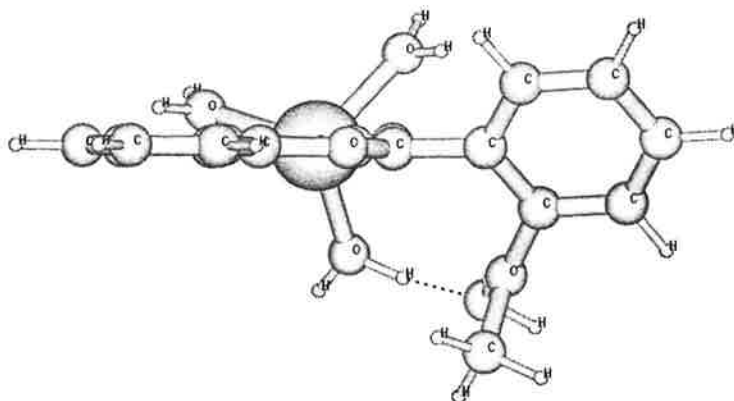
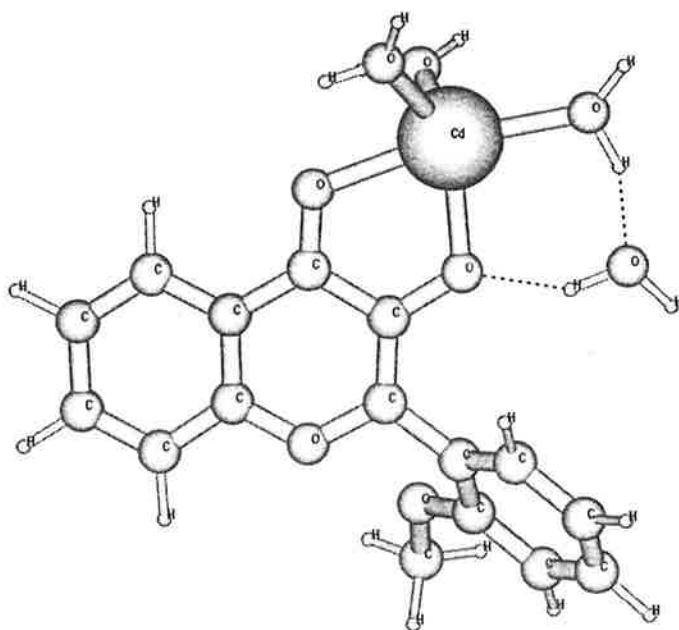


**Figure 2.56:** The global energy minimised structure of the  $[\text{Zn}(\text{H}_2\text{O})_4]^+$  complex as calculated by the use of Gaussian 94. Figure a) represents the view perpendicular to the AC ring plane and Figure b) represents the view parallel to the AC ring plane.

a)



b)

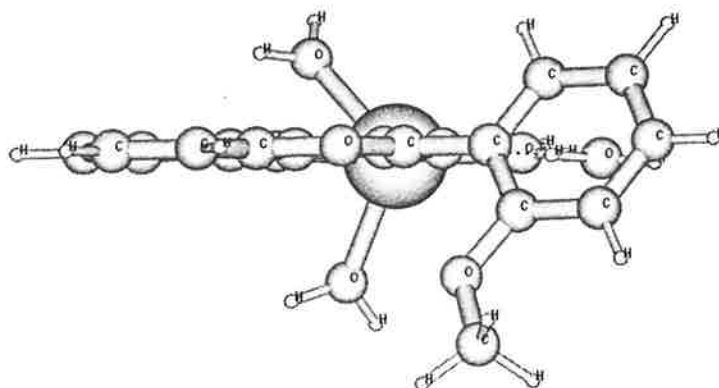
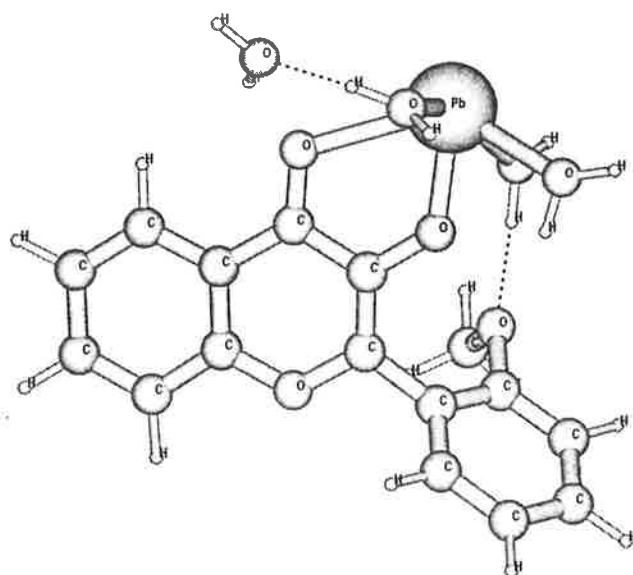


**Figure 2.57:** The global energy minimised structure of the  $[Cd(H_2O)_4]^+$  complex as calculated by the use of Gaussian 94. Figure a) represents the view perpendicular to the AC ring plane and Figure b) represents the view parallel to the AC ring plane.

a)



b)

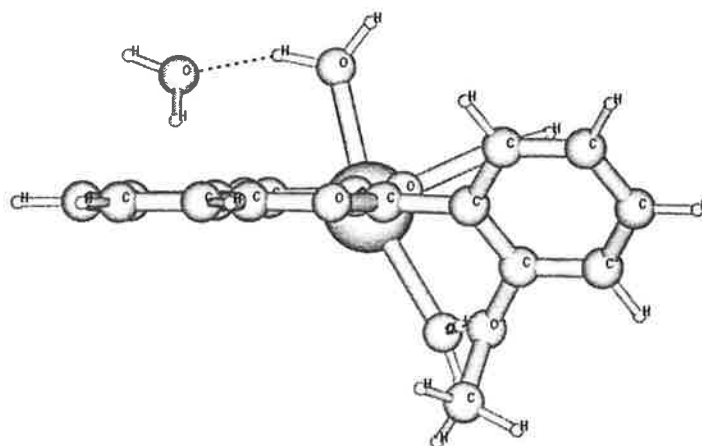


**Figure 2.58:** The global energy minimised structure of the  $[\text{Pb}(\text{H}_2\text{O})_4]^{4+}$  complex as calculated by the use of Gaussian 94. Figure a) represents the view perpendicular to the AC ring plane and Figure b) represents the view parallel to the AC ring plane.

accurate correlations between experimental data and molecular geometry optimisations of complexes, future Gaussian 94 calculations would require modelling with many water molecules in the model.

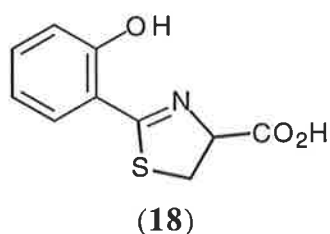
**Table 2.10:** *The Gibbs free energies of hydration of the studied metal ions.*<sup>61</sup>

<b>Metal Ions</b>	<b>Pb<sup>2+</sup></b>	<b>Cd<sup>2+</sup></b>	<b>Zn<sup>2+</sup></b>	<b>Al<sup>3+</sup></b>
<b><math>\Delta G_H</math> (kJ mol<sup>-1</sup>)</b>	-1497.0	-1801.2	-2027.6	-4616.2

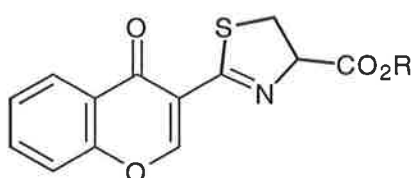
## Chapter 3: Thiazolines and Thiazoles

### 3.1 Synthesis

The synthesis of a series of compounds based on the structure of morin (**2**) has been described in Chapter 2, and these ligands were tested for their suitability as fluorescent probes for  $\text{Pb}^{2+}$ . Although these ligands produced moderately stable and moderately fluorescent  $\text{Pb}^{2+}$  complexes, none of them were highly specific for  $\text{Pb}^{2+}$ . Therefore, further synthetic studies were required to develop a ligand that would produce a highly specific, highly stable and highly fluorescent  $\text{Pb}^{2+}$  complex.

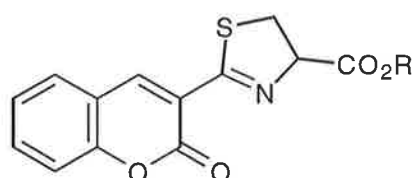


Research by Pratt *et al.*, investigating the synthesis of potential  $\text{Zn}^{2+}$  fluorescent probes, reported the formation of a very stable complex between  $\text{Pb}^{2+}$  and an aromatic thiazoline (**18**).<sup>87</sup> Although the low fluorescence of this ligand was quenched on complexation with  $\text{Pb}^{2+}$ , which rendered it unsuitable as a  $\text{Pb}^{2+}$  fluorescent probe, the coordinating affinity of this ligand for  $\text{Pb}^{2+}$  provided a basis on which other potentially successful probes could be designed. The fluorescent nature of the flavone series (see Section 2.5.4) and the formation of a stable  $\text{Pb}^{2+}$  complex by the thiazolines suggested that **19** - **24** would be suitable targets as potential fluorescent probes for  $\text{Pb}^{2+}$ .



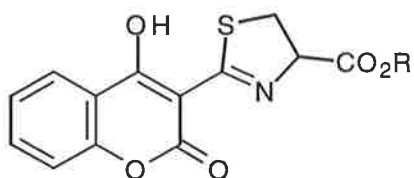
R =  $\text{CH}_2\text{CH}_3$  (**19**)

R = H (**20**)



R =  $\text{CH}_2\text{CH}_3$  (**21**)

R = H (**22**)

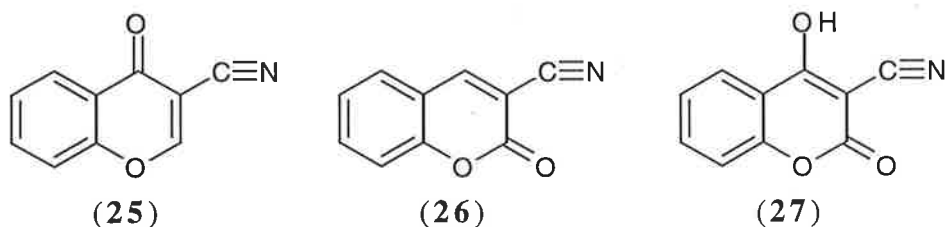


R =  $\text{CH}_2\text{CH}_3$  (**23**)

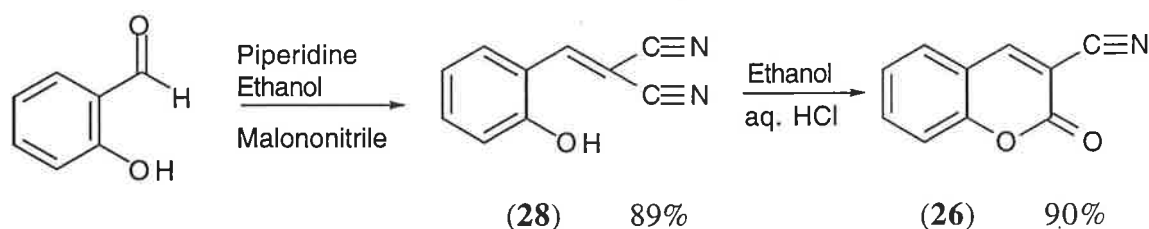
R = H (**24**)

Compounds **19** and **20** were chosen since they combine the fluorescent properties of the benzopyran-4-one chromophore and the  $\text{Pb}^{2+}$  complexing thiazoline moiety to produce potentially stable  $\text{Pb}^{2+}$  fluorescent complexes. The coumarins **21** to **24** were also selected to compare the metal ion selectivity and fluorescence intensity between the benzopyran-4-one and coumarin chromophores. Synthesis of both the carboxylic acid and ester forms of the target molecules were pursued in order to test the effects of the different substituents on complex stability. The presence of an ester group may also be essential to the hydrophobic properties of the potential ligand which allow the probe to traverse the outer membrane of the cell and remain within the cytosol.<sup>23,25</sup> It has been reported that  $\text{Zn}^{2+}$  and  $\text{Ca}^{2+}$  fluorescent probes loaded into living cells appear to require the presence of an ester to enable penetration of the cell wall.<sup>23,25</sup> Once the probe is within the cell, cytosolic esterases cleave the ester group forming charged species which are often membrane impermeable.<sup>23,25</sup>

To synthesise the thiazolines **19** - **24**, the precursor nitriles **25**, **26** and **27** were required. The adopted route involved the direct reaction of each nitrile with L-cysteine hydrochloride to produce the required thiazolines, using the method described by Mathur and coworkers.<sup>88</sup>



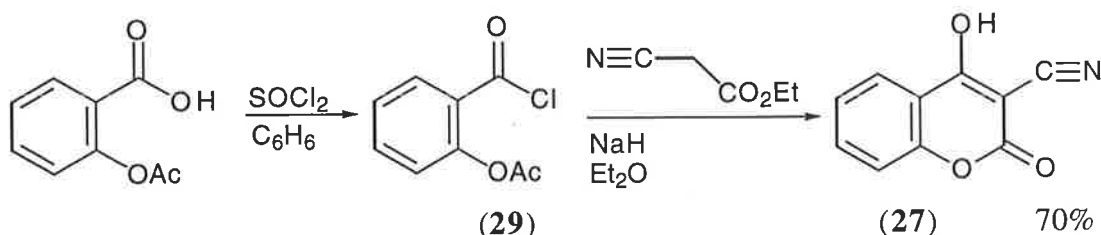
Nitrile **25** was commercially available. 2-Oxo-2H-1-benzopyran-3-carbonitrile (**26**) was synthesised using a literature procedure which involved reaction of salicylaldehyde with malononitrile in ethanol containing a catalytic amount of piperidine (Scheme 3.1).<sup>89</sup> The intermediate compound **28** was reacted directly without further purification in dilute hydrochloric acid/ethanol to produce nitrile **26** in 90% yield.



**Scheme 3.1**

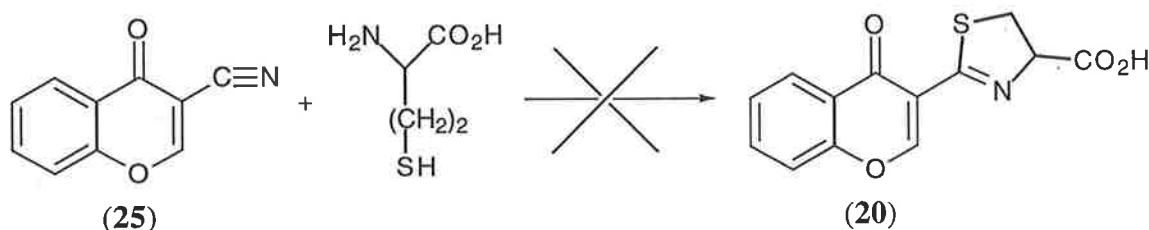


4-Hydroxy-2-oxo-2H-1-benzopyran-3-carbonitrile (**27**) was produced by a literature procedure outlined in Scheme 3.2.<sup>90</sup> Acetylsalicylic acid was converted to its acid chloride **29** using thionyl chloride in benzene at reflux. The acid chloride **29** was reacted with ethyl cyanoacetate which had previously been treated with sodium hydride in ether to give the required nitrile in 70% yield.



**Scheme 3.2**

The condensation of compound **25** with L-cysteine hydrochloride was then attempted (Scheme 3.3).



**Scheme 3.3**

After many attempts in various solvents (ethanol, DMF, THF), with various bases (NaHCO<sub>3</sub>, triethylamine and sodium hydroxide) and varying reaction times it was not possible to obtain any of the condensation product **20**. <sup>1</sup>H NMR indicated only the presence of starting materials. This lack of reactivity was attributed to the electron rich nature of the nitriles which would deactivate nucleophilic attack (Figure 3.1).



**Figure 3.1:** Resonance structures of nitrile **25** indicating the delocalisation of electrons which decrease the susceptibility for nucleophilic attack by L-cysteine.

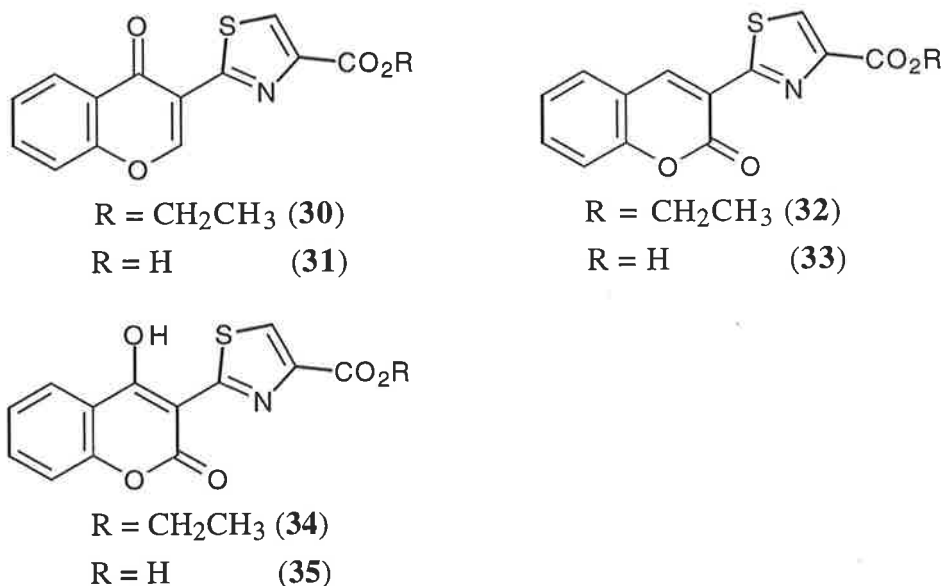
Attempts to react the nitriles **26** and **27** with L-cysteine hydrochloride in various solvents and bases produced no reaction for nitrile **27** and product mixtures containing predominantly

starting materials and hydrolysed lactone in the reactions of **26** according to  $^1\text{H}$  NMR data. The hydrolysed starting material was detected by the presence of a phenolic OH signal at  $\delta$  10.96 ppm, and a carboxylic acid OH signal at  $\delta$  9.84 ppm in the  $^1\text{H}$  NMR spectrum. Again the electron rich coumarin nitriles have presumably hindered the nucleophilic attack by L-cysteine significantly which prevents reaction (Figure 3.2).



**Figure 3.2:** General resonance structures of coumarin nitriles indicating the delocalisation of electrons which decrease the susceptibility for nucleophilic attack by L-cysteine.

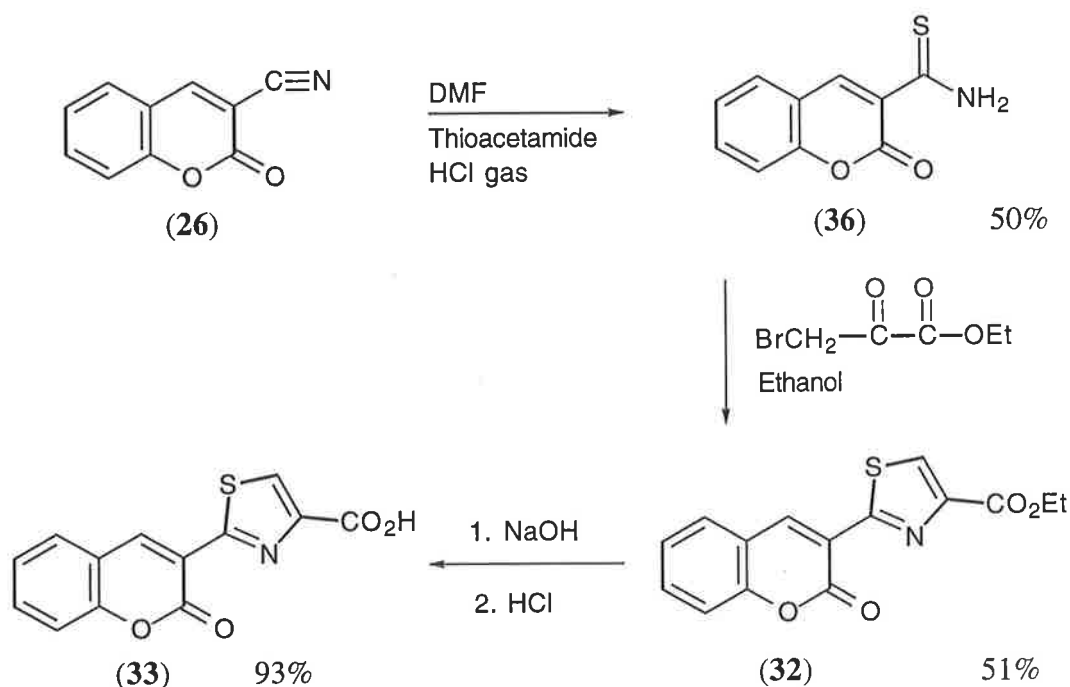
The lack of reactivity of the nitriles **25** - **27** towards nucleophilic attack by L-cysteine prompted synthesis of the thiazoles (**30** - **35**) in place of the thiazolines. Since the conjugation is less extensive in thiazolines **19** to **24** by comparison with their corresponding fully aromatic thiazoles **30** to **35**, it was anticipated that the thiazoles may have greater fluorescence properties. Consequently another series of target compounds was devised (**30** - **35**).



The route to produce the target thiazoles involved conversion of the nitriles **25**, **26** and **27** to their corresponding thioamides followed by reaction with ethyl bromopyruvate using similar methods to those developed by Yamada *et al.*<sup>91</sup> Procedures for converting nitriles to thioamides, using aromatic and aliphatic nitriles, have been reported in the literature with poor

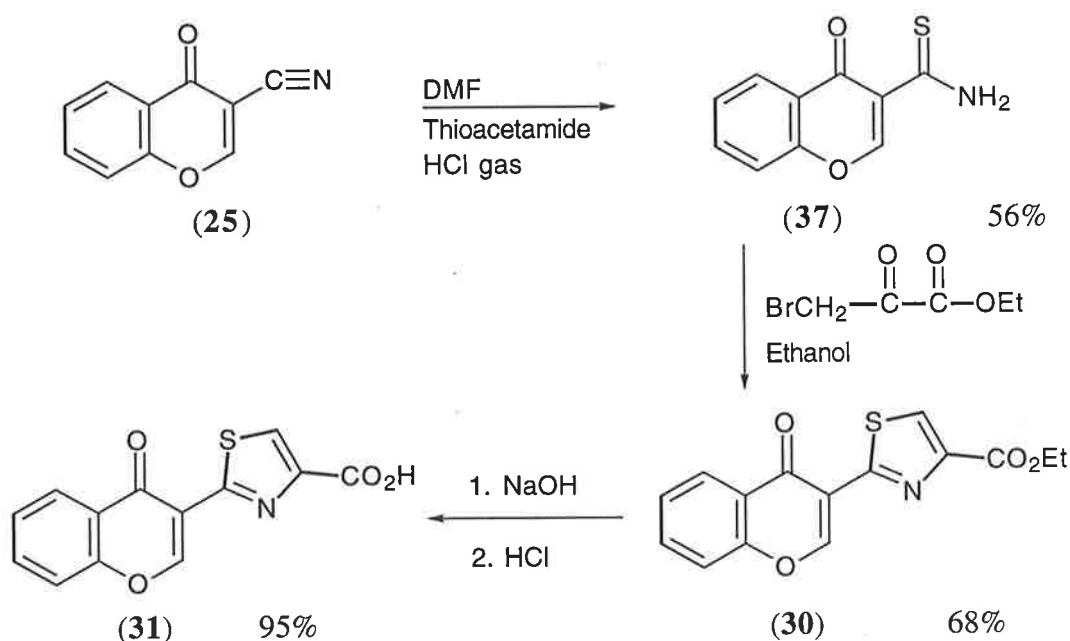
to moderate yields.<sup>92</sup> The method involves the reaction of nitriles with dry hydrogen chloride gas in DMF, followed by treatment with thioacetamide (Scheme 3.4). Using this procedure for 2-oxo-2H-1-benzopyran-3-carbonitrile (**26**), 2-oxo-2H-1-benzopyran-3-carbothioamide (**36**) was produced in a non optimised yield of 50%. When thioamide **36** was refluxed in ethanol with one molar equivalent of ethyl bromopyruvate, the thiazole ester ethyl-2-(3-2-oxo-2H-1-benzopyran)-2-thiazole-4-carboxylate (**32**) was formed. Microanalytical, NMR and mass spectral data were consistent with structure **32** (see Section 6.3).

Due to the possibility that a carboxylate group on the thiazole could introduce another coordinating site on the potential ligand and increase specificity for  $\text{Pb}^{2+}$ , the thiazole ester **32** was hydrolysed to the carboxylic acid **33** using sodium hydroxide in ethanol. Upon work up, a white solid was produced with spectroscopic and microanalytical data supporting the expected structure **33** (Scheme 3.4). The mass spectrum produced a molecular ion at  $m/z$  273.



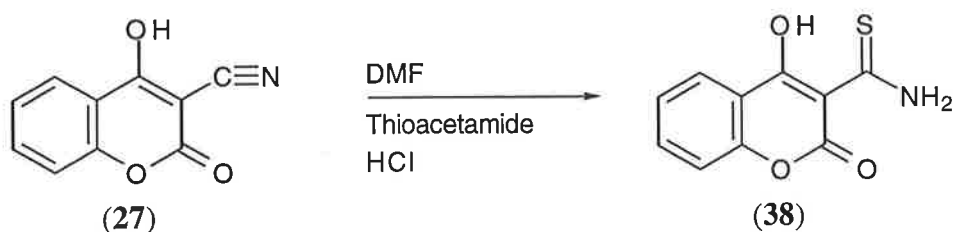
Scheme 3.4

Commercially available 4-oxo-4H-1-benzopyran-3-carbonitrile (**25**) was subjected to the same reaction conditions as mentioned above (illustrated in Scheme 3.5) to give the thiazole ester **30** and acid **31** in the yields shown.



Scheme 3.5

The thioamide **38** was similarly produced from nitrile **27** via the reaction with thioacetamide and hydrogen chloride gas in DMF (Scheme 3.6).



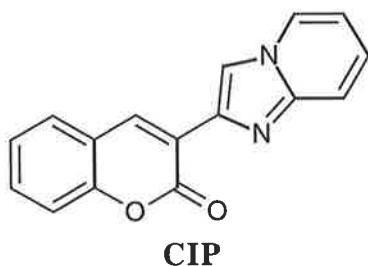
Scheme 3.6

The thioamide product was refluxed with ethyl bromopyruvate in dry ethanol and after a half hour reaction time, an insoluble compound precipitated out of solution. Efforts to dissolve or recrystallise this material in various solvents proved fruitless. As a result of this insolubility,  $^1\text{H}$  NMR experiments could not be performed on the product to identify its structure. Analysis by mass spectrometry indicated the presence of a large molecular weight structure possibly a polymer. Since the purpose of producing these compounds was to assess their potential as possible water soluble metal ion specific probes, it was thought inappropriate to further study this particular molecule.

The next stage was to determine whether the four thiazoles **30**, **31**, **32** and **33** coordinated the series of metal ions using previously described methods (see Section 2.3).

### 3.2 Specificity

Gudasi and Goudar have reported the use of a coumarin imidazo compound, CIP (2-(3-coumarinyl)imidazo[1,2-a]pyridine), as a bidentate coordinating ligand for a series of metal ions.<sup>93</sup> This ligand was found, through IR spectroscopic studies, to act as a neutral bidentate ligand by coordinating to all of the metal ions tested through the lactone carbonyl and the imidazo imine nitrogen of the ligand.<sup>85</sup>



Since the ligands **32** and **33** contain a five membered, nitrogen containing, heterocyclic ring attached to a coumarin ring system on position C<sub>3</sub> as in CIP, it was considered that these ligands might similarly coordinate metal ions through the lactone carbonyl and thiazole nitrogen. Due to the ligands **30** and **31** only varying in structure from **32** and **33** by the position of the carbonyl group, similar coordination through the carbonyl and thiazole nitrogen was envisaged. To ascertain this, the complexing ability of the ligands **30** - **33** needed to be assessed.

The complexing ability of the ligands **30** - **33**, were determined using UV-visible absorption spectroscopy as described in Section 2.3. The sample solutions for the UV-visible absorption measurements were prepared in a similar manner to those for the flavone and thioflavone ligands (Section 2.3.3). This allowed for a direct comparison of the results obtained for the thiazoles **30** - **33**, with those of the flavones and thioflavones **4** - **12**. The preparation of the sample solutions and the method used for the absorption measurements are described in Section 6.7.1 and the conditions used to determine the absorption measurements have been summarised in Table 3.1.

**Table 3.1:** A summary of the conditions under which the UV-visible spectra of the ligands **30 - 33** in the absence and presence of the listed metal ions were determined.

Ligands	<b>30 - 33</b>
Metal ions	Pb <sup>2+</sup> , Zn <sup>2+</sup> , Ca <sup>2+</sup> , Al <sup>3+</sup> , Cd <sup>2+</sup> , Ni <sup>2+</sup> , Cu <sup>2+</sup> , Co <sup>2+</sup> , Mg <sup>2+</sup>
Solvent	25% H <sub>2</sub> O/75% DMF
Ionic strength	0.10 M
pH	Approximately 7 *
[Ligand]	4.0 x 10 <sup>-5</sup> M
[Metal ion]	8.0 x 10 <sup>-3</sup> M *

\* Variable value in the solutions containing Pb<sup>2+</sup>, Al<sup>3+</sup> or Cu<sup>2+</sup>.

### 3.2.1 Determination of Metal Ion-Thiazole Complexation

The esters **30** and **32**, were the first thiazole type ligands to be investigated for their complexing properties with the metal ions listed in Table 3.1. Their UV-visible absorption spectra were recorded in the absence and presence of the series of metal ions and are presented in Appendix A (figures A.2.1 and A.2.2). No significant changes in the absorption spectra of ligands **30** and **32** were noted upon the addition of any of the tested metal ions. Therefore, under these conditions, ligand **30** and **32** do not coordinate significantly to any of the metal ions studied.

To determine whether the carboxylic acid analogues of the esters **30** and **32** may provide another metal ion coordinating group, metal ion coordination studies on **31** and **33** were required. Under the same conditions of those for the esters **30** and **32**, the UV-visible absorption spectra of the acids **31** and **33** were recorded (Appendix A, figures A.2.3 and A.2.4). The absorption maxima and the absorbance values at the absorption maxima for the ligands **31** and **33** and their complexes are listed in Table 3.2.

The UV-visible absorption spectrum of ligand **31** significantly changed in the presence of all of the metal ions except for  $\text{Ca}^{2+}$  and  $\text{Mg}^{2+}$ . This is consistent with all of the studied metal ions coordinating ligand **31** except for  $\text{Ca}^{2+}$  and  $\text{Mg}^{2+}$ , under these conditions. As can be seen from Table 3.2, the absorbance and absorption maxima of ligand **31** are the same as the absorbance and absorption maxima in the presence of  $\text{Ca}^{2+}$  and  $\text{Mg}^{2+}$ .

**Table 3.2:** UV-visible absorption maxima of the ligands (**31**) and (**33**) in the absence and presence of the listed metal ions.

Ligand	Metal Ion	Absorption Wavelength Maxima <sup>a</sup> (nm)	Absorbance at Maxima
<p>2-(3-(4-Oxo-4H-1-benzopyran)-2-thiazole-4-carboxylate (<b>31</b>)<sup>b</sup></p>		307	0.442
	$\text{Pb}^{2+}$	321	0.475
	$\text{Co}^{2+}$	301	0.531
	$\text{Ni}^{2+}$	316	0.630
	$\text{Cu}^{2+}$	294	0.465
	$\text{Al}^{3+}$	310	0.483
	$\text{Ca}^{2+}$	307	0.442
	$\text{Mg}^{2+}$	307	0.442
	$\text{Cd}^{2+}$	314	0.615
	$\text{Zn}^{2+}$	316	0.620
<p>2-(3-(2-Oxo-2H-1-benzopyran)-2-thiazole-4-carboxylate (<b>33</b>)<sup>c</sup></p>		355	0.630
	$\text{Pb}^{2+}$	355	0.594
	$\text{Co}^{2+}$	350	0.558
	$\text{Ni}^{2+}$	349	0.543
	$\text{Cu}^{2+}$	352	0.506
	$\text{Al}^{3+}$	351	0.660
	$\text{Ca}^{2+}$	355	0.702
	$\text{Mg}^{2+}$	355	0.638
	$\text{Cd}^{2+}$	353	0.598
	$\text{Zn}^{2+}$	352	0.582

<sup>a</sup> Errors in the absorption maxima values are  $\pm 1$  nm

<sup>b</sup> Measured between wavelengths 280 - 400 nm

<sup>c</sup> Measured between wavelengths 280 - 450 nm

The coumarin carboxylic acid derivative, ligand **33**, coordinated all the tested metal ions. This was shown by either a hyperchromic or hypochromic shift in the UV-visible spectrum of ligand **33** in the presence of the coordinating metal ions. Although some of the metal

complexes did not produce a change in the wavelength maxima as compared with the free ligand (see Table 3.2), a change in the absorbance intensity was observed.

From the results of the coordination studies of the ligands **30** to **33** with various metal ions, it became apparent that under the conditions used (ie. the solvent system, ionic strength and pH {Table 3.1}) the carboxylate group was an important functional group for coordination. It appears that none of the metal ions studied coordinated the esters **30** and **32**, whereas all of the metal ions coordinated to the carboxylate **33** and seven out of nine metal ions coordinated to the carboxylate **31**. This suggests that the complexes of ligands **31** and **33** may form stable terdentate species with chelation occurring through the carboxylate group, the nitrogen on the heterocyclic ring and the carbonyl functional group. However, the esters **30** and **32** do not appear to form sufficiently stable complexes to be detected under the conditions of this study.

Once the ability of ligands **31** and **33** to form complexes with various metal ions had been qualitatively established, the next stage was to determine the fluorescence properties of these complexes. Although the esters **30** and **32** did not form detectable complexes in 75% DMF/25% H<sub>2</sub>O in the presence of NaPIPES buffer, these compounds may form stable complexes in 95% ethanol 5% H<sub>2</sub>O in the presence of perchloric acid, which are the conditions previously used for fluorescence determination (see Section 2.5). Therefore the esters **30** and **32** were also tested for fluorescence enhancement or fluorescence quenching in the presence of metal ions.

### 3.3 Fluorescence Measurements on Compounds **30** - **33**

To carry out the fluorescence measurements on **30** - **33**, the conditions under which the measurements were performed and the method of measurement were the same as those used for the fluorescence measurements made on the flavones and thioflavones **4** - **7** in  $1.0 \times 10^{-5}$  M perchloric acid (Section 2.5) so that a direct comparison of the results obtained for **30** - **33** could be made with those obtained previously. The method used, and the preparation of the sample solutions are outlined in Section 6.8.4. All sample solutions contained perchloric acid and sodium perchlorate at the respective concentrations of  $1.0 \times 10^{-5}$  M and 0.10 M, and the ligand concentration was  $1.0 \times 10^{-6}$  M. The metal ions studied were Pb<sup>2+</sup>, Zn<sup>2+</sup>, Cd<sup>2+</sup>, Mg<sup>2+</sup>



and  $\text{Al}^{3+}$ . Their concentrations were  $1.0 \times 10^{-4}$  M which is 100 times greater than that of the ligand.

**Table 3.3:** Comparison of the fluorescence intensities of the metal complexes of the ligands 30 - 33.

Ligand	Metal Ion	Excitation Wavelength (nm)	Maximum Emission Intensity	Maximum Emission Wavelength (nm)
(30)	$\text{Pb}^{2+}$	305	14	359
	$\text{Pb}^{2+}$	305	17	357
	$\text{Zn}^{2+}$	305	54	356
	$\text{Cd}^{2+}$	305	44	355
	$\text{Al}^{3+}$	305	57	355
	$\text{Mg}^{2+}$	305	43	358
(31)	$\text{Pb}^{2+}$	305	25	360
	$\text{Pb}^{2+}$	305	57	358
	$\text{Zn}^{2+}$	305	96	359
	$\text{Cd}^{2+}$	305	87	358
	$\text{Al}^{3+}$	305	49	443
	$\text{Mg}^{2+}$	305	92	358
(32)	$\text{Pb}^{2+}$	353	651	416
	$\text{Pb}^{2+}$	353	661	414
	$\text{Zn}^{2+}$	353	637	415
	$\text{Cd}^{2+}$	353	658	415
	$\text{Al}^{3+}$	353	651	415
	$\text{Mg}^{2+}$	353	654	415
(33)	$\text{Pb}^{2+}$	353	594	422
	$\text{Pb}^{2+}$	353	251	422
	$\text{Zn}^{2+}$	353	604	424
	$\text{Cd}^{2+}$	353	568	422
	$\text{Al}^{3+}$	353	484	417
	$\text{Mg}^{2+}$	353	612	422

Since the UV-visible absorption maxima of the ligands 30 - 33 did not vary significantly from the absorption maxima of their complexes, the fluorescence emission spectra were measured by irradiating the solutions of each compound with monochromatic light at wavelengths equal to those of the UV-visible maxima of the free ligand. The fluorescence spectra of ligands 30 -

**33** and their complexes are shown in Appendix C (Figures C.2.1 - C.2.4), and the excitation wavelengths, maximum emission intensities and maximum emission wavelengths of the complexes are shown in Table 3.3.

### 3.3.1 The Benzopyran-4-ones **30** and **31**

The ester **30** is weakly fluorescent, but its fluorescence increases upon complexation as seen from Table 3.3. The most highly fluorescent complex of ligand **30** was that of  $\text{Al}^{3+}$ , which produced only a 4 fold enhancement when compared to the fluorescence of the free ligand. The order of decreasing fluorescence with the metal ion was  $\text{Al}^{3+} > \text{Zn}^{2+} > \text{Cd}^{2+} = \text{Mg}^{2+} > \text{Pb}^{2+}$ .

Ligand **31** (the carboxylic acid analogue of **30**) produced a low level of fluorescence in its free state, and various levels of enhanced fluorescence in metal complexes. The most highly fluorescent complex of ligand **31** was that of  $\text{Zn}^{2+}$ , which produced a 4 fold fluorescence enhancement when compared to the fluorescence of the free ligand. The order of decreasing fluorescence with metal ion was  $\text{Zn}^{2+} > \text{Mg}^{2+} > \text{Cd}^{2+} > \text{Pb}^{2+} > \text{Al}^{3+}$ . By comparison with the determined fluorescence order for ligands **30** and **31**, the order of decreasing fluorescence with metal ion is similar except for  $\text{Al}^{3+}$ . Without quantitative stability constants being available for the metal complexes of **30** and **31**, these spectral variations with the nature of the metal ion cannot be interpreted with confidence. However, it is noteworthy that the complexes of the smallest (Table 3.4) and hardest metal ion shows the greatest fluorescence variation. This warrants further study.

**Table 3.4:** *The effective ionic radii of the metal ions (with a coordination number of 6) used in the fluorescence determinations of the complexes of ligands **30** - **33**.<sup>55</sup>*

Metal Ion	$\text{Pb}^{2+}$	$\text{Cd}^{2+}$	$\text{Zn}^{2+}$	$\text{Mg}^{2+}$	$\text{Al}^{3+}$
Effective Ionic Radii (Å)	1.190	0.950	0.740	0.720	0.535

### 3.3.2 The coumarins **32** and **33**

The fluorescence spectra of compound **32** in the presence and absence of  $\text{Pb}^{2+}$ ,  $\text{Zn}^{2+}$ ,  $\text{Cd}^{2+}$ ,  $\text{Mg}^{2+}$  and  $\text{Al}^{3+}$  were examined (Table 3.3, page 104). The ester **32**, in the absence of the studied metal ions, produced a fluorescent spectrum with a maximum fluorescence emission of

615 at a wavelength of 416 nm. Although the preferred condition for a metal ion fluorescent probe is that the probe is weakly or non-fluorescent in the uncomplexed state and highly fluorescent as the metal ion complex, ester **32** could still prove useful as a probe if its fluorescence is selectively quenched by  $\text{Pb}^{2+}$ . The ester **32** in the presence of each of the metal ions produced fluorescence values that did not vary significantly from the value of the fluorescence of **32** in the absence of the metal ions (see spectrum C.2.3 in Appendix C). This suggests that either the metal ions are not coordinating to ester **32** (as previously concluded in Section 3.2.1) and that the difference between the fluorescence maxima is due to experimental and instrumental error, or that the metal ions are producing complexes with **32** whose fluorescence does not vary significantly from the fluorescence of **32** alone. In either case, ester **32** is unsuitable as a  $\text{Pb}^{2+}$ , or any other metal ion specific fluorescent probe.

As with its ethyl ester analogue **32**, the carboxylic acid **33** produced a highly fluorescent spectrum in the absence of the metal ions with a fluorescence maximum of 594 at a wavelength of 422 nm. However, unlike ester **32**, the acid **33** did produce significantly different fluorescence levels in the presence of  $\text{Pb}^{2+}$ ,  $\text{Cd}^{2+}$  and  $\text{Al}^{3+}$ , but comparable fluorescence levels in the presence of  $\text{Mg}^{2+}$  and  $\text{Zn}^{2+}$  (Table 3.3 and Figure C.2.4 in Appendix C). The fluorescence of ligand **33** was partially quenched upon the addition of  $\text{Pb}^{2+}$ ,  $\text{Al}^{3+}$  and  $\text{Cd}^{2+}$  producing respective maximum fluorescence values of 251, 484 and 568, and the fluorescence of **33** was slightly enhanced in the presence of  $\text{Zn}^{2+}$  and  $\text{Mg}^{2+}$  producing maximum fluorescence values of 604 and 612 respectively.

Comparison of the fluorescence emission spectra of the different metal ion complexes of **33** shows that the relative order of the least fluorescent to the most fluorescent complex parallels the relative order of the largest to smallest effective ionic radii (see Table 3.4) of the metal ions studied except for  $\text{Al}^{3+}$ . It is possible that the larger the metal ion in the complex, the more likely the ion breaks down the planarity of the conjugated coumarin and thiazole systems upon complex formation, thus restricting the delocalisation of the  $\pi$  electrons and therefore significantly quenching the fluorescence of ligand **33**. The loss of fluorescence upon complexation can also be attributed to the heavy metal effect. The heavy metal ions  $\text{Pb}^{2+}$  and  $\text{Cd}^{2+}$  (as well as  $\text{Al}^{3+}$ ) quench the fluorescence of **33** most significantly with the  $\text{Zn}^{2+}$  and

Mg<sup>2+</sup> complexes producing comparable fluorescence emission spectra with that of ligand **33** alone. However, these conclusions must be considered provisional at best, as the complex stability constants are unavailable. These observations provide an opportunity for further study.

### 3.3.3 Summary

In summary, the benzopyran-4-one ester ligand **30** and its carboxylic acid derivative **31** did not produce significant fluorescence in the uncomplexed state. However, both ligands produced various levels of enhanced fluorescence when complexed to each of the studied metal ions which include Pb<sup>2+</sup>, Cd<sup>2+</sup>, Zn<sup>2+</sup>, Mg<sup>2+</sup> and Al<sup>3+</sup>. The most fluorescent complex of **30** was the Al<sup>3+</sup> complex which produced only a 4 fold fluorescence enhancement as compared with the fluorescence of the free ligand. The most fluorescent complex of **31** was the Zn<sup>2+</sup> complex which also produced only a 4 fold fluorescence enhancement. As it required a 100 fold excess of metal ion to ligand concentration to produce poorly fluorescent complexes of both ligands **30** and **31** of which neither were specific for one particular metal ion, the ligands **30** and **31** do not appear to be useful as fluorescent probes for Pb<sup>2+</sup> or any other metal ion.

The coumarin ester **32** and its carboxylic analogue **33** were found to be highly fluorescent when irradiated at a wavelength of 353 nm with respective fluorescence emission values of 651 and 594. The fluorescence of compound **32** was found not to vary significantly in the absence and presence of the studied metal ions suggesting that either all the metal ions did not coordinate to **32** or that they each coordinated in a manner not effecting the fluorescence emission of **32**. In comparison, the fluorescence of **33** was found to vary significantly in the presence of Pb<sup>2+</sup> and Al<sup>3+</sup>, moderately in the presence of Cd<sup>2+</sup> and insignificantly in the presence of Zn<sup>2+</sup> and Mg<sup>2+</sup>.

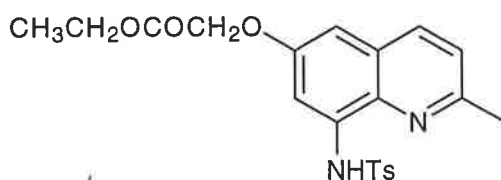
Although ligands **30** - **33** themselves do not appear to act as sufficient fluorescent probes for Pb<sup>2+</sup> or other metal ions, these compounds may be used as models on which more successful metal ion fluorescent probes could be designed.

## Chapter 4: Quinoline and Pyridine Analogues

### 4.1 Synthesis

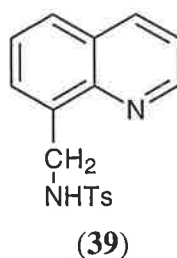
#### 4.1.1 C<sub>8</sub> Substituted Quinoline Derivatives

Zinquin-Ester, as mentioned previously (Section 1.3), is a fluorescent probe specific for Zn<sup>2+</sup>, which has been used to detect exchangeable Zn<sup>2+</sup> within living cells. This probe has the required specificity and sensitivity for Zn<sup>2+</sup>.<sup>25</sup> Since its structure could be modified to selectively coordinate larger metal ions, Zinquin-Ester was chosen as the basis for the synthesis of potential ligands for Pb<sup>2+</sup>.



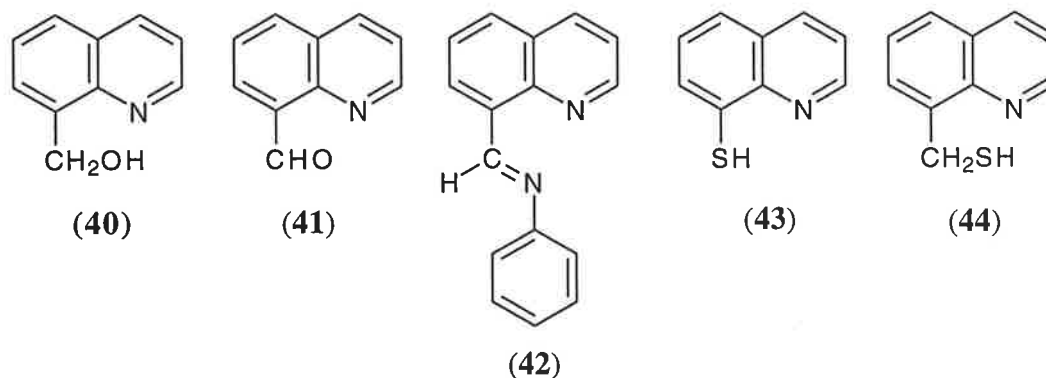
Zinquin Ester

It was anticipated that synthesis of a Zinquin analogue (with a coordination site that differed from Zinquin) may produce a compound which could coordinate Pb<sup>2+</sup> in preference to or as well as Zn<sup>2+</sup>. *N*1-(8-Quinolylmethyl)-4-methyl-1-benzene sulfonamide (**39**) was chosen as the first such ligand. This ligand contains a methylene group between C<sub>8</sub> of the quinoline ring and the nitrogen of the sulfonamide group as compared with Zinquin-Ester. Although the introduction of the methylene group disrupts the conjugation between the quinoline ring and the sulfonamide group (which may reduce the fluorescence of the ligand) it was hoped that investigation into the physical properties of **39** would provide further understanding of the physical properties of Zinquin-Ester.

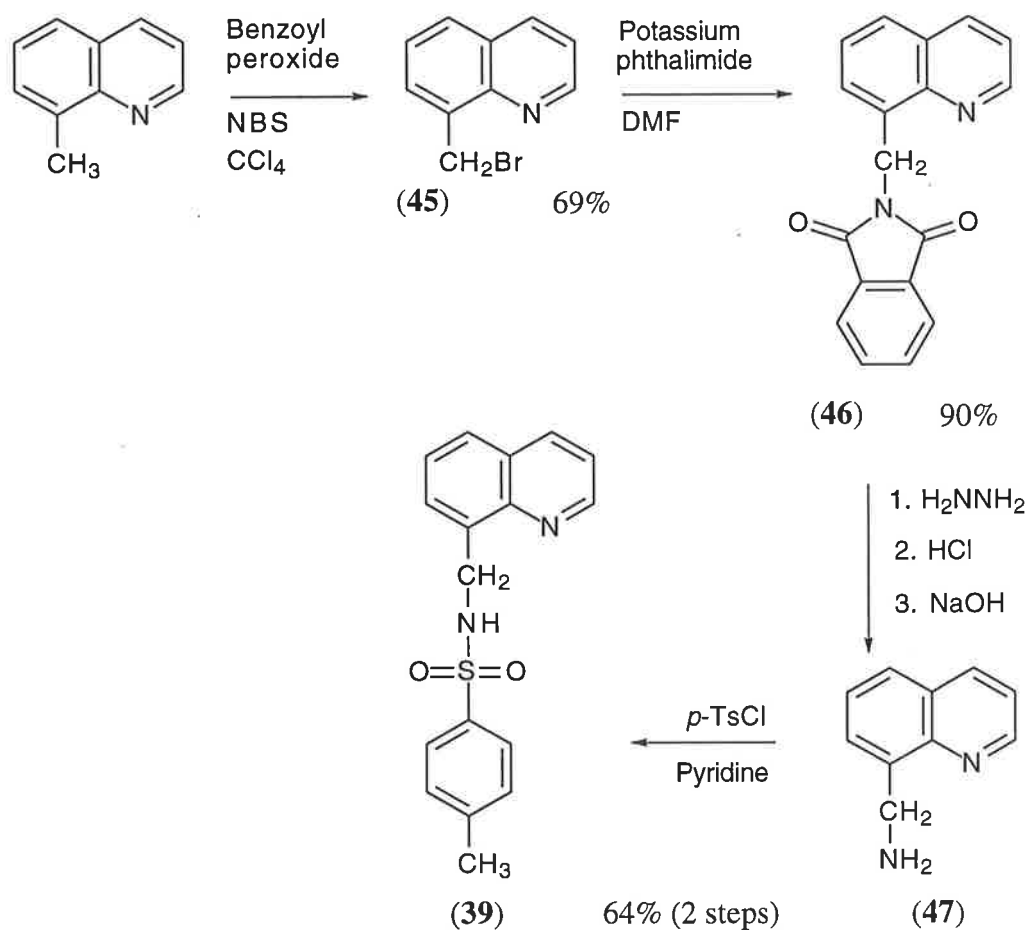


To allow comparisons to be made with the electron donating ability of the sulfonamide nitrogen on the sulfonamide **39** with other donor atoms such as oxygen and sulfur, a series of potential

ligands (**40 - 44**) which contained various other heteroatoms in place of nitrogen were synthesised.



The sulfonamide **39** was synthesised *via* the route outlined in Scheme 4.1.

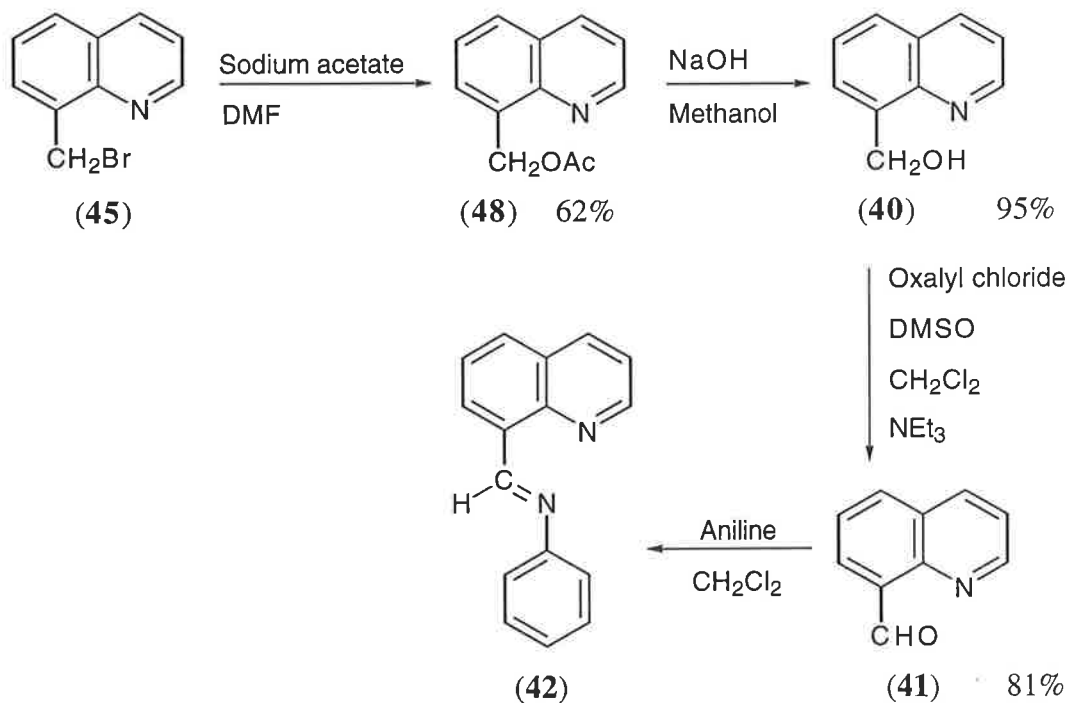


Scheme 4.1

8-Methylquinoline was brominated with *N*-bromosuccinimide in carbon tetrachloride giving 8-(bromomethyl)quinoline (**45**) in 69% yield.<sup>94</sup> This reaction was followed by an  $S_N2$  reaction with potassium phthalimide in DMF to produce, in 90% yield, the phthalimido compound **46**. The protecting phthalimide group was removed using hydrazine hydrate giving the free amine 8-methylaminoquinoline (**47**) which was reacted further without purification to form the

sulfonamide **39** using *p*-toluenesulfonyl chloride in pyridine at room temperature. The overall yield for the two steps was 64% (Scheme 4.1). The  $^1\text{H}$  NMR spectrum of **39** contained a triplet at  $\delta$  6.64 ppm for the sulfonamide proton and a doublet at  $\delta$  4.65 ppm for the methylene protons to which the sulfonamide proton is coupled. All other peaks in the  $^1\text{H}$  NMR spectrum were consistent with the proposed structure **39**. The IR spectrum of **39** confirmed the presence of the sulfonamide showing a N-H stretch at  $3276\text{ cm}^{-1}$  and the mass spectrum produced a mass peak at a  $m/z$  of 312.

8-Quinolylmethanol (**40**) was synthesised so that comparisons could be made with sulfonamide **39**, and consequently between nitrogen and oxygen as coordinating atoms. To prepare **40**, 8-(bromomethyl)quinoline (**45**) was subject to a nucleophilic attack by sodium acetate to produce the acetate **48**. This was followed by hydrolysis of the acetate group to produce the required alcohol **40** in 95% yield (Scheme 4.2).<sup>95</sup> The  $^1\text{H}$  NMR spectrum of the product was consistent with that of the literature containing a broad signal at  $\delta$  5.09 ppm for the hydroxyl proton, a singlet at  $\delta$  5.20 ppm for the methylene protons and a multiplet between  $\delta$  8.21 ppm and  $\delta$  8.86 ppm for the aromatic protons.



Scheme 4.2

The facile synthesis of the alcohol **40** led to the production of the further conjugated 8-quinoline carbaldehyde **41** via a Swern oxidation. The aldehyde carbonyl in **41** is conjugated to the

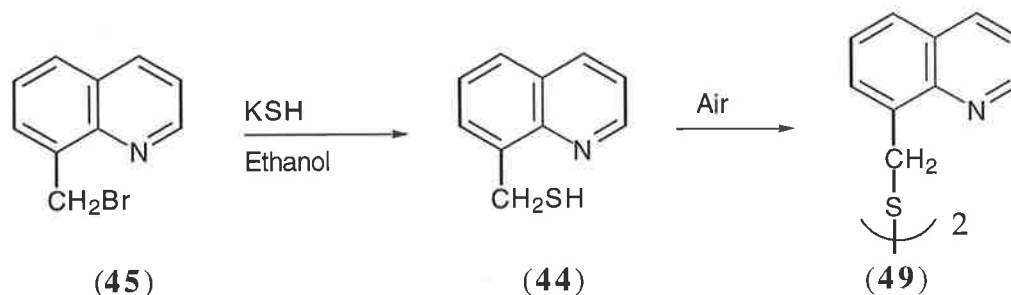
quinoline ring system which is likely to be an important requirement for the fluorescence of the ligand, whereas the hydroxy oxygen in **40** is not conjugated to the quinoline ring. According to Bridges, for an organic molecule to fluoresce structural rigidity, planarity and extensive conjugation are required (see section 2.5.2).<sup>76</sup> The alcohol **40** was reacted with oxalyl chloride in dichloromethane and one molar equivalent of DMSO at  $-70^{\circ}\text{C}$  to produce 8-quinolinecarbaldehyde (**41**) (Scheme 4.2). The product was identified by its  $^1\text{H}$  NMR spectrum which contained a signal at  $\delta$  11.47 ppm for the aldehyde proton, and its melting point was consistent with the literature melting point.<sup>96</sup>

To produce a compound with more extensive conjugation than that of aldehyde **41** (and hence a potentially greater fluorescence) the imine **42** was synthesised (Scheme 4.2). Treatment of **41** with aniline in dichloromethane in the presence of crushed  $4\text{\AA}$  molecular sieves yielded **42** as a crude oil. In an attempt to purify crude **42** using column silica chromatography, hydrolysis of the imine to form aldehyde **41** occurred. The only impurity in the product mixture was the excess, unreacted aniline (shown by the presence of the broad singlet at  $\delta$  3.64 ppm corresponding to the amide protons, and the multiplets in the chemical shift ranges of  $\delta$  6.64 - 6.80 ppm and  $\delta$  7.15 - 7.25 ppm corresponding to the aromatic protons in the  $^1\text{H}$  NMR spectrum) the reaction was repeated and the resulting crude oil was purified by the evaporation of the excess aniline under reduced pressure. The yellow solid was sufficiently pure to characterise by  $^1\text{H}$  NMR and was identified as structure **42** according to mass spectral (molecular ion at  $m/z$  232) and  $^1\text{H}$  NMR data. The  $^1\text{H}$  NMR spectrum contained a multiplet between  $\delta$  7.26 - 9.00 ppm for the aromatic protons and a singlet at  $\delta$  9.94 ppm for the imine proton ( $-\text{CH}=\text{N}-$ ).

Lead(II) is a soft acid metal ion and should therefore have a preferential affinity for soft base sulfur donor atoms over oxygen and nitrogen donor atoms. It was anticipated that a thiol analogue of quinolines **39** and **40** would produce a stable, more selective ligand for  $\text{Pb}^{2+}$ . Attempts to make thiol **44** were made following the procedure of Bankovskis *et al.* (Scheme 4.3).<sup>94</sup> 8-(Bromomethyl)quinoline (**45**) was treated with an ethanolic solution of potassium hydrosulfide which was prepared by saturating a solution of potassium hydroxide in ethanol with hydrogen sulfide gas.  $^1\text{H}$  NMR analysis of the pale yellow oil that was obtained

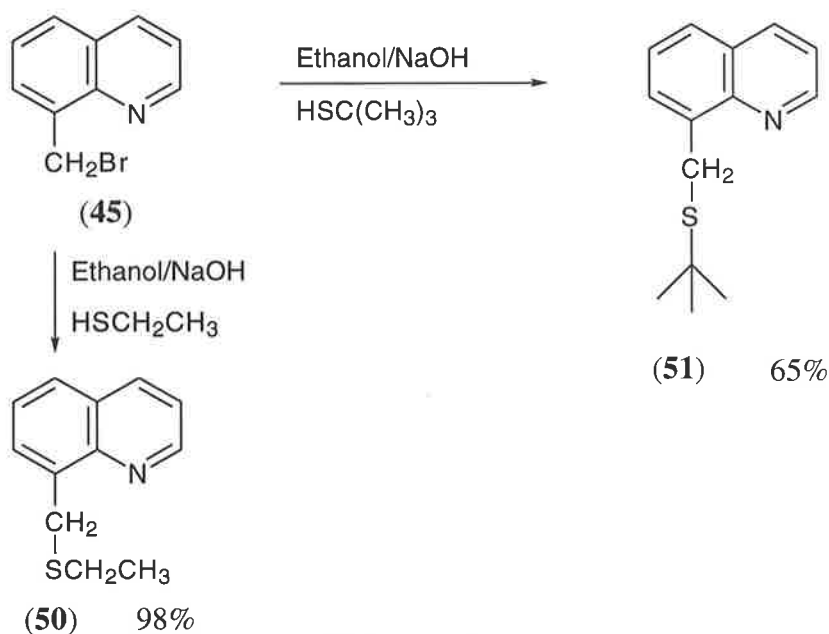


supported thiol structure **44** (Scheme 4.3). The  $^1\text{H}$  NMR spectrum showed a triplet at  $\delta$  2.35 ppm for the thiol proton and a doublet at  $\delta$  4.26 ppm for the methylene protons.



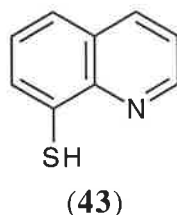
Scheme 4.3

The thiol **44** was unstable in air and within an hour it had oxidised to the disulfide (**49**).<sup>94</sup> This was evident from the  $^1\text{H}$  NMR spectrum of **49** which showed a singlet at  $\delta$  4.49 ppm for the methylene protons (as compared to a doublet in the spectrum of **44**) and no signal for a thiol. As a consequence of the instability of 8-quinolylmethanethiol (**44**), the protected thiols **50** and **51** were synthesised to produce more stable structures capable of coordinating to  $\text{Pb}^{2+}$  (Scheme 4.4). Two different thiol protected analogues were prepared, one with a bulky *t*-butyl group and the other with a less hindering ethyl group, to determine if steric factors influenced the binding capabilities of  $\text{Pb}^{2+}$ . Both of the thioethers **50** and **51** were made from 8-(bromomethyl)quinoline (**45**) (Scheme 4.4) which was treated with the respective thiols in an alkaline ethanolic solution heated to  $50^\circ\text{C}$ . Microanalytical, mass spectral and NMR data confirmed the structure of thioether **51**. Only NMR data was collected for **50**, as this compound decomposed within days of production.



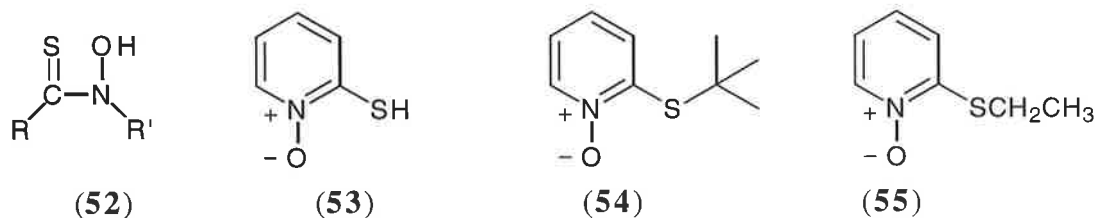
Scheme 4.4

The use of 8-quinolinethiol (**43**) for the fluorometric determination of  $\text{Zn}^{2+}$  contained in Portland cement has been described in the literature.<sup>97</sup> Removal of interfering cations, including  $\text{Pb}^{2+}$ , by the use of sodium thiosulfate prior to analysis was required using this method, suggesting  $\text{Pb}^{2+}$  forms a fluorescent complex with ligand **43**. Consequently 8-quinolinethiol (**43**) (commercially available as the hydrogen chloride salt) was also chosen as a ligand to be studied.



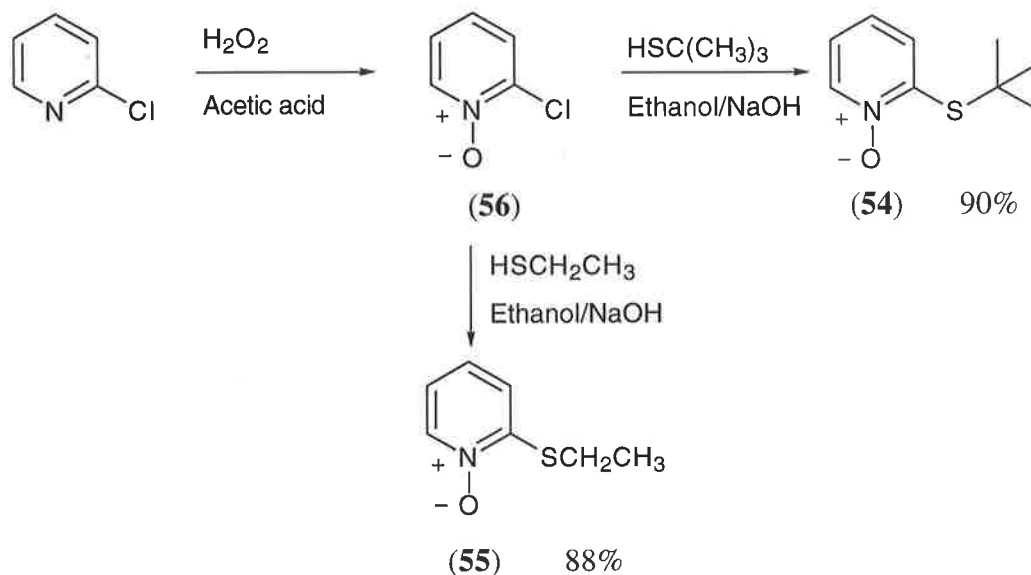
#### 4.1.2 Pyridine and Quinoline 1-Oxides

In pursuit of a chelating agent that was powerful and selective for  $\text{Pb}^{2+}$ , Raymond *et al.* discovered that thiohydroxamic acids (**52**) formed stable complexes with  $\text{Pb}^{2+}$ .<sup>3,98,99</sup> The ligands synthesised in their research were of the 1-hydroxypyridinethione (**53**) type, which were reported in 1963 by Robinson as being capable of forming heavy metal derivatives.<sup>100</sup> The research of Raymond and Robinson provided a basis on which a rational design for  $\text{Pb}^{2+}$  selective fluorescent probes could be established.



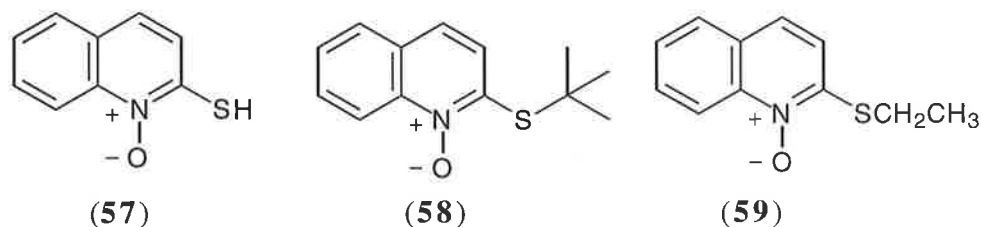
Thione **53** is commercially available as its hydrated sodium salt. The instability of this compound in air and solution made the S-protected *t*-butyl and ethyl derivatives **54** and **55** more attractive as synthetic targets. To prepare these derivatives, 2-chloropyridine was treated with aqueous hydrogen peroxide in acetic acid followed by digestion with potassium carbonate to form the 1-oxide **56** in 70% yield (Scheme 4.5).<sup>101</sup> Treatment of 2-chloropyridine-1-oxide (**56**) with *t*-butylthiol and ethanethiol respectively in ethanol containing sodium hydroxide produced **54** and **55** in good yields (Scheme 4.5). The <sup>1</sup>H NMR spectra of **54** and **55** indicated the presence of the 1-oxide functional groups by the chemical shifts of the H<sub>6</sub> protons which were at  $\delta$  8.22 ppm and  $\delta$  8.27 ppm respectively (further downfield than the H<sub>6</sub> protons on other pyridyl analogues). The spectrum of **54** also showed a singlet at  $\delta$  1.46 ppm with an

integration of 9 for the *t*-butyl protons and the spectrum of **55** showed a triplet at  $\delta$  1.46 ppm and a quartet at  $\delta$  2.94 ppm for the ethyl protons.

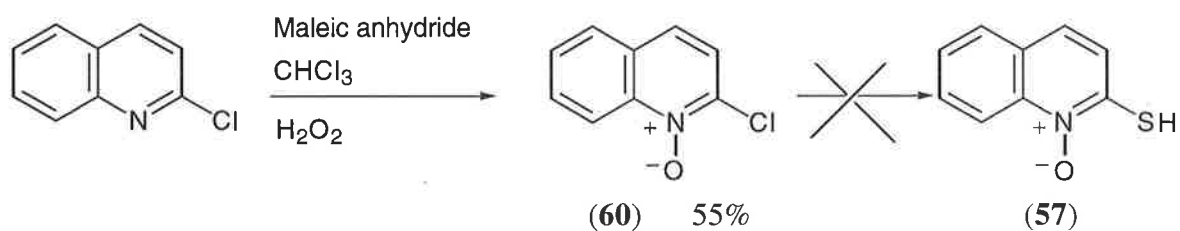


**Scheme 4.5**

Although the pyridinethione analogues may form stable complexes with  $\text{Pb}^{2+}$ , their extent of conjugation is restricted to a monocyclic system. To improve UV-visible absorption and fluorescence properties, quinoline type analogues of the pyridinethiones (**53**, **54** and **55**) were required. Thus compounds **57**, **58** and **59** were prepared.



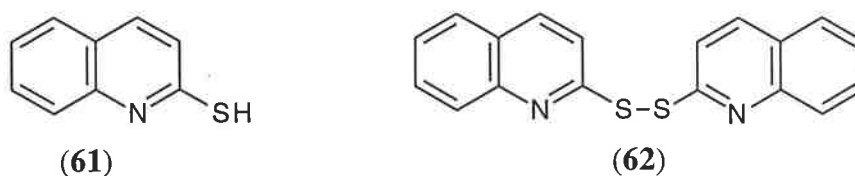
2-Chloroquinoline-1-oxide (**60**) was prepared from 2-chloroquinoline by treatment with 32% hydrogen peroxide in chloroform with excess maleic anhydride at room temperature for five days in a 55% yield (Scheme 4.6).<sup>102</sup>



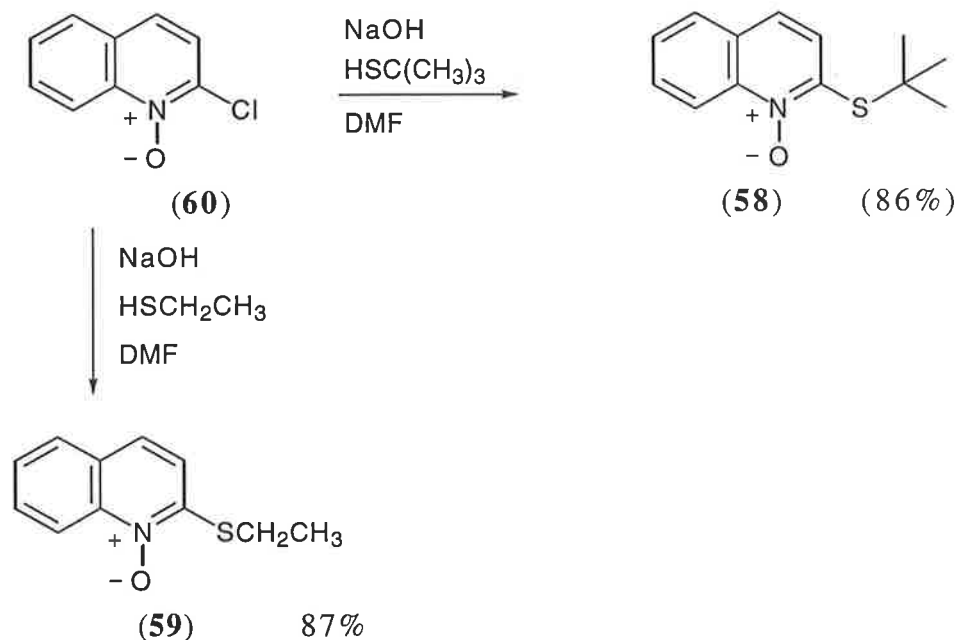
**Scheme 4.6**

Treatment of the 1-oxide **60** with sodium hydrosulfide in ethanol (Scheme 4.6) did not produce the required 2-mercaptoquinoline-1-oxide (**57**). Under these conditions it was evident from  $^1\text{H}$

NMR, that redox transfer of the oxygen from **60** or even possibly **57** occurred resulting in reduction of the respective quinoline-1-oxide. The presence of quinoline-1-oxides are typically indicated in  $^1\text{H}$  NMR spectra by the chemical shift of the  $\text{H}_8$  proton which is found further downfield compared with the other quinoline aromatic protons (e.g.  $\text{H}_8 = 8.74$  ppm in the  $^1\text{H}$  NMR spectrum of **60**), however, no peaks were found above  $\delta$  8.04 ppm in the  $^1\text{H}$  NMR spectrum of the reaction mixture. The  $^1\text{H}$  NMR spectrum of the product indicated the presence of 2-chloroquinoline and possibly the thiol **61** and the disulfide **62** in reference to the  $^1\text{H}$  NMR spectra of **61** and 2-chloroquinoline obtained from The Aldrich Library of  $^{13}\text{C}$  and  $^1\text{H}$  FT NMR Spectra, Edition 3.<sup>103</sup>



To overcome the problem of the reduction of **60** (which is most likely due to **61** and/or the sodium hydrosulfide) the thiol protected compounds **58** and **59** were produced. The protected *t*-butyl and ethyl quinoline-1-oxide thiols **58** and **59** were synthesised in good yields by treating 2-chloroquinoline-1-oxide (**60**) with *t*-butylthiol and ethanethiol respectively (Scheme 4.7). The mass spectra of **58** and **59** contained the relevant respective molecular ions of  $m/z$  233 and  $m/z$  205.



Scheme 4.7

## 4.2 Investigations into the Chelating Properties of the Quinoline and Pyridine Analogues

To determine whether the pyridine and quinoline compounds **39 - 44**, **50**, **51**, **53 - 55**, **58** and **59** coordinate  $\text{Pb}^{2+}$ , the UV-visible absorption spectra of these compounds were recorded in the presence and absence of  $\text{Pb}^{2+}$ , as similarly described in Chapters 2 and 3 with the flavone and thiazole type ligands. The metal ions  $\text{Cd}^{2+}$  and  $\text{Zn}^{2+}$  as well as  $\text{Pb}^{2+}$  were also studied as part of this investigation due to the added interest of developing a probe for the toxic heavy metal ion  $\text{Cd}^{2+}$ . Zinc (II) was chosen due to its closely related chemical properties to  $\text{Cd}^{2+}$ .

Since the colourless oils **50** and **54** decomposed to brown oils, and the thiol **44** oxidised to the disulfide **49** within a few hours on standing at room temperature, these ligands were omitted from the UV-visible determined chelation studies. The instability of these compounds rendered them unsuitable as analytical reagents for metal ion detection. Therefore only the UV-visible absorption spectra of the compounds **39 - 43**, **51**, **53**, **55**, **58** and **59** under the conditions used in Sections 2.2 and 3.2 in the absence and presence of  $\text{Pb}^{2+}$ ,  $\text{Cd}^{2+}$  and  $\text{Zn}^{2+}$  were recorded. The spectra are presented in Appendix A.

No significant shifts in the UV-visible absorbance spectra of any of the compounds were observed in the presence of the metal ions studied except for the ligands **43** and **53**. Both of these ligands produced shifts in their spectra when complexed to  $\text{Pb}^{2+}$ ,  $\text{Zn}^{2+}$  and  $\text{Cd}^{2+}$  with the spectra of the complexes of **43** producing bathochromic shifts and the complexes of **53** producing hypsochromic shifts (Table 4.1).

From these results it was concluded that all of the  $\text{C}_8$  substituted quinoline compounds studied (**39 - 43**, **50**, **51**), except for **43**, did not produce detectable complexes with  $\text{Pb}^{2+}$ ,  $\text{Cd}^{2+}$  or  $\text{Zn}^{2+}$  under the experimental conditions. Therefore, based on the above observations, a bite through 4 bonds for  $\text{C}_8$  substituted quinolines is not as suitable as a bite through 3 bonds when considering metal ion coordination (Figure 4.1). In further support to this theory other  $\text{C}_8$  substituted quinoline ligands with a bite through 3 bonds, such as Zinquin-Ester and 8-hydroxyquinoline, have demonstrated the ability to form stable, detectable complexes.<sup>25,104,105</sup>

**Table 4.1:** UV-visible absorption wavelength maxima of the ligands **43** and **53** in the presence and absence of the listed metal ions.

Ligand	Metal Ion	Absorption Wavelength Maxima (nm)
8-Mercaptoquinoline ( <b>43</b> ) <sup>a</sup>		320
	Pb <sup>2+</sup>	387
	Cd <sup>2+</sup>	389
	Zn <sup>2+</sup>	387
2-Mercaptopyridine-N-oxide ( <b>53</b> ) <sup>b</sup>		278:333
	Pb <sup>2+</sup>	268:324
	Cd <sup>2+</sup>	279:330
	Zn <sup>2+</sup>	275:324

<sup>a</sup> Measured between the wavelengths 280 - 500 nm

<sup>b</sup> Measured between the wavelengths 260 - 400 nm

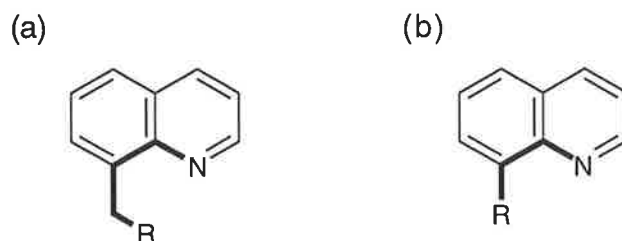


**Figure 4.1:** A diagram of C<sub>8</sub> substituted quinolines with a bite through (a) 4 bonds as represented by compounds **39** - **42**, **50** and **51** and (b) 3 bonds as represented by compound **43**.

Although **43** was the only C<sub>8</sub> substituted quinoline compound found to chelate to Pb<sup>2+</sup>, Cd<sup>2+</sup> and Zn<sup>2+</sup>, it could not serve adequately as an analytical agent because of its facile oxidation to the bisquinolyl disulfide. Previous studies on the metal ion chelates of 8-mercaptoquinoline (**43**) found that the absorbance of the chelates decreased as a function of time even in the presence of reducing agents such as glucose and hydroxylamine hydrochloride.<sup>106</sup> Based on the above observations and the fact that **43** is not specific for Pb<sup>2+</sup> (according to stability constant measurements, Table 4.2) further physical studies were not performed using this compound.

**Table 4.2:** Formation constants ( $\log K_{f1}$ ) for 1:1 chelates of 8-mercaptoquinoline in 50% aqueous dioxane as reported by Corsini et al.<sup>106</sup>

Metal Ion	Cu <sup>2+</sup>	Pb <sup>2+</sup>	Zn <sup>2+</sup>	Ni <sup>2+</sup>	Mn <sup>2+</sup>
Formation Constants ( $\log K_{f1}$ )	12 - 14 <sup>a</sup>	11.85	11.05	10.95	6.74

<sup>a</sup> Quantitative data for the Cu chelate were not obtained since reduction of Cu<sup>2+</sup> to Cu<sup>+</sup> was suspected

Further conclusions drawn from these chelation studies are that of the quinoline and pyridine-1-oxides examined (**53**, **55**, **58** and **59**) only **53** coordinated to the metal ions studied. As **53** was the only 1-oxide which did not have its thiol group protected with a *t*-butyl or ethyl group, this suggests that the free thiol or thione form of the thiohydroxamate group is vital for metal ion coordination. Although **53** did chelate the metal ions studied, and does contain the thiohydroxamate group which has been found to be the most stable and specific functional group for the chelation to Pb<sup>2+</sup>,<sup>3</sup> further physical measurements were not carried out. As **53** has a great propensity towards oxidation to form the disulfide, it was believed that **53** and other such aromatic thiohydroxamate ligands would be too unstable to act as Pb<sup>2+</sup> fluorescent probes.<sup>100</sup>

In conclusion, a series of C<sub>8</sub> substituted quinolines and pyridine and quinoline-1-oxides have been synthesised and assessed for their ability to chelate Pb<sup>2+</sup>, Cd<sup>2+</sup> and Zn<sup>2+</sup>. This assessment has emphasised the pitfalls in utilising thiolate compounds as analytical reagents and has demonstrated that these ligand types are unsuitable as fluorescent ligands for Pb<sup>2+</sup>.

## Chapter 5: Summary and Suggested Future Work

This thesis describes the development of potential  $\text{Pb}^{2+}$  selective fluorescent ligands which could be used as probes to detect and measure  $\text{Pb}^{2+}$  in biological and aqueous samples. Due to the adverse health effects of  $\text{Pb}^{2+}$  in humans, there is a demand for more sophisticated clinical screening and  $\text{Pb}^{2+}$  detection methods. Also of interest were the development of fast and efficient methods for detecting other metal ions which are known to be, or suspected as being, harmful to humans such as  $\text{Al}^{3+}$  and  $\text{Cd}^{2+}$ .

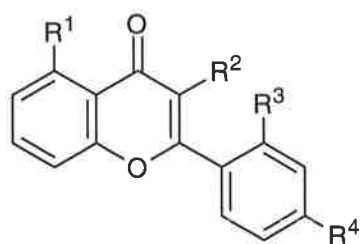
### The Flavones and Thioflavones

A series of ligands were synthesised based on the structure of morin (**2**) which is a polyoxygenated, naturally occurring flavone. The flavones prepared were those of the  $\text{C}_3$  hydroxy and  $\text{C}_5$  hydroxy type, **4**, **5** and **8**, along with their corresponding thioflavone analogues **6**, **7** and **9**. Also synthesised were the methoxy flavone analogues **10**, **11** and **12**, which do not contain a  $\text{C}_3$  or  $\text{C}_5$  hydroxy group. These compounds were then studied for their ability to coordinate to a series of metal ions as part of a selectivity test.

A series of metal ions were chosen to determine whether they formed complexes with the synthesised compounds **4** - **12**. Selection criteria for each metal ion were based on whether the metal ion is present in biological systems or is one of environmental interest. The metal ions selected were  $\text{Pb}^{2+}$ ,  $\text{Mg}^{2+}$ ,  $\text{Ca}^{2+}$ ,  $\text{Co}^{2+}$ ,  $\text{Cu}^{2+}$ ,  $\text{Ni}^{2+}$ ,  $\text{Zn}^{2+}$ ,  $\text{Cd}^{2+}$  and  $\text{Al}^{3+}$ . The coordination of these metal ions to the compounds **4** - **12** was investigated using UV-visible absorption spectroscopy. The ligands **4** and **5** coordinated all of those metal ions studied except  $\text{Ca}^{2+}$ . The ligands **6** and **7** (the thio analogues of **4** and **5** respectively) were found to be more selective than their oxygenated counterparts as they coordinated all of the metal ions studied except  $\text{Mg}^{2+}$ ,  $\text{Ca}^{2+}$  and  $\text{Al}^{3+}$ . None of the compounds **8** - **12** coordinated to  $\text{Pb}^{2+}$ , with **8** coordinating to  $\text{Mg}^{2+}$ ,  $\text{Co}^{2+}$ ,  $\text{Cu}^{2+}$ ,  $\text{Ni}^{2+}$ ,  $\text{Zn}^{2+}$ ,  $\text{Al}^{3+}$ , **9** coordinated  $\text{Cu}^{2+}$  and  $\text{Ni}^{2+}$  only, and **10** - **12** coordinating none of the studied metal ions. The absence of significant coordination of any of the metal ions to the compounds **10** - **12** suggested that a hydroxyl group in the  $\text{C}_3$  or  $\text{C}_5$  positions is essential for metal ion coordination to flavones of this type.

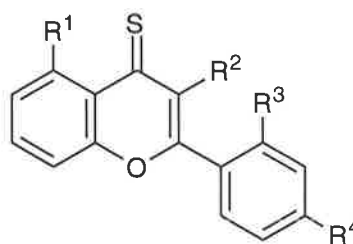


Since **4** - **7** were the only ligands to coordinate to  $\text{Pb}^{2+}$ , the physical properties (stability constants and fluorescence emission spectra) of these ligands as  $\text{Pb}^{2+}$  fluorescent probes were evaluated.



(4)  $\text{R}^1 = \text{R}^4 = \text{H}$   $\text{R}^2 = \text{OH}$   $\text{R}^3 = \text{OMe}$

(5)  $\text{R}^1 = \text{R}^3 = \text{H}$   $\text{R}^2 = \text{OH}$   $\text{R}^4 = \text{OMe}$



(6)  $\text{R}^1 = \text{R}^4 = \text{H}$   $\text{R}^2 = \text{OH}$   $\text{R}^3 = \text{OMe}$

(7)  $\text{R}^1 = \text{R}^3 = \text{H}$   $\text{R}^2 = \text{OH}$   $\text{R}^4 = \text{OMe}$

The stability constants of the complexes formed between the ligands **4** - **7** and  $\text{Pb}^{2+}$ ,  $\text{Zn}^{2+}$ ,  $\text{Cd}^{2+}$  and  $\text{Al}^{3+}$  were determined using UV-visible absorption spectroscopy. The stability constants were determined for all complexes in solutions containing both  $[\text{H}^+] = 1.0 \times 10^{-2}$  M and  $[\text{H}^+] = 1.0 \times 10^{-5}$  M.

The complexes of the oxygenated flavones **4** and **5** produced the same relative metal ion stability order with  $\text{Al}^{3+} > \text{Pb}^{2+}$  in solutions containing  $[\text{H}^+] = 1.0 \times 10^{-2}$  M, and  $\text{Pb}^{2+} > \text{Al}^{3+} > \text{Zn}^{2+} > \text{Cd}^{2+}$  in solutions containing  $[\text{H}^+] = 1.0 \times 10^{-5}$  M. Each complex formed with ligand **5** was found to be more stable than the complex formed with ligand **4** and the same metal ion.

Stability constants for the  $\text{Pb}^{2+}$ ,  $\text{Cd}^{2+}$  and  $\text{Zn}^{2+}$  complexes formed with ligand **6** were also determined. Under the conditions where  $[\text{H}^+] = 1.0 \times 10^{-2}$  M,  $\text{Pb}^{2+}$  was the only metal ion to coordinate to **6**. Under the conditions where  $[\text{H}^+] = 1.0 \times 10^{-5}$  M, the determined stability order was  $\text{Pb}^{2+} > \text{Zn}^{2+} > \text{Cd}^{2+}$ . Most importantly the  $\text{Pb}^{2+}$  complexes formed with ligand **6** were significantly more stable than the  $\text{Pb}^{2+}$  complexes formed with ligands **4** and **5**.

Due to the instability of ligand **7** and its  $\text{Pb}^{2+}$  complex in solution in the presence of light, the stability constants of the complexes of ligand **7** were not determined.

The fluorescence of the complexes formed by the ligands **4** - **7** with  $\text{Pb}^{2+}$ ,  $\text{Al}^{3+}$ ,  $\text{Zn}^{2+}$ ,  $\text{Cd}^{2+}$  and  $\text{Mg}^{2+}$  in  $[\text{H}^+] = 10^{-2}$  M and  $[\text{H}^+] = 10^{-5}$  M were examined. All four ligands produced no fluorescence or low levels of fluorescence when not coordinated to any metal ions.

The oxygenated flavones **4** and **5**, under the higher acid concentration conditions, produced highly fluorescent  $\text{Al}^{3+}$  complexes giving a relative fluorescence of 346 for ligand **4** with  $\text{Al}^{3+}$  at 5 times the concentration of the ligand ( $1.0 \times 10^{-6} \text{ M}$ ), and a relative fluorescence of 931 for ligand **5** with  $\text{Al}^{3+}$  at 2.5 times the concentration of the ligand ( $3.33 \times 10^{-7} \text{ M}$ ). The relative fluorescence of **4** and **5** in the presence of all the other studied metal ions, under the higher acid concentration conditions, did not differ significantly from the fluorescence levels of the ligands **4** and **5** alone when irradiated at the same wavelength. Therefore it can be stated that under the high acid concentration conditions ( $[\text{H}^+] = 10^{-2} \text{ M}$ ) the ligands **4** and **5** are highly selective for  $\text{Al}^{3+}$  with **5** forming a more highly fluorescent  $\text{Al}^{3+}$  complex than **4**.

The oxygenated flavones **4** and **5**, under the conditions of the lower acid concentration ( $[\text{H}^+] = 10^{-5} \text{ M}$ ) produced fluorescent  $\text{Al}^{3+}$  complexes whose fluorescence decreased over time. This loss of fluorescence was attributed to the high concentration of hydroxo aluminium(III) species which are most likely to deconjugate the flavone system by attack at the  $\text{C}_2$  position (ie. through a coordinated hydroxide attack).

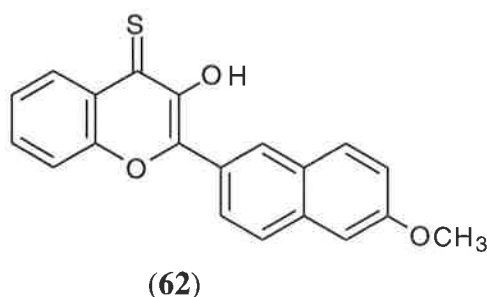
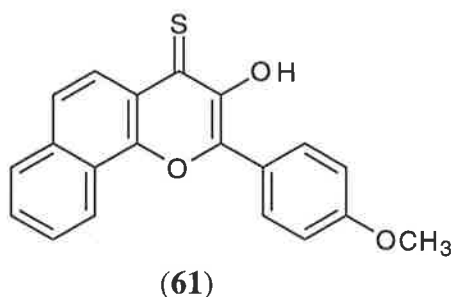
The ligands **4** and **5**, in solutions containing  $1.0 \times 10^{-5} \text{ M}$  acid, produced moderate to weakly fluorescent species with  $\text{Zn}^{2+}$  and weakly fluorescent complexes with  $\text{Pb}^{2+}$  and  $\text{Cd}^{2+}$ , and fluorescent levels comparable to the fluorescence of the free ligands for  $\text{Mg}^{2+}$ . These ligands were not metal ion selective under these low acid concentration conditions ( $[\text{H}^+] = 10^{-5} \text{ M}$ ) and did not produce high fluorescence levels with any metal ion.

On assessing the value of ligands **4** and **5** as metal ion specific probes it appears that ligand **5**, under highly acidic conditions (where  $[\text{H}^+] = 10^{-2} \text{ M}$ ), is the most suitable as a fluorescent probe for  $\text{Al}^{3+}$ . Ligand **5** produced high levels of fluorescence in the presence of  $\text{Al}^{3+}$ , and low levels of fluorescence (comparable to the fluorescence values of ligand **5** in the free state when irradiated at the same wavelength) in a 100 fold excess of the metal ions  $\text{Pb}^{2+}$ ,  $\text{Zn}^{2+}$ ,  $\text{Cd}^{2+}$  and  $\text{Mg}^{2+}$ . Aluminium(III) in a concentration as low as  $3.33 \times 10^{-8} \text{ M}$  produced twice the fluorescence as that of the free ligand **5**. This inherent sensitivity and selectivity of ligand **5** for  $\text{Al}^{3+}$  provides a strong basis for the development of an  $\text{Al}^{3+}$  fluorescent probe.

The fluorescence spectra of ligand **6** and its  $\text{Pb}^{2+}$ ,  $\text{Zn}^{2+}$  and  $\text{Cd}^{2+}$  complexes were also examined. The metal ions  $\text{Al}^{3+}$  and  $\text{Mg}^{2+}$  were not studied with this ligand due to no coordination being observed in the chelation studies of ligand **6**. Ligand **6** in its free state produced no fluorescence in solutions containing  $[\text{H}^+] = 10^{-2}$  M and  $[\text{H}^+] = 10^{-5}$  M. It also produced negligible or low fluorescence levels in the presence of metal ions suggesting that this ligand is unsuitable as a fluorescent probe.

The fluorescence spectra of ligand **7** were examined along with those of the metal complexes which ligand **7** forms. Under the conditions where  $[\text{H}^+] = 10^{-2}$  M, ligand **7** appears to be quite selective for  $\text{Pb}^{2+}$  giving a weak fluorescence of 47. Comparatively, the relative fluorescence values for the unbound ligand and other metal complexes were negligible. However, under the conditions where  $[\text{H}^+] = 10^{-5}$  M the ligand **7** produced a more highly fluorescent  $\text{Zn}^{2+}$  complex (relative fluorescence of 331) than a  $\text{Pb}^{2+}$  complex (relative fluorescence of 115) with  $\text{Cd}^{2+}$  producing a relative fluorescence value of 69.

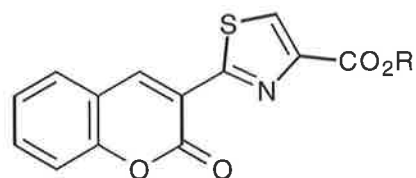
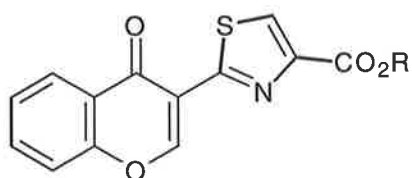
Although ligand **7** was found to decompose in its complexed and uncomplexed state in the presence of light, of the flavones studied, **7** possessed the most favourable qualities for a  $\text{Pb}^{2+}$  fluorescent probe. Under the higher acid concentration conditions ( $[\text{H}^+] = 10^{-2}$  M) ligand **7** is quite selective for  $\text{Pb}^{2+}$ . Besides its potential to decompose in solution the other main disadvantage with ligand **7** is that its  $\text{Pb}^{2+}$  complex is only moderately fluorescent. Therefore analogues of **7** with further conjugation (such as compounds **61** and **62**) may be more suitable target compounds with the potential to produce more intense fluorescence.



From the metal ion coordination, complex stability and fluorescence studies performed using the flavones it would appear that 3 hydroxyl groups, stable sulfur containing functional groups, electron donating substituents and conjugating aromatic groups should be incorporated into future flavone  $\text{Pb}^{2+}$  fluorescent probe designs.

## The Thiazoles

Based upon the  $\text{Pb}^{2+}$  stable thiazoline ligand **18** and the benzopyran sub structure (the A-C substructure of the flavones), the compounds **30** - **33** were synthesised as potential  $\text{Pb}^{2+}$  fluorescent probes. The compounds **30** - **33** were tested for their ability to coordinate to a series of metal ions using UV-visible absorption spectroscopy. The metal ions chosen were the same as those used for the flavone chelation studies which are  $\text{Pb}^{2+}$ ,  $\text{Mg}^{2+}$ ,  $\text{Ca}^{2+}$ ,  $\text{Co}^{2+}$ ,  $\text{Cu}^{2+}$ ,  $\text{Ni}^{2+}$ ,  $\text{Zn}^{2+}$ ,  $\text{Cd}^{2+}$  and  $\text{Al}^{3+}$ .

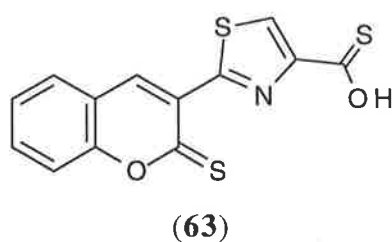


The ester ligands **30** and **32** did not produce detectable complexes under the conditions used as there was no change in the UV-visible absorption spectra of these ligands in the presence of the studied metal ions. However, ligand **33** coordinated to all the metal ions, and **31** coordinated to all the metal ions except  $\text{Ca}^{2+}$  and  $\text{Mg}^{2+}$ . These results suggest that the complexes of **31** and **33** may form stable terdentate species with chelation probably occurring through the carboxylate group, the nitrogen on the heterocyclic ring and the carbonyl functional group, whereas the esters **30** and **32** do not form stable enough complexes to be detected under the conditions of this study.

The fluorescence spectra of **30** - **33** were determined in the absence and presence of  $\text{Pb}^{2+}$ ,  $\text{Al}^{3+}$ ,  $\text{Mg}^{2+}$ ,  $\text{Zn}^{2+}$  and  $\text{Cd}^{2+}$ . The benzopyran-4-one type compounds **30** and **31** produced poor fluorescence in the absence of the studied metal ions and slightly enhanced but still poor fluorescent levels in the presence of each metal ion. These non selective and poor fluorescent qualities rendered **30** and **31** unsuitable as  $\text{Pb}^{2+}$  or any other metal ion probe. The coumarin ester **32** and its carboxylic analogue **33** were found to be highly fluorescent in the free ligand state producing respective relative fluorescence emission values of 651 and 594. The fluorescence of **32** was found not to vary significantly in the absence and presence of the studied metal ions suggesting no significant coordination. In comparison, the fluorescence of

**33** was found to vary significantly in the presence of  $\text{Pb}^{2+}$  and  $\text{Al}^{3+}$ , moderately in the presence of  $\text{Cd}^{2+}$  and insignificantly in the presence of  $\text{Zn}^{2+}$  and  $\text{Mg}^{2+}$ .

Although the synthesised compounds **30** - **33** were found to be inappropriate as metal ion probes, the studies performed on these compounds has provided insight into the design of potentially more efficient  $\text{Pb}^{2+}$  fluorescent probes. The conclusions drawn from the coordination and fluorescence studies of ligand **33** suggest that the free ligand is too fluorescent (as it is preferred that the ligand is non fluorescent in the free state and highly fluorescent as the complex) and that the ligand is not specific for  $\text{Pb}^{2+}$ . To overcome these problems, a strongly quenching group could be introduced into the molecule which would reduce the fluorescence of the free ligand and possible coordination of this new ligand to the less strongly quenching  $\text{Pb}^{2+}$  might lead to a net fluorescence enhancement. This process was adopted successfully by Czarnik in his attempts to produce a water soluble  $\text{Pb}^{2+}$  chemosensor (see section 1.4). Also the introduction of more soft donor atoms (since  $\text{Pb}^{2+}$  is a soft metal ion) on ligands of this type may increase the specificity for  $\text{Pb}^{2+}$ . For instance the conversion of ligand **33** to its bithiocarbonyl analogue (**63**) may produce a non fluorescent molecule (due to the heavy atom quenching effect of the large S atoms) which could form a highly fluorescent species upon  $\text{Pb}^{2+}$  complexation. This molecule would also possibly be highly selective for  $\text{Pb}^{2+}$  due to the soft S donor atoms and the potentially larger bite size (as typically thiocarbonyl  $\text{S}=\text{C}$  bonds are longer than carbonyl  $\text{O}=\text{C}$  bonds). Therefore ligand **33** may provide a sufficient basis on which potential fluorescent probes for  $\text{Pb}^{2+}$  could be designed.



### The Quinoline and Pyridine Analogues

To widen the survey of molecules used to test as  $\text{Pb}^{2+}$  probes, another series of potential ligands were synthesised (compounds **39** - **44**, **50**, **51**, **53** - **55**, **58** and **59**). The structures of these ligands were based on a quinoline chromophore, and 1-hydroxypyridine-2-thione

which forms stable complexes with  $\text{Pb}^{2+}$ . These compounds were tested for their ability to coordinate to  $\text{Pb}^{2+}$ ,  $\text{Zn}^{2+}$  and  $\text{Cd}^{2+}$  using UV-visible absorption spectroscopy.

The results from the UV-visible absorption determined chelation studies indicated that of the compounds tested, only **43** and **53** produced detectable complexes with  $\text{Pb}^{2+}$ ,  $\text{Zn}^{2+}$  and  $\text{Cd}^{2+}$ . Since **43** and **53** are also both unstable thiols which are susceptible to oxidation, they were deemed unsuitable as analytical reagents. Therefore none of these quinoline or pyridine compounds were found to possess the crucial initial requirements for a compound to be used as a metal ion specific fluorescent probe, which include compound stability in solution and the ability to coordinate metal ions.

## Chapter 6: Experimental

### 6.1 General Synthesis

A Koffler hot stage melting point apparatus equipped with Reichert microscope was used to record all melting points (mp), which are uncorrected. Microanalyses were performed by the Chemistry Department, University of Otago, Dunedin, New Zealand.

Infra red (IR) spectra were recorded as nujol mulls, using a Hitachi 270-30 infra red spectrophotometer and data processor. Ultraviolet/visible (UV-visible) spectra were recorded on a Cary 2200 spectrophotometer using 25% H<sub>2</sub>O/ 75% DMF (by volume) as the solvent.

<sup>1</sup>H and <sup>13</sup>C NMR spectra were obtained using a Bruker ACP 300 Fourier Transform or a Gemini Varian 200 nuclear magnetic resonance (NMR) spectrophotometer. The NMR samples were dissolved in deuteriochloroform (CDCl<sub>3</sub>), or *d*<sub>6</sub>-dimethylsulfoxide (DMSO-*d*<sub>6</sub>) where indicated, using tetramethylsilane as an internal standard. Chemical shifts are quoted as  $\delta$  in parts per million and coupling constants (*J*) are given in Hertz (Hz). Multiplicities are abbreviated as follows: s, singlet; d, doublet; t, triplet; q, quartet; m, multiplet; br, broad. Ar represents aromatic protons.

Mass spectra (MS) were recorded as electron impact mass spectra using an AEI-GEC MS3074 mass spectrometer or as fast atom bombardment (FAB) mass spectra on a Vacuum Generators ZAB 2HF mass spectrometer.

Squat and flash columns <sup>107,108</sup> were made using Merk Silica Gel 60. Analytical TLC was carried out using Merk DC-Alufolien Kieselgel 60 F<sub>254</sub> and was visualised by ultraviolet light (254 and 365 nm).

Purification and drying of reagents was carried out according to Perrin, Armarego and Perrin.<sup>109</sup>

## 6.2 Flavone and Thioflavone Syntheses

### 1-(2-Hydroxyphenyl)-3-(2-methoxyphenyl)-2-propene-1-one (13)<sup>42</sup>

A mixture of 2-hydroxyacetophenone (2.72 g, 0.02 mol), *o*-methoxybenzaldehyde (2.72 g, 0.02 mol), and potassium hydroxide (5.6 g, 0.1 mol) in water (20 cm<sup>3</sup>) and ethanol (20 cm<sup>3</sup>) was stirred at room temperature for 24 h. The reaction mixture was acidified with dilute hydrochloric acid (50 cm<sup>3</sup>) and extracted with dichloromethane (100 cm<sup>3</sup>). The organic layer was dried (MgSO<sub>4</sub>) and the solvent evaporated under reduced pressure producing a yellow solid which was recrystallised from ethanol (3.5 g, 69% yield). mp 110-112 °C (lit.<sup>42</sup> 112-114 °C); IR 3420 (broad), 1640, 1578, 1462 cm<sup>-1</sup>; <sup>1</sup>H NMR (CDCl<sub>3</sub>) δ 3.90 (s, 3H, -OCH<sub>3</sub>), 6.88 - 7.93 (m, 9H, Ar and -CH=CH-), 8.18 - 8.26 (m, 1H, Ar); <sup>13</sup>C NMR (CDCl<sub>3</sub>) δ 55.5, 111.2, 118.4, 118.7, 120.1, 120.6, 120.7, 123.5, 129.5, 129.6, 132.1, 136.0, 141.0, 158.9, 163.5, 194.2; MS *m/z* 254 (M<sup>+</sup>, 51%), 223 (100), 147 (19), 134 (16), 121 (50), 91 (30), 77 (25), 65 (30).

### 1-(2-Hydroxyphenyl)-3-(4-methoxyphenyl)-2-propene-1-one (14)<sup>43</sup>

An aqueous sodium hydroxide solution (50%, 20 cm<sup>3</sup>) was added to a warm solution of *p*-anisaldehyde (5.0 g, 36.7 mmol) and 2-hydroxyacetophenone (5.0 g, 36.7 mmol) in ethanol (50 cm<sup>3</sup>) and the solution was warmed on a hot plate until a yellow-orange precipitate formed. Dilute hydrochloric acid (100 cm<sup>3</sup>) was added and the product was collected by vacuum filtration. The orange solid was recrystallised from ethanol producing orange plates (4.7 g, 50%). mp 90-92 °C (lit.<sup>43</sup> 92-94 °C); IR 1640, 1608, 1562, 1514 cm<sup>-1</sup>; <sup>1</sup>H NMR (CDCl<sub>3</sub>) δ 3.86 (s, 3H, -OCH<sub>3</sub>), 6.89 - 7.65 (m, 9H, Ar and -CH=CH-), 7.86 - 7.94 (m, 1H, Ar); <sup>13</sup>C NMR (CDCl<sub>3</sub>) δ 55.7, 114.8, 117.9, 118.8, 119.0, 120.4, 127.6, 129.8, 130.8, 136.4, 145.6, 162.3, 163.8, 193.9.

### 3-Hydroxy-2-(2-methoxyphenyl)-4H-1-benzopyran-4-one (4)<sup>44</sup>

1-(2-Hydroxyphenyl)-3-(2-methoxyphenyl)-2-propene-1-one (13) (1.0 g, 0.004 mol) was dissolved in a solution of ethanol (30 cm<sup>3</sup>) and aqueous sodium hydroxide (10%, 15 cm<sup>3</sup>) and the mixture was heated to boiling. The boiling solution was removed from the heat to which hydrogen peroxide (32%, 3 cm<sup>3</sup>) was slowly added. The reaction mixture was allowed to stand



for 24 h after which the solution was diluted with water (50 cm<sup>3</sup>) and acidified with aqueous hydrochloric acid (10%, 50 cm<sup>3</sup>). The resulting solid was recrystallised from ethanol (7.0 g, 65%). mp 210-212 °C (lit.<sup>44</sup> 213-214 °C). IR 3296 (broad), 1612, 1288 cm<sup>-1</sup>; UV-vis  $\lambda_{\text{max}}$  330 nm; <sup>1</sup>H NMR (CDCl<sub>3</sub>)  $\delta$  3.79 (s, 3H, -OCH<sub>3</sub>), 6.45 (br s, 1H, OH) 7.05 - 7.72 (m, 7H, Ar), 8.25 - 8.30 (m, 1H, H<sub>5</sub>); <sup>13</sup>C NMR (DMSO-*d*<sub>6</sub>)  $\delta$  55.8, 112.0, 118.4, 120.1, 120.2, 122.1, 124.3, 125.1, 131.1, 131.7, 133.3, 139.3, 147.0, 155.2, 157.3, 172.9; MS *m/z* 268 (M<sup>+</sup>, 64%), 237 (40), 147 (19), 121 (100), 91 (25), 77 (29).

### 3-Hydroxy-2-(4-methoxyphenyl)-4H-1-benzopyran-4-one (5)<sup>44</sup>

1-(2-Hydroxyphenyl)-3-(4-methoxyphenyl)-2-propene-1-one (**14**) (1.0 g, 4.0 mmol) was subject to the same conditions as described above. A yellow crystalline solid was produced (0.6 g, 56%). mp 232-234 °C (lit.<sup>44</sup> 236-237 °C); IR 3225 (broad) 1604, 1568, 1512, 1484 cm<sup>-1</sup>; UV-vis  $\lambda_{\text{max}}$  356 nm; <sup>1</sup>H NMR (CDCl<sub>3</sub>)  $\delta$  3.90 (s, 3H, -OCH<sub>3</sub>), 6.97 (br s, 1H, OH) 7.03 - 8.27 (m, 8H, Ar); MS *m/z* 268 (M<sup>+</sup>, 100%), 253 (19), 197 (37), 92 (91), 63 (74), 41 (43).

### Lawesson's Reagent (15)<sup>48</sup>

Phosphorus pentasulfide (14.0 g, 31.5 mmol) was stirred in anisole (40 cm<sup>3</sup>, 370 mmol) under nitrogen and the solution was heated for 6 h at 155 °C. The yellow precipitate was collected from the cooled reaction mixture and washed with chloroform (50 cm<sup>3</sup>) and ether (50 cm<sup>3</sup>), then dried under vacuum, in a desiccator over phosphorous pentoxide, yielding Lawesson's reagent (**15**) (11.79 g, 93%). mp 222-226 °C (lit.<sup>48</sup> 226-228 °C).

### 3-Hydroxy-2-(2-methoxyphenyl)-4H-1-benzopyran-4-thione (6)

The benzopyranone (**4**) (0.5 g, 1.86 mmol) and Lawesson's reagent (**15**) (0.75 g, 1.86 mmol) were refluxed in THF for 4 h. The solvent was removed under reduced pressure and the residue was purified by squat chromatography (dichloromethane). The resulting solid was recrystallised from ethanol yielding orange crystals (360 mg, 68%). mp 155-157 °C; IR 3100 (broad) cm<sup>-1</sup>; UV-vis  $\lambda_{\text{max}}$  411 nm; <sup>1</sup>H NMR (CDCl<sub>3</sub>)  $\delta$  3.86 (s, 3H, -OCH<sub>3</sub>), 7.05 - 7.73 (m, 7H, Ar), 8.07 (br s, 1H, OH), 8.60-8.63 (m, 1H, H<sub>5</sub>); <sup>13</sup>C NMR (CDCl<sub>3</sub>)  $\delta$  55.8, 111.9,

118.6, 119.5, 120.4, 125.5, 128.3, 128.5, 131.0, 132.3, 132.8, 141.8, 146.7, 150.9, 157.8, 188.0; MS  $m/z$  285, 253, 223, 165, 145, 137, 76. Anal. Calcd for  $C_{16}H_{12}O_3S$ : C, 67.59; H, 4.25. Found: C, 67.49; H, 4.00.

### 3-Hydroxy-2-(4-methoxyphenyl)-4H-1-benzopyran-4-thione (7)

3-Hydroxy-2-(4-methoxyphenyl)-4H-1-benzopyran-4-one (**5**) (0.2 g, 0.75 mmol) was subject to the same reagent and conditions as described above. A red orange solid was produced (0.15 g, 70%). mp 138-139 °C; IR 1606, 1586, 1546, 1506  $cm^{-1}$ ; UV-vis  $\lambda_{max}$  449 nm;  $^1H$  NMR ( $CDCl_3$ )  $\delta$  3.90 (s, 3H,  $-OCH_3$ ), 7.03 - 8.41 (m, 7H, Ar), 8.54 - 8.59 (m, 1H,  $H_5$ ), 8.72 (br s, 1H, OH);  $^{13}C$  NMR ( $CDCl_3$ )  $\delta$  55.5, 114.4, 118.2, 123.2, 125.7, 127.8, 128.8, 130.8, 132.8, 142.0, 145.9, 150.2, 161.9, 186.6; MS  $m/z$  284 ( $M^+$ , 11%), 152 (14), 92 (45), 77 (61), 69 (100), 41 (85). Anal. Calcd for  $C_{16}H_{12}O_3S$ : C, 67.59; H, 4.25. Found: C, 67.74; H, 4.01.

### 1-[2-Hydroxy-6-(phenylmethoxy)phenyl]-ethanone (16)<sup>50</sup>

2,6-Dihydroxyacetophenone (0.5 g, 3.3 mmol) and sodium hydride (60%, 131 mg, 3.3 mmol) in DMSO (10  $cm^3$ ) were stirred at room temperature for 10 min. Benzyl bromide (0.4  $cm^3$ , 3.4 mmol) was added and stirring was continued for 1 h. The reaction mixture was acidified with dilute hydrochloric acid (10%, 75  $cm^3$ ) and extracted with dichloromethane (2 x 50  $cm^3$ ). The organic layers were combined, dried ( $MgSO_4$ ) and the solvent evaporated under reduced pressure producing a solid residue which was purified by flash chromatography (dichloromethane). The resultant pale yellow crystalline solid was recrystallised from toluene/ether to give **16** (500 mg, 63%). mp 109-110 °C (lit.<sup>50</sup> 109-110 °C);  $^1H$  NMR ( $CDCl_3$ )  $\delta$  2.60 (s, 3H,  $-CH_3$ ), 5.11 (s, 2H,  $-OCH_2Ph$ ), 6.45 (d, 1H,  $J=8$  Hz, Ar), 6.58 (d, 1H,  $J=8$  Hz, Ar), 7.32 - 7.43 (m, 6H, Ar), 13.30 (s, 1H,  $-OH$ ).

### 1-[2-Hydroxy-6-(phenylmethoxy)phenyl]-3-(2-methoxyphenyl)-2-propene-1-one (17)

1-[2-Hydroxy-6-(phenylmethoxyphenyl)]-ethanone (**16**) (0.5 g, 2.1 mmol), *o*-anisaldehyde (0.29 g, 2.1 mmol), aqueous potassium hydroxide (50%, 2  $cm^3$ ) and ethanol (5  $cm^3$ ) were

stirred at room temperature for 6 h. The reaction mixture was acidified with aqueous hydrochloric acid (10%, 40 cm<sup>3</sup>) giving a precipitate which was extracted with dichloromethane (2 x 50 cm<sup>3</sup>). The combined extracts were dried (MgSO<sub>4</sub>) and the solvent removed under reduced pressure to give an orange solid. Recrystallisation from ethanol afforded the orange crystalline solid **17** (0.75 g, 99%). mp 146-148 °C; IR 1626, 1596, 1578, 1556 cm<sup>-1</sup>; <sup>1</sup>H NMR (CDCl<sub>3</sub>) δ 3.77 (s, 3H, -OCH<sub>3</sub>), 5.10 (s, 2H, -OCH<sub>2</sub>-Ar), 6.47 - 6.90 (m, 5H, Ar), 7.23 - 7.48 (m, 7H, Ar), 7.85 (d, 1H, *J* = 15.7 Hz, -CO-CH=CH-), 8.18 (d, 1H, *J* = 15.7 Hz, -CO-CH=CH-); <sup>13</sup>C NMR (CDCl<sub>3</sub>) δ 55.6, 71.5, 102.6, 111.2, 111.5, 112.3, 120.8, 124.3, 127.9, 128.3, 128.4, 128.6, 129.0, 131.7, 135.9, 136.0, 138.5, 158.8, 160.4, 165.5, 195.0; MS *m/z* 360 (M<sup>+</sup>, 6%), 269 (38), 91 (100). Anal. Calcd for C<sub>23</sub>H<sub>20</sub>O<sub>4</sub>: C, 76.65; H, 5.59. Found C, 76.74; H, 5.41.

#### 5-Hydroxy-2-(2-methoxyphenyl)-4H-1-benzopyran-4-one (**8**)

1-[(2-Hydroxy)-6-(phenylmethoxyphenyl)-3-(2-methoxyphenyl)]-2-propene-1-one (**17**) (0.4 g, 1.11 mmol) was refluxed in dry DMSO (5 cm<sup>3</sup>) for 2 h with one crystal of iodine. The DMSO was removed by evaporation producing a red-brown residue which was purified by flash chromatography (dichloromethane) followed by recrystallisation from ethanol to give **8** as pale yellow crystals (0.27 g, 91%). mp 138-139 °C (lit.<sup>110</sup> 136-137 °C); IR 3410 (broad), 1650, 1616, 1580, 1568 cm<sup>-1</sup>; UV-vis λ<sub>max</sub> 336 nm (lit.<sup>110</sup> (MeOH) 331 nm); <sup>1</sup>H NMR (CDCl<sub>3</sub>) δ 3.93 (s, 3H, -OCH<sub>3</sub>), 6.76 - 7.91 (m, 8H, Ar), 12.67 (s, 1H, OH); <sup>13</sup>C NMR (CDCl<sub>3</sub>) δ 56.0, 107.1, 111.0, 111.2, 111.4, 112.1, 120.5, 121.1, 129.6, 133.1, 135.4, 156.9, 158.4, 161.0, 162.2, 184.2; MS *m/z* 268 (M<sup>+</sup>, 100), 253 (3), 237 (7), 137 (93), 107 (80).

#### 5-Hydroxy-2-(2-methoxyphenyl)-4H-1-benzopyran-4-thione (**9**)

The benzopyranone (**8**) (75 mg, 0.28 mmol) and Lawesson's reagent (**15**) (0.104 g, 0.28 mmol) were refluxed in THF (20 cm<sup>3</sup>) for 1/2 h. The solvent was removed under reduced pressure and the residue was purified by flash chromatography (dichloromethane). The resulting solid was recrystallised from ethanol to give **9** as red crystals (70 mg, 88%). mp 147-149 °C; IR 3453 (broad), 1613, 1547 cm<sup>-1</sup>; UV-vis λ<sub>max</sub> 409 nm; <sup>1</sup>H NMR (CDCl<sub>3</sub>, D<sub>2</sub>O) δ

3.97 (s, 3H, -OCH<sub>3</sub>), 6.87 - 7.97 (m, 8H, Ar); <sup>13</sup>C NMR (CDCl<sub>3</sub>) δ 55.1, 107.2, 111.1, 113.0, 118.0, 119.2, 121.0, 124.5, 129.6, 133.2, 134.9, 152.7, 152.8, 158.4, 161.0, 200.8; MS *m/z* 284 (M<sup>+</sup>, 100%), 253 (10), 153 (21), 77 (32), 63 (31), 39 (69). Anal. Calcd for C<sub>16</sub>H<sub>12</sub>O<sub>3</sub>S: C, 67.59; H, 4.25. Found C, 67.01, H, 4.29.

### **2-(2-Methoxyphenyl)-4H-1-benzopyran-4-one (10)**

1-(2-Hydroxyphenyl)-3-(2-methoxyphenyl)-2-propene-1-one (**13**) (450 mg, 1.8 mmol) was refluxed in DMSO (3 cm<sup>3</sup>) with one crystal of iodine for 10 min. Water (50 cm<sup>3</sup>) was added to the cooled reaction mixture and the aqueous layer was extracted with dichloromethane (2 x 50 cm<sup>3</sup>). The combined organic layers were washed with 20% aqueous sodium thiosulfate, separated, dried (MgSO<sub>4</sub>), and the solvent evaporated under reduced pressure. The residue was crystallised from ethanol giving off-white crystals (420 mg, 93%). mp 101-103 °C (lit.<sup>111</sup> 102-104 °C); IR 1635, 1566 cm<sup>-1</sup>; UV-vis λ<sub>max</sub> 308 nm; <sup>1</sup>H NMR (CDCl<sub>3</sub>) δ 3.93 (s, 3H, -OCH<sub>3</sub>), 7.01 - 7.93 (m, 8H, Ar), 8.20 - 8.25 (m, 1H, H<sub>5</sub>).

### **2-(4-Methoxyphenyl)-4H-1-benzopyran-4-one (11)<sup>52</sup>**

1-(2-Hydroxyphenyl)-3-(4-methoxyphenyl)-2-propene-1-one (**14**) (660 mg, 2.60 mmol) was treated with the same conditions as mentioned above producing an off-white crystalline solid (590 mg, 90%). mp 158-160 °C (lit.<sup>52</sup> 161-163 °C); IR 1648, 1607, 1513 cm<sup>-1</sup>; UV-vis λ<sub>max</sub> 320 nm; <sup>1</sup>H NMR (CDCl<sub>3</sub>) δ 3.97 (s, 3H, -OCH<sub>3</sub>), 6.73 (s, 1H, H<sub>3</sub>), 6.97 - 7.91 (m, 7H, Ar), 8.18 - 8.23 (m, 1H, H<sub>5</sub>).

### **3-Methoxy-2-(2-methoxyphenyl)-4H-1-benzopyran-4-one (12)**

Sodium hydride (60% in mineral oil, 48 mg, 1.2 mmol) was added to benzopyranone (**4**) (268 mg, 1.0 mmol) dissolved in DMSO (5 cm<sup>3</sup>), and the solution was allowed to stir at room temperature for 5 min. Iodomethane (0.852 g, 6.0 mmol) was added dropwise to the stirring solution over 3 min and the mixture was left to stir for 3 h. The DMSO was removed by evaporation and the residue was dissolved in dichloromethane (30 cm<sup>3</sup>) and washed with dilute hydrochloric acid (2 x 15 cm<sup>3</sup>). The dichloromethane layer was dried (MgSO<sub>4</sub>), filtered and the solvent removed under reduced pressure. The remaining solid was recrystallised from ethanol to give **12** (250 mg, 88%). mp 149-150 °C; IR 1644, 1626, 1608, 1494 cm<sup>-1</sup>; UV-vis λ<sub>max</sub>

310 nm;  $^1\text{H}$  NMR ( $\text{CDCl}_3$ )  $\delta$  3.82 (s, 3H,  $-\text{OCH}_3$ ), 3.85 (s, 3H,  $-\text{OCH}_3$ ), 7.02 - 7.69 (m, 7H, Ar), 8.29 (dd, 1H,  $J=1.9, 8.1$  Hz,  $\text{H}_5$ ); MS  $m/z$  282 ( $\text{M}^+$ , 53), 267 (17), 251 (100), 181 (22), 121 (37) 92 (45), 65 (43). Anal. Calcd for  $\text{C}_{17}\text{H}_{14}\text{O}_4$ : C, 72.33; H, 5.00. Found C, 72.03, H, 5.09.

## 6.4 Thiazoles Syntheses

### 2-Hydroxybenzylidenemalononitrile (**28**)<sup>89</sup>

2-Salicylaldehyde (5.0 g, 41.0 mmol) and malononitrile (2.6 g, 33.0 mmol) were stirred at room temperature in ethanol (20  $\text{cm}^3$ ) with piperidine (2 drops) for 15 min. The solution was cooled in an ice bath yielding **28** as a yellow precipitate which was collected by vacuum filtration (5.0 g, 89%). This product was used in the next step without further purification.

### 2-Oxo-2H-1-benzopyran-3-carbonitrile (**26**)<sup>89</sup>

2-Hydroxybenzylidenemalononitrile (**28**) (2.0 g, 12.0 mmol) was warmed with stirring in dilute aqueous hydrochloric acid (10%, 10  $\text{cm}^3$ ) for 10 min. The cooled solution produced an off-white precipitate which was collected by vacuum filtration. The precipitate was purified by squat chromatography (dichloromethane) followed by recrystallisation from ethanol to produce **26** as a white crystalline solid (1.85 g, 90%). mp 184-185 °C (lit.<sup>89</sup> 184-185 °C); IR 2224, 1726, 1604, 1554  $\text{cm}^{-1}$ ;  $^1\text{H}$  NMR ( $\text{CDCl}_3$ )  $\delta$  7.36 - 7.76 (m, 4H, Ar), 8.28 (s, 1H,  $\text{H}_4$ );  $^{13}\text{C}$  NMR ( $\text{CDCl}_3$ )  $\delta$  103.5, 113.6, 117.3, 117.6, 125.8, 129.4, 135.6, 151.9, 154.7, 156.5.

### 2-Acetoxybenzoylchloride (**29**)<sup>90</sup>

A mixture of acetylsalicylic acid (2.0 g, 0.011 mol) and thionyl chloride (2  $\text{cm}^3$ , 0.027 mol) dissolved in dry benzene (10  $\text{cm}^3$ ) was refluxed for 6 h, cooled, and evaporated to dryness to give 2-acetoxybenzoylchloride (**29**) which, due to instability to moisture, was used rapidly without further purification.

### 4-Hydroxy-2-oxo-2H-1-benzopyran-3-carbonitrile (**27**)<sup>90</sup>

2-Acetoxybenzoylchloride (**29**) (0.011 mol) in dry ether (50  $\text{cm}^3$ ) was added slowly to a stirred, refluxing suspension of the sodium salt of ethyl cyanoacetate [prepared from ethyl

cyanoacetate (3.42 g, 0.03 mol) and a 60% dispersion of NaH in mineral oil (1.14 g) in dry ether (15 cm<sup>3</sup>)]. After a further 18 h at reflux, the cooled mixture was poured into aqueous sodium hydroxide (10%, 100 cm<sup>3</sup>). The aqueous phase was separated, washed with ether (3 x 50 cm<sup>3</sup>), acidified with cold concentrated hydrochloric acid (20 cm<sup>3</sup>) and filtered. Recrystallisation of the solid from ethanol gave **27**. mp 266-269 °C (decomp.) (lit.<sup>90</sup> 267-269 °C); IR 3298 (broad), 1645, 1604, 1549 cm<sup>-1</sup>; <sup>1</sup>H NMR (DMSO-*d*<sub>6</sub>) δ 7.17 - 7.84 (m, 4H, Ar), 9.27 (br s, 1H, OH); <sup>13</sup>C NMR (DMSO-*d*<sub>6</sub>) δ 76.3, 117.3, 119.7, 121.2, 124.1, 125.6, 133.6, 154.5, 163.7, 176.5.

### 2-Oxo-2H-1-benzopyran-3-carbothioamide (**36**)

2-Oxo-2H-1-benzopyran-3-carbonitrile (**26**) (684 mg, 4.0 mmol) and thioacetamide (600 mg, 8.0 mmol) were stirred in DMF (10 cm<sup>3</sup>) at 90 °C in an oil bath. The solution was saturated with dry hydrogenchloride gas and allowed to stir for 30 min, after which water was added (100 cm<sup>3</sup>) producing a precipitate. The collected precipitate was purified by squat chromatography (dichloromethane) followed by recrystallisation from ethanol to give a golden-brown crystalline solid **36** (410 mg, 50%). mp 232-235 °C; IR 3288, 3144, 1698, 1610, 1598, 1562 cm<sup>-1</sup>; <sup>1</sup>H NMR (CDCl<sub>3</sub>) δ 7.37 - 7.80 (m, 4H, Ar), 8.01 (br s, 1H, -NH), 9.50 (s, 1H, H<sub>4</sub>), 10.35 (br s, 1H, -NH); <sup>13</sup>C NMR (DMSO-*d*<sub>6</sub>) δ 116.3, 118.7, 125.0, 125.4, 130.5, 134.3, 148.2, 153.8, 159.2, 193.4; MS *m/z* 204 (M<sup>+</sup>, 87%), 171 (100), 118 (23), 89 (40), 63 (27), 40 (19). Anal. Calcd for C<sub>10</sub>H<sub>7</sub>NO<sub>2</sub>S: C, 58.52; H, 3.43; N, 6.83. Found: C, 58.24; H, 3.58; N, 6.84.

### Ethyl-2-(3-2-oxo-2H-1-benzopyran)-2-thiazole-4-carboxylate (**32**)

The thioamide **36** (205 mg, 1.0 mmol) and ethyl bromopyruvate (125 mg, 1.0 mmol) were refluxed in dry ethanol (7 cm<sup>3</sup>) for 1 h. The solvent was removed under reduced pressure and the red solid was purified by flash chromatography (dichloromethane) followed by a recrystallisation from ethanol to which decolourising charcoal was added. The solution was filtered and left to cool producing **32** as white fluffy crystals (153 mg, 51%). mp 159-161 °C; IR 1726, 1604, 1562, 756 cm<sup>-1</sup>; UV-vis λ<sub>max</sub> 350 nm; <sup>1</sup>H NMR (CDCl<sub>3</sub>) δ 1.43 (t, 3H, *J* = 7.1 Hz, -CH<sub>2</sub>CH<sub>3</sub>), 4.46 (q, 2H, *J* = 7.1 Hz, -CH<sub>2</sub>CH<sub>3</sub>), 7.33 - 7.73 (m, 4H, Ar), 8.30 (s, 1H, -S-CH=C-), 9.06 (s, 1H, H<sub>4</sub>); <sup>13</sup>C NMR (CDCl<sub>3</sub>) δ 14.4, 61.6, 116.8, 118.9, 119.4,

125.3, 129.3, 129.8, 133.1, 140.8, 147.2, 153.6, 159.8, 159.9, 161.5; MS  $m/z$  301 ( $M^+$ , 59%), 273 (4), 256 (20), 229 (100), 189 (34), 69 (29). Anal. Calcd for  $C_{15}H_{11}NO_4S$ : C, 59.79; H, 3.68; N, 4.65. Found C, 59.55; H, 3.73; N, 4.65.

### **2-(3-2-Oxo-2H-1-benzopyran)-2-thiazole-4-carboxylate (33)**

An aqueous sodium hydroxide solution (10%, 2 cm<sup>3</sup>) was added to a stirred suspension of ethyl-2-(3-2-oxo-2H-1-benzopyran)-2-thiazole-4-carboxylate (**32**) (100 mg, 0.33 mmol) in ethanol (4 cm<sup>3</sup>) and the solution was allowed to stir at room temperature for 24 h. Concentrated hydrochloric acid (10 cm<sup>3</sup>) was added to the solution forming a white precipitate which was collected and recrystallised from ethanol (84 mg, 93%). Decomp. pt. 280-285 °C; IR 1714, 1694, 1606, 1580 cm<sup>-1</sup>; UV-vis  $\lambda_{max}$  355 nm; <sup>1</sup>H NMR. (DMSO-*d*<sub>6</sub>)  $\delta$  3.26 (br s, 1H, -CO<sub>2</sub>H), 7.34 - 7.89 (m, 4H, Ar), 8.39 (s, 1H, -S-CH=C-), 9.04 (s, 1H, H<sub>4</sub>); <sup>13</sup>C NMR (DMSO-*d*<sub>6</sub>)  $\delta$  114.8, 117.2, 117.6, 123.7, 128.2, 128.5, 131.6, 139.0, 146.1, 151.7, 157.6, 157.9, 160.9; MS  $m/z$  273 ( $M^+$ , 33%), 229 (10), 201 (54), 185 (56), 69 (90), 57 (81), 43 (100). Anal. Calcd for  $C_{13}H_7NO_4S$ : C, 57.14; H, 2.58; N, 5.13. Found C, 56.57; H, 2.59; N, 5.07.

### **4-Oxo-4H-1-benzopyran-3-carbothioamide (37)**

4-Oxo-4H-1-benzopyran-3-carbonitrile (**25**) (450 mg, 2.65 mmol) and thioacetamide (400 mg, 5.30 mmol) were stirred in a DMF solution saturated with dry hydrogenchloride gas at 90 °C in an oil bath. After 30 min, water (70 cm<sup>3</sup>) was added, producing a yellow precipitate. The solid was recrystallised from ethanol yielding **37** as yellow-orange crystals (300 mg, 56%). mp 220-223 °C; IR 3240, 3097, 1642, 1612, 1580 cm<sup>-1</sup>; <sup>1</sup>H NMR (CDCl<sub>3</sub>)  $\delta$  7.24 - 7.61 (m, 3H, Ar), 8.03 - 8.07 (m, 1H, H<sub>5</sub>), 9.05 (br s, 1H, -NH), 9.40 (s, 1H, H<sub>2</sub>), 10.75 (br s, 1H, -NH); <sup>13</sup>C NMR (CDCl<sub>3</sub>) 118.5, 119.0, 124.3, 126.6, 126.7, 135.0, 155.8, 166.5, 177.1, 194.5; MS  $m/z$  204 ( $M^+$ , 100%), 172 (65), 121 (16), 92 (7). Anal. Calcd for  $C_{10}H_7NO_2S$ : C, 58.52; H, 3.44; N, 6.83. Found: C, 58.28; H, 3.59; N, 6.81.

### **Ethyl-2-(3-4-oxo-4H-1-benzopyran)-2-thiazole-4-carboxylate (30)**

The thioamide **37** (100 mg, 0.488 mmol) and ethyl bromopyruvate (0.06 cm<sup>3</sup>, 0.488 mmol) were refluxed in dry ethanol (5 cm<sup>3</sup>) for 3 h. The solvent was removed under reduced pressure

to produce a solid which was purified by flash chromatography (dichloromethane) followed by recrystallisation from ethanol. The product, **30**, was obtained as a fluffy white crystalline solid (100 mg, 68%). mp 181-183 °C; IR 1722, 1644, 1616  $\text{cm}^{-1}$ ; UV-vis  $\lambda_{\text{max}}$  303 nm;  $^1\text{H}$  NMR ( $\text{CDCl}_3$ )  $\delta$  1.43 (t, 3H,  $J = 7.2$  Hz,  $-\text{CH}_2\text{CH}_3$ ), 4.45 (q, 2H,  $J = 7.2$  Hz,  $-\text{CH}_2\text{CH}_3$ ), 7.48 - 7.81 (m, 3H, Ar), 8.26 (s, 1H,  $-\text{S}-\text{CH}=\text{C}-$ ), 8.34 - 8.39 (m, 1H,  $\text{H}_5$ ), 9.29 (s, 1H,  $\text{H}_2$ ); MS  $m/z$  301 ( $\text{M}^+$ , 89%), 256 (29), 229 (100), 189 (47), 168 (56), 141 (53), 115 (51), 92 (29), 77 (52).

### 2-(3-4-Oxo-4H-1-benzopyran)-2-thiazole-4-carboxylate (**31**)

An aqueous sodium hydroxide solution (10%, 2  $\text{cm}^3$ ) was added to a stirred suspension of ethyl-2-(3-4-oxo-4H-1-benzopyran)-2-thiazole-4-carboxylate (**30**) (100 mg, 0.33 mmol) in ethanol (4  $\text{cm}^3$ ) and the solution was allowed to stir at room temperature for 24 h. Concentrated hydrochloric acid (10  $\text{cm}^3$ ) was added to the solution forming **31** as a white precipitate which was collected and recrystallised from ethanol (86 mg, 95%). mp 268-270 °C; IR 3420 (broad), 1704, 1644, 1614, 1570  $\text{cm}^{-1}$ ; UV-vis  $\lambda_{\text{max}}$ ;  $^1\text{H}$  NMR ( $\text{DMSO}-d_6$ )  $\delta$  3.21 (br s, 1H,  $-\text{CO}_2\text{H}$ ), 7.46 - 7.82 (m, 3H, Ar), 8.21 - 8.27 (m, 1H,  $\text{H}_5$ ), 8.26 (s, 1H,  $-\text{S}-\text{CH}=\text{C}$ ), 9.25 (s, 1H,  $\text{H}_2$ );  $^{13}\text{C}$  NMR ( $\text{DMSO}-d_6$ )  $\delta$  117.1, 119.0, 123.1, 125.6, 126.7, 129.5, 135.2, 146.4, 155.7, 156.8, 157.6, 162.4, 174.2; MS  $m/z$  273 ( $\text{M}^+$ , 80), 229 (59), 189 (30), 173 (85), 120 (35), 92 (86), 58 (100). Anal. Calcd for  $\text{C}_{13}\text{H}_7\text{NO}_4\text{S}$ : C, 57.14; H, 2.58; N, 5.13. Found C, 56.94; H, 2.73; N, 5.08.

### 4-Hydroxy-2-oxo-2H-1-benzopyran-3-carbothioamide (**38**)

4-Hydroxy-2-oxo-2H-1-benzopyran-3-carbonitrile (**27**) (500 mg, 2.67 mmol) and thioacetamide (400 mg, 5.34 mmol) was dissolved in DMF (10  $\text{cm}^3$ ) with stirring and the solution was saturated with dry hydrogen chloride gas at 90 °C. After 15 min, water (50  $\text{cm}^3$ ) was added to the reaction mixture forming a yellow precipitate which was recrystallised from ethanol to give **38** as yellow-orange needles (200 mg, 34%). mp 215-218 °C; IR 3322, 3210, 1672, 1594, 1536  $\text{cm}^{-1}$ ;  $^1\text{H}$  NMR ( $\text{CDCl}_3$ )  $\delta$  7.32 - 7.75 (m, 3H, Ar), 8.11 - 8.16 (m, 1H,  $\text{H}_5$ ), 11.00 (br s, 3H,  $-\text{NH}_2$  and OH);  $^{13}\text{C}$  NMR ( $\text{CDCl}_3$ )  $\delta$  97.4, 115.9, 116.7, 125.0, 126.0, 135.6, 152.5, 162.3, 175.0, 192.9; MS  $m/z$  221 ( $\text{M}^+$ , 100%), 188 (71), 121 (88), 92



(49). Anal. Calcd. for C<sub>10</sub>H<sub>7</sub>NO<sub>3</sub>S: C, 54.29; H, 3.19; N, 6.33. Found: C, 54.08; H, 3.41; N, 6.32.

## 6.4 Quinoline and Pyridine Analogues Syntheses

### 8-(Bromomethyl)quinoline (45)<sup>94</sup>

8-Methylquinoline (2.3 g, 16.1 mmol), *N*-bromosuccinimide (2.9 g, 16.5 mol) and benzoyl peroxide (0.1 g, 0.41 mmol) were refluxed in carbon tetrachloride for 4 h. The solution was cooled to 0 °C, filtered, and the filtrate evaporated under reduced pressure to dryness producing a solid which was recrystallised from hexane. White crystals of 8-(bromomethyl)quinoline (6) were obtained (2.33 g, 69%). mp 80-82 °C (lit.<sup>94</sup> 83-84 °C); <sup>1</sup>H NMR (CDCl<sub>3</sub>) δ 5.23 (2H, s, -CH<sub>2</sub>Br), 7.40 - 8.18 (m, 5H, Ar), 8.99 - 9.02 (m, 1H, H<sub>2</sub>).

### 2-(8-Quinolylmethyl)-1,3-isoindolinedione (46)

8-(Bromomethyl)quinoline (45) (1.1 g, 5.0 mmol) and potassium phthalimide (1.85 g, 0.01 mol) were heated in DMF (10 cm<sup>3</sup>) at 80-90 °C for 2 h. The DMF was removed under reduced pressure and the residue was purified by squat chromatography (dichloromethane). The solvent was removed under reduced pressure producing 46 as a white solid (1.3 g, 90%) which was used in the next step without further purification.

### 8-Quinolylmethylamine (47)

2-(8-Quinolylmethyl)-1,3-isoindolinedione (46) (1.0 g, 3.5 mmol) and hydrazine hydrate (1.1 cm<sup>3</sup>, 53 mmol) were refluxed in ethanol (20 cm<sup>3</sup>) for 3 h. Concentrated hydrochloric acid (0.2 cm<sup>3</sup>) was added and the solution was allowed to reflux for a further 2 h. The cooled solution was acidified to pH 1, filtered, washed with dichloromethane (50 cm<sup>3</sup>), basicified to pH 12-14 using dilute aqueous sodium hydroxide and was extracted with dichloromethane (4 x 50 cm<sup>3</sup>). The combined organic layers were dried (MgSO<sub>4</sub>), filtered and the solvent removed under reduced pressure producing 47 as a brown oil. Amine 47 was used without further purification.

***N*1-(8-Quinolylmethyl)-4-methyl-1-benzene sulfonamide (39)**

*p*-Toluene-sulfonylchloride (0.95 g, 5.0 mmol) was added to a stirred solution of 8-quinolylmethylamine (47) in pyridine (5 cm<sup>3</sup>) and the mixture was allowed to stir for 5 h. Water (50 cm<sup>3</sup>) was added to the mixture and the aqueous layer was extracted with dichloromethane (3 x 50 cm<sup>3</sup>). The combined organic layers were dried (MgSO<sub>4</sub>), filtered and the solvent was removed under reduced pressure. The residual pyridine was removed under vacuum on an oil pump producing a solid which was recrystallised from ethyl acetate/hexane to yield 39 (600 mg, 64% for two steps). mp 108-110 °C; IR 3276, 1595, 1500 cm<sup>-1</sup>. UV-vis λ<sub>max</sub> 283 nm; <sup>1</sup>H NMR (300 MHz, CDCl<sub>3</sub>) δ 2.27 (s, 3H, -CH<sub>3</sub>), 4.65 (d, 2H, *J* = 6.56 Hz, -CH<sub>2</sub>-NH-), 6.64 (t, 1H, 6.56 Hz, -NH-), 6.99 - 8.10 (m, 9H, Ar), 8.82 - 8.85 (m, 1H, H<sub>2</sub>); <sup>13</sup>C NMR. (200 MHz, CDCl<sub>3</sub>) δ 21.1, 46.1, 121.0, 125.9, 126.6, 127.6, 128.1, 128.8, 129.2, 133.7, 136.3, 137.2, 142.4, 146.2, 149.2; MS *m/z* 312 (M<sup>+</sup>, 16%), 255 (9), 157 (100), 128 (22), 97 (23), 69 (81), 43 (61). Anal. Calcd for C<sub>17</sub>H<sub>16</sub>N<sub>2</sub>O<sub>2</sub>S: C, 65.36, H, 5.16, N, 8.97. Found C, 65.64, H, 5.10, N, 9.33.

**8-(Quinolylmethyl)acetate (48)<sup>95</sup>**

A suspension of 8-(bromomethyl)quinoline (45) (0.38 g, 1.71 mmol) and sodium acetate (281 mg, 3.42 mmol) was stirred in DMF at 90 °C for 2 h. The solvent was removed under reduced pressure producing a residue which was purified by radial chromatography (3% ethyl acetate/dichloromethane) followed by recrystallisation from ethyl acetate/hexane (210 mg, 62%). mp 40-41 °C (lit.<sup>11</sup> 40-41 °C); <sup>1</sup>H NMR (CDCl<sub>3</sub>) δ 2.14 (s, 3H, -OC(O)CH<sub>3</sub>), 5.84 (s, 2H, -CH<sub>2</sub>-O-), 7.40 - 8.16 (m, 5H, Ar), 8.93 - 8.96 (m, 1H, H<sub>2</sub>).

**8-Quinolylmethanol (40)<sup>95</sup>**

A mixture of 8-(quinolylmethyl)acetate (48) (200 mg, 1.0 mmol) and sodium hydroxide (5 cm<sup>3</sup>, 30%) in methanol (10 cm<sup>3</sup>) was refluxed for 1.5 h. The methanol was removed under reduced pressure, water (50 cm<sup>3</sup>) was added and the solution was extracted with dichloromethane (50 cm<sup>3</sup>). The organic layer was dried (MgSO<sub>4</sub>), filtered and the solvent removed under reduced pressure. The resulting solid 40 was recrystallised from ethyl acetate/hexane (161 mg, 95%). mp 73-75 °C (lit.<sup>95</sup> 73.5-74.5 °C); IR 3262, 1594, 1500 cm<sup>-1</sup>;

UV-vis  $\lambda_{\max}$  290 nm;  $^1\text{H}$  NMR ( $\text{CDCl}_3$ )  $\delta$  5.09 (br s, 1H, OH), 5.20 (s, 2H,  $-\text{CH}_2\text{-OH}$ ), 7.40 - 8.21 (m, 5H, Ar), 8.87 - 8.90 (m, 1H, H<sub>2</sub>); MS  $m/z$  159 ( $\text{M}^+$ , 81%), 142 (17), 130 (100), 102 (21), 77 (24).

### 8-Quinolinecarbaldehyde (41)

Oxalyl chloride (0.3 cm<sup>3</sup>, 3.3 mmol) was added, with stirring, to dichloromethane (10 cm<sup>3</sup>) at  $-78^\circ\text{C}$ . DMSO (0.47 cm<sup>3</sup>, 6.6 mmol) dissolved in dichloromethane (5 cm<sup>3</sup>) was added to the mixture which was stirred for a further 5 min. 8-Quinolylmethanol (40) (0.5 g, 3.1 mmol) in dichloromethane (5 cm<sup>3</sup>) was added to the reaction over 5 min and the mixture was left to stir for 15 min, after which triethylamine (2.0 cm<sup>3</sup>, 16.5 mmol) was added and the mixture stirred for a further 5 min. The reaction mixture was warmed to room temperature and washed with water (30 cm<sup>3</sup>). The organic layer was dried ( $\text{MgSO}_4$ ), filtered and the solvent removed under reduced pressure producing a solid which was recrystallised from hexane giving 41 as sharp, white needles (0.4 g, 81%). mp  $93\text{-}95^\circ\text{C}$  (lit.<sup>96</sup>  $94\text{-}95^\circ\text{C}$ ); IR  $1682\text{ cm}^{-1}$ ; UV-vis  $\lambda_{\max}$  300 nm;  $^1\text{H}$  NMR ( $\text{CDCl}_3$ )  $\delta$  7.53 - 8.34 (m, 5H, Ar), 9.07 (m, 1H, H<sub>2</sub>), 11.47 (s, 1H,  $-\text{C(O)H}$ ).  $^{13}\text{C}$  NMR ( $\text{CDCl}_3$ )  $\delta$  121.8, 126.2, 128.3, 129.3, 131.8, 134.2, 136.3, 147.7, 151.3, 192.6; MS  $m/z$  158 ( $\text{M}^+$ , 92%), 129 (100), 102 (51), 76 (15), 51(12).

### *N*-1-[(*E*)-1-(8-quinolyl)methylidene]-aniline (42)

Aniline (0.05 cm<sup>3</sup>, 0.6 mmol) was added to 8-quinolinecarbaldehyde (41) (78.5 mg, 0.5 mmol) dissolved in dichloromethane (10 cm<sup>3</sup>) containing a crushed regenerated 4Å molecular sieve and the mixture was stirred at room temperature for 3 h. Dichloromethane (10 cm<sup>3</sup>) was added to the reaction mixture which was then gravity filtered followed by removal of solvent under reduced pressure. Imine 42 was produced as a yellow solid (100 mg, 86%). mp  $83\text{-}85^\circ\text{C}$ . UV-vis  $\lambda_{\max}$  299 nm.  $^1\text{H}$  NMR ( $\text{CDCl}_3$ )  $\delta$  7.26 - 9.00 (m, 11H, Ar), 9.94 (s, 1H,  $-\text{CH=N-}$ ); MS  $m/z$  232 ( $\text{M}^+$ , 65%), 155 (100), 129 (42), 77 (39), 51 (24).

### 8-Quinolylmethanethiol (44)<sup>94</sup>

A solution of potassium hydroxide (2.4 g, 43 mmol) in ethanol (50 cm<sup>3</sup>) was saturated with hydrogen sulfide gas which was generated by the dropwise addition of dilute hydrochloric acid onto iron(II) sulfide. This reaction produced an ethanolic solution of potassium mono hydrogen

sulfide which was added to 8-(bromomethyl)quinoline (**45**) (1.2 g, 5.4 mmol) and the mixture was warmed on a hot plate for 5 min. The ethanol was removed under reduced pressure producing a residue to which water (50 cm<sup>3</sup>) was added. The aqueous mixture was adjusted to pH 7 using dilute hydrochloric acid (10%) and the product was extracted with ether (2 x 50 cm<sup>3</sup>). The combined ether layers were dried (MgSO<sub>4</sub>), filtered and the solvent removed under reduced pressure. The air sensitive oil **44** was stored under nitrogen at 0 °C. <sup>1</sup>H NMR (CDCl<sub>3</sub>) δ 2.35 (t, 1H, *J* = 8.1 Hz, -CH<sub>2</sub>-SH), 4.36 (d, 2H, *J* = 8.0 Hz, -CH<sub>2</sub>-SH), 7.39 - 8.14 (m, 5H, Ar), 8.94 - 8.97 (m, 1H, H<sub>2</sub>).

### 8-Quinolylmethane disulfide (**49**)<sup>94</sup>

Thiol **44** was subject to air in a round bottomed flask for 2 hours producing **49** as a yellow solid. <sup>1</sup>H NMR (CDCl<sub>3</sub>) δ 4.49 (s, 2H, -CH<sub>2</sub>-S-), 7.36 - 8.16 (m, 5H, Ar), 8.92 - 8.95 (m, 1H, H<sub>2</sub>).

### 8-[(Ethylthio)methyl]-quinoline (**50**)

Ethanethiol (0.3 cm<sup>3</sup>, 4.0 mol) and sodium hydroxide (0.16 g, 4.0 mol.), dissolved in ethanol (10 cm<sup>3</sup>), was added to a solution of 8-(bromomethyl)quinoline (**45**) (444 mg, 2.0 mmol) in ethanol (10 cm<sup>3</sup>) and the mixture was heated at 50 °C for 1 h. The ethanol and excess ethanethiol were removed under reduced pressure, and the residue dissolved in dichloromethane (50 cm<sup>3</sup>) and washed with water (2 x 50 cm<sup>3</sup>). The organic layer was dried (MgSO<sub>4</sub>) and the solvent removed under reduced pressure to produce **50** as an oil which was distilled at 150 °C/0.05 Torr using a kugelrohr apparatus (398 mg, 98%). <sup>1</sup>H NMR (CDCl<sub>3</sub>) δ 1.27 (t, 3H, *J* = 7.36 Hz, -CH<sub>3</sub>), 2.55 (q, 2H, *J* = 7.32 Hz, -S-CH<sub>2</sub>-CH<sub>3</sub>), 4.43 (s, 2H, Ar-CH<sub>2</sub>-S-), 7.36 - 8.12 (m, 5H, Ar), 8.95 - 8.97 (m, 1H, H<sub>2</sub>); <sup>13</sup>C NMR (CDCl<sub>3</sub>) δ 14.6, 26.3, 31.3, 121.2, 126.2, 127.1, 128.6, 129.4, 136.3, 137.5, 146.5, 149.7.

### 8-[(2-Methyl-2-propanethio)methyl]-quinoline (**51**)

8-(Bromomethyl)quinoline (**45**) (444 mg, 2.0 mmol) and 2-methyl-2-propanethiol (0.45 cm<sup>3</sup>, 4.0 mmol) were subject to the same conditions described above except that the resulting residue was purified by flash chromatography (ethyl acetate) followed by distillation (100 °C at 0.06

Torr) to produce **51** as a white solid (300 mg, 65%). mp 41-44 °C; UV-vis  $\lambda_{\text{max}}$  291 nm;  $^1\text{H}$  NMR ( $\text{CDCl}_3$ )  $\delta$  1.44 (s, 9H,  $-\text{C}(\text{CH}_3)_3$ ), 4.51 (s, 2H, Ar- $\text{CH}_2$ -S-), 7.38 - 8.14 (m, 5H, Ar), 8.96 - 8.99 (m, 1H, H<sub>2</sub>); MS  $m/z$  (FAB) 232 ( $\text{MH}^+$ , 98%), 174 (100), 154 (22), 142 (38), 56 (47). Anal. Calcd for  $\text{C}_{14}\text{H}_{17}\text{NS}$ : C, 72.68; H, 7.41; N, 6.05. Found: C, 72.80; H, 7.26; N, 6.16

### 2-Chloropyridine-1-oxide (**56**)<sup>101</sup>

2-Chloropyridine (2.26 g, 0.02 mol) and hydrogen peroxide (32% aqueous solution, 5 cm<sup>3</sup>) were stirred in acetic acid (15 cm<sup>3</sup>) at 80 °C for 15 h. The solvent was reduced by evaporation, chloroform (20 cm<sup>3</sup>) and  $\text{K}_2\text{CO}_3$  (1.7 g) were added and the mixture was digested at 65 °C for 5 min. The solid was filtered off and washed with chloroform (20 cm<sup>3</sup>). Evaporation of the filtrate and washings under reduced pressure gave the pyridine-1-oxide **56** which was recrystallised from ethyl acetate (1.8 g, 70%). mp 67-69 °C (lit.<sup>101</sup> 67-68.5 °C);  $^1\text{H}$  NMR ( $\text{DMSO}-d_6$ )  $\delta$  7.21 - 7.52 (m, 3H, Ar), 8.35 - 8.39 (m, 1H, H<sub>6</sub>).

### 2-[(2-Methyl-2-propyl)thio]-pyridine-1-oxide (**54**)

2-Methyl-2-propanethiol (0.45 cm<sup>3</sup>, 4.0 mmol) and sodium hydroxide (0.16 g, 4.0 mmol) were dissolved in dry ethanol (5 cm<sup>3</sup>) at 50 °C with stirring. To the mixture was added 2-chloropyridine-1-oxide (**56**) (0.26 g, 2.0 mmol) dissolved in ethanol (5 cm<sup>3</sup>), and the solution was allowed to stir for 2 h at 50 °C. Unreacted 2-methyl-2-propanethiol was removed by purging nitrogen through the solution into a sodium hypochlorite solution. The resultant residue was dissolved in dichloromethane (50 cm<sup>3</sup>) and washed with water (2 x 50 cm<sup>3</sup>). The organic layer was dried ( $\text{MgSO}_4$ ), filtered, and the solvent evaporated producing pyridine-1-oxide **54** as an oil which was purified by squat chromatography (ethyl acetate) (330 mg, 90%).  $^1\text{H}$  NMR ( $\text{CDCl}_3$ )  $\delta$  1.46 (s, 9H,  $-\text{C}(\text{CH}_3)_3$ ), 7.04 - 7.50 (m, 3H, Ar), 8.20 - 8.24 (m, 1H, H<sub>6</sub>); MS  $m/z$  184 ( $\text{MH}^+$ , 21%), 127 (100), 110 (17), 79 (28), 57 (30).

### 2-(Ethylthio)-pyridine-1-oxide (**55**)

Ethanethiol (0.19 cm<sup>3</sup>, 4.0 mmol), 2-chloropyridine-1-oxide (**56**) (0.26 g, 2.0 mmol) and sodium hydroxide (0.16 g, 4.0 mmol) were subject to the same conditions as described above

producing **55** as a white solid which was recrystallised from dichloromethane/hexane (273 mg, 88%). mp 103-105 °C (lit.<sup>112</sup> 104-105 °C); <sup>1</sup>H NMR (CDCl<sub>3</sub>) δ 1.46 (t, 3H, *J* = 7.4 Hz, -CH<sub>2</sub>CH<sub>3</sub>), 2.94 (q, 2H, *J* = 7.4 Hz, -CH<sub>2</sub>CH<sub>3</sub>), 7.16 - 7.27 (m, 3H, Ar), 8.25 - 8.29 (m, 1H, H<sub>6</sub>); <sup>13</sup>C NMR (CDCl<sub>3</sub>) δ 13.5, 25.1, 120.8, 121.8, 126.2, 139.3, 171.1; MS *m/z* 155 (M<sup>+</sup>, 100%), 138 (37), 78 (20), 45 (14), 39 (14).

### 2-Chloroquinoline-1-oxide (**60**)<sup>102</sup>

Aqueous hydrogen peroxide (32%, 2.8 g) was added to maleic anhydride (14 g, 0.14 mol) dissolved in chloroform (30 cm<sup>3</sup>) on ice, and the mixture was allowed to stir for 2 h. 2-Chloroquinoline (1.6 g, 0.01 mol) was added to the mixture and the solution was left to stir at room temperature for 5 days. The solution was filtered and the maleic acid was washed with chloroform (30 cm<sup>3</sup>). The filtrate was washed with water (50 cm<sup>3</sup>) and the aqueous layer was separated and washed with chloroform (50 cm<sup>3</sup>). The combined organic layers were washed with a saturated aqueous K<sub>2</sub>CO<sub>3</sub> solution (100 cm<sup>3</sup>), which in turn was washed with chloroform and the recombined organic layers were washed again with saturated aqueous K<sub>2</sub>CO<sub>3</sub> (100 cm<sup>3</sup>). The organic layer was dried (MgSO<sub>4</sub>) and the solvent removed under reduced pressure producing a residue which was purified by flash alumina chromatography (acetone) followed by recrystallisation from acetone/benzene. The product **60** was received as colourless crystals (0.98 g, 55%). mp 89-93 °C (lit.<sup>102</sup> 90-93 °C); <sup>1</sup>H NMR (CDCl<sub>3</sub>) δ 7.46 - 7.87 (m, 5H, Ar), 8.74 - 8.79 (m, 1H, H<sub>8</sub>); MS *m/z* 179 (M<sup>+</sup>, 100), 163 (31), 144 (13), 128 (38), 116 (94), 89 (44).

### 2-[(2-Methyl-2-propyl)thio]-quinoline-1-oxide (**59**)

2-Methyl-2-propanethiol (0.135 cm<sup>3</sup>, 1.2 mmol) and sodium hydroxide (50 mg, 1.2 mmol) were dissolved with stirring in dry DMF (3 cm<sup>3</sup>) at 50 °C in an oil bath for 10 min. 2-Chloroquinoline-1-oxide (**60**) (180 mg, 1.0 mmol) was added to the mixture and the solution was allowed to stir at 50 °C for 2.5 h. Residual 2-methyl-2-propanethiol was removed by purging nitrogen through the system into a sodium hypochlorite solution. The DMF was removed under reduced pressure producing an off-white solid which was recrystallised from ethyl acetate giving **59** as white crystals (200 mg, 86%). mp 149-150 °C; UV-vis λ<sub>max</sub> 332

nm;  $^1\text{H}$  NMR ( $\text{CDCl}_3$ )  $\delta$  1.62 (s, 9H,  $-\text{C}(\text{CH}_3)_3$ ), 7.56 - 7.83 (m, 5H, Ar), 8.69 - 8.73 (m, 1H, H<sub>8</sub>); MS  $m/z$  233 ( $\text{M}^+$ , 4%), 177 (100), 160 (20), 145 (14), 128 (56), 102 (22), 57 (33), 41 (42). Anal. Calcd for  $\text{C}_{13}\text{H}_{15}\text{NOS}$ : C, 66.92, H, 6.48, N, 6.00. Found C, 67.12, H, 6.20, N, 6.04.

### 2-(Ethylthio)-quinoline-1-oxide (58)

Ethanethiol (104 mg, 1.68 mmol.), 2-chloroquinoline-1-oxide (**60**) (100 mg, 0.56 mmol) and sodium hydroxide (67 mg, 1.68 mmol) were subject to the same conditions as described above. The white solid received was recrystallised from acetone/hexane producing **58** as sharp colourless crystals (250 mg, 87%). mp 106-108 °C; UV-vis  $\lambda_{\text{max}}$  331 nm;  $^1\text{H}$  NMR ( $\text{CDCl}_3$ )  $\delta$  1.47 (t, 3H,  $J=7.4$  Hz,  $-\text{CH}_2\text{CH}_3$ ), 3.00 (q, 2H,  $J=7.4$  Hz,  $-\text{CH}_2\text{CH}_3$ ), 7.20-7.81 (m, 5H, Ar), 8.64 - 8.68 (m, 1H, H<sub>8</sub>);  $^{13}\text{C}$  NMR ( $\text{CDCl}_3$ )  $\delta$  13.5, 24.6, 117.5, 118.7, 125.4, 127.0, 127.2, 128.0, 130.7, 141.2, 149.1; MS  $m/z$  205 ( $\text{M}^+$ , 25), 188 (100), 177 (16), 145 (16), 128 (76). Anal. Calcd for  $\text{C}_{11}\text{H}_{11}\text{NOS}$ : C, 64.36, H, 5.40, N, 6.82. Found C, 64.42, H, 5.23, N, 7.19.

## 6.5 General Physical Methods

UV-visible absorption solutions, used to determine ligand metal ion selectivity, were prepared from stock solvent containing 25% water and 75% DMF, by volume. These solutions were buffered with the sodium salt of piperazine-*N,N*-bis-(2-ethanesulfonic acid), NaPIPES, which has a  $\text{pK}_a$  of 6.8 at 293.2 K. The deionised water used was purified with a Milli Q Reagent system, boiled to expel dissolved gases and protected from carbon dioxide by a drying tube containing soda lime. Laboratory grade DMF was distilled under reduced pressure before use.

UV-visible absorption solutions, used to determine metal-ligand stability constants,  $K_{\text{stab}}$ , were prepared from stock solvent containing 5% water and 95% ethanol by volume. Milli Q water and freshly distilled ethanol were used in the preparation.

All ligands were prepared and purified by the methods described in Sections 6.2 to 6.4, and were dried over phosphorus pentoxide under vacuum for a minimum of 2 h before use.

The analytical grade metal perchlorate and nitrate salts used were dried over phosphorus pentoxide under vacuum prior to their use. Prestandardised 1.0 M aqueous solutions of the required metal ions were used to make metal ion stock solutions. Accurate standardisations were carried out using a Dowex AG 50W-X2 ion exchange column with standard aqueous stock solutions of 1.0 M sodium hydroxide and 0.1 M hydrochloric acid prepared from Convol<sup>®</sup> ampoules. Solutions requiring perchloric acid were prepared using analytical grade 70% aqueous perchloric acid.

## 6.6 Standardisation of Metal Ion Solutions

Prior to standardisation, the hygroscopic metal salts  $\text{Al}(\text{ClO}_4)_3$ ,  $\text{Pb}(\text{ClO}_4)_2$ ,  $\text{Mg}(\text{ClO}_4)_2$ ,  $\text{Cd}(\text{ClO}_4)_2$  and  $\text{Zn}(\text{NO}_3)_2$ , were dried for a minimum of 24 h over phosphorus pentoxide under vacuum, and total dehydration was assumed. Aqueous solutions of the afore mentioned metal salts at an approximate concentration of 1.0 M, were prepared using Milli Q water and then sequentially standardised. A Dowex AG 50W-X2 ion exchange column, which had been previously washed twice with hydrochloric acid (0.1 M) and twice with water, was loaded with an aqueous metal ion solution ( $2 \text{ cm}^3$ ). The loaded column was then eluted with purified Milli Q water until a change in the pH of the eluent from approximately pH 1 to pH 6 was observed. Universal indicator paper was used to monitor the changes in pH. Bromothymol blue (2 drops) was added to the eluent and the solution was titrated against sodium hydroxide (1.0 M) to determine the number of moles of hydrochloric acid, which in turn allowed the determination of the metal ion concentration. At least three of these titrations were performed, and the concentration of the metal salt was taken as an average of the two most precise values which were obtained within an error range of  $\pm 0.05 \text{ cm}^3$ . This procedure was repeated for each metal ion solution.

The sodium hydroxide, used in the above mentioned titrations, was accurately determined by standardisation against potassium hydrogen phthalate ( $10 \text{ cm}^3$ ,  $5.0 \times 10^{-2} \text{ M}$ ) using a Metrohm E665 Dosimat autoburette, an Orion SA720 potentiometer and an Orion 8172 Sure Flow Ross pH electrode. Titrations were controlled and data collected using an IMB compatible program, AUTOTIT7.



## 6.7 UV-visible Absorption Measurements

A Cary 2200 ultraviolet/visible spectrophotometer was used to record all UV-visible absorption spectra of the studied compounds and their metal complexes. The solutions were thermostatted to  $298.2 \pm 0.2$  K using a Julabo P water pump which circulated water through the cell compartment of the spectrophotometer. Data was collected and recorded through an IBM compatible personal computer. The spectral bandwidth of the spectrophotometer was set to 1.0 nm and measurements were made at a rate of 2 nm/sec. The wavelength range varied for each ligand tested. Baseline reference solutions were recorded for every sample solution and were subtracted from each individual absorption spectrum prior to data processing. The data was collated, and the plots of the absorption spectra were produced using the computer programs Microsoft Excel 5.0 and MATLAB.

### 6.7.1 Selectivity

The solutions used for UV-visible absorption metal ion selectivity measurements all contained 0.1 M sodium perchlorate and  $1.0 \times 10^{-3}$  M NaPIPES. To measure the absorption of the free ligand, the solutions also contained the ligand at a concentration of  $5.0 \times 10^{-5}$  M, except for the solutions of ligands (4), (5), (6), and (7) which were measured at a concentration of  $4.0 \times 10^{-5}$  M. In all complex solutions the metal ion concentration was in a 200 fold excess of the required ligand. Baseline measurements were run for all spectra of the sample solutions, using reference solutions containing either 0.1 M sodium perchlorate and  $1.0 \times 10^{-3}$  M NaPIPES, or these and the metal salt at the required concentration, for baselines of the absorption spectra of the ligands alone and those of the ligand in the presence of metal ions respectively.

### 6.7.2 Stability Constant Determination

Each ligand and its metal complex solution were recorded at two perchloric acid concentrations,  $1.0 \times 10^{-2}$  M, and  $1.0 \times 10^{-5}$  M, with all solutions containing 0.10 M sodium perchlorate. The concentration of the ligand being measured was held constant for each solution measured with 3-Hydroxy-2'-methoxyflavone (4) at a concentration of  $5.0 \times 10^{-5}$  M, and 3-hydroxy-4'-methoxyflavone (5) and 3-hydroxy-2'-methoxythioflavone (6) at  $3.33 \times 10^{-5}$  M. The concentration of the metal ions in the complex solutions varied according to which acid concentration and ligand were measured (see Appendix B). Baseline measurements were run

for all spectra of the sample solutions using reference solutions containing either 0.1 M sodium perchlorate and  $1.0 \times 10^{-2}$  M perchloric acid or 0.1 M sodium perchlorate and  $1.0 \times 10^{-5}$  M perchloric acid, corresponding to the perchloric acid concentration at which the sample solutions were measured. These solutions used for absorption spectra measurements were prepared from stock solutions as shown in Appendix B.

The wavelength range within which the absorption spectra were recorded varied according to which ligand was being measured. Ligand **4** was recorded from 260 - 450 nm, ligand **5** from 260 - 500 nm and ligand **6** was recorded from 260 - 550 nm.

The values of the stability constants,  $K_{\text{stab}}$ , and their corresponding errors were calculated using the computer program Specfit<sup>67</sup>, which was written from the IBM compatible version of the program MATLAB. Specfit fits data by minimising the square sum of the differences between the measured and calculated data of all components in solution. The UV-visible absorption data within the following wavelength ranges was used to determine the stability constants, 310 - 338 nm and 370 - 410 nm for ligand **4**, 342 - 370 nm and 400 - 440 nm for ligand **5**, and 380 - 420 nm and 430 - 480 nm for ligand **6**.

### 6.7.3 Light Decomposition of Ligand 7

A series of four solutions were prepared (in glassware covered by aluminium foil) using ligand **7** at a concentration of  $2.5 \times 10^{-5}$  M in 95% ethanol/5% water with  $\text{NaClO}_4$  at 0.1 M and  $\text{HClO}_4$  at a concentration of  $1.0 \times 10^{-5}$  M. Two of the solutions also contained  $\text{Pb}(\text{ClO}_4)_2$  at a concentration of  $5.0 \times 10^{-5}$  M. Each solution's UV-visible absorption spectrum was recorded within the wavelength range 260 - 600 nm every 20 minutes over a 60 minute period (0, 20, 40 and 60 minutes). Of the two solutions which did not contain  $\text{Pb}(\text{ClO}_4)_2$ , one was stored in the dark and the other was exposed to natural sunlight between measurements over the 60 minute duration. Of the two solutions which did contain  $\text{Pb}(\text{ClO}_4)_2$ , again, one was stored in the dark and the other was exposed to natural light between measurements over the 60 minute duration.

## 6.8 Fluorescence Measurements

Fluorescence emission spectra of the free ligands and their various metal complexes were measured using a Perkin Elmer Luminescence Spectrometer LS50B with the excitation and

emission slit widths set to 2.5 mm. All sample solutions were prepared in solvent with composition 95% ethanol/5% water and 0.1 M sodium perchlorate, and were thermostatted to  $298.2 \pm 0.2$  K by circulation of temperature controlled water through the cell compartment of the spectrometer, using a Grant Technical Specification Thermostatic Bath/Circulator Type ZD. Excitation of solutions and the recording of emission spectra were carried out using the computer application, Fluorescence Data Manager, FLDM, an LS50B instrument control program by Perkin Elmer, and a personal computer, which was directly connected to the spectrometer. Plots of the emission spectra were then produced using the computer program Microsoft Excel 5.0.

### **6.8.1 Stability Constant Determinations of Ligands 4 and 5 Al<sup>3+</sup> Complexes using Fluorescence Spectroscopy**

Ligands **4** and **5**, and their Al<sup>3+</sup> complex solutions all contained perchloric acid at a concentration of  $1.0 \times 10^{-2}$  M. The concentration of the ligand being measured was held constant for each solution measured with ligand **4** at  $1.0 \times 10^{-6}$  M and ligand **5** at  $3.33 \times 10^{-7}$  M. The concentration of Al<sup>3+</sup> in the complex solutions varied according to which ligand was being measured (Appendix B).

The wavelength ranges and excitation wavelengths at which the fluorescence spectra were recorded are 390 - 600 nm and 385 nm for ligand **4** and 420 - 600 nm and 416 nm for ligand **5**.

The values of the stability constants,  $K_{stab}$ , and their corresponding errors were calculated using the computer program Specfit<sup>67</sup>. The fluorescence data within the wavelength range 440 - 500 nm was used to determine the stability constants for the Al<sup>3+</sup> complexes of ligands **4** and **5**.

### **6.8.2 Fluorescence Determinations of Flavones 4 - 7 and their Complexes**

The relative fluorescence of the flavones **4** - **7** and their metal complex solutions were recorded at two perchloric acid concentrations,  $1.0 \times 10^{-2}$  M and  $1.0 \times 10^{-5}$  M. To measure the fluorescence spectra of the free ligand, the solutions also contained the ligand at a concentration of  $1.0 \times 10^{-6}$  M for the solutions containing **4**,  $3.33 \times 10^{-7}$  M for the solutions containing **5**,  $3.33 \times 10^{-6}$  M for the solutions containing **6**, and  $2.5 \times 10^{-6}$  M for those containing **7**. In all of the metal-ligand complex solutions the metal ion concentration was in a 100 fold excess of the

required ligand concentration. All the fluorescence spectra were recorded within the following wavelength ranges and at the corresponding excitation wavelengths, 400 - 600 nm and 385 nm for **4**, 430 - 600 nm and 416 nm for **5**, 470 - 650 and 460 nm for **6**, and 500 - 650 nm and 492 nm for **7**.

### 6.8.3 Fluorescence and UV-visible Absorption Time Experiments

All solutions were prepared from stock solvent containing 5% water, 95% ethanol, 0.1 M sodium perchlorate and perchloric acid at a concentration of  $10^{-5}$  M. The concentrations of ligand and  $\text{Al}(\text{ClO}_4)_3$  used in each experiment are listed in the table below. The UV-visible absorption measurements and the Fluorescence measurements were performed using the instruments described in sections 6.7 and 6.8 and were all recorded over 2 hours.

Experiment	Excitation Wavelength	Ligand	[Ligand] M	$[\text{Al}^{3+}]$ M	Result
RF vs Time <sup>a</sup>	385 nm	<b>4</b>	$1.0 \times 10^{-6}$	$5.0 \times 10^{-6}$	Fluorescence decrease
Abs vs Time <sup>b</sup>	385 nm	<b>4</b>	$5.0 \times 10^{-5}$	$1.0 \times 10^{-4}$	Constant absorbance
Abs vs Time	385 nm	<b>4</b>	$5.0 \times 10^{-6}$	$1.0 \times 10^{-5}$	Absorbance decrease
Abs vs Time	330 nm	<b>4</b>	$5.0 \times 10^{-5}$	0	Constant absorbance
Abs vs Time	330 nm	<b>4</b>	$5.0 \times 10^{-6}$	0	Constant absorbance
RF vs Time	416 nm	<b>5</b>	$3.33 \times 10^{-6}$	$6.66 \times 10^{-6}$	Fluorescence decrease

<sup>a</sup> Relative Fluorescence is abbreviated RF

<sup>b</sup> Absorbance is abbreviated Abs

### 6.8.4 Fluorescence Determinations of Thiazoles **30** - **33** and their Complexes

Ligands **30** - **33**, and their metal ion complex solutions all contained perchloric acid at a concentration of  $1.0 \times 10^{-5}$  M. To measure the fluorescence spectra of the free ligand, the solutions also contained the corresponding ligand at a concentration of  $1.0 \times 10^{-6}$  M. In all of the metal - ligand complex solutions, the metal ion concentration was in a 100 fold excess of the required ligand concentration (ie  $1.0 \times 10^{-4}$  M). The fluorescence spectra of the benzopyran-4-one thiazoles **30** and **31** and their metal - complexes were recorded between the wavelength range 310 - 600 nm with an excitation wavelength of 305 nm. The fluorescence spectra of the

coumarin thiazoles **32** and **33** and their metal complexes were recorded between the wavelength range 360 - 600 nm with an excitation wavelength of 353 nm.

## 6.9 Molecular Modelling

The structure geometries studied in this thesis were all calculated using GUASSIAN 94 software.<sup>62</sup> All calculations were performed using the LanL2DZ basis set.<sup>83</sup> Computational platforms on which the calculations were performed include the DECStation 5000/25 and Silicone Graphics Indigo2xZ workstations, as well as a Silicon Graphics Power Challenge Computer.

## Appendix A: UV-visible Absorption Spectra

This appendix contains the UV-visible absorption spectra of the ligands, **4 - 7** (Appendix A.1), **30 - 33** (Appendix A.2) and **39 - 43, 51, 53, 55, 58** and **59** (Appendix A.3) and their metal ion complexes. Each spectral plot displays a comparison of the UV-visible absorption spectra of the ligand when measured in the presence and in the absence of the metal ions which are listed in the legend of each plot. Only the spectra of the ligands in the presence of coordinating metal ions, as shown by a shift in the absorption maxima of the ligand, have been included in **A.1** of Appendix A, since they display large spectral changes. The spectra of these ligands when in the presence of non-coordinating metal ions have been omitted as they overlay the spectra of the free ligand itself. The spectra of the ligands in the presence of non-coordinating metal ions in **A.2** and **A.3** of Appendix A have been included in the spectral plots to illustrate the insignificant spectral changes with the studied metal ions. All the solutions used to measure the spectra of the complexed and free ligands were made up in a solvent system comprising of 75% DMF and 25% H<sub>2</sub>O by volume, and 0.10 M NaClO<sub>4</sub>, and all spectra were recorded at 298.2 K. The solutions used to record the spectra of the ligands in the absence of metal ions for **A.1** and **A.2** also contained 4.0 x 10<sup>-5</sup> M ligand and 1.0 x 10<sup>-3</sup> M NaPIPES whereas the solutions used to record the spectra of the ligands in the presence of metal ions contained 4.0 x 10<sup>-5</sup> M ligand, 1.0 x 10<sup>-3</sup> M NaPIPES and 8.0 x 10<sup>-3</sup> M metal perchlorate. The solutions used to record the spectra of the ligands in the absence and presence of metal ions for **A.3** contained 1.0 x 10<sup>-4</sup> M ligand, and 1.0 x 10<sup>-4</sup> M ligand and 1.0 x 10<sup>-2</sup> M metal perchlorate respectively.

## A.1 Flavones and Thioflavones

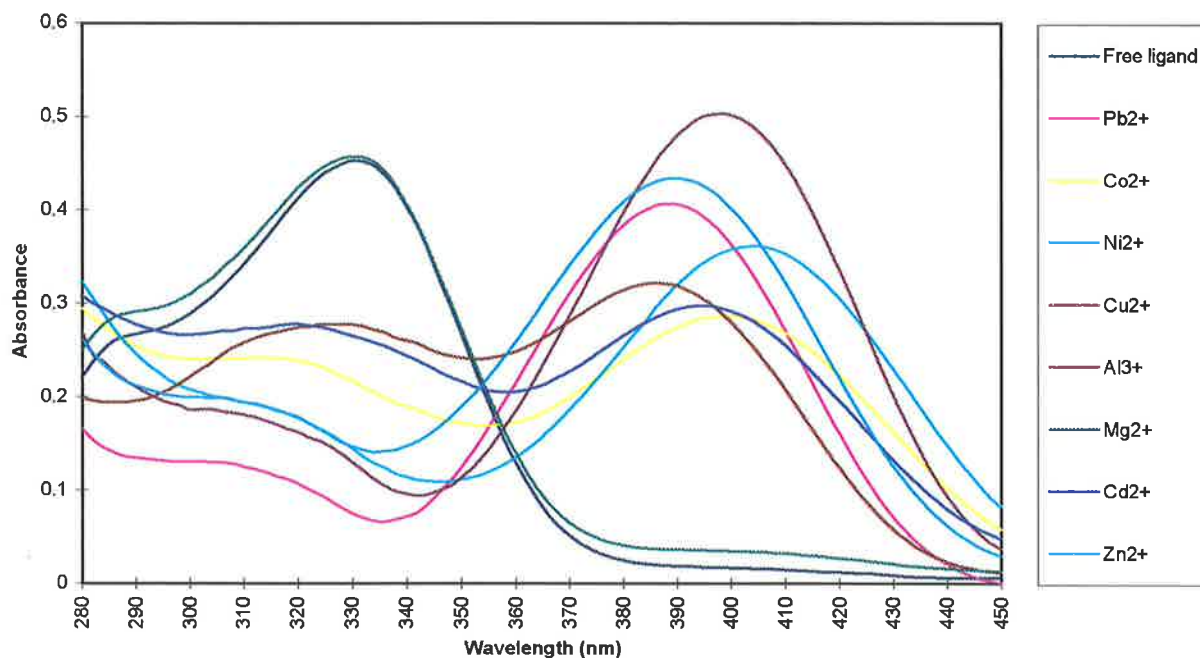


**Figure A.1.1:** The UV-visible absorption spectra of the ligand 3-hydroxy-2'-methoxyflavone (4) in the presence and absence of the metal ions listed in the vertical, right legend.

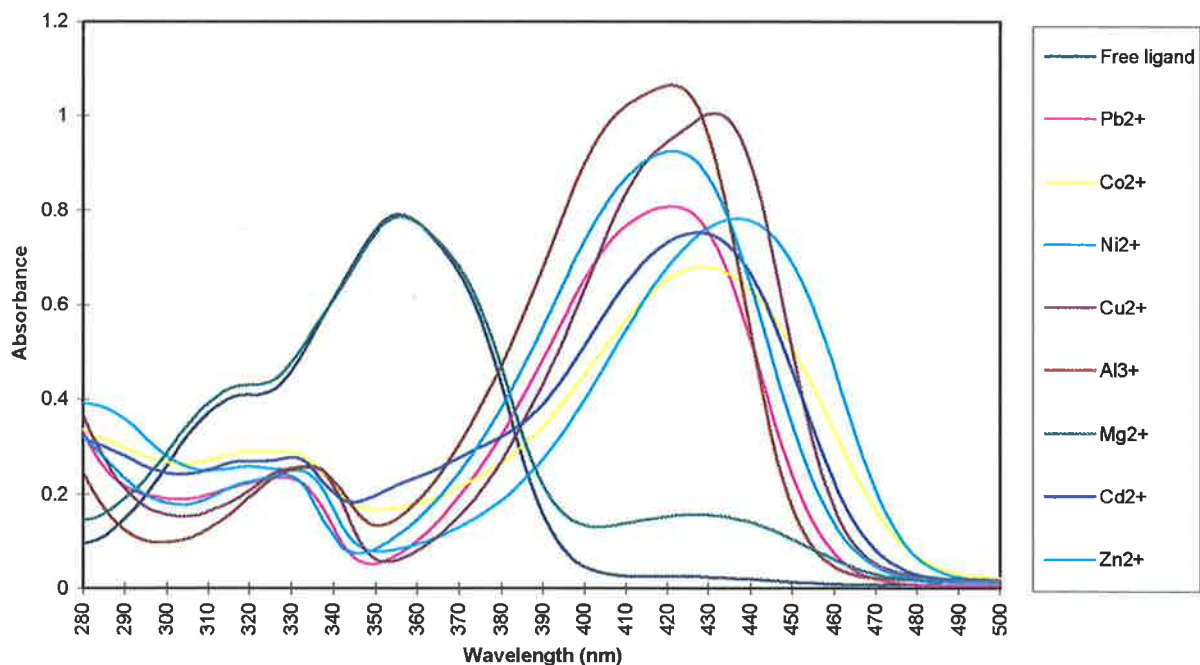


**Figure A.1.2:** The UV-visible absorption spectra of the ligand 3-hydroxy-4'-methoxyflavone (5) in the presence and absence of the metal ions listed in the vertical, right legend.

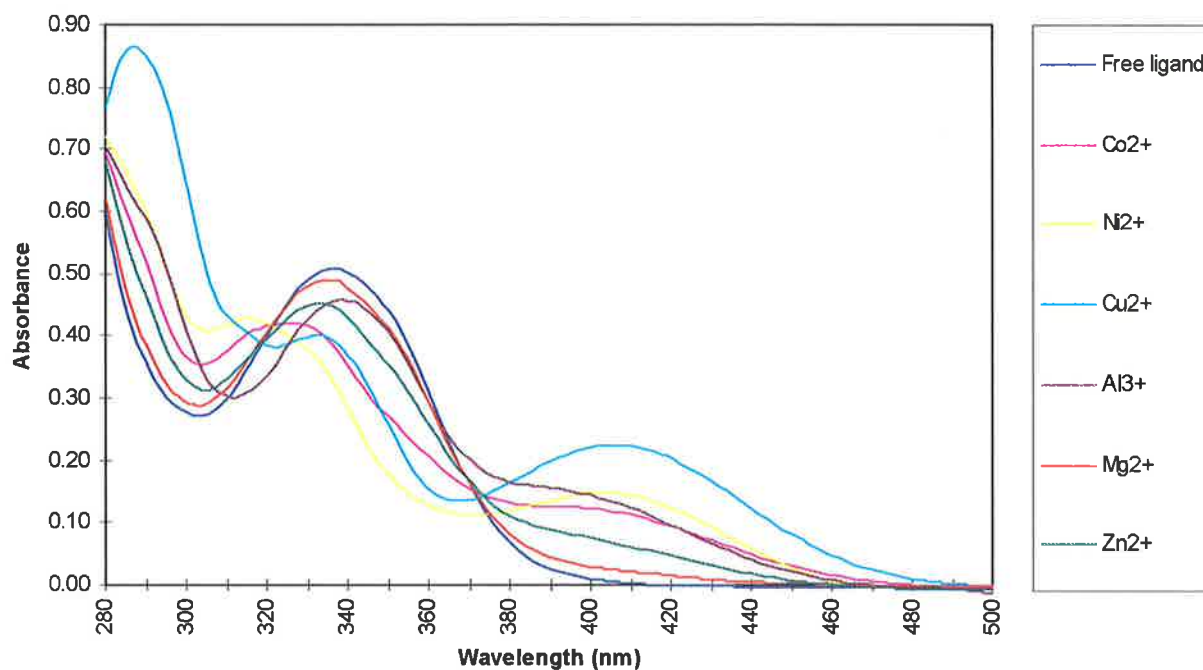


**Figure A.1.3:** The UV-visible absorption spectra of the ligand 5-hydroxy-2'-methoxyflavone (8) in the presence and absence of the metal ions listed in the vertical, right legend.

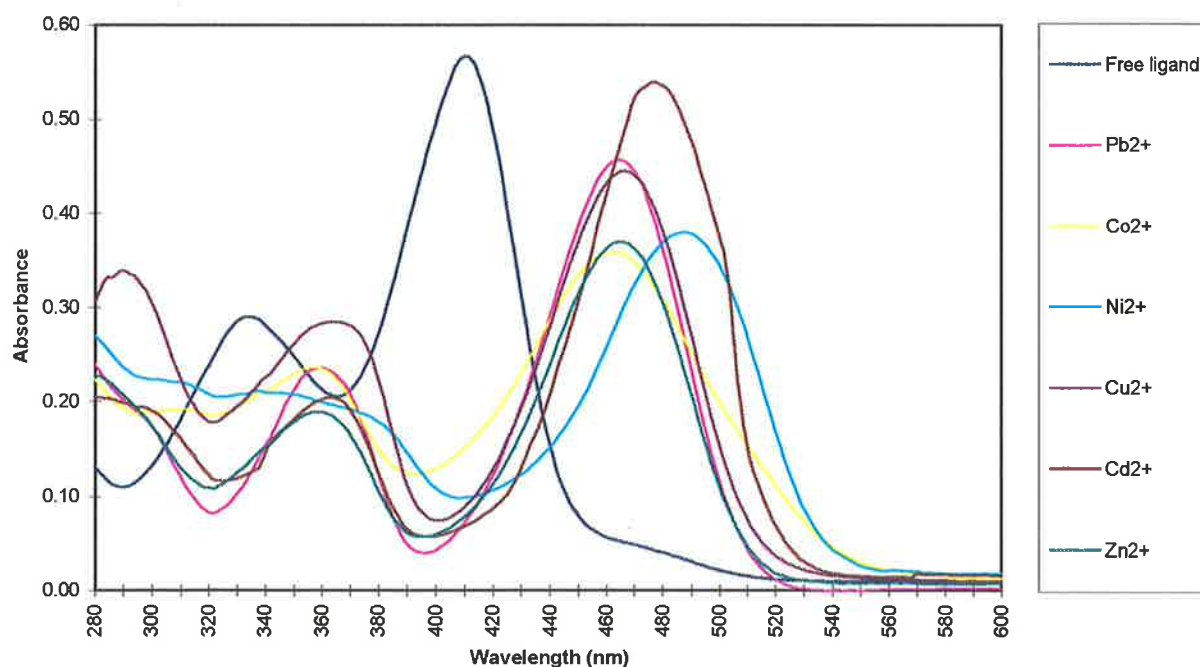


**Figure A.1.4:** The UV-visible absorption spectra of the ligand 3-hydroxy-2'-methoxythioflavone (6) in the presence and absence of the metal ions listed in the vertical, right legend.



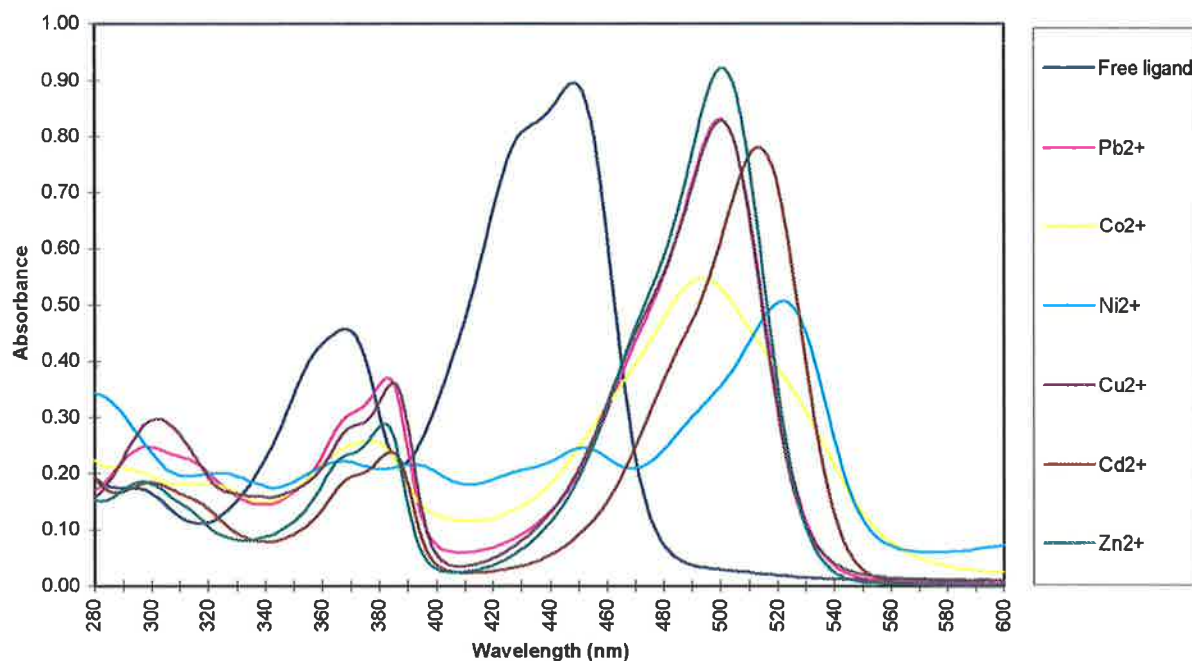


**Figure A.1.5:** The UV-visible absorption spectra of the ligand 3-hydroxy-4'-methoxythioflavone (7) in the presence and absence of the metal ions listed in the vertical, right legend.

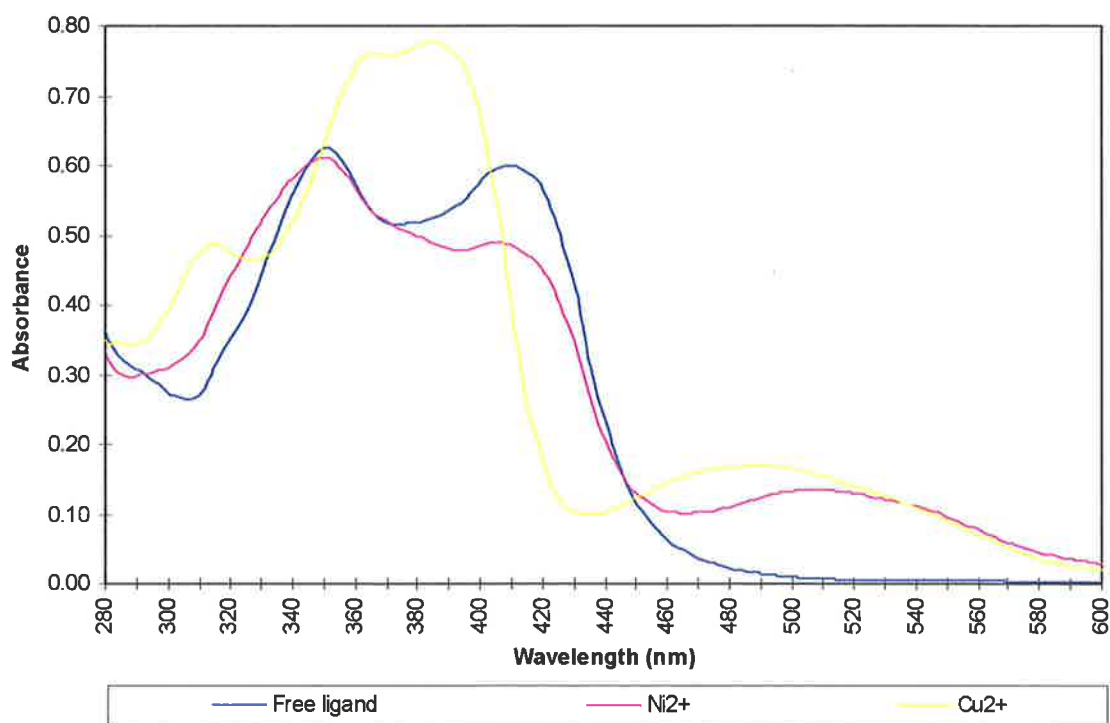


**Figure A.1.6:** The UV-visible absorption spectra of the ligand 5-hydroxy-2'-methoxythioflavone (9) in the presence and absence of the metal ions listed in the bottom legend.

## A.2 Thiazoles 30 - 33 and their Complexes

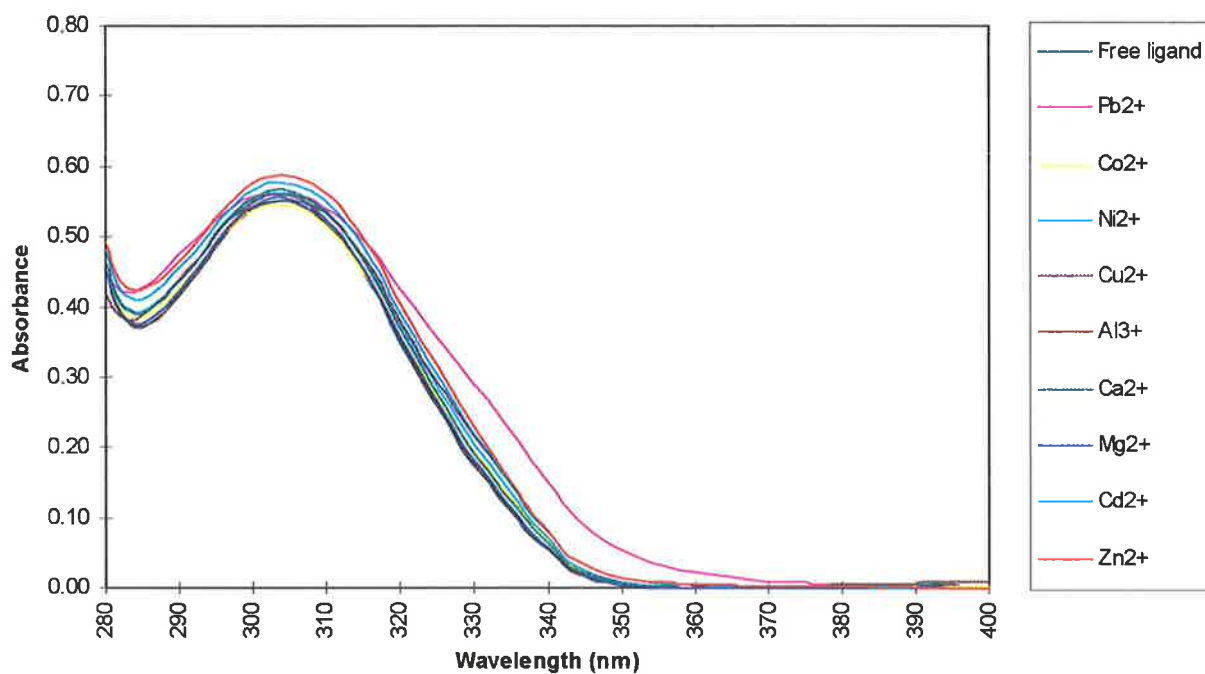


**Figure A.2.1:** Comparison of the UV-visible absorption spectra of the benzopyran thiazole ester 30 in the absence and presence of the metal ions listed in the vertical, right legend.

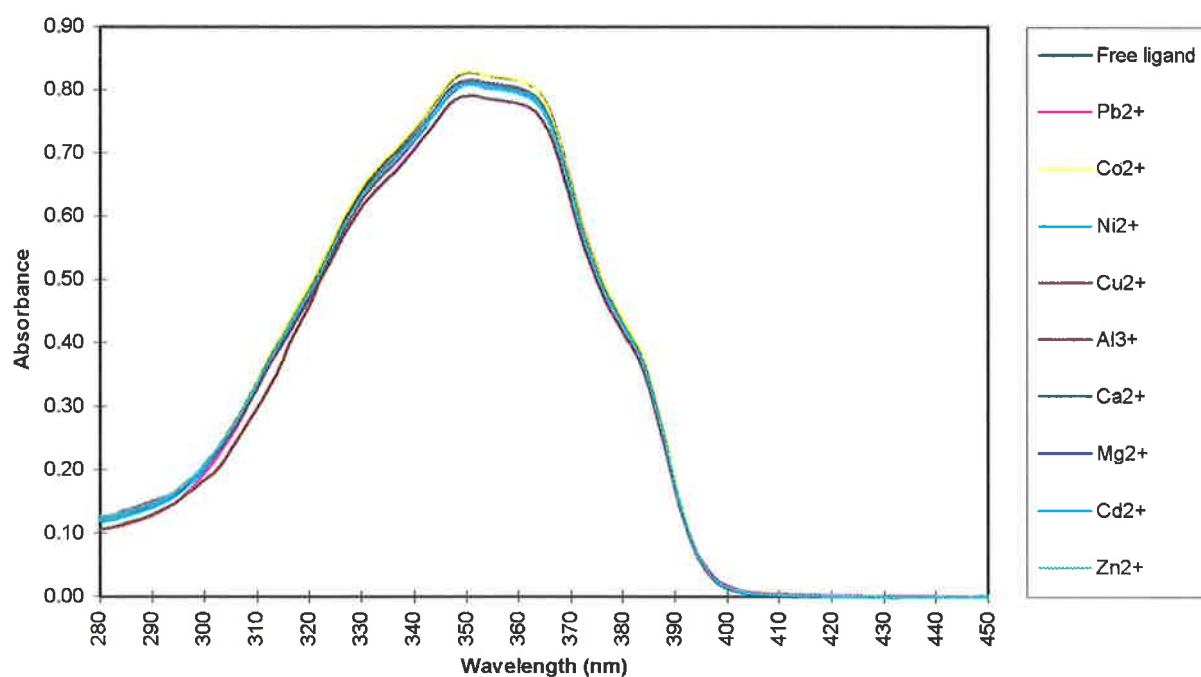


**Figure A.2.2:** Comparison of the UV-visible absorption spectra of the coumarin thiazole ester 32 in the absence and presence of the metal ions listed in the vertical, right legend.

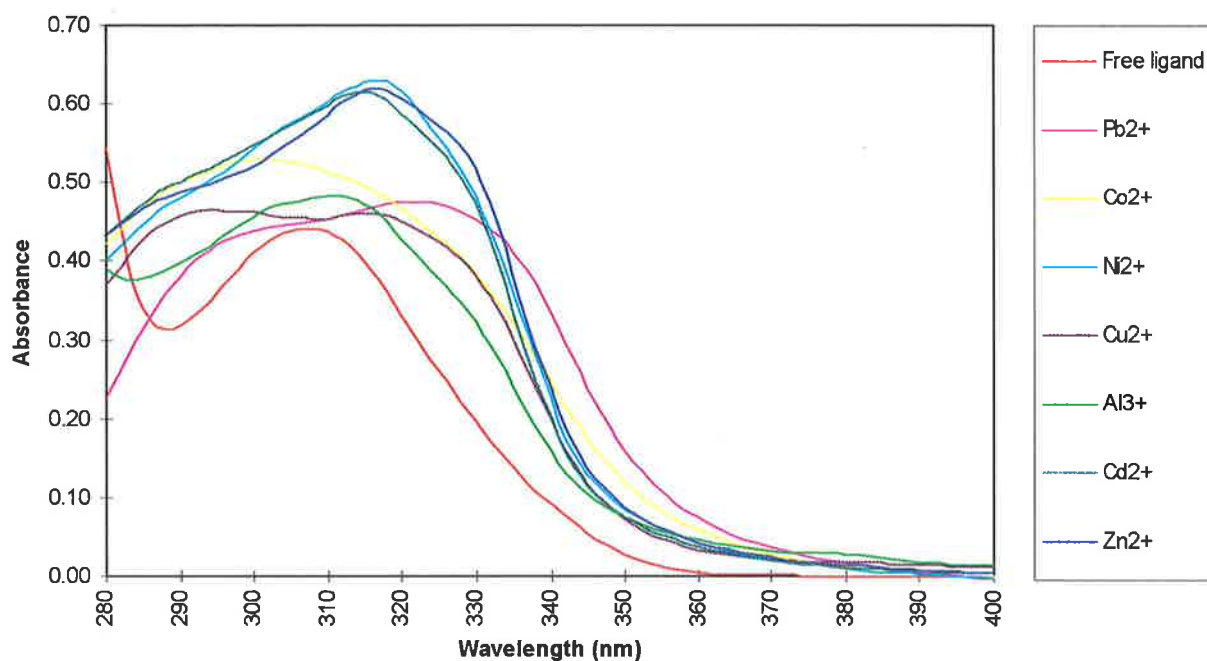


**Figure A.2.3:** Comparison of the UV-visible absorption spectra of the benzopyran thiazole acid **31** in the absence and presence of the metal ions listed in the vertical, right legend.

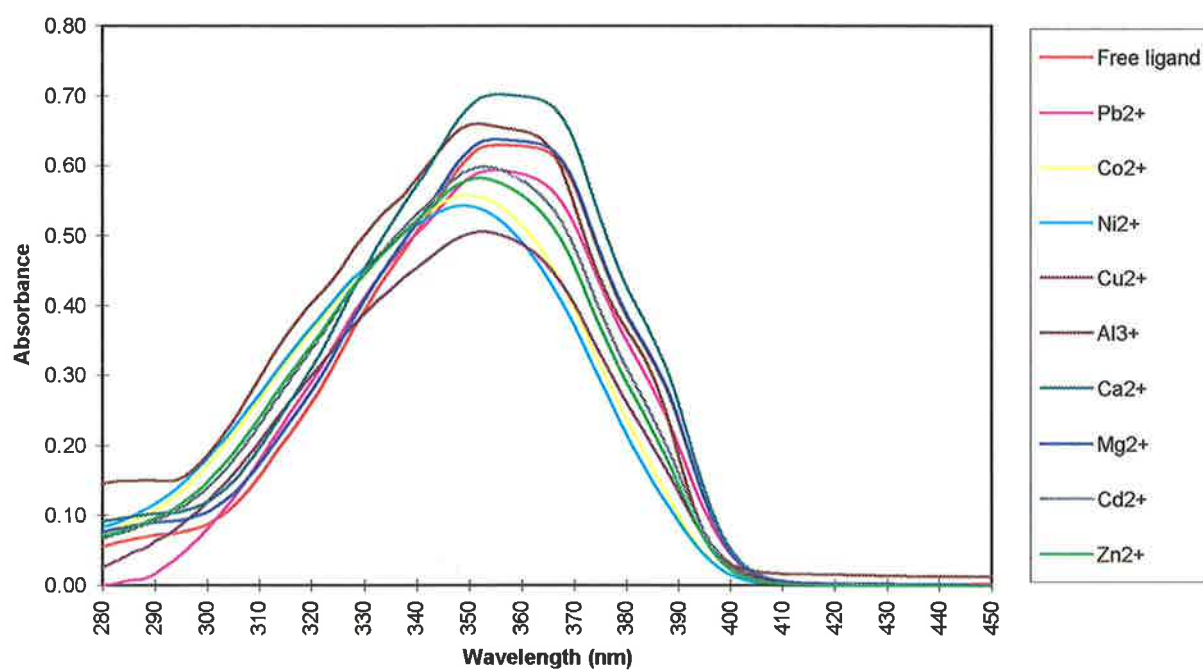


**Figure A.2.4:** Comparison of the UV-visible absorption spectra of the coumarin thiazole acid **33** in the absence and presence of the metal ions listed in the vertical, right legend.

### A.3 Quinoline and Pyridine Analogues

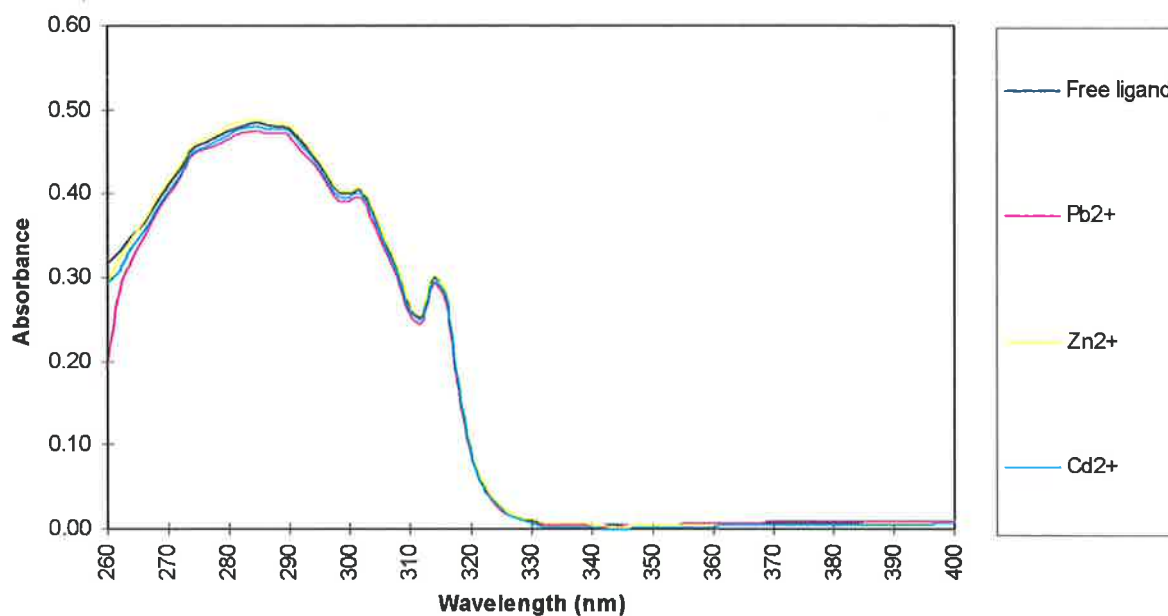


**Figure A.3.1:** Comparison of the UV-visible absorption spectra of the quinoline sulphonamide **39** in the presence and absence of the metal ions in the vertical, right legend.

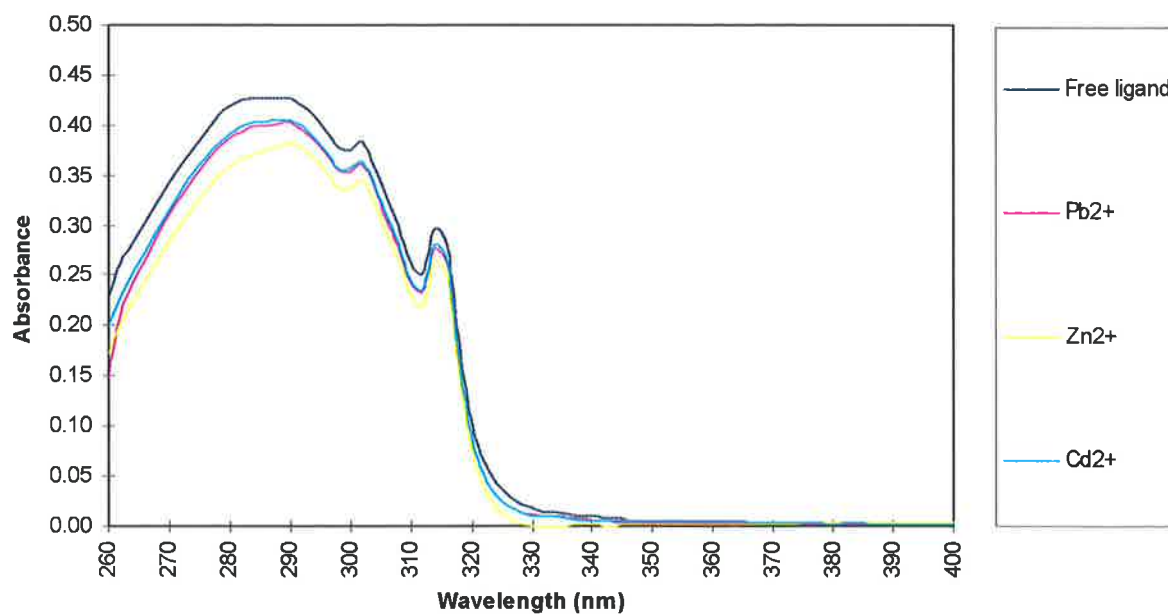


**Figure A.3.2:** Comparison of the UV-visible absorption spectra of the quinoline alcohol **40** in the presence and absence of the metal ions listed in the vertical, right legend.

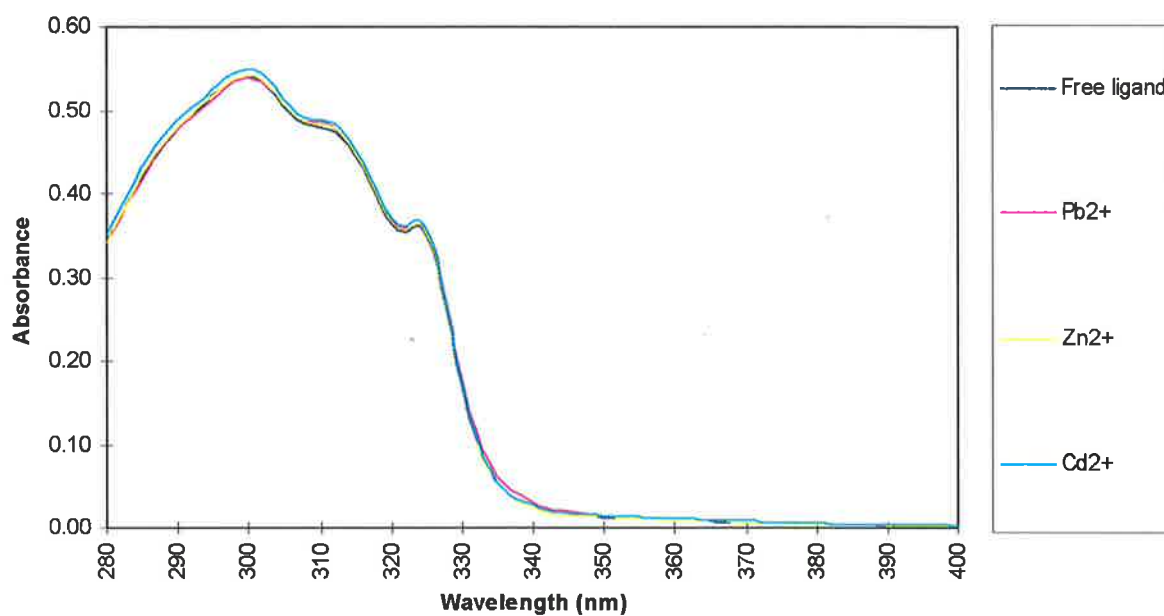


**Figure A.3.3:** Comparison of the UV-visible absorption spectra of the quinoline aldehyde 41 in the presence and absence of the metal ions listed in the vertical, right legend.

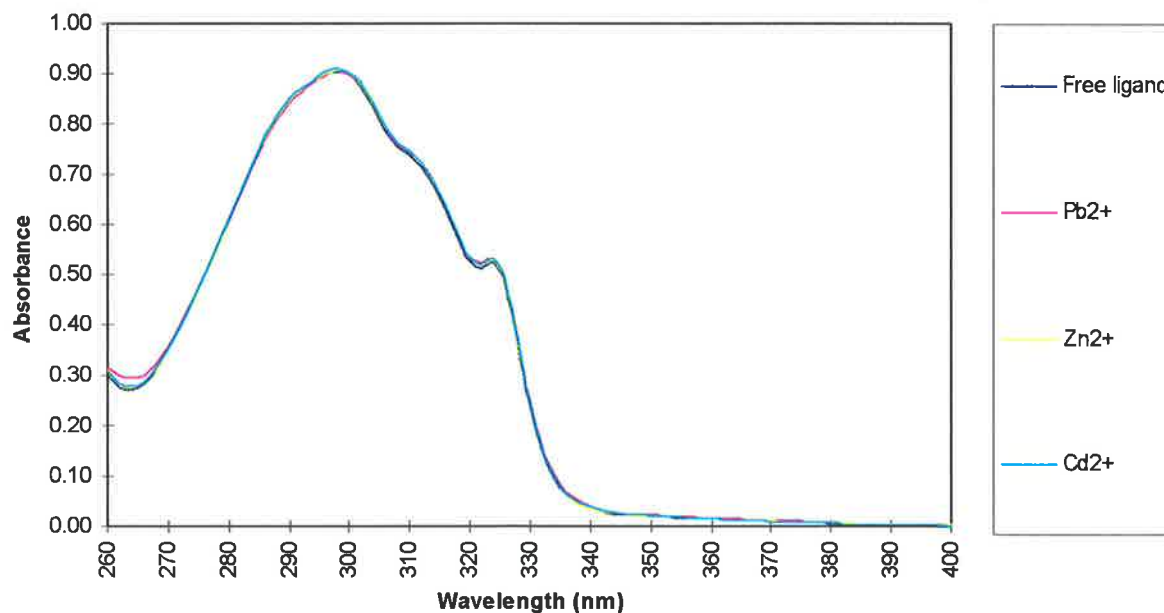


**Figure A.3.4:** Comparison of the UV-visible absorption spectra of the quinoline imine 42 in the presence and absence of the metal ions listed in the vertical, right legend.

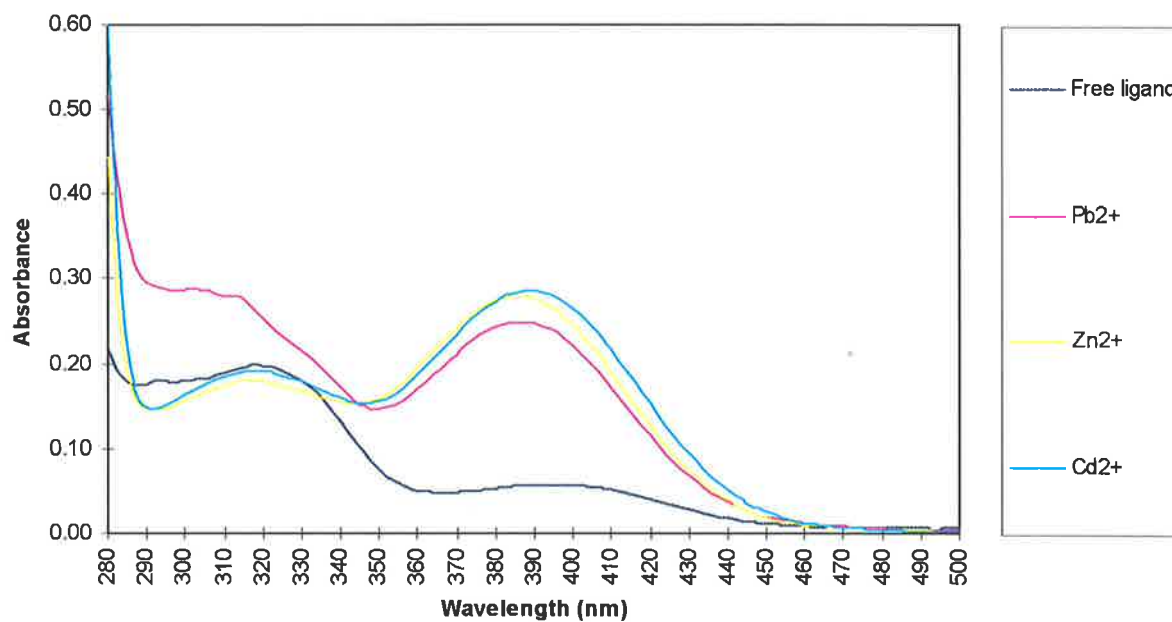


**Figure A.3.5:** Comparison of the UV-visible absorption spectra of the quinoline thiol 43 in the absence and presence of the metal ions listed in the vertical, right legend.

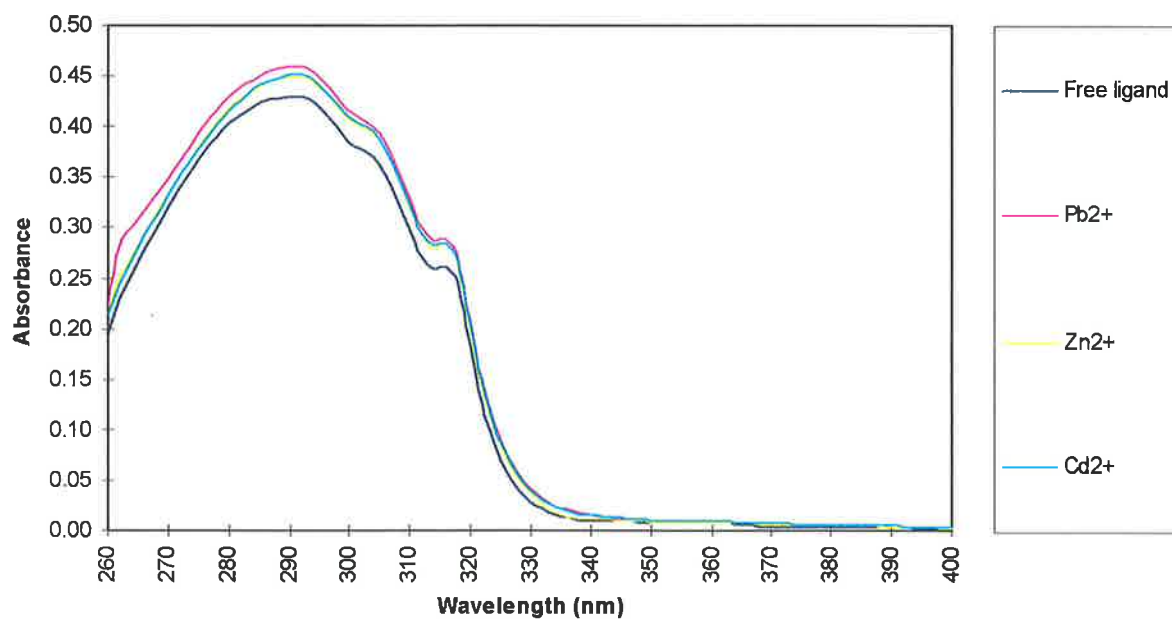


**Figure A.3.6:** Comparison of the UV-visible absorption spectra of the quinoline 51 in the presence and absence of the metal ions listed in the vertical, right legend.

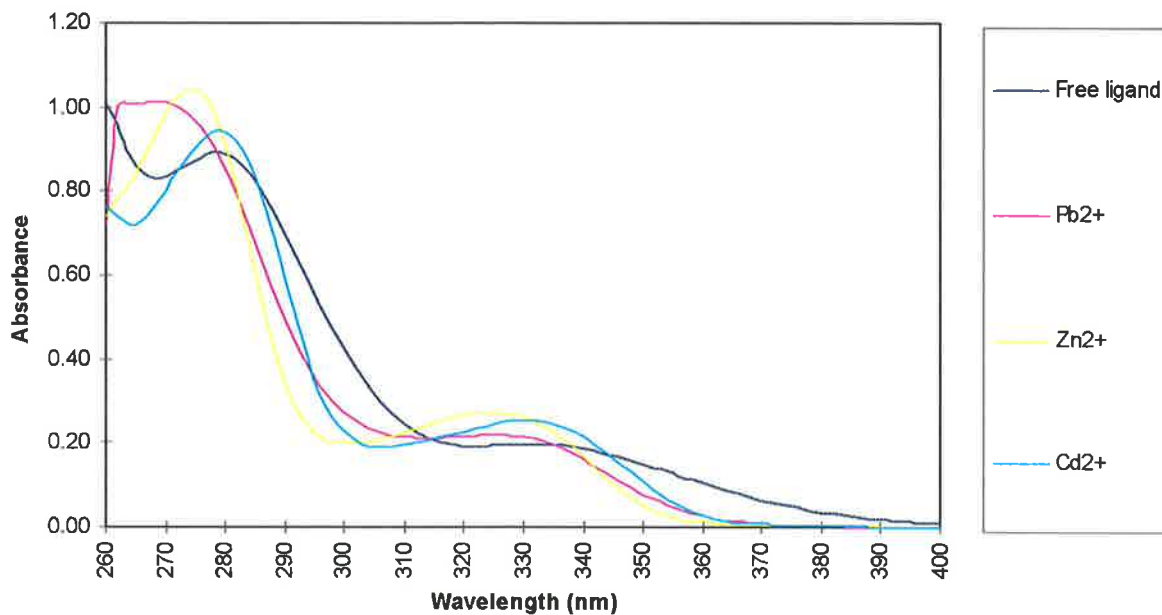


**Figure A.3.7:** Comparison of the UV-visible absorption spectra of the pyridine-1-oxide 53 in the presence and absence of the metal ions listed in the vertical, right legend.

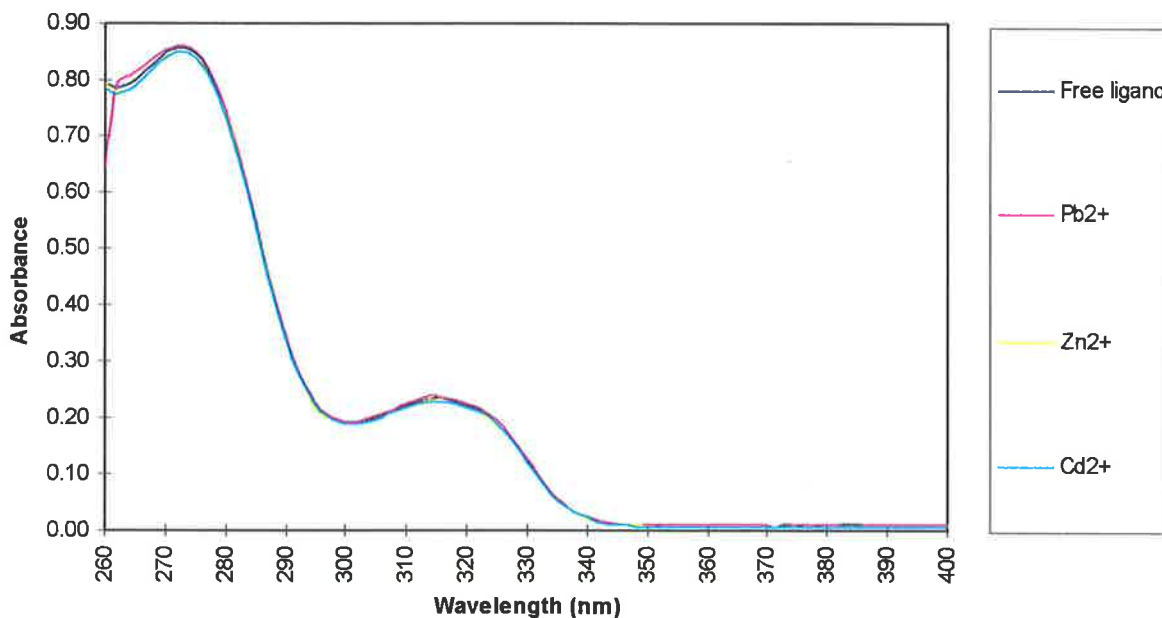


**Figure A.3.8:** Comparison of the UV-visible absorption spectra of the pyridine-1-oxide 55 in the presence and absence of the metal ions listed in the vertical, right legend.

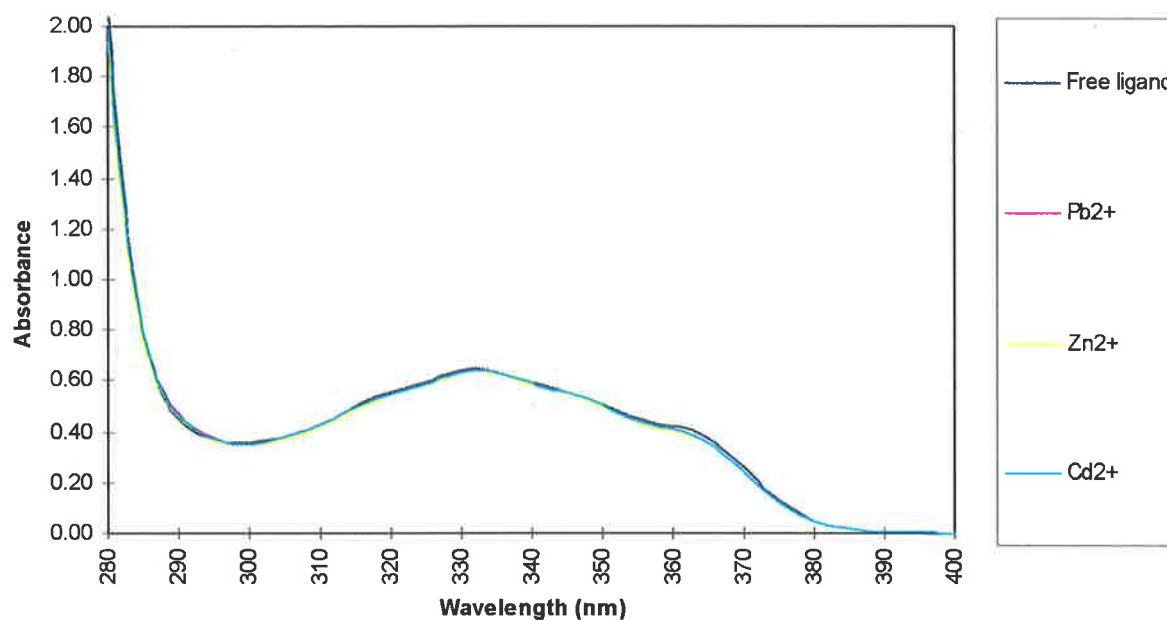


**Figure A.3.9:** Comparison of the UV-visible absorption spectra of the quinoline-1-oxide **58** in the presence and absence of the metal ions listed in the vertical, right legend.

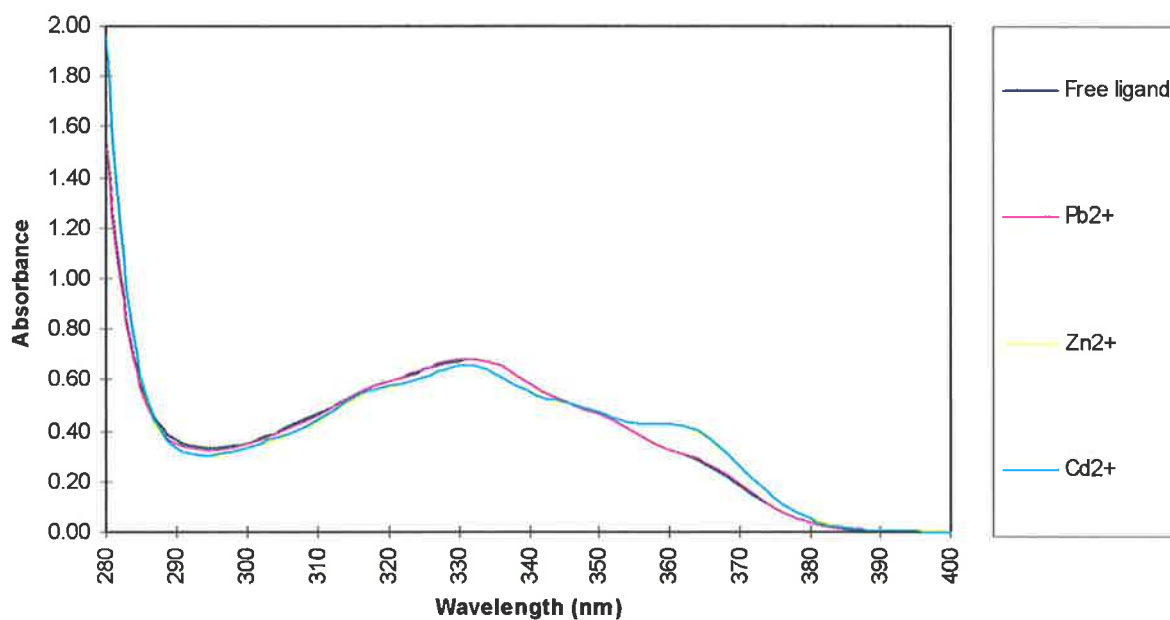


**Figure A.3.10:** Comparison of the UV-visible absorption spectra of the quinoline-1-oxide **59** in the presence and absence of the metal ions listed in the vertical, right legend.



## Appendix B: Metal Ion Concentrations for UV-visible Absorption and Fluorescence

The following tables present the various concentrations of the metal ion solutions used to measure the UV-visible absorption and fluorescence spectra of the flavone and thioflavone (4, 5 and 6) complexes for stability constant determination. Each table has a column titled soln n<sup>o</sup>. which represents the solution number that corresponds to a UV-visible absorption or fluorescence spectrum. Solution number 1 refers to the free ligand, and the numbers thereof increase respectively with the increasing concentration of metal ion. The abbreviation *lig* refers to the ligand that is mentioned in the title of the table. All solutions contained 0.1M sodium perchlorate.

**Table B.1:** Solutions of 3-hydroxy-2'-methoxyflavone (4) at  $5.0 \times 10^{-5} \text{ M}$  in  $[H^+] = 1.0 \times 10^{-2} \text{ M}$  with varying concentrations of  $Pb(ClO_4)_2$  as represented in Figure 2.6. All solutions were made from  $Pb(ClO_4)_2$  stock solutions of  $1.0 \times 10^{-2} \text{ M}$  or  $2.0 \times 10^{-2} \text{ M}$ .

Soln n <sup>o</sup> .	[Pb <sup>2+</sup> ] M	[lig]:[Pb <sup>2+</sup> ]	Soln n <sup>o</sup> .	[Pb <sup>2+</sup> ] M	[lig]:[Pb <sup>2+</sup> ]
1	0	1:0	13	$6.0 \times 10^{-3}$	1:120
2	$5.0 \times 10^{-4}$	1:10	14	$6.5 \times 10^{-3}$	1:130
3	$1.0 \times 10^{-3}$	1:20	15	$7.0 \times 10^{-3}$	1:140
4	$1.5 \times 10^{-3}$	1:30	16	$7.5 \times 10^{-3}$	1:150
5	$2.0 \times 10^{-3}$	1:40	17	$8.0 \times 10^{-3}$	1:160
6	$2.5 \times 10^{-3}$	1:50	18	$8.5 \times 10^{-3}$	1:170
7	$3.0 \times 10^{-3}$	1:60	19	$9.0 \times 10^{-3}$	1:180
8	$3.5 \times 10^{-3}$	1:70	20	$9.5 \times 10^{-3}$	1:190
9	$4.0 \times 10^{-3}$	1:80	21	$1.0 \times 10^{-2}$	1:200
10	$4.5 \times 10^{-3}$	1:90	22	$1.25 \times 10^{-2}$	1:250
11	$5.0 \times 10^{-3}$	1:100	23	$1.50 \times 10^{-2}$	1:300
12	$5.5 \times 10^{-3}$	1:110	24	$1.75 \times 10^{-2}$	1:350

**Table B.2:** Solutions of 3-hydroxy-2'-methoxyflavone (**4**) at  $5.0 \times 10^{-5} \text{ M}$  in  $[\text{H}^+] = 1.0 \times 10^{-5} \text{ M}$  with varying concentrations of  $\text{Pb}(\text{ClO}_4)_2$  as represented in Figure 2.10. All solutions were made from a  $\text{Pb}(\text{ClO}_4)_2$  stock solution of concentration  $2.5 \times 10^{-4} \text{ M}$ .

Soln n <sup>o</sup> .	$[\text{Pb}^{2+}] \text{ M}$	[lig]: $[\text{Pb}^{2+}]$	Soln n <sup>o</sup> .	$[\text{Pb}^{2+}] \text{ M}$	[lig]: $[\text{Pb}^{2+}]$
1	0	1:0	10	$8.75 \times 10^{-5}$	1:1.75
2	$6.25 \times 10^{-6}$	1:0.125	11	$1.00 \times 10^{-5}$	1:2
3	$1.25 \times 10^{-5}$	1:0.25	12	$1.13 \times 10^{-5}$	1:2.25
4	$1.88 \times 10^{-5}$	1:0.375	13	$1.25 \times 10^{-5}$	1:2.5
5	$2.50 \times 10^{-5}$	1:0.5	14	$1.38 \times 10^{-5}$	1:2.75
6	$3.75 \times 10^{-5}$	1:0.75	15	$1.50 \times 10^{-4}$	1:3
7	$5.00 \times 10^{-5}$	1:1	16	$2.00 \times 10^{-4}$	1:4
8	$6.25 \times 10^{-5}$	1:1.25	17	$2.50 \times 10^{-4}$	1:5
9	$7.50 \times 10^{-5}$	1:1.5			

**Table B.3:** Solutions of 3-hydroxy-2'-methoxyflavone (**4**) at  $5.0 \times 10^{-5} \text{ M}$  in  $[\text{H}^+] = 1.0 \times 10^{-2} \text{ M}$  with varying concentrations of  $\text{Al}(\text{ClO}_4)_3$  as represented in Figure 2.8. All solutions were made from an  $\text{Al}(\text{ClO}_4)_3$  stock solution of  $5.0 \times 10^{-4} \text{ M}$ .

Soln n <sup>o</sup> .	$[\text{Al}^{3+}] \text{ M}$	[lig]: $[\text{Al}^{3+}]$	Soln n <sup>o</sup> .	$[\text{Al}^{3+}] \text{ M}$	[lig]: $[\text{Al}^{3+}]$
1	0	1:0	12	$1.13 \times 10^{-4}$	1:2.25
2	$6.25 \times 10^{-6}$	1:0.125	13	$1.25 \times 10^{-4}$	1:2.5
3	$1.25 \times 10^{-5}$	1:0.25	14	$1.38 \times 10^{-4}$	1:2.75
4	$1.88 \times 10^{-5}$	1:0.375	15	$1.50 \times 10^{-4}$	1:3
5	$2.50 \times 10^{-5}$	1:0.5	16	$1.63 \times 10^{-4}$	1:3.25
6	$5.00 \times 10^{-5}$	1:1	17	$1.75 \times 10^{-4}$	1:3.5
7	$5.63 \times 10^{-5}$	1:1.125	18	$1.88 \times 10^{-4}$	1:3.75
8	$6.25 \times 10^{-5}$	1:1.25	19	$2.00 \times 10^{-4}$	1:4
9	$7.50 \times 10^{-5}$	1:1.5	20	$2.13 \times 10^{-4}$	1:4.25
10	$1.00 \times 10^{-4}$	1:2	21	$2.25 \times 10^{-4}$	1:4.5
11	$1.06 \times 10^{-4}$	1:2.125	22	$2.50 \times 10^{-4}$	1:5

**Table B.4:** Solutions of 3-hydroxy-2'-methoxyflavone (4) at  $5.0 \times 10^{-5}$  M in  $[H^+] = 1.0 \times 10^{-5}$  M with varying concentrations of  $Al(ClO_4)_3$  as represented in Figure 2.12. All solutions were made from an  $Al(ClO_4)_3$  stock solution of  $1.0 \times 10^{-4}$  M.

Soln n <sup>o</sup> .	$[Al^{3+}]$ M	[lig]: $[Al^{3+}]$	Soln n <sup>o</sup> .	$[Al^{3+}]$ M	[lig]: $[Al^{3+}]$
1	0	1:0	10	$5.63 \times 10^{-5}$	1:1.125
2	$6.25 \times 10^{-6}$	1:0.125	11	$6.25 \times 10^{-5}$	1:1.25
3	$1.25 \times 10^{-5}$	1:0.25	12	$6.88 \times 10^{-5}$	1:1.375
4	$1.88 \times 10^{-5}$	1:0.375	13	$7.50 \times 10^{-5}$	1:1.5
5	$2.50 \times 10^{-5}$	1:0.5	14	$8.31 \times 10^{-5}$	1:1.625
6	$3.13 \times 10^{-5}$	1:0.625	15	$8.75 \times 10^{-4}$	1:1.75
7	$3.75 \times 10^{-5}$	1:0.75	16	$9.38 \times 10^{-4}$	1:1.875
8	$4.38 \times 10^{-5}$	1:0.875	17	$1.00 \times 10^{-4}$	1:2
9	$5.00 \times 10^{-5}$	1:1			

**Table B.5:** Solutions of 3-hydroxy-2'-methoxyflavone (4) at  $5.0 \times 10^{-5}$  M in  $[H^+] = 1.0 \times 10^{-5}$  M with varying concentrations of  $Zn(NO_3)_2$  as represented in Figure 2.14. All solutions were made from a  $Zn(NO_3)_2$  stock solution of  $5.0 \times 10^{-3}$  M.

Soln n <sup>o</sup> .	$[Zn^{2+}]$ M	[lig]: $[Zn^{2+}]$	Soln n <sup>o</sup> .	$[Zn^{2+}]$ M	[lig]: $[Zn^{2+}]$
1	0	1:0	10	$1.25 \times 10^{-3}$	1:25
2	$1.25 \times 10^{-4}$	1:2.5	11	$1.50 \times 10^{-3}$	1:30
3	$2.50 \times 10^{-4}$	1:5	12	$1.75 \times 10^{-3}$	1:30
4	$3.75 \times 10^{-4}$	1:7.5	13	$2.00 \times 10^{-3}$	1:40
5	$5.00 \times 10^{-4}$	1:10	14	$2.25 \times 10^{-3}$	1:45
6	$6.25 \times 10^{-4}$	1:12.5	15	$2.50 \times 10^{-3}$	1:50
7	$7.50 \times 10^{-4}$	1:15	16	$3.50 \times 10^{-3}$	1:70
8	$1.00 \times 10^{-3}$	1:20	17	$4.50 \times 10^{-3}$	1:90
9	$1.13 \times 10^{-3}$	1:22.5	18	$5.00 \times 10^{-3}$	1:100

**Table B.6:** Solutions of 3-hydroxy-2'-methoxyflavone (**4**) at  $5.0 \times 10^{-5}$  M in  $[H^+] = 1.0 \times 10^{-5}$  M with varying concentrations of  $Cd(ClO_4)_2$  as represented in Figure 2.16. All solutions were made from  $Cd(ClO_4)_2$  stock solutions at concentrations of  $2.5 \times 10^{-3}$  M and 0.02 M.

Soln n <sup>o</sup> .	[Cd <sup>2+</sup> ] M	[lig]:[Cd <sup>2+</sup> ]	Soln n <sup>o</sup> .	[Cd <sup>2+</sup> ] M	[lig]:[Cd <sup>2+</sup> ]
1	0	1:0	9	$3.75 \times 10^{-3}$	1:75
2	$5.00 \times 10^{-5}$	1:1	10	$5.00 \times 10^{-3}$	1:100
3	$1.00 \times 10^{-4}$	1:2	11	$7.50 \times 10^{-3}$	1:150
4	$2.50 \times 10^{-4}$	1:5	12	$1.00 \times 10^{-2}$	1:200
5	$5.00 \times 10^{-4}$	1:10	13	$1.25 \times 10^{-2}$	1:250
6	$1.00 \times 10^{-3}$	1:20	14	$1.50 \times 10^{-2}$	1:300
7	$1.50 \times 10^{-3}$	1:30	15	$1.75 \times 10^{-2}$	1:350
8	$2.50 \times 10^{-3}$	1:50	16	$2.0 \times 10^{-2}$	1:400

**Table B.7:** Solutions of 3-hydroxy-4'-methoxyflavone (**5**) at  $3.33 \times 10^{-5}$  M in  $[H^+] = 1.0 \times 10^{-2}$  M with varying concentrations of  $Pb(ClO_4)_2$  as represented in Figure 2.18. All solutions were made from  $Pb(ClO_4)_2$  stock solutions of  $6.66 \times 10^{-3}$  M and  $1.33 \times 10^{-2}$  M.

Soln n <sup>o</sup> .	[Pb <sup>2+</sup> ] M	[lig]:[Pb <sup>2+</sup> ]	Soln n <sup>o</sup> .	[Pb <sup>2+</sup> ] M	[lig]:[Pb <sup>2+</sup> ]
1	0	1:0	11	$3.33 \times 10^{-3}$	1:100
2	$3.33 \times 10^{-4}$	1:10	12	$4.00 \times 10^{-3}$	1:120
3	$6.66 \times 10^{-4}$	1:20	13	$4.66 \times 10^{-3}$	1:140
4	$9.99 \times 10^{-4}$	1:30	14	$5.33 \times 10^{-3}$	1:160
5	$1.33 \times 10^{-4}$	1:40	15	$5.99 \times 10^{-3}$	1:180
6	$1.67 \times 10^{-4}$	1:50	16	$6.66 \times 10^{-3}$	1:200
7	$2.00 \times 10^{-3}$	1:60	17	$8.33 \times 10^{-3}$	1:250
8	$2.33 \times 10^{-3}$	1:70	18	$9.99 \times 10^{-3}$	1:300
9	$2.66 \times 10^{-3}$	1:80	19	$1.17 \times 10^{-2}$	1:350
10	$3.00 \times 10^{-3}$	1:90	20	$1.33 \times 10^{-2}$	1:400

**Table B.8:** Solutions of 3-hydroxy-4'-methoxyflavone (5) at  $3.33 \times 10^{-5} \text{ M}$  in  $[\text{H}^+] = 1.0 \times 10^{-5} \text{ M}$  with varying concentrations of  $\text{Pb}(\text{ClO}_4)_2$  as represented in Figure 2.20. All solutions were made from  $\text{Pb}(\text{ClO}_4)_2$  stock solutions of  $3.33 \times 10^{-5} \text{ M}$  and  $1.67 \times 10^{-4} \text{ M}$ .

Soln n <sup>o</sup> .	$[\text{Pb}^{2+}] \text{ M}$	[lig]: $[\text{Pb}^{2+}]$	Soln n <sup>o</sup> .	$[\text{Pb}^{2+}] \text{ M}$	[lig]: $[\text{Pb}^{2+}]$
1	0	1:0.0	10	$3.00 \times 10^{-5}$	1:0.9
2	$3.33 \times 10^{-6}$	1:0.1	11	$3.33 \times 10^{-5}$	1:1.0
3	$6.66 \times 10^{-6}$	1:0.2	12	$5.00 \times 10^{-5}$	1:1.5
4	$9.99 \times 10^{-6}$	1:0.3	13	$6.66 \times 10^{-5}$	1:2.0
5	$1.33 \times 10^{-5}$	1:0.4	14	$8.33 \times 10^{-5}$	1:2.5
6	$1.67 \times 10^{-5}$	1:0.5	15	$9.99 \times 10^{-5}$	1:3.0
7	$2.00 \times 10^{-5}$	1:0.6	16	$1.33 \times 10^{-4}$	1:4.0
8	$2.33 \times 10^{-5}$	1:0.7	17	$1.50 \times 10^{-4}$	1:4.5
9	$2.66 \times 10^{-5}$	1:0.8			

**Table B.9:** Solutions of 3-hydroxy-4'-methoxyflavone (5) at  $3.33 \times 10^{-5} \text{ M}$  in  $[\text{H}^+] = 1.0 \times 10^{-2} \text{ M}$  with varying concentrations of  $\text{Al}(\text{ClO}_4)_3$  as represented in Figure 2.22. All solutions were made from an  $\text{Al}(\text{ClO}_4)_3$  stock solution of concentration  $1.67 \times 10^{-4} \text{ M}$ .

Soln n <sup>o</sup> .	$[\text{Al}^{3+}] \text{ M}$	[lig]: $[\text{Al}^{3+}]$	Soln n <sup>o</sup> .	$[\text{Al}^{3+}] \text{ M}$	[lig]: $[\text{Al}^{3+}]$
1	0	1:0.0	10	$3.00 \times 10^{-5}$	1:0.9
2	$3.33 \times 10^{-6}$	1:0.1	11	$3.33 \times 10^{-5}$	1:1.0
3	$6.66 \times 10^{-6}$	1:0.2	12	$4.00 \times 10^{-5}$	1:1.2
4	$9.99 \times 10^{-6}$	1:0.3	13	$4.66 \times 10^{-5}$	1:1.4
5	$1.33 \times 10^{-5}$	1:0.4	14	$5.33 \times 10^{-5}$	1:1.6
6	$1.67 \times 10^{-5}$	1:0.5	15	$5.99 \times 10^{-5}$	1:1.8
7	$2.00 \times 10^{-5}$	1:0.6	16	$6.66 \times 10^{-5}$	1:2.0
8	$2.33 \times 10^{-5}$	1:0.7	17	$7.33 \times 10^{-5}$	1:2.2
9	$2.66 \times 10^{-5}$	1:0.8			

**Table B.10:** Solutions of 3-hydroxy-4'-methoxyflavone (5) at  $3.33 \times 10^{-5}$  M in  $[H^+] = 1.0 \times 10^{-5}$  M with varying concentrations of  $Al(ClO_4)_3$  as represented in Figure 2.25. All solutions were made from  $Al(ClO_4)_3$  stock solutions at concentrations  $6.66 \times 10^{-5}$  M or  $1.33 \times 10^{-4}$  M.

Soln n <sup>o</sup> .	$[Al^{3+}]$ M	[lig]: $[Al^{3+}]$	Soln n <sup>o</sup> .	$[Al^{3+}]$ M	[lig]: $[Al^{3+}]$
1	0	1:0.0	10	$3.00 \times 10^{-5}$	1:0.9
2	$3.33 \times 10^{-6}$	1:0.1	11	$3.33 \times 10^{-5}$	1:1.0
3	$6.66 \times 10^{-6}$	1:0.2	12	$4.00 \times 10^{-5}$	1:1.2
4	$9.99 \times 10^{-6}$	1:0.3	13	$4.66 \times 10^{-5}$	1:1.4
5	$1.33 \times 10^{-5}$	1:0.4	14	$5.33 \times 10^{-5}$	1:1.6
6	$1.67 \times 10^{-5}$	1:0.5	15	$5.99 \times 10^{-5}$	1:1.8
7	$2.00 \times 10^{-5}$	1:0.6	16	$6.66 \times 10^{-5}$	1:2.0
8	$2.33 \times 10^{-5}$	1:0.7	17	$7.33 \times 10^{-5}$	1:2.2
9	$2.66 \times 10^{-5}$	1:0.8			

**Table B.11:** Solutions of 3-hydroxy-4'-methoxyflavone (5) at  $3.33 \times 10^{-5}$  M in  $[H^+] = 1.0 \times 10^{-5}$  M with varying concentrations of  $Zn(NO_3)_2$  as represented in Figure 2.26. All solutions were made from a  $Zn(NO_3)_2$  stock solution of concentration  $3.33 \times 10^{-3}$  M.

Soln n <sup>o</sup> .	$[Zn^{2+}]$ M	[lig]: $[Zn^{2+}]$	Soln n <sup>o</sup> .	$[Zn^{2+}]$ M	[lig]: $[Zn^{2+}]$
1	0	1:0	11	$8.33 \times 10^{-4}$	1:25
2	$8.33 \times 10^{-5}$	1:2.5	12	$9.99 \times 10^{-4}$	1:30
3	$1.67 \times 10^{-4}$	1:5	13	$1.17 \times 10^{-3}$	1:35
4	$2.50 \times 10^{-4}$	1:7.5	14	$1.33 \times 10^{-3}$	1:40
5	$3.33 \times 10^{-4}$	1:10	15	$1.50 \times 10^{-3}$	1:45
6	$4.16 \times 10^{-4}$	1:12.5	16	$1.67 \times 10^{-3}$	1:50
7	$5.00 \times 10^{-4}$	1:15	17	$2.33 \times 10^{-3}$	1:70
8	$5.83 \times 10^{-4}$	1:17.5	18	$3.00 \times 10^{-3}$	1:90
9	$6.66 \times 10^{-4}$	1:20	19	$3.33 \times 10^{-3}$	1:100
10	$7.50 \times 10^{-4}$	1:22.5			

**Table B.12:** Solutions of 3-hydroxy-4'-methoxyflavone (5) at  $3.33 \times 10^{-5} \text{ M}$  in  $[\text{H}^+] = 1.0 \times 10^{-5} \text{ M}$  with varying concentrations of  $\text{Cd}(\text{ClO}_4)_2$  as represented in Figure 2.28. All solutions were made from  $\text{Cd}(\text{ClO}_4)_2$  stock solutions at concentrations of  $2.5 \times 10^{-3} \text{ M}$  and  $0.02 \text{ M}$ .

Soln n <sup>o</sup> .	$[\text{Cd}^{2+}] \text{ M}$	[lig]: $[\text{Cd}^{2+}]$	Soln n <sup>o</sup> .	$[\text{Cd}^{2+}] \text{ M}$	[lig]: $[\text{Cd}^{2+}]$
1	0	1:0	9	$2.50 \times 10^{-3}$	1:75
2	$1.67 \times 10^{-5}$	1:0.5	10	$3.33 \times 10^{-3}$	1:100
3	$3.33 \times 10^{-5}$	1:1	11	$5.00 \times 10^{-3}$	1:150
4	$6.66 \times 10^{-5}$	1:2	12	$6.66 \times 10^{-3}$	1:200
5	$1.67 \times 10^{-4}$	1:5	13	$8.33 \times 10^{-3}$	1:250
6	$3.33 \times 10^{-4}$	1:10	14	$9.99 \times 10^{-3}$	1:300
7	$9.99 \times 10^{-4}$	1:30	15	$1.17 \times 10^{-2}$	1:350
8	$1.67 \times 10^{-3}$	1:50	16	$1.33 \times 10^{-2}$	1:400

**Table B.13:** Solutions of 3-hydroxy-2'-methoxythioflavone (6) at  $3.33 \times 10^{-5} \text{ M}$  in  $[\text{H}^+] = 1.0 \times 10^{-2} \text{ M}$  with varying concentrations of  $\text{Pb}(\text{ClO}_4)_2$  as represented in Figure 2.32. All solutions were made from  $\text{Pb}(\text{ClO}_4)_2$  stock solutions at  $6.66 \times 10^{-3} \text{ M}$  and  $1.33 \times 10^{-2} \text{ M}$  concentrations.

Soln n <sup>o</sup> .	$[\text{Pb}^{2+}] \text{ M}$	[lig]: $[\text{Pb}^{2+}]$	Soln n <sup>o</sup> .	$[\text{Pb}^{2+}] \text{ M}$	[lig]: $[\text{Pb}^{2+}]$
1	0	1:0	10	$2.00 \times 10^{-3}$	1:60
2	$1.67 \times 10^{-4}$	1:5	11	$2.33 \times 10^{-3}$	1:70
3	$3.33 \times 10^{-4}$	1:10	12	$2.66 \times 10^{-3}$	1:80
4	$5.00 \times 10^{-4}$	1:15	13	$3.33 \times 10^{-3}$	1:100
5	$6.66 \times 10^{-4}$	1:20	14	$4.00 \times 10^{-3}$	1:120
6	$8.33 \times 10^{-4}$	1:25	15	$4.66 \times 10^{-3}$	1:140
7	$9.99 \times 10^{-4}$	1:30	16	$5.33 \times 10^{-3}$	1:160
8	$1.33 \times 10^{-3}$	1:40	17	$6.66 \times 10^{-3}$	1:200
9	$1.67 \times 10^{-3}$	1:50	18	$8.33 \times 10^{-3}$	1:250

**Table B.14:** Solutions of 3-hydroxy-2'-methoxythioflavone (6) at  $3.33 \times 10^{-5} \text{ M}$  in  $[\text{H}^+] = 1.0 \times 10^{-5} \text{ M}$  with varying concentrations of  $\text{Pb}(\text{ClO}_4)_2$  as represented in Figure 2.34. All solutions were made from an  $\text{Pb}(\text{ClO}_4)_2$  stock solution of  $6.66 \times 10^{-5} \text{ M}$ .

Soln n <sup>o</sup> .	$[\text{Pb}^{2+}] \text{ M}$	[lig]: $[\text{Pb}^{2+}]$	Soln n <sup>o</sup> .	$[\text{Pb}^{2+}] \text{ M}$	[lig]: $[\text{Pb}^{2+}]$
1	0	1:0	10	$2.33 \times 10^{-5}$	1:0.7
2	$5.00 \times 10^{-6}$	1:0.15	11	$2.66 \times 10^{-5}$	1:0.8
3	$6.66 \times 10^{-6}$	1:0.2	12	$3.00 \times 10^{-5}$	1:0.9
4	$8.33 \times 10^{-6}$	1:0.25	13	$3.33 \times 10^{-5}$	1:1
5	$9.99 \times 10^{-6}$	1:0.3	14	$4.00 \times 10^{-5}$	1:1.2
6	$1.17 \times 10^{-5}$	1:0.35	15	$4.66 \times 10^{-5}$	1:1.4
7	$1.33 \times 10^{-5}$	1:0.4	16	$5.33 \times 10^{-5}$	1:1.6
8	$1.66 \times 10^{-5}$	1:0.5	17	$5.99 \times 10^{-4}$	1:1.8
9	$2.20 \times 10^{-5}$	1:0.6	18	$6.66 \times 10^{-5}$	1:2

**Table B.15:** Solutions of 3-hydroxy-2'-methoxythioflavone (6) at  $3.33 \times 10^{-5} \text{ M}$  in  $[\text{H}^+] = 1 \times 10^{-5} \text{ M}$  with various concentrations of  $\text{Zn}(\text{NO}_3)_2$  as represented in Figure 2.36. All solutions were made from a stock  $\text{Zn}(\text{NO}_3)_2$  solution at a concentration of  $8.33 \times 10^{-4} \text{ M}$ .

Soln n <sup>o</sup> .	$[\text{Zn}^{2+}] \text{ M}$	[lig]: $[\text{Zn}^{2+}]$	Soln n <sup>o</sup> .	$[\text{Zn}^{2+}] \text{ M}$	[lig]: $[\text{Zn}^{2+}]$
1	0	1:0	10	$2.00 \times 10^{-4}$	1:6
2	$1.67 \times 10^{-5}$	1:0.5	11	$2.66 \times 10^{-4}$	1:8
3	$3.33 \times 10^{-5}$	1:1	12	$3.33 \times 10^{-4}$	1:10
4	$5.00 \times 10^{-5}$	1:1.5	13	$4.00 \times 10^{-4}$	1:12
5	$6.66 \times 10^{-5}$	1:2	14	$4.66 \times 10^{-4}$	1:14
6	$8.33 \times 10^{-5}$	1:2.5	15	$5.33 \times 10^{-4}$	1:16
7	$9.99 \times 10^{-5}$	1:3	16	$6.66 \times 10^{-4}$	1:20
8	$1.33 \times 10^{-4}$	1:4	17	$8.33 \times 10^{-4}$	1:25
9	$1.67 \times 10^{-4}$	1:5			



**Table B.16:** Solutions of 3-hydroxy-2'-methoxythioflavone (**6**) at  $3.33 \times 10^{-5}$  M in  $[H^+] = 1.0 \times 10^{-5}$  M with varying concentrations of  $Cd(ClO_4)_2$  as represented in Figure 2.38. All solutions were made from a  $Cd(ClO_4)_2$  stock solution at a concentration of  $6.66 \times 10^{-3}$  M.

Soln n <sup>o</sup> .	$[Cd^{2+}]$ M	[lig]: $[Cd^{2+}]$	Soln n <sup>o</sup> .	$[Cd^{2+}]$ M	[lig]: $[Cd^{2+}]$
1	0	1:0	10	$7.50 \times 10^{-4}$	1:22.5
2	$8.33 \times 10^{-5}$	1:2.5	11	$9.16 \times 10^{-4}$	1:27.5
3	$1.67 \times 10^{-4}$	1:5	12	$9.99 \times 10^{-4}$	1:30
4	$2.50 \times 10^{-4}$	1:7.5	13	$1.17 \times 10^{-3}$	1:35
5	$3.33 \times 10^{-4}$	1:10	14	$1.33 \times 10^{-3}$	1:40
6	$4.16 \times 10^{-4}$	1:12.5	15	$1.50 \times 10^{-3}$	1:45
7	$5.00 \times 10^{-4}$	1:15	16	$3.33 \times 10^{-3}$	1:100
8	$5.83 \times 10^{-4}$	1:17.5	17	$6.66 \times 10^{-3}$	1:200
9	$6.66 \times 10^{-4}$	1:20			

**Table B.17:** Solutions for fluorescence determination of 3-hydroxy-2'-methoxyflavone (**4**) at  $1.0 \times 10^{-6}$  M in  $[H^+] = 1.0 \times 10^{-2}$  M with varying concentrations of  $Al(ClO_4)_3$  as represented in Figure 2.45. All solutions were made from an  $Al(ClO_4)_3$  stock solution of  $5.0 \times 10^{-4}$  M.

Soln n <sup>o</sup> .	$[Al^{3+}]$ M	[lig]: $[Al^{3+}]$	Soln n <sup>o</sup> .	$[Al^{3+}]$ M	[lig]: $[Al^{3+}]$
1	0	1:0	11	$2.00 \times 10^{-6}$	1:2
2	$1.25 \times 10^{-7}$	1:0.125	12	$2.25 \times 10^{-6}$	1:2.25
3	$2.50 \times 10^{-7}$	1:0.25	13	$2.50 \times 10^{-6}$	1:2.5
4	$3.75 \times 10^{-7}$	1:0.375	14	$2.75 \times 10^{-6}$	1:2.75
5	$5.00 \times 10^{-7}$	1:0.5	15	$3.00 \times 10^{-6}$	1:3
6	$7.50 \times 10^{-7}$	1:0.75	16	$3.50 \times 10^{-6}$	1:3.5
7	$1.00 \times 10^{-6}$	1:1	17	$4.00 \times 10^{-6}$	1:4
8	$1.25 \times 10^{-6}$	1:1.25	18	$4.45 \times 10^{-6}$	1:4.5
9	$1.50 \times 10^{-6}$	1:1.5	19	$5.00 \times 10^{-6}$	1:5
10	$1.75 \times 10^{-6}$	1:1.75			

**Table B.18:** Solutions for fluorescence determination of 3-hydroxy-4'-methoxyflavone (5) at  $3.33 \times 10^{-7} \text{ M}$  in  $[\text{H}^+] = 1.0 \times 10^{-2} \text{ M}$  with varying concentrations of  $\text{Al}(\text{ClO}_4)_3$  as represented in Figure 2.51. All solutions were made from an  $\text{Al}(\text{ClO}_4)_3$  stock solution of concentration  $1.67 \times 10^{-4} \text{ M}$ .

Soln n <sup>o</sup> .	$[\text{Al}^{3+}] \text{ M}$	[lig]: $[\text{Al}^{3+}]$	Soln n <sup>o</sup> .	$[\text{Al}^{3+}] \text{ M}$	[lig]: $[\text{Al}^{3+}]$
1	0	1:0.0	10	$3.00 \times 10^{-7}$	1:0.9
2	$3.33 \times 10^{-8}$	1:0.1	11	$3.33 \times 10^{-7}$	1:1.0
3	$6.66 \times 10^{-8}$	1:0.2	12	$4.00 \times 10^{-7}$	1:1.2
4	$9.99 \times 10^{-8}$	1:0.3	13	$4.66 \times 10^{-7}$	1:1.4
5	$1.33 \times 10^{-7}$	1:0.4	14	$5.33 \times 10^{-7}$	1:1.6
6	$1.67 \times 10^{-7}$	1:0.5	15	$5.99 \times 10^{-7}$	1:1.8
7	$2.00 \times 10^{-7}$	1:0.6	16	$6.66 \times 10^{-7}$	1:2.0
8	$2.33 \times 10^{-7}$	1:0.7	17	$8.33 \times 10^{-7}$	1:2.5
9	$2.66 \times 10^{-7}$	1:0.8			

## Appendix C: Fluorescence Spectra

This appendix contains the fluorescence emission spectra of the ligands **4** - **7** in the absence and presence of  $\text{Pb}^{2+}$ ,  $\text{Cd}^{2+}$ ,  $\text{Zn}^{2+}$  and  $\text{Mg}^{2+}$  (Figures C.1.1 - C.1.7), and the ligands **30** - **33** in the absence and presence of  $\text{Pb}^{2+}$ ,  $\text{Cd}^{2+}$ ,  $\text{Zn}^{2+}$ ,  $\text{Mg}^{2+}$  and  $\text{Al}^{3+}$  (Figures C.2.1 - C.2.4).

All the solutions used to record the fluorescence spectra were made up in a solvent system comprising of 95% ethanol and 5% water by volume and 0.1 M  $\text{NaClO}_4$  and were thermostated at 298.2 K.

The relative fluorescence levels of the flavones **4** - **7** and their metal complex solutions were recorded at two perchloric acid concentrations,  $1.0 \times 10^{-2}$  M and  $1.0 \times 10^{-5}$  M. To measure the fluorescence spectra of the free ligand, the solutions also contained the ligand at a concentration of  $1.0 \times 10^{-6}$  M for the solutions containing **4**,  $3.33 \times 10^{-7}$  M for the solutions containing **5**,  $3.33 \times 10^{-6}$  M for the solutions containing **6**, and  $2.5 \times 10^{-6}$  M for those containing **7**. In all of the metal-ligand complex solutions the metal ion concentration was in a 100 fold excess of the required ligand concentration.

Ligands **30** - **33**, and their metal ion complex solutions all contained perchloric acid at a concentration of  $1.0 \times 10^{-5}$  M. To measure the fluorescence spectra of the free ligand, the solutions also contained the corresponding ligand at a concentration of  $1.0 \times 10^{-6}$  M. In all of the metal - ligand complex solutions, the metal ion concentration was in a 100 fold excess of the required ligand concentration

## C.1 Flavones and Thioflavones

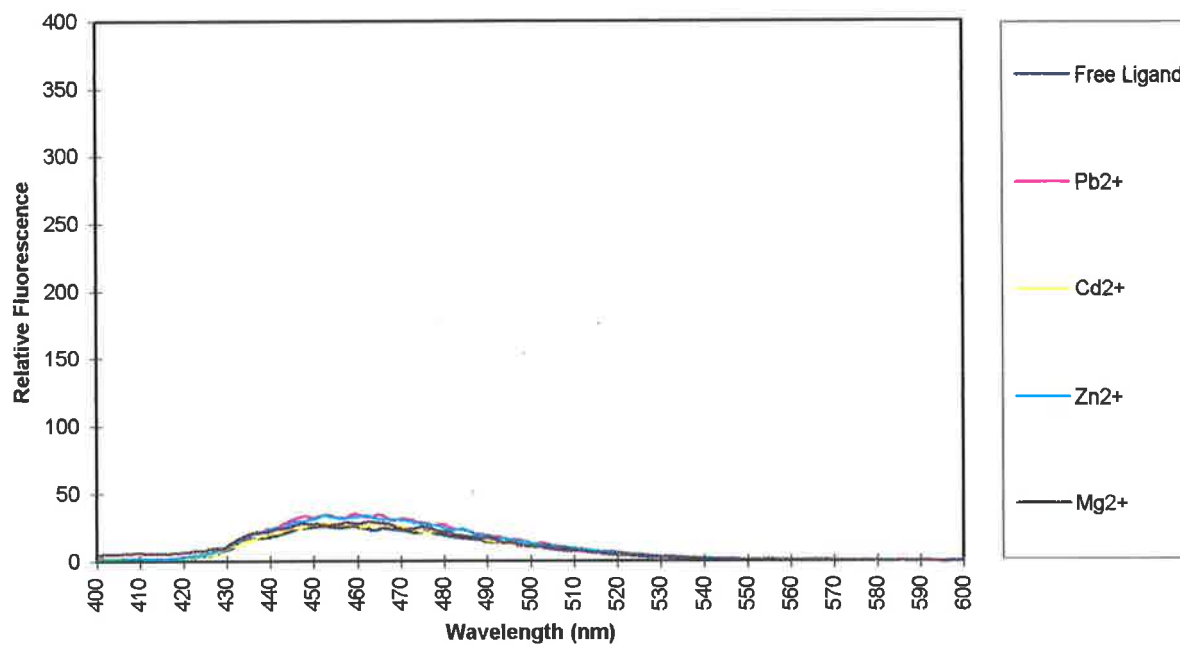


**Figure C.1.1:** A comparison of the fluorescence spectra of ligand 4 in solutions containing  $[H^+] = 10^{-2} M$  in the presence and absence of the metal ions listed in the vertical, right legend.

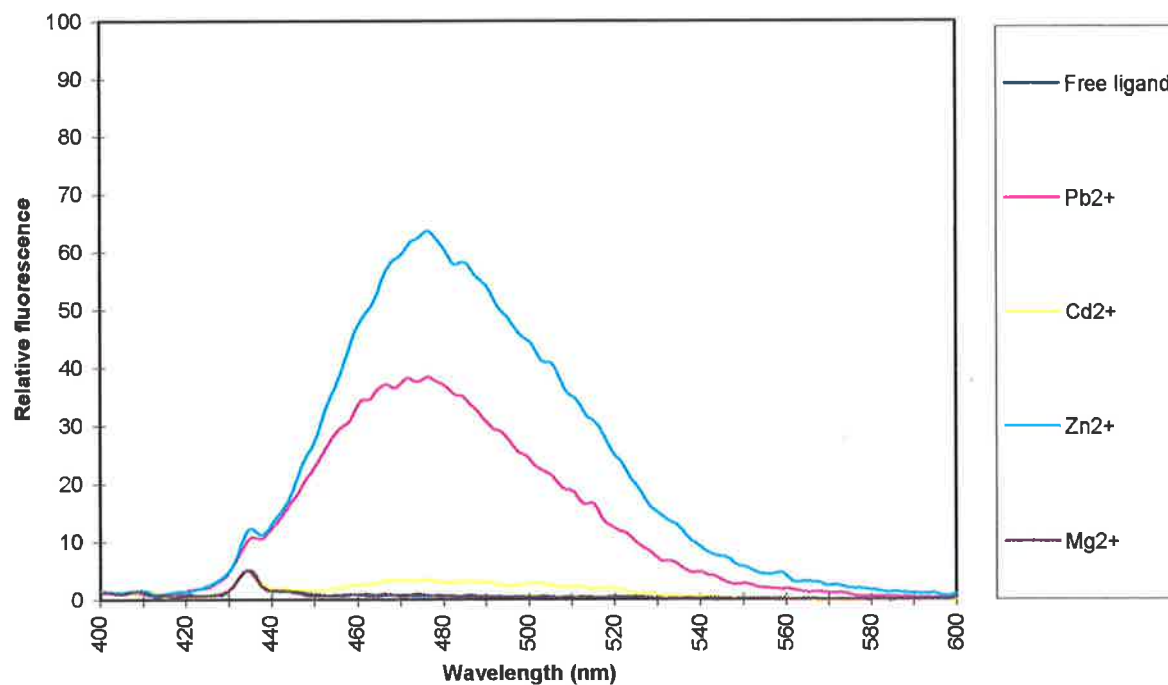


**Figure C.1.2:** A comparison of the fluorescence spectra of ligand 4 in solutions containing  $[H^+] = 10^{-5} M$  in the presence and absence of the metal ions listed in the vertical, right legend.

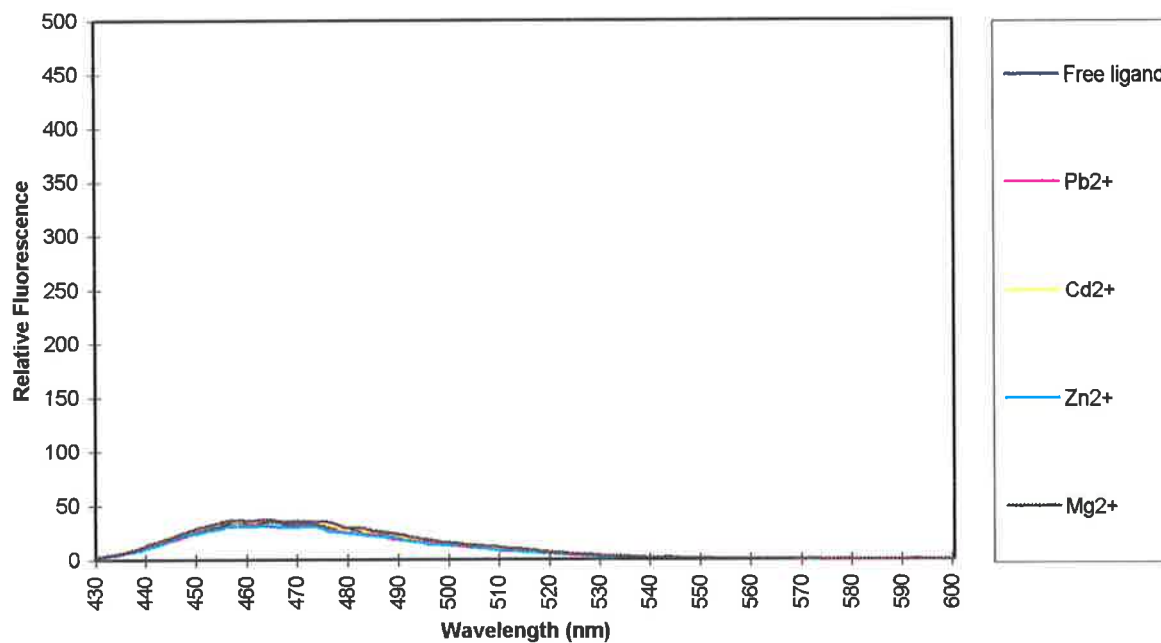


**Figure C.1.3:** A comparison of the fluorescence spectra of ligand 5 in solutions containing  $[H^+] = 10^{-2} M$  in the absence and presence of the metal ions listed in the vertical, right legend.

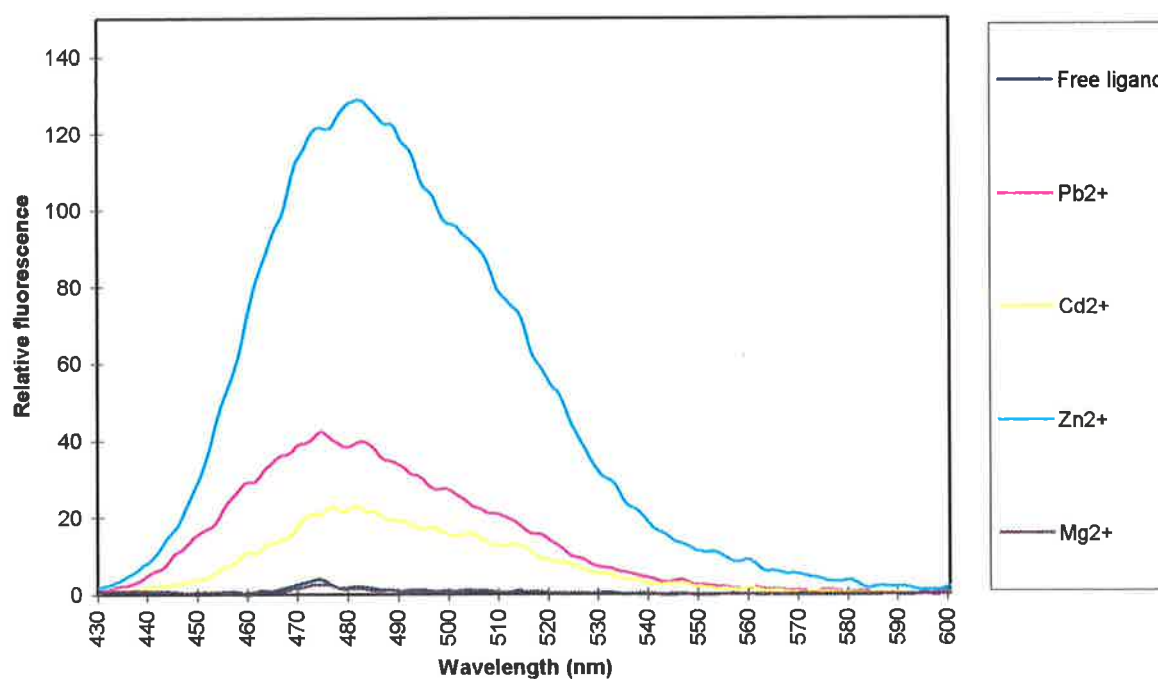


**Figure C.1.4:** A comparison of the fluorescence spectra of ligand 5 in solutions containing  $[H^+] = 10^{-5} M$  in the absence and presence of the metal ions listed in the vertical, right legend.

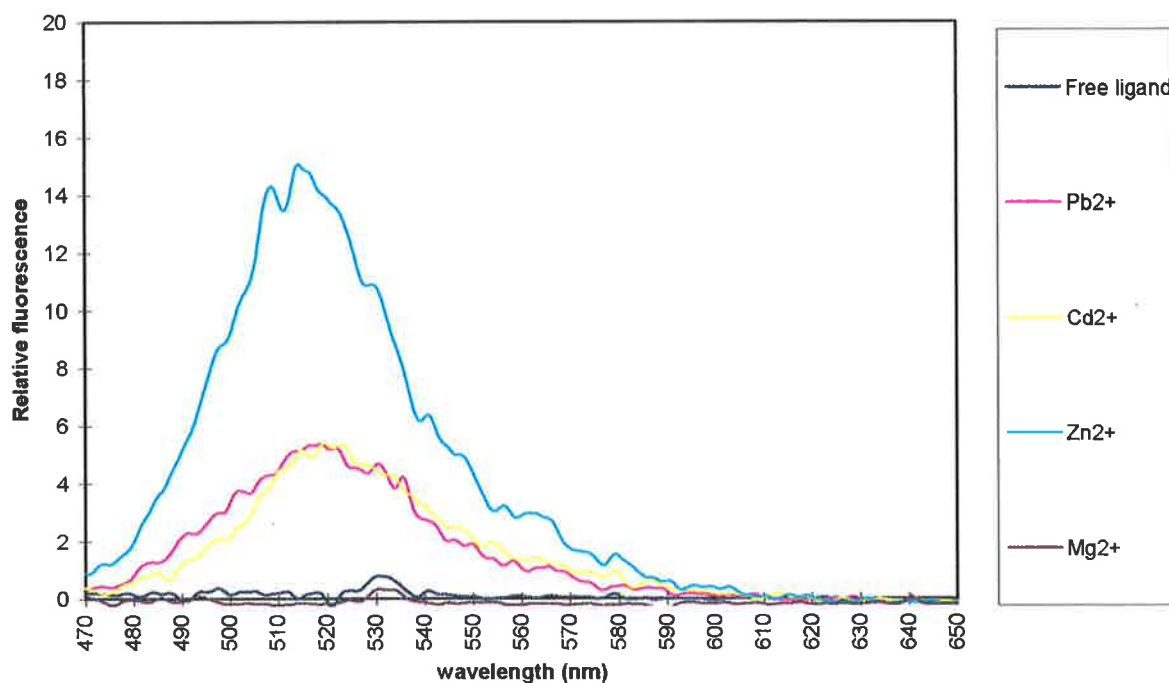


**Figure C.1.5:** A comparison of the fluorescence spectra of ligand 6 in solutions containing  $[H^+] = 10^{-5} M$  in the absence and presence of the metal ions listed in the vertical, right legend.

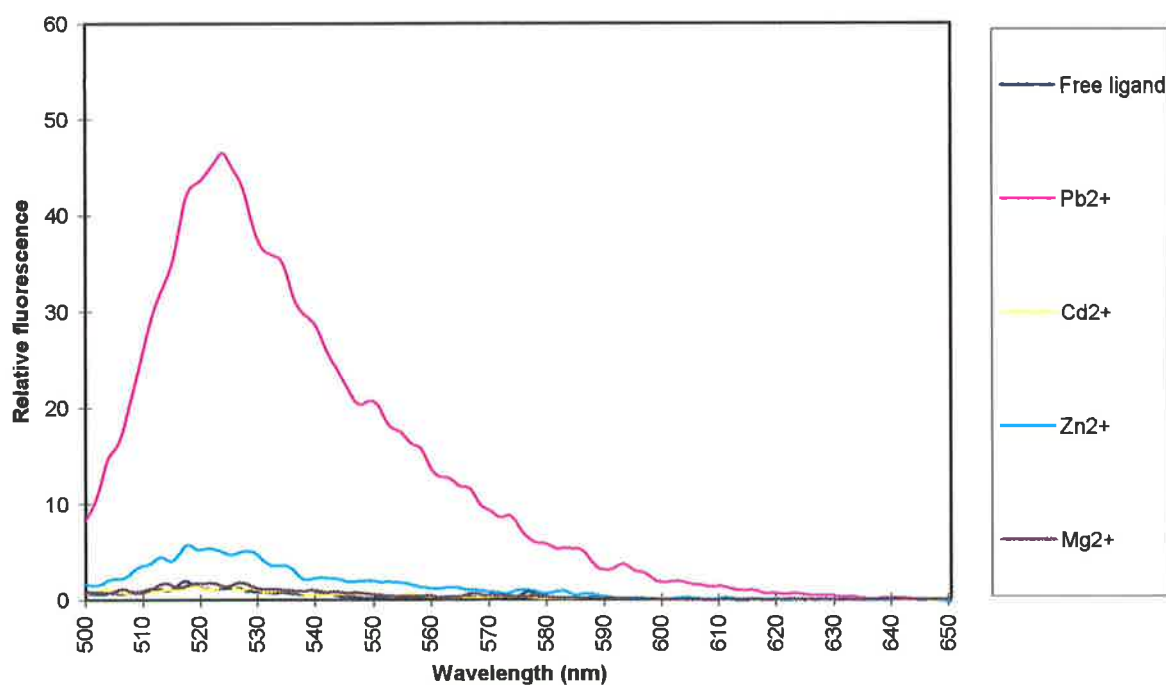


**Figure C.1.6:** A comparison of the fluorescence spectra of ligand 7 in solutions containing  $[H^+] = 10^{-2} M$  in the absence and presence of the metal ions listed in the vertical, right legend.

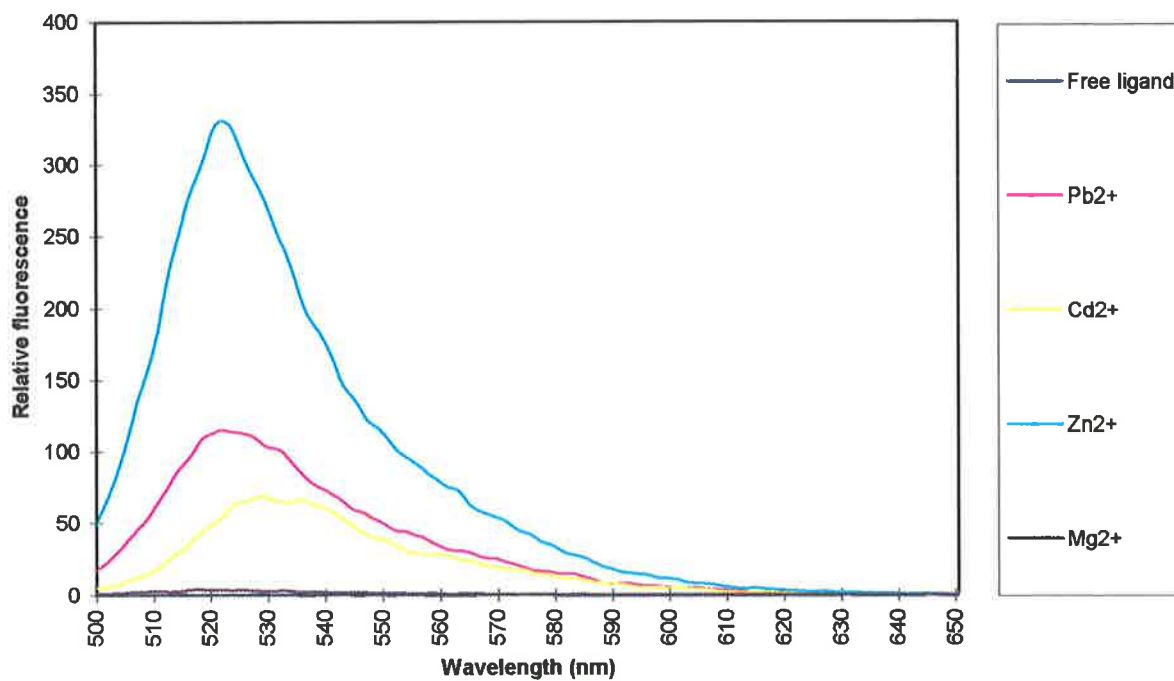


**Figure C.1.7:** A comparison of the fluorescence spectra of ligand 7 in solutions containing  $[H^+] = 10^{-5} M$  in the absence and presence of the metal ions listed in the vertical, right legend.

## C.2 Thiazoles 30 - 33

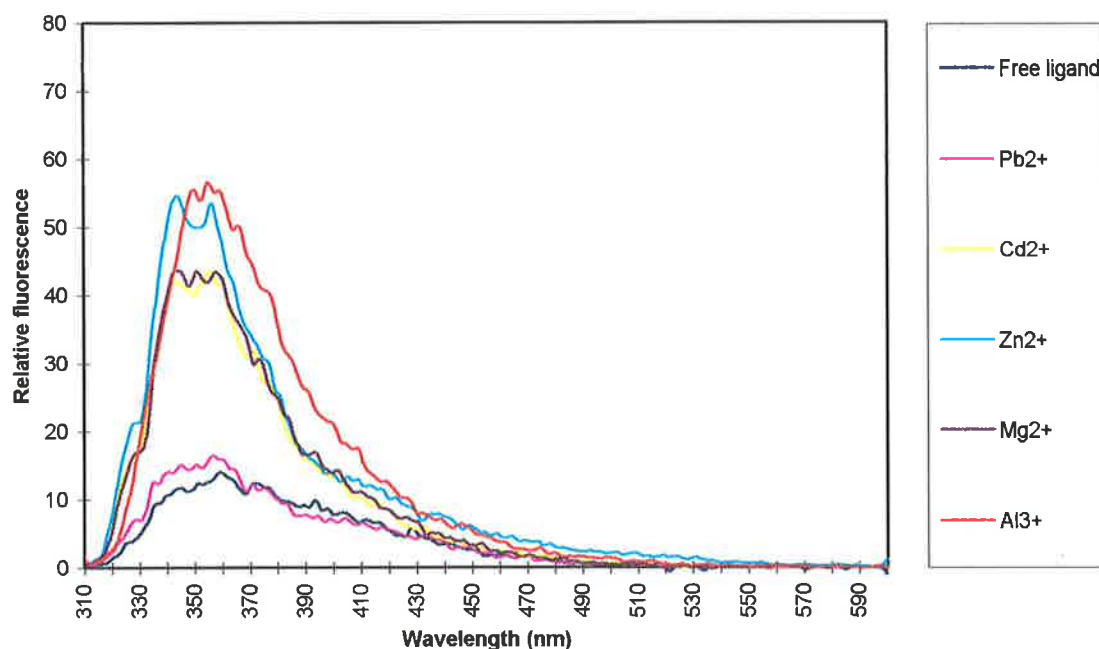


**Figure C.2.1:** The fluorescence emission spectra of the benzopyran-4-one thiazole ester **30** in the absence and presence of the metal ions listed in the right, vertical legend. An incident wavelength of 305 nm was used to determine the spectra.

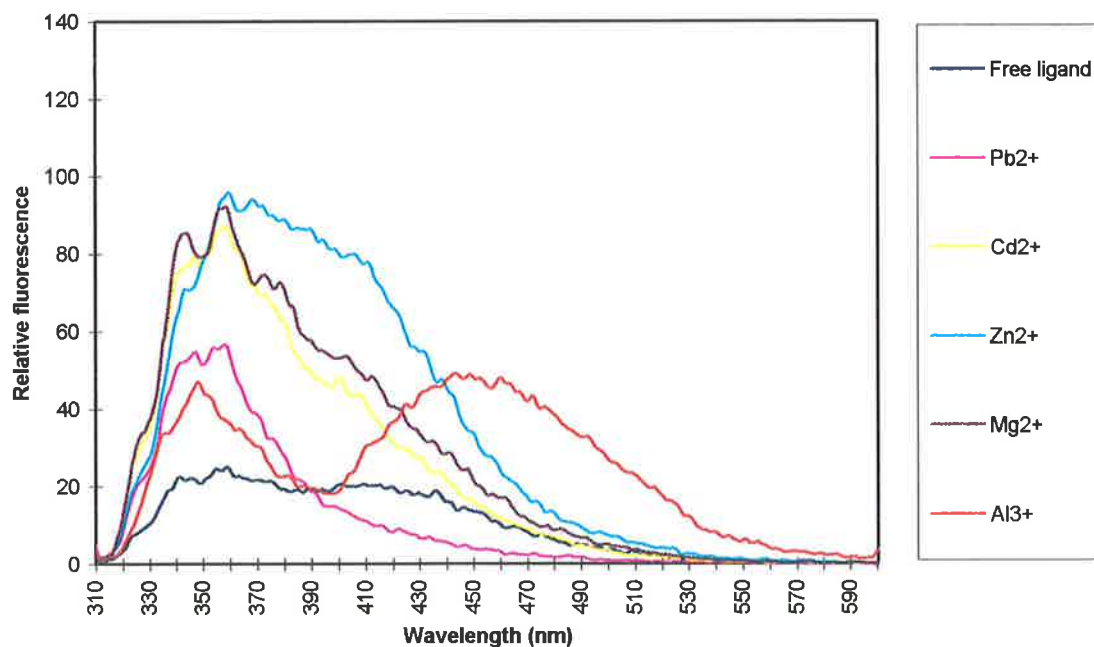


**Figure C.2.2:** The fluorescence emission spectra of the benzopyran-4-one thiazole acid **31** in the absence and presence of the metal ions listed in the right, vertical legend. An incident wavelength of 305 nm was used to determine the spectra.



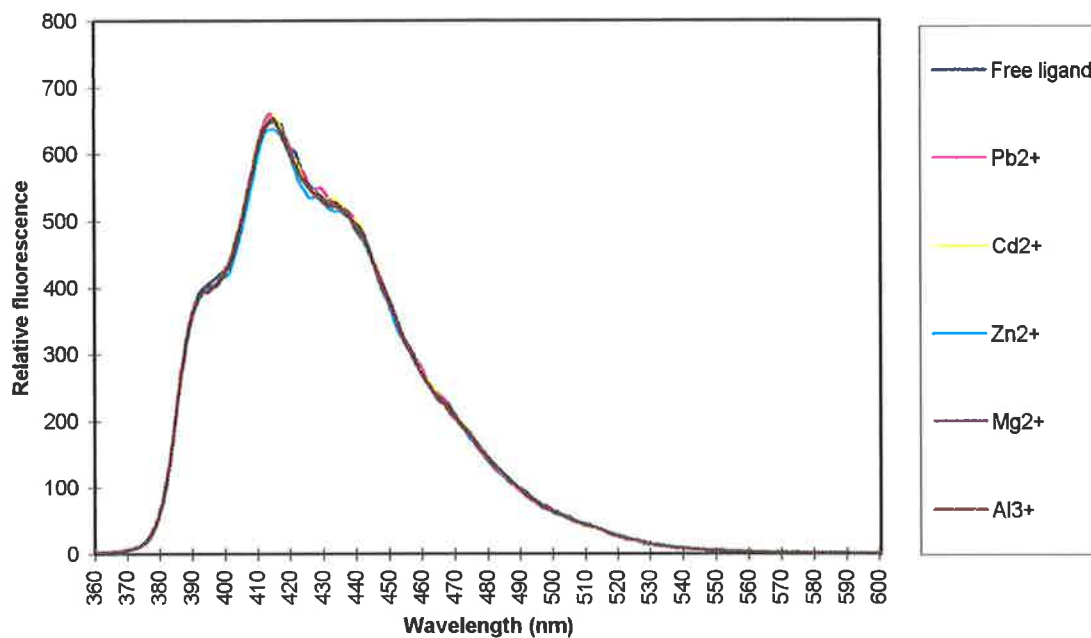


**Figure C.2.3:** The fluorescence emission spectra of the coumarin thiazole ester **32** in the absence and presence of the metal ions listed in the right, vertical legend. An incident wavelength of 353 nm was used to determine the spectra.

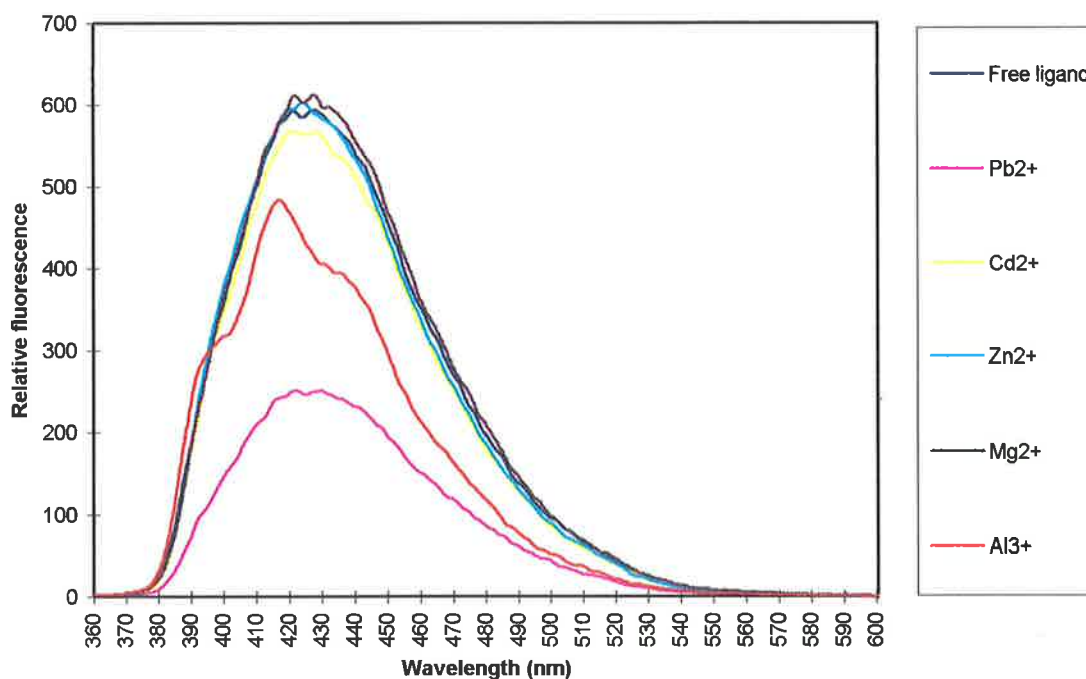


**Figure C.2.4:** The fluorescence emission spectra of the coumarin thiazole acid **33** in the absence and presence of the metal ions listed in the right, vertical legend. An incident wavelength of 353 nm was used to determine the spectra.

## Bibliography

- (1) Boggess, W. R.; Wixson, B. G. *Lead in the Environment*; Castle House Publications Ltd: 1979.
- (2) Green, V. A.; Wise, G. W.; Callenbach, J. *Clin. Toxicol.* **1976**, *9*, 33.
- (3) Abu-Dari, K.; Ekkehardt Hahn, F.; Raymond, K. N. *J. Am. Chem. Soc.* **1990**, *112*, 1519.
- (4) Ratcliffe, J. M. *Lead in Man and the Environment*; Ellis Horwood Limited: Chichester, 1981.
- (5) Australian Academy of Science. *Health and Environmental Lead in Australia* ; Canberra, 1981.
- (6) Alperstein, G.; Taylor, R.; Vimpani, G. *Lead Alert: A Guide for Health Professionals*; Australian Government publishing Service: Canberra, 1994.
- (7) Lippmann, M. *Environmental Toxicants: Human Exposures and Their Health Effects*; Van Nostrand Reinhold: New York, 1992.
- (8) National Research Council. *Measuring Lead Exposure in Infants, Children, and Other Sensitive Populations*; National Academy Press: Washington, D.C., 1993.
- (9) Nathanson, J.A.; Bloom, F.E. *Nature* **1975**, *255*, 419.
- (10) Schaffer, S.J.; Szilagyi, P.G.; Weitzman, M. *Pediatrics* **1994**, *93*(2), 159.
- (11) Friedheim, E.; Gorvi, C. *J. Pharm. Pharmacol.* **1975**, *27*, 624.
- (12) Tandon, S.K.; Behari, J.R.; Singh, S. *Bull. Environ. Contam. Toxicol.* **1983**, *30*, 552.
- (13) Tandon, S.K.; Flora, S.J.S.; Singh, S. *Bull. Environ. Contam. Toxicol.* **1986**, *37*, 317.
- (14) Peter, R.A.; Stucken, L.A.; Thompson, J.J.S. *Nature* **1945**, *156*, 616.
- (15) Haust, H.L.; Ali, H.; Haines, D.S.M. *J. Biochem.* **1986**, *2*, 897.
- (16) Twarog, T.A.; Cherian, M.G. *Bull. Environ. Contam. Toxicol.* **1983**, *30*, 165.
- (17) Graziano, J.H.; Leong, J.K.; Friedheim, E. *J. Pharmacol. Exp. Ther.* **1978**, *206*, 699.
- (18) Abu-Dari, K.; Karpishin, T. B.; Raymond, K. N. *Inorg. Chem.* **1993**, *32*, 3052.
- (19) Harrison, R. M.; Laxen, D. P. H. *Lead Pollution: Causes and Control*; Chapman and Hall Ltd: London, 1981.
- (20) Mason, W. T. *Fluorescent and Luminescent Probes for Biological Activity.*; Academic Press Limited.: London, 1993.
- (21) Haugland, R. P. *Molecular Probes' Handbook of Fluorescent Probes and Research Chemicals.*; Molecular Probes, Inc.: Eugene, 1996.
- (22) Mintá, A.; Kao, J. P. Y.; Tsien, R. Y. *J. Biol. Chem.* **1989**, *264*, 8171.

- (23) Grynkiewicz, G.; Poenie, M.; Tsien, R. Y. *J. Biol. Chem.* **1985**, *260*, 3440.
- (24) Hendrickson, K. M.; Rodopoulos, T.; Pittet, P.A.; Mahadevan, I.; Lincoln, S. F.; Ward, A. D.; Kurucsev, T.; Duckworth, P. A.; Forbes, I. J.; Zalewski, P. D.; Betts, W.H. *J. Chem. Soc., Dalton Trans.* **1997**, 3879.
- (25) Mahadevan, I.; Kimber, M. C.; Lincoln, S. F.; Tiekink, E. R. T.; Ward, A. D.; Betts, W.H.; Forbes, I. J.; Zalewski, P. D. *Aust. J. Chem.* **1996**, *49*, 561.
- (26) Zalewski, P. D.; Millard, S. H.; Forbes, I. J.; Kapaniris, O.; Slavotinek, A.; Betts, W. H.; Ward, A. D.; Lincoln, S. F.; Mahadevan, I. *J. Histochem. Cytochem.* **1994**, *42*, 877.
- (27) Zalewski, P. D.; Forbes, I. J.; Betts, W. H. *Biochem. J.* **1993**, *296*, 403.
- (28) Coyle, P.; Zalewski, P. D.; Philcox, J. C.; Forbes, I. J.; Ward, A. D.; Lincoln, S. F.; Mahadevan, I.; Roe, A. M. *Biochem. J.* **1994**, *303*, 781.
- (29) Zalewski, P. D.; Forbes, I. J.; Seamark, R. F.; Borlinghaus, R.; Betts, W. H.; Ward, A. D.; Lincoln, S. F. *Chem. Biol.* **1994**, *1*, 153.
- (30) Brand, I. A.; Kleineke, J. *J. Biol. Chem.* **1996**, *271*, 1941.
- (31) Berendji, D.; Kolb-Bachofen, V.; Meyer, K. L.; Grapenthin, O.; Weber, H.; Wahn, V.; Kroncke, K. D. *FEBS Letts.* **1997**, *405*, 37.
- (32) Unterreitmaier, E.; Schuster, M. *Anal. Chim. Acta.* **1995**, *309*, 339.
- (33) Czarnik, A. W. *Acc. Chem. Res.* **1994**, *27*, 302.
- (34) Katyal, M. *Talanta* **1968**, *15*, 95.
- (35) Geissman, T.A. *The Chemistry of Flavonoid Compounds*; Pergamon Press: Oxford, 1962
- (36) Katyal, M.; Prakash, S. *Talanta* **1977**, *24*, 367.
- (37) Goto, H. *Chem. Abs.* **1941**, *35*, 17209.
- (38) Hayashi, T.; Kawai, S.; Ohno, T. *Chem. Pharm. Bull.* **1973**, *21*, 1147.
- (39) Pearson, R. *Hard and Soft Acids and Bases*; Dowden, Hutchinson and Ross: Stroudsburg, 1973.
- (40) Sutton, L. E. *Tables of Interatomic Distances and Configuration in Molecules and Ions: Supplement 1956 - 1959*; The Chemical Society: London, 1965.
- (41) Pauling, L. C. *The Nature of the Chemical Bond and the Structure of Molecules and Crystals: An Introduction to Modern Structural Chemistry 3rd Ed.*; Cornell University Press: Ithica, 1960.
- (42) Tambar, J.; Gubler, H. *Helv. Chim. Acta.* **1918**, *2*, 101.
- (43) Herstein, F.; Konstanecki, S. v. *Ber. Dtsch. Chem. Ges.* **1899**, *32*, 318.
- (44) Hayashi, T.; Hara, K.; Kawai, S.; Ohno, T. *Chem. Pharm. Bull.* **1970**, *18*, 2407.
- (45) Briggs, M. T.; Duncan, G. L. S.; Thornber, C. W. *J. Chem. Research (M)*. **1982**, 2461.

- (46) Baker, W.; Harborne, J. B.; Ollis, W. D. *J. Chem. Soc.* **1952**, 1303.
- (47) Durand, R. J. F.; Sheenen, J. N.; Orme, P. H. *J. Synthesis* **1973**, 149.
- (48) Thomsen, I.; Clausen, K.; Scheibye, S.; Lawesson, S. *Organic Syntheses*, **62**, 158.
- (49) Miles, C. O.; Main, L.; Nicholson, B. K. *Aust. J. Chem.* **1989**, *42*, 1103.
- (50) Tsuda, Y.; Hosoi, S.; Goto, Y. *Chem. Pharm. Bull.* **1991**, *39(1)*, 18.
- (51) Silva, A. M. S.; Pinto, D. C. G. A.; Cavalerio, J. A. S. *Tetrahedron Lett.* **1994**, *35*, 5899.
- (52) Doshi, A. G.; Soni, P. A.; Ghiya, B. J. *Indian J. Chem.* **1986**, *25B*, 759.
- (53) Prasad, A. *Clinical, Biochemical and Nutritional Aspects of Trace Elements*; Alan R. Liss, Inc.: New York, 1982.
- (54) Ochiai, E. *J. Chem. Educ.* **1988**, *65*, 943.
- (55) Shannon, R.D. *Acta Cryst.* **1976**, *A32*, 751.
- (56) Knowles, A.; Burgess, C. *Practical Absorption Spectrometry*; Chapman and Hall: New York, 1984.
- (57) Jurd, L.; Geissman, T. A. *J. Org. Chem.* **1956**, *21*, 1395.
- (58) Atkins, P. W. *Physical Chemistry: 5th Edition*; Oxford University Press: Oxford, 1994.
- (59) Beck, M. T.; Nagypal, I. *Chemistry of Complex Equilibria*; Halsted Press: Chichester, 1990.
- (60) Hayashi, T.; Kawai, S.; Ohno, T. *Chem. Pharm. Bull.* **1970**, *18*, 2407.
- (61) Burgess, J. *Metal Ions in Solution*; Ellis Horwood Limited: Chichester, 1978.
- (62) Gaussian 94, Revision C.3, Frisch, M. J.; Trucks, G. W.; Schlegel, H. B.; Gill, P. M. W.; Johnson, B. G.; Robb, M. A.; Cheesman, J. R.; Keith, T.; Petersson, G. A.; Montgomery, J. A.; Raghavachari, K.; Al-Laham, M. A.; Zakrzewski, V. G.; Ortiz, J. V.; Foresman, J. B.; Cioslowski, J.; Stefanov, B. B.; Nanayakkara, A.; Challacombe, M.; Peng, C. Y.; Ayala, P. Y.; Chen, W.; Wong, M. W.; Andres, J. L.; Replogle, E. S.; Gomperts, R.; Martin, R. L.; Fox, D. J.; Binkley, J. S.; Defrees, D. J.; Baker, J.; Stewart, J. P.; Head-Gordan, M.; Gonzalez, C.; and Pople, J. A. Gaussian, Inc., Pittsburg PA, 1995.
- (63) Martell, A.E.; Montekaitis, R.J. *The Determination and Use of Stability Constants.*; VCH publishers: New York, 1988.
- (64) Bauman, R.P. *Absorption Spectroscopy*; John Wiley & Sons: New York, 1976.
- (65) Chaberek, S; Martell, A. E. *Organic Sequestering Agents*; John Wiley & Sons: New York, 1959.
- (66) Jaffe, H. H.; Orchin, M. *Theory and Application of Ultraviolet Spectroscopy*; John Wiley & Sons: New York, 1962.
- (67) Kurucsev, T. *Specfit*, personal communication.
- (68) Martell, A. E.; Calvin, M. *Chemistry of the Metal Chelate Compounds*; Prentice-Hall: New Jersey, 1962.

- (69) Taylor, T. A.; Patterson, H. H. *Anal. Chim. Acta* **1993**, *278*, 249.
- (70) Saarl, L. A.; Seltz, W. R. *Anal. Chem.* **1983**, *55*, 667.
- (71) Basolo, F.; Johnson, R. C. *Coordination Chemistry - The Chemistry of Metal Complexes*; W.A. Benjamin Inc.: New York, 1964.
- (72) Kettle, S.F.A. *Coordination Compounds*; Thomas Nelson and Sons: London, 1969.
- (73) Rao, C. N. R. *Ultra-Violet and Visible Spectroscopy*; Butterworth & Co: London, 1961.
- (74) Lakowicz, J.R. *Principles of Fluorescence Spectroscopy*; Plenum Press: New York, 1983.
- (75) Becker, R. S. *Theory and Interpretation of Fluorescence and Phosphorescence*; John Wiley & Sons, Inc.: New York; 1969.
- (76) Bridges, J. W. *Luminescence in Chemistry*; Bowden, E. J., Ed.; D. Van Nostrand Company: London, 1968; pp 77-115.
- (77) McGlynn, S.P.; Azumi, T.; Kinoshita, M. *Molecular Spectroscopy of the Triplet State*; Prentice-Hall, Inc.: Englewood Cliffs, N.J.; 1969.
- (78) Hayashi, T.; Kawai, S.; Ohno, T. *Chem. Pharm. Bull.*, **1971**, *19*, 792.
- (79) Grant, G.H.; Richards, W.G. *Computational Chemistry*; Oxford University Press Inc.: New York, 1995.
- (80) Clark, T. *A Handbook of Computational Chemistry: A Practical Guide to Chemical Structure and Energy Calculations*; John Wiley and Sons: New York, 1985.
- (81) Hehre, W.J.; Radom, L.; Schleyer, P.R.; Pople, J.A. *Ab Initio Molecular Orbital Theory*; John Wiley and Sons: New York, 1986.
- (82) Foresman, J.B.; Frisch, A. *Exploring Chemistry with Electronic Structure Methods 2nd Ed.*; Gaussian, Inc.: Pittsburg, 1996.
- (83) Dunning, Jr, T.H.; Hay, P.J. *Modern Theoretical Chemistry*; Schaefer III, H.F., Ed: Plenum: New York, 1976.
- (84) Stewart, G.M.; Tiekink, E.R.T.; Buntine, M.A. *J. Phys. Chem. A*, **1997**, *101*, 5368.
- (85) Buntine, M.A.; Hall, V.J.; Kosovel, F.J.; Tiekink, E.R.T. *J. Phys. Chem. A*, **1988**, *102*, 2472.
- (86) Hay, P.J.; Wadt, W.R. *J. Chem. Phys.*, **1985**, *82(1)*, 299.
- (87) Pratt, J. M. Ph.D. thesis, The University of Adelaide, Adelaide, Australia, **1995**.
- (88) Mathur, K.; Iyer, R.; Dhar, M. *J. Sci. Ind. Res.* **1962**, *21B*, 34.
- (89) Baker, W.; Howes, C. S. *J. Chem. Soc.* **1953**, 119.
- (90) Buckle, D. R.; Cantello, B. C. C.; Smith, H.; Spicer, B. A. *J. Med Chem.* **1977**, *20* (2), 265.
- (91) Yamada, Y.; Seki, N.; Kitahara, T.; Takahashi, M.; Matsui, M. *Agr. Biol. Chem.* **1970**, *34*, 780.

- (92) Taylor, E. C.; Zoltewicz, J. A. *J. Am. Chem. Soc.* **1960**, *82*, 2656.
- (93) Gudasi, K. B.; Goudar, T. R. *Indian J. Chem.* **1994**, *33A*, 346.
- (94) Bankovskis, J.; Misulovina, Z.; Ievins, A.; Buka, M. *Latvijas PSR Zinatnu Akad. Vestis* **1960**, *11*, 103. *Chem. Abs.* **1961**, *55*, 14458g.
- (95) Uchida, M.; Chihiro, M.; Morita, S.; Kanbe, T.; Yamashita, H.; Yamasaki, K.; Yabuuchi, Y.; Nakagawa, K. *Chem. Pharm Bull.* **1989**, *37*, 2109.
- (96) Rodionov, V.M.; Berkengeim, M.A. *J. Gen. Chem (U.S.S.R)* **1944**, *14*, 330. *Chem. Abs.* **1945**, *39*, 4077<sub>1</sub>.
- (97) Watanabe, K.; Kawagaki, K. *Bull. Chem. Soc. Jpn.* **1975**, *48*, 1945.
- (98) Rupprecht, S.; Franklin, S. J.; Raymond, K. N. *Inorg. Chim. Acta* **1995**, *235*, 185.
- (99) Rupprecht, S.; Langemann, K.; Lugger, T.; McCormick, J. M.; Raymond, K. N. *Inorg. Chim. Acta* **1996**, *243*, 79.
- (100) Robinson, M. A. *J. Inorg. Nucl. Chem.* **1964**, *26*, 1277.
- (101) Katritzky, A. R. *J. Chem. Soc.* **1957**, *1*, 191.
- (102) Yamazaki, M.; Honjo, N.; Noda, K.; Chono, Y.; Hamana, M. *J. Pharm. Soc. Jpn.* **1966**, *86*, 749.
- (103) Pouchert, C. J.; Behnke, J. *The Aldrich Library of <sup>13</sup>C and <sup>1</sup>H FT NMR Spectra, Edition 3.*; Aldrich Chemical Company, 1993.
- (104) Steger, H. F.; Corsini, A. *J. Inorg. Nucl. Chem.* **1973**, *35*, 1637.
- (105) Hamaya, T.; Hiratani, K.; Ohashi, K. *Chemistry Letters* **1994**, 615.
- (106) Corsini, A.; Fernando, Q.; Freiser, H. *Anal. Chem.* **1963**, *35*, 1424.
- (107) Harwood, L. M. *Aldrichimica Acta* **1985**, *18(1)*, 25.
- (108) Still, W. C.; Kahn, M.; Mitra, A. *J. Org. Chem.* **1978**, *43(14)*, 2923.
- (109) Perrin, D. D.; Armarego, W.L.F.; *Purification of Laboratory Chemicals*, 3rd ed; Pergamon Press: Oxford, 1988.
- (110) Wollenweber, E.; Mann, K. *Biochem. Physiol. Pflanz.* **1986**, *181*, 665.
- (111) Sanicanin, Z.; Tabakovic, I. *Electrochimica Acta* **1988**, *33(11)*, 1595.
- (112) Sakurai, T.; Inoue, H. *J. Chem. Soc. Perkin Trans. 2*, **1984**, 2031.